CURRENT MEG RESEARCH IN PSYCHIATRY

EDITED BY: Yoji Hirano and Peter Uhlhaas
PUBLISHED IN: Frontiers in Psychiatry

frontiers Research Topics

frontiers

ISSN 1664-8714
ISBN 978-2-88966-608-9
DOI 10.3389/978-2-88966-608-9

About Frontiers

Frontiers is more than just an open-access publisher of scholarly articles: it is a pioneering approach to the world of academia, radically improving the way scholarly research is managed. The grand vision of Frontiers is a world where all people have an equal opportunity to seek, share and generate knowledge. Frontiers provides immediate and permanent online open access to all its publications, but this alone is not enough to realize our grand goals.

Frontiers Journal Series

The Frontiers Journal Series is a multi-tier and interdisciplinary set of open-access, online journals, promising a paradigm shift from the current review, selection and dissemination processes in academic publishing. All Frontiers journals are driven by researchers for researchers; therefore, they constitute a service to the scholarly community. At the same time, the Frontiers Journal Series operates on a revolutionary invention, the tiered publishing system, initially addressing specific communities of scholars, and gradually climbing up to broader public understanding, thus serving the interests of the lay society, too.

Dedication to Quality

Each Frontiers article is a landmark of the highest quality, thanks to genuinely collaborative interactions between authors and review editors, who include some of the world's best academicians. Research must be certified by peers before entering a stream of knowledge that may eventually reach the public - and shape society; therefore, Frontiers only applies the most rigorous and unbiased reviews.
Frontiers revolutionizes research publishing by freely delivering the most outstanding research, evaluated with no bias from both the academic and social point of view. By applying the most advanced information technologies, Frontiers is catapulting scholarly publishing into a new generation.

What are Frontiers Research Topics?

Frontiers Research Topics are very popular trademarks of the Frontiers Journals Series: they are collections of at least ten articles, all centered on a particular subject. With their unique mix of varied contributions from Original Research to Review Articles, Frontiers Research Topics unify the most influential researchers, the latest key findings and historical advances in a hot research area! Find out more on how to host your own Frontiers Research Topic or contribute to one as an author by contacting the Frontiers Editorial Office: frontiersin.org/about/contact

CURRENT MEG RESEARCH IN PSYCHIATRY

Topic Editors:
Yoji Hirano, Kyushu University, Japan
Peter Uhlhaas, University of Glasgow, United Kingdom

Citation: Hirano, Y., Uhlhaas, P., eds. (2021). Current MEG Research in Psychiatry. Lausanne: Frontiers Media SA. doi: 10.3389/978-2-88966-608-9

Table of Contents

frontiers in Psychiatry

EDITORIAL
published: 02 February 2021
doi: 10.3389/fpsyt.2021.647085

Editorial: Current MEG Research in Psychiatry

Yoji Hirano[1,2]* *and Peter J. Uhlhaas*[3,4]*

[1] Department of Neuropsychiatry, Graduate School of Medical Sciences, Kyushu University, Fukuoka, Japan, [2] Department of Psychiatry, Harvard Medical School, VA Boston Healthcare System, Boston, MA, United States, [3] Department of Child and Adolescent Psychiatry, Charité - Universitätsmedizin, Berlin, Germany, [4] Institute of Neuroscience and Psychology, University of Glasgow, Glasgow, United Kingdom

Keywords: magnetoencephalography, MEG, brain imaging, spatiotemporal resolution, neurobiology, psychiatric disorders, biomarkers

Editorial on the Research Topic

Current MEG Research in Psychiatry

The identification of biomarkers for psychiatric disorders has the potential to revolutionize and redefine psychiatry, as these could aid diagnosis and identify novel treatment targets (1). Toward this goal, neuroimaging studies of psychiatric disorders have greatly accelerated over the past two decades. Specifically, neurophysiological approaches, such as electro- and magneto-encephalography (EEG/MEG) have revealed novel insights into sensory and cognitive abnormalities in psychiatric conditions due to their excellent temporal resolution in the ms range (2–10).

More than 50 years ago since the first MEG measurement of brain signals by Cohen (11), MEG is now a widely adopted method for the understanding of normal brain functions and their relationship to sensory and cognitive processes (12). MEG has an advantage of capturing neuronal dynamics with greater spatiotemporal and spectral detail than EEG. In addition, MEG has seen over the last years an emerging application as a tool to investigate pathophysiological mechanisms and biomarkers in psychiatric conditions (9). Given its exquisite temporal and good spatial resolution, MEG has provided novel insights into the role of rhythmic activity in autism spectrum disorder (ASD) and schizophrenia (SZ) (8, 9) as well as the first indication that MEG may contribute toward early detection and diagnosis in early-stage SZ and Alzheimer's disease (AD) (13, 14).

This special issue on "Current MEG Research in Psychiatry" provides a state-of-the-art overview of the potential and scope of MEG, ranging from recent developments in MEG methods (Hironaga et al.) to the study of cognitive and sensory dysfunctions in ASD (Yuk et al.) and SZ (Coffmann et al., Sauer et al., and Ohara et al.) including functional connectivity in psychosis (Candelaria-Cook and Stephen and Sunaga et al.), to the role of alterations nervous system (ANS) activity in major depression disorder (MDD) (Zhou et al.). While MEG has been largely used to study magnetic fields generated by the activity of the neural networks in the brain, cardio-vascular activity is also associated with a strong electrical dipole resulting in a measurable magnetic field. Two papers (Zhou et al., Kato et al.) use this approach to examine the relationship between ANS during emotion processing. Specifically, Zhou et al. show that the changes in heart rate variability (HRV) are associated with inhibitory dysfunctions of functional connectivity in the prefrontal cortex (PFC) in MDD while Kato et al. demonstrate changes in heart-rate evoked fields (HEFs) and disgust.

A particular focus of MEG-applications has been investigations into the neurophysiology of sensory and cognitive deficits in SZ and the papers by Coffmann et al., Sauer et al., and Ohara et al. provide novel perspectives on this topic. Coffmann et al. examined contralateral alpha suppression (CAS) during visual short-term memory and observed a failure to modulate alpha-band power in a load-dependent manner in first-episode SZ (FESZ) patients. Changes in neural oscillations

Edited and reviewed by:
Stefan Borgwardt,
University of Basel, Switzerland

***Correspondence:**
Yoji Hirano
yhouji@mac.com
Peter J. Uhlhaas
peter.uhlhaas@charite.de

Specialty section:
This article was submitted to Neuroimaging and Stimulation, a section of the journal Frontiers in Psychiatry

Received: *29 December 2020*
Accepted: *08 January 2021*
Published: *02 February 2021*

Citation:
Hirano Y and Uhlhaas PJ (2021) Editorial: Current MEG Research in Psychiatry. Front. Psychiatry 12:647085. doi: 10.3389/fpsyt.2021.647085

and event-related fields (ERFs) during repetition suppression were investigated by Sauer et al. Analysis of virtual-channel MEG-data revealed that both repetition suppression and enhancement were impaired in a sample of chronic SZ patients as indicated by deficits in the modulation of beta/gamma-band power as well as in ERFs in thalamic and occipital cortices. Finally, Ohara et al. examined whether the M170 indexes a specific deficit in face-processing in SZ. Patients with SZ showed a selective deficit to face-stimuli in the fusiform face area (FFA) that correlated with the severity of negative symptoms.

Spectral signatures of resting-state activity are currently attracting a lot of attention in psychosis research (15–19) and the reports by Candelaria-Cook and Stephen as well as Sunaga et al. provide advanced perspectives on this theme. Candelaria-Cook and Stephen tested the reliability of MEG-based functional connectivity metrics in HC and SZ. They found that HC had higher reliability compared to SZ, and the default mode, cognitive control, and visual networks had higher test-retest reliability compared to somatosensory and auditory networks. In addition, both eyes open and eyes closed resting-state networks were found to be reliable over sessions. Sunaga et al. explored the frequency-specific resting-state connectome including limbic network (LM) and default mode network (DMN) in bipolar psychosis (BP) *via* a novel graph analysis. BP patients show frequency-specific alterations in the inter-community (between right LM–right DMN) in the gamma-band and intra-community edges (within left LM) in the high beta-band, and the intra-community edges in the left LM at beta-band frequencies were positively correlated with depressive symptoms.

Investigations into the developmental trajectories of potential biomarkers are also crucial for early detection and intervention, in particular for disorders with an onset in childhood, such as ASDs (20). A longitudinal MEG study by Edgar et al. examined the development of auditory cortex M50 and M100 ERFs in children (6–8 years of age). The authors show significant between-subject as well as within-subject (left- and right-hemisphere) variability, in particular for M100 responses during normal brain development. Yuk et al. examined phase-synchronization during working memory in adult with ASDs to investigate the contribution of long-range synchronization toward cognitive deficits. While adults with ASD appropriately employed alpha-band oscillations to facilitate maintenance of novel visual stimuli in short-term and working memory, the topology and networks involved were different from controls, indicating more effortful processing in adults with ASDs.

Hironaga et al. provide a state-of-the-art review on the future prospects of MEG research in psychiatric disorders through addressing key empirical and methodological challenges. Despite the relatively small number of systems worldwide and high maintenance costs (12), MEG has the potential to significantly contribute toward the development of biomarkers for early detection and diagnosis for major syndromes [e.g., (13)]. Groundbreaking innovations, such as the new optically-pumped magnetometer (OPM) or wearable OPMs (21), will lead to a deeper understanding of the neural basis of psychiatric disorders as well as facilitate the development of novel treatment targets including neurofeedback treatments (22). Accordingly, we believe that the continued development of MEG hardware and analyses approaches will open up new perspectives for establishing neurophysiological biomarkers for psychiatric disorders.

AUTHOR CONTRIBUTIONS

PU and YH prepared the first draft of the manuscript and edited the manuscript. All authors contributed to and have approved the final manuscript.

FUNDING

This research was supported, in part, by AMED under Grant Number JP20dm0207069 and GAJJ020620 (JP19dm0107124h0004) (YH); Fund for the Promotion of Joint International: JP20KK0193 (YH) from the Japan Society for the Promotion of Science (JSPS); SIRS Research Fund Award (YH) from Schizophrenia International Research Society.

REFERENCES

1. Insel TR, Cuthbert BN. Brain disorders? Precisely. *Science*. (2015) 348:499–500. doi: 10.1126/science.aab2358
2. Kwon JS, O'Donnell BF, Wallenstein GV, Greene RW, Hirayasu Y, et al. Gamma frequency-range abnormalities to auditory stimulation in schizophrenia. *Arch Gen Psychiatry*. (1999) 56:1001–5. doi: 10.1001/archpsyc.56.11.1001
3. Spencer KM, Nestor PG, Perlmutter R, Niznikiewicz MA, Klump MC, Frumin M, et al. Neural synchrony indexes disordered perception and cognition in schizophrenia. *Proc Natl Acad Sci USA*. (2004) 101:17288–93. doi: 10.1073/pnas.0406074101
4. Hirano S, Spencer KM, Onitsuka T, Hirano Y. Language-related neurophysiological deficits in schizophrenia. *Clin EEG Neurosci*. (2020) 51:222–33. doi: 10.1177/1550059419886686
5. Oribe N, Onitsuka T, Hirano S, Hirano Y, Maekawa T, Obayashi C, et al. Differentiation between bipolar disorder and schizophrenia revealed by neural oscillation to speech sounds: an MEG study. *Bipolar Disord*. (2010) 12:804–12. doi: 10.1111/j.1399-5618.2010.00876.x
6. Oribe N, Hirano Y, Del Re E, Mesholam-Gately RI, Woodberry KA, Ueno T, et al. Longitudinal evaluation of visual P300 amplitude in clinical high-risk subjects: an event-related potential study. *Psychiatry Clin Neurosci*. (2020) 74:527–34. doi: 10.1111/pcn.13083
7. Oribe N, Hirano Y, Del Re E, Seidman LJ, Mesholam-Gately RI, Woodberry KA, et al. Progressive reduction of auditory evoked gamma in first episode schizophrenia but not clinical high risk individuals. *Schizophr Res*. (2019) 208:145–52. doi: 10.1016/j.schres.2019.03.025
8. Uhlhaas PJ, Singer W. Neuronal dynamics and neuropsychiatric disorders: toward a translational paradigm for dysfunctional large-scale networks. *Neuron*. (2012) 75:963–80. doi: 10.1016/j.neuron.2012.09.004
9. Uhlhaas PJ, Liddle P, Linden DEJ, Nobre AC, Singh KD, Gross J. Magnetoencephalography as a tool in psychiatric research: current status and perspective. *Biol Psychiatry Cogn Neurosci Neuroimaging*. (2017) 2:235–44. doi: 10.1016/j.bpsc.2017.01.005

10. Hamilton HK, Boos AK, Mathalon DH. Electroencephalography and event-related potential biomarkers in individuals at clinical high risk for psychosis. *Biol Psychiatry*. (2020) 88:294–303. doi: 10.1016/j.biopsych.2020.04.002
11. Cohen D. Magnetoencephalography: evidence of magnetic fields produced by alpha-rhythm currents. *Science*. (1968) 161:784–6. doi: 10.1126/science.161.3843.784
12. Baillet S. Magnetoencephalography for brain electrophysiology and imaging. *Nat Neurosci*. (2017) 20:327–39. doi: 10.1038/nn.4504
13. Grent-'t-Jong T, Gajwani R, Gross J, Gumley AI, Krishnadas R, Lawrie SM, et al. Association of magnetoencephalographically measured high-frequency oscillations in visual cortex with circuit dysfunctions in local and large-scale networks during emerging psychosis. *JAMA Psychiatry*. (2020) 77:852–62. doi: 10.1001/jamapsychiatry.2020.0284
14. Nakamura A, Cuesta P, Fernández A, Arahata Y, Iwata K, Kuratsubo I, et al. Electromagnetic signatures of the preclinical and prodromal stages of Alzheimer's disease. *Brain*. (2018) 141:1470–85. doi: 10.1093/brain/awy044
15. Hirano Y, Oribe N, Kanba S, Onitsuka T, Nestor PG, Spencer KM. Spontaneous gamma activity in schizophrenia. *JAMA Psychiatry*. (2015) 72:813–21. doi: 10.1001/jamapsychiatry.2014.2642
16. Hirano Y, Oribe N, Onitsuka T, Kanba S, Nestor PG, Hosokawa T, et al. Auditory cortex volume and gamma oscillation abnormalities in schizophrenia. *Clin EEG Neurosci*. (2020) 51:244–51. doi: 10.1177/1550059420914201
17. Grent-'t-Jong T, Gross J, Goense J, Wibral M, Gajwani R, Gumley AI, et al. Resting-state gamma-band power alterations in schizophrenia reveal E/I-balance abnormalities across illness-stages. *Elife*. (2018) 7:e37799. doi: 10.7554/eLife.37799
18. Mackintosh AJ, de Bock R, Lim Z, Trulley VN, Schmidt A, Borgwardt S, et al. Psychotic disorders, dopaminergic agents and EEG/MEG resting-state functional connectivity: a systematic review. *Neurosci Biobehav Rev*. (2020). doi: 10.1016/j.neubiorev.2020.10.021. [Epub ahead of print].
19. Hirano Y, Nakamura I, Tamura S, Onitsuka T. Long-term test-retest reliability of auditory gamma oscillations between different clinical EEG systems. *Front Psychiatry*. (2020) 11:876. doi: 10.3389/fpsyt.2020.00876
20. Edgar JC. Identifying electrophysiological markers of autism spectrum disorder and schizophrenia against a backdrop of normal brain development. *Psychiatry Clin Neurosci*. (2020) 74:1–11. doi: 10.1111/pcn.12927
21. Hill RM, Boto E, Rea M, Holmes N, Leggett J, Coles LA, et al. Multi-channel whole-head OPM-MEG: helmet design and a comparison with a conventional system. *NeuroImage*. (2020) 219:116995. doi: 10.1016/j.neuroimage.2020.116995
22. Hirano Y, Tamura S. Recent findings on neurofeedback training for auditory hallucinations in schizophrenia. *Curr Opin Psychiatry*. (2021) doi: 10.1097/YCO.0000000000000693

Conflict of Interest: PU reports having received research funding from Lilly UK and Lundbeck UK outside the submitted work.

The remaining author declares that the research was conducted in the absence of any commercial or financial relationships that could be construed as a potential conflict of interest.

frontiers in Psychiatry

ORIGINAL RESEARCH
published: 22 January 2020
doi: 10.3389/fpsyt.2019.00989

Decreased Task-Related HRV Is Associated With Inhibitory Dysfunction Through Functional Inter-Region Connectivity of PFC in Major Depressive Disorder

Hongliang Zhou[1], Zongpeng Dai[2], Lingling Hua[1], Haiteng Jiang[2], Shui Tian[2], Yinglin Han[1], Pinhua Lin[1], Haofei Wang[1], Qing Lu[2,3] and Zhjjian Yao[1,4]**

[1] Department of Psychiatry, the Affiliated Brain Hospital of Nanjing Medical University, Nanjing, China, [2] School of Biological Sciences & Medical Engineering, Southeast University, Nanjing, China, [3] Child Development and Learning Science, Key Laboratory of Ministry of Education, Nanjing, China, [4] Nanjing Brain Hospital, Medical School of Nanjing University, Nanjing, China

OPEN ACCESS

Edited by:
Yoji Hirano,
Kyushu University,
Japan

Reviewed by:
Yutaka Kato,
Tsutsuji Mental Hospital,
Japan
Murat İlhan Atagun,
Yıldırım Beyazıt University,
Turkey

***Correspondence:**
Qing Lu
luq@seu.edu.cn
Zhjjian Yao
zjyao@njmu.edu.cn

Specialty section:
This article was submitted to Neuroimaging and Stimulation, a section of the journal Frontiers in Psychiatry

Received: 28 October 2019
Accepted: 12 December 2019
Published: 22 January 2020

Citation:
Zhou H, Dai Z, Hua L, Jiang H, Tian S, Han Y, Lin P, Wang H, Lu Q and Yao Z (2020) Decreased Task-Related HRV Is Associated With Inhibitory Dysfunction Through Functional Inter-Region Connectivity of PFC in Major Depressive Disorder. Front. Psychiatry 10:989. doi: 10.3389/fpsyt.2019.00989

The regulation of the autonomic nervous system (ANS) can improve cognitive function in major depressive disorders (MDD). Heart rate variability (HRV) derives from the dynamic control of the ANS and reflects the balance between the activities of the sympathetic and parasympathetic nervous systems by measuring tiny changes in adjacent heart beats. Task-related HRV may reflect the association between the flexibility of cognition and ANS function. The study was to investigate the neural mechanism of interactions between ANS and cognitive function in MDD with Magnetoencephalography (MEG) measurements. Participants included 20 MDD patients and 18 healthy controls (HCs). All participants were measured with a go/no-go task MEG. HRV indices, the standard deviation of the average normal-to-normal (NN) interval calculated over short periods (SDANN) and the square root of the mean squared differences of successive NN intervals (RMSSD), were derived from the raw MEG data. Results showed that MDD patients showed decreased SDANN and RMSSD. In MDD patients, both resting-state and task-related RMSSD were related to inhibitory and control dysfunction. In the go/no-go task, many areas in the prefrontal cortex (PFC) are responsible for an individual's inhibitory function. A brain MEG functional connectivity analysis revealed that there were significant differences in four brain regions within the prefrontal cortex (PFC) between MDD patients and HCs. Task-related RMSSD in HCs were related to the functional connectivity between the left middle frontal gyrus and the anterior cingulate cortex (ACC), while in MDD patients, these values were not related to the above functional connectivity but were related to the functional connectivity between

the left middle frontal gyrus and insula. However, the resting-state RMSSD value was not related to these significant difference functional connectivity networks in all participants. It concludes that the decreased task-related HRV is associated with inhibitory dysfunction through functional inter-region connectivity in the PFC in MDD, and the task-related HRV can be used as an index of the association between MDD and autonomic dysregulation.

Keywords: major depressive disorders, magnetoencephalography, task-related heart rate variability, functional connectivity, go/no-go task

INTRODUCTION

Major depressive disorder (MDD) is a serious health care problem worldwide, according to the report of illness-induced disability (1). MDD is a more severe state of depressive symptomatology in which patients present multiple depressive symptoms and show significant distress or impaired functioning. Of the many depressive symptoms, cognitive impairments are common in MDD. Cognitive function is an individual's ability to process information. Cognitive dysfunction is prevalent and is associated with the early onset of depression and with longer depressive episodes in MDD patients; it also has an adverse impact on treatment outcomes, as well as on functional recovery (2). Inhibitory and control function is a critical cognitive function that can be defined as interference control, prepotent response inhibition, and resistance to interference. Prepotent response inhibition is the ability to suppress or withhold a (motor) response, which can be measured by the go/no-go task (3).

Inhibitory and control function includes two levels: a central level, which is related to the cerebral cortex, and a peripheral level, which is mediated by the autonomic nervous system (ANS) (4). At the central level, many studies using neuroimaging methods have reported that in the go/no-go task, many areas in the prefrontal cortex (PFC), such as BA9, BA10, and BA47, are responsible for an individual's inhibitory function (5–9). At the peripheral level, the ANS, especially the vagus nerve, plays an important role in an individual's inhibitory and control function (4). Many studies have shown that the decreased vagus tone is associated with abnormal inhibitory and control function under the emotional stop-signal task or the Stroop test (10, 11).

Magnetoencephalography (MEG) has high temporal and spatial resolution and has been used to investigate the neural mechanism of many cognitive functions (12). Functional connectivity measures how brain regions are temporally coordinated and is employed to probe brain network architecture (13). MEG has been used for investigations of brain cortical activity and functional connectivity in MDD (14). MEG in MDD patients allows inter-regional and intraregional connectivity interactions in brain function to be related to cognition, which can provide mechanistic insights into interactions between the ANS and cognitive function.

Individual ANS functioning relies on a balance between the activities of the sympathetic and parasympathetic nervous systems. Although cardiac automaticity is originated in pacemaker tissues, heart rate and rhythm largely depend on the control of ANS (15). By releasing neurotransmitters such as acetylcholine, epinephrine, and norepinephrine, the sympathetic and parasympathetic nervous systems can affect heart beats which lead to the changes of heart rate variability (HRV). HRV derives from the dynamic control of the ANS and reflects the balance between the activities of the sympathetic and parasympathetic nervous systems by measuring tiny changes in adjacent heart beats. The measurement of HRV contains time domain methods, frequency domain methods and rhythm pattern analysis. Time domain methods and frequency domain methods are mostly applied to clinical researches. Although frequency domain methods are computed by decomposing waveform of electrocardiogram (ECG)–RR intervals (interbeat interval or RRIs) and are considered to better distinguish the influence of the parasympathetic and sympathetic nervous systems, they may be affected by different therapeutic regimes and other factors easily comparing with time domain methods which may also reflect the activities of the sympathetic and parasympathetic nervous systems (16–18). The standard deviation of the average normal-to-normal (NN) intervals (SDANN), which is calculated over a short period (usually within 5 min), and the square root of the mean squared differences of successive normal sinus intervals (RMSSD) are components of HRV from the time-domain analysis. SDANN represents sympathetic function, and RMSSD represents the flexibility of vagal (parasympathetic) tone (19, 20). It is accepted that HRV is decreased in MDD (21–23), and decreased HRV might be associated with abnormal perseveration cognition (24). A recent study proved that yoga could be an add-on treatment for MDD by adjusting HRV (25). In addition, HRV biofeedback (HRVB), which has been extensively applied in the clinic, can improve cognition and other symptoms of MDD (26–30). It is worth noting that according to the different experimental conditions, HRV can be measured as the resting-state HRV or task-related HRV. Previous studies that used resting-state HRV investigated the association between the ANS and cognition in MDD, and confirmed that resting-state HRV can be used as a characteristic biological marker for MD (23, 24, 31).

Because task-related HRV may reflect the association between the flexibility of cognition and ANS function, task-related HRV can be used as a sensitive index to reflect inhibitory control function at the peripheral level (32). However, to date, no studies on the association between the ANS and cognition (i.e. inhibitory control function) in MDD, which was shown to be involved in task-related HRV, have been reported. Most importantly, the neural mechanism of interactions between the ANS and inhibitory and control function in MDD remains unclear.

In this study, both resting-state HRV and task-related HRV were used to assess ANS function; a go/no-go task was employed to measure cognitive function (inhibitory and control function), and MEG was used to measure brain cortical activity and functional connectivity. To guarantee cognition along different psychophysiological dimensions, task-related HRV indices were derived from the raw MEG data. The purpose of this study is to 1) uncover the neural mechanism of interactions between the ANS and inhibitory and control function in MDD and 2) confirm whether task-related HRV can be used as an index of the association between MDD and autonomic dysregulation.

MATERIALS AND METHODS

Time and Setting

The experiment was completed in the Department of Psychiatry, Affiliated Nanjing Brain Hospital of Nanjing Medical University, Nanjing, People's Republic of China, from January 1, 2017, to July 28, 2019. All experimental procedures were approved by the Ethics Committee on Human Studies, Affiliated Nanjing Brain Hospital of Nanjing Medical University, Nanjing, People's Republic of China and were conducted depending on the Declaration of Helsinki (Ethical review number: 2016KY12). All patients and healthy controls signed an informed consent form, and they received 20 United States dollars as a reward after finishing the experiment. Considering that some patients could not sign the consent form, legal guardians who could represent these patients were also asked to provide consent for all experimental procedures.

Diagnostic Approaches and Participants

This study included an MDD group and an HC group. The criteria for the MDD group were as follows: 1) only meet the criteria of Diagnostic and Statistical Manual of Mental Disorders, Fifth edition (DSM-5) for major depression; 2) age from 18 years old to 65 years old; 3) Hamilton Depression Scale (17-item edition, HAMD) scores ≥ 17; 4) no fewer than two episodes of depression; 5) had not taken medication for the last two weeks; 6) were not treated with electroconvulsive therapy within the last month; 7) no diagnosis of alcohol, drug, or other substance dependency, any kind of head injury, neurological disorder, or systemic disease that might have an effect on the central nervous system; and 8) no contraindications for the MEG measurements. The criteria for the HC group were as follows: 1) did not meet the criteria of any DSM-5 axis I disorder or personality disorders according to the Structured Clinical Interview for DSM-5 (SCID-5, Chinese version); 2) age from 18 years old to 65 years old; 3) HAMD (17-item edition) scores ≤ 7; 4) no history of any kind of psychiatric disorder; 5) no diagnosis of alcohol, drug, or other substance dependence; and 6) no diagnosis of any kind of head injury, neurological disorder or systemic disease that might have an effect on the central nervous system. All participants needed to be free of any form of cardiac disease, lung disease, beta-blocker medication, or any other disease that could influence the physiological data, and they were forbidden to drink any coffee or tea on the day of the test session. In addition, to reduce the stress caused by MEG examination, patients were informed the whole process of the research and were asked to fit the environment in advance after 8 min resting.

According to the above criteria, twenty patients with MDD were chosen from thirty-four inpatients, and eighteen healthy persons were chosen from thirty healthy volunteers. These HCs were citizens who lived in Nanjing city, Jiangsu Province, People's Republic of China. All participants were Chinese.

On the day of the experiment, with the assistance of a psychiatric resident physician, a psychiatric associate chief physician was asked to collect medication information, demographic and clinical characteristics, and confirm/exclude the MDD diagnosis of participants. We used the Annett Handedness Scale to evaluate handedness. The standards of handedness were as follows: Annett score (1) = right, (2–7) = mixed, and (8) = left. All participants were right handed.

MEG Task and Procedure

Go/No-Go Task

The go/no-go task was edited by BrainX software, which was based on DirectX (Microsoft Corporation, Redmond, WA, USA). One hundred eighty stimuli were used in this task, and the total duration of the task was 300 s. Three types of stimuli were used in this task: a red lamp picture, a green lamp picture, and a gray cross. These stimuli were shown serially on a white background against a black background (1.5 × 1.5 cm in size) on a computer screen. The whole task contained both go and no-go trials. In a go trial, the participant was shown a gray cross on a white background that was presented for 2,500 millisecond (ms) followed by a green lamp picture. The green lamp picture remained on the screen for either 150 or 500 ms, decided at random. In a no-go trial, a red lamp picture was presented for 400 ms duration, followed by a gray cross picture and then a green lamp picture. The duration of the gray fixation cross presentation was 2,500 ms and that of the green lamp was 150 ms. After every picture was presented, there was an interval time of 300 ms. The duration of no-go trials accounts for 25% of the entire task. There were 20 go trials and 5 no-go trials in this experiment in the practice phase, and the data in the practice phase were not recorded or analyzed (**Figure 1**).

Behavioral Data Measurements

The behavioral data included the accuracy rate (hit rate, i.e. the percentage of correct responses), reaction times (RTs), and false alarms (error rate, i.e. the opposite of the intended action was selected on accident). The accuracy rate and RTs were recorded for go trials, and false alarms were recorded for no-go trials.

MEG Data Acquisition

A 275-channel whole-head CTF MEG system (Omega 2000, VSM Med Tech Inc., Port Coquitlam, Canada) was used for the MEG recordings. The sampling rate of the machine was adjusted to 1,200 Hz. Any metal on participants' bodies was removed, and people were asked to lay in the supine position in a special magnetically shielded room. With a third-order synthetic gradient, the system could cancel background and noise

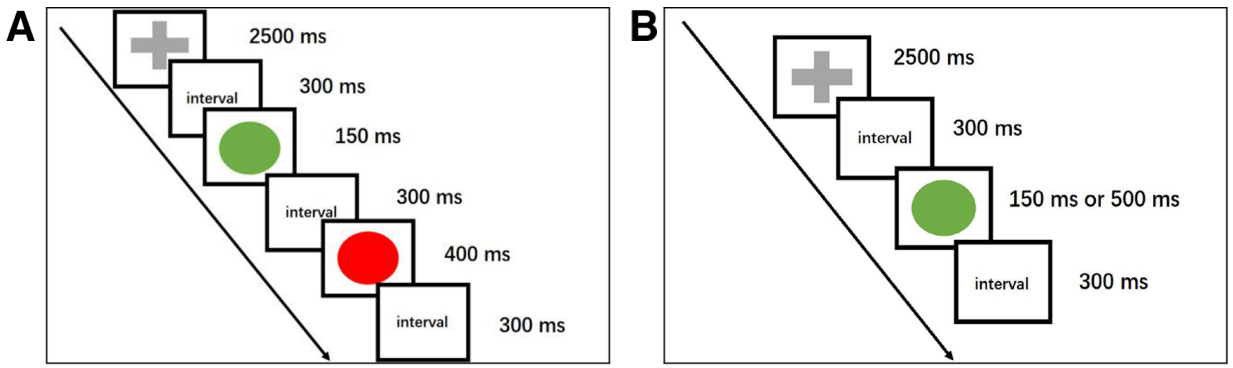

FIGURE 1 | A cartoon illustrating the go/no-go task. ms, millisecond. **(A)** This schematic representation of a no-go trial begins with the presentation of a gray fixation cross (go stimulus), followed by a green lamp (go stimulus). Then, a red lamp, which indicates a no-go trial, is shown, and participants need to respond. The no-go trials accounted for 25% of the entire session, and every picture was followed by a 300 ms interval. **(B)** The go trials consisted of a gray fixation cross whose duration was 2,500 ms and a green lamp. The duration of the green lamp was randomly either 150 or 500 ms.

interference effectively. During MEG measurements, the movement of head motion and localization could be tolerated within 5 millimeter (mm). The T1-weighted imaging data were obtained from Siemens Verio 3.0 Tesla Magnetic Resonance Imaging (MRI) scanner (Erlangen, Germany). The T1-weighted axial image parameters were as follows: repetition time/echo time (TR/TE) = 1,900/2.48 ms, thickness/gap = 1.0/0 mm, field of view (FOV) = 240 × 240 mm^2, matrix = 256 × 256 × 192, and voxel size = 1 × 1 × 1 mm^3. Three energizing coils were set at the nasion, left preauricular, and right preauricular locations to measure the participant's head location within the scanner and for offline co-registration of MRI and MEG data.

Pre-Processing

The Fieldtrip toolbox (http://www.ru.nl/fcdonders/fieldtrip/) in a MATLAB software environment (http://www.mathworks.com) was used to pre-process MEG data. After removing the frequency band between 49.5 and 50.5 Hz, which indicated big noise that could affect the authenticity of the data, the raw MEG data were separated into three parts: go epochs, no-go epochs and interval epochs. Only correct no-go epochs were used in the MEG analysis. The time range of 200 ms pre-stimulus and 900 ms post-stimulus during no-go epochs was selected. The SPM megheadloc function was applied to screen the data for head motion by removing any epochs with motion greater than 5 mm or when intertrial movement was >10 mm. Then, we used independent component analysis (ICA) to eliminate eye movement and cardiac artifacts. The 1- to 120-Hz frequency band was chosen for analysis.

Source Reconstruction and Functional Connectivity Calculations

The minimum-norm estimates algorithm was used to complete source reconstruction after pre-processing the raw MEG data (33). We used averaged envelope correlation (AEC) to compute the functional connectivity networks within brain regions between MDD patients and HCs under the go/no-go task. The filtered time series gotten after source reconstruction were transformed by Hilbert transform to get the analytic signal, and then the absolute value of the signal was extracted and divided into several parts. The time consistency between each two parts of them was calculated by average correlation value with Pearson correlation analysis. Considering that there had been no similar study carried out before, according to previous studies (34, 35), we chose the prefrontal lobe, which is the area primarily reactive to the go/no-go task. Significantly, the anterior cingulate cortex was specifically chosen for its tight association with HRV. Although there are some doubts surrounding exploring deep brain areas by MEG, considering that the important role of the insula plays in HRV, this region was chosen as an auxiliary brain area for the explanation of our results. The brain areas chosen to compute function connectivity in the no-go epoch are shown in **Table 1**.

TABLE 1 | Brain regions chosen from previous studies.

Area	H	X	Y	Z	BA
Superior frontal gyrus	L	−24	48	22	9
	L	−26	62	8	10
	L	−48	28	−16	47
	R	26	46	42	8
	R	42	60	2	10
	R	24	54	34	8
	R	30	60	−14	10
	R	22	62	24	9
Middle frontal gyrus	L	−28	56	−2	10
	L	−30	48	36	8
	R	−50	48	18	46
	R	38	38	30	9
	R	22	36	42	8
Insula	L	−35.13	6.65	3.44	13
	L	−32	16	−16	13
	L	−34	12	−14	13
	R	44	−6	−4	
Anterior cingulate cortex		4	26	−4	

HRV Data Acquisition and Analysis

To guarantee HRV could reflect task-related state more precisely, ECG record was directly collected from the MEG raw data under the go/no-go task after ICA (36). There were two reasons to choose time domain analysis. Firstly, the bandpass frequency range of MEG data was set from 0 HZ to 120 HZ, which could disturb the indices of frequency domain analysis. Secondly, time domain analysis is not sensitive to the usage of medication other than tricyclic and tetracyclic antidepressants (37), which could minimize the influence of medication. By recording continuous ECG data, each QRS complex was detected with the pan-tompkin function in the MATLAB software environment, and the normal-to-normal (NN) intervals which were all intervals between adjacent QRS complexes resulting from instantaneous heart rate were determined. And HRV components SDANN and RMSSD were selected to be analyzed. The pan-tompkin function in the MATLAB software environment was applied to lock the R wave. Then, the RMSSD and SDANN were measured with the following formulas: SDANN (which represents the activity of sympathetic nervous system) $= \sqrt{\frac{1}{N}\sum_{i-1}^{N}(RR_i - \overline{RR})^2}$ and RMSSD (which represents the activity of parasympathetic nervous system) $= \sqrt{\frac{1}{N-1}\sum_{i=1}^{N-1}(RR_{i+1} - RR_i)^2}$ (38). Resting-state HRV was derived from the recording data of HRV biofeedback software after 8 min resting at the same time (about 2 o'clock in the afternoon) on the next day to reduce the effect of circadian rhythm on experiment. Although the data contain all indices of HRV, to match task-related HRV, only the SDANN and RMSSD values were used for analysis.

Data and Statistical Analysis

Data are shown as the means (standard deviation, SD). Statistical Program for Social Sciences software version 19.0 (SPSS, IBM Corporation, Armonk, NY, USA) was applied to statistical analysis. Independent-samples *t*-tests and paired-sample *t*-tests were applied to compare mean age, education, The Hamilton Depression Scale (HAMD, 17-item edition) scores, the Hamilton Anxiety Scale (HAMA) scores, behavioral data, HRV values, and functional connectivity of brain regions between the MDD and the HC groups, and the Pearson chi-square test was used to investigate the gender ratio. A general linear correlation method was used to investigate the relationship between HRV indices and significant difference functional connectivity networks, and HAMD scores used Pearson's *r* in the MDD patients and the HCs. To reduce the likelihood of false positives, the false-discovery rate (FDR) correction was used to correct multiple comparisons (39). Alpha values of 0.05 were considered to have significance.

RESULTS

Demographic Characteristics of Participants

As shown in **Table 2**. There were no significant differences between the demographic characteristics of the participants in the MDD group and the HC group. The HAMA scores were higher in the MDD group than in the HC group; however, there were no significant differences. The HAMD scores of the MDD group were higher than those of the HC group.

TABLE 2 | Demographic and clinical characteristics of participants.

	MDD	HC	Test statistic
Gender ratio (M/F)	20 (8/12)	18 (7/11)	$\chi^2 = 0.005$, $p = 0.944$
Mean age (SD)	31.6 (9.8)	30.7 (8.2)	$t = 0.291$, $p = 0.773$
Age range	19–48	19–44	—
Age of onset (SD)	27.9 (6.04)	—	—
Education (SD)	12.6 (2.3)	14.1 (2.8)	$t = 1.89$, $p = 0.67$
Total duration of depressive episode (month, SD)	39.6 (10.7)	—	—
Number of depressive episode onset (SD)	3.7 (1.1)	—	—
HAMA (SD)	7.8 (2.1)	5.0 (3.3)	$t = 1.985$, $p = 0.060$
HAMD (SD)	24.9 (6.3)	5 (1.4)	$t = 13.749$, $p = 0.000$

MDD: major depressive disorders; HC, healthy control; F, female, M, male; SD, standard deviation; R, right, M, mixed, L, left;. HAMA, Hamilton Anxiety Scale; HAMD, Hamilton Depression Scale.

Behavioral Data Analysis

As shown in **Table 3**, RTs for go trials in the MDD group were longer than those in the HC group; the hit rate for go trials in the MDD group was lower than that in the HC group, and the rate of false alarms for no-go trials in the MDD group was higher than that in the HC group.

HRV Indices Analysis

Comparisons of HRV Indices Between Different States

As shown in **Figure 2A**, by paired-sample *t*-test, there were no differences in SDANN values in the resting state and task-related state (in the Go/No-go task) in the HC group or in the MDD group (for HC group, $t = 1.661$,$p = 0.115$; for MDD group, $t = 1.856$, $p = 0.079$). However, there were significant differences in the RMSSD value in both the HC group and the MDD group (for the HC group, $t = 5.667$, $p = 0.000028$; for the MDD group, $t = 2.993$, $p = 0.007$); the RMSSD value in both the HC group and the MDD group in the resting state were lower than that in the task-related state.

TABLE 3 | Comparisons of behavioral data between MDD and HC group [present as mean (SD)].

Group	MDD (n = 20)	HC (n = 18)	*t*	*p*
RTs (go trials, ms)	470.5 (26.1)	385.8 (12.9)	9.701	0.000
Hit rate (go trials)	0.823 (0.040)	0.916 (0.025)	7.187	0.000
False alarms (no-go trials)	0.209 (0.050)	0.102 (0.112)	3.641	0.000

MDD, major depressive disorder group; HC, healthy control group; ms, millisecond.

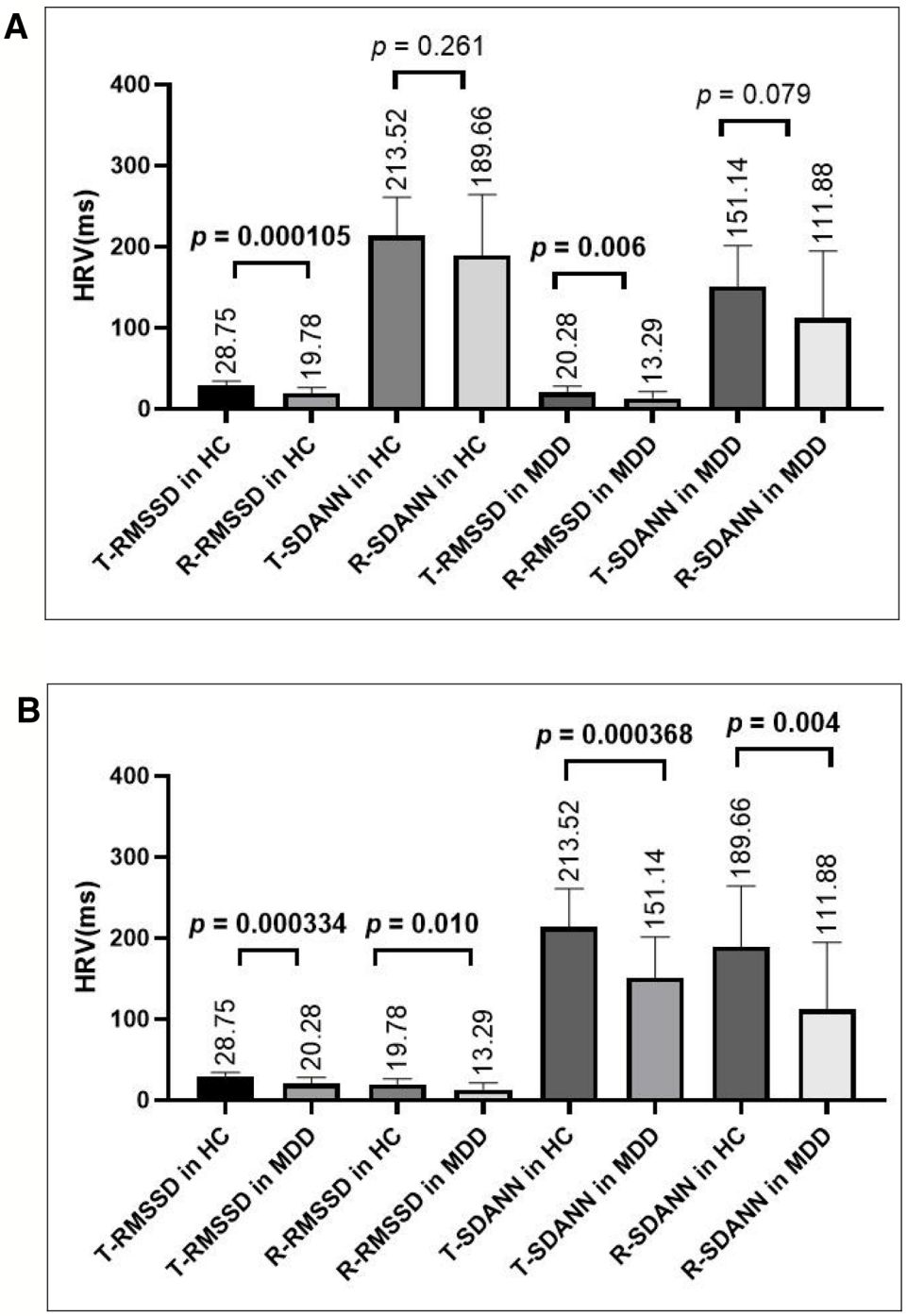

FIGURE 2 | (A) Comparing HRV indices in the task-related state or resting state within the HC group or MDD group, there was no difference in the SDANN value, but there was a significant difference in the RMSSD value. **(B)** Comparing HRV indices in the resting state or the task-related state between the HC and MDD group, there were significant differences in both the RMSSD and SDANN values. T-RMSSD, task-related RMSSD, R-RMSSD, resting-state RMSSD; T-SDANN, task-related SDANN, R-SDANN, resting-state SDANN.

Comparisons of HRV Indices Between the HC Group and the MDD Group

As shown in **Figure 2B**, by independent sample *t*-test, there were significant differences in both the SDANN and RMSSD values in the resting state (for SDANN, $t = 3.034$, $p = 0.004$; for RMSSD, $t = 2.712$, $p = 0.010$) and in the task-related state (for SDANN, $t = 3.932$, $p = 0.000368$; for RMSSD, $t = 3.965$, $p = 0.000334$) between HCs and MDD patients. Both SDANN and RMSSD values in MDD patients were lower than those in HCs in both the resting state and the task-related state.

Correlation Analysis Between HRV Indices and Behavioral Data

The general linear correlation method was used to investigate the relationship among HRV indices (resting-state SDANN and RMSSD values and task-related SDANN and RMSSD values) and behavioral data (RTs, hit rate, and false alarms). The results showed that only the resting-state RMSSD value and the task-related RMSSD value were correlated with RTs in the MDD group (for resting-state RMSSD: $r = -0.476$, $p = 0.034$; for task-related RMSSD: $r = -0.522$, $p = 0.018$).

MEG Analysis

As shown in **Figure 3**, compared to the brain regions in the HC group, there were three regional functional connectivities in the brain that passed FDR correction in the MDD group, including the functional connectivity between the left middle frontal gyrus (−28, 56, −2) and right superior frontal gyrus (42, 60, 2) ($t = -3.573$, $p = 0.001027$), the functional connectivity between the left middle frontal gyrus (−28, 56, −2) and left superior frontal gyrus (−48, 28, −16) ($t = 3.972$, $p = 0.000375$), and the functional connectivity between the left middle frontal gyrus (−28, 56, −2) and anterior cingulate cortex (4, 26, −14) ($t = -3.851$, $p = 0.000569$).

Correlation Analysis Between the RMSSD Value and Significant Difference Functional Connectivity Networks

Task-Related RMSSD Value

A general linear correlation method was used to investigate the relationship between task-related HRV indices and the three above mentioned brain regional functional connectivity networks; this analysis showed that in the HC group, the task-related RMSSD value is positively correlated with the functional connectivity between left middle frontal gyrus (−28, 56, −2) and anterior cingulate cortex (4, 26, −14) ($r = 0.605$, $p = 0.008$), while in the MDD group, the task-related RMSSD value is not correlated with above functionally connected regions ($r = -0.117$, $p = 0.625$), and, instead, the task-related RMSSD value is negatively correlated with the functional connectivity between left middle frontal gyrus (−28, 56, −2) and insula (44, −6, −4) ($r = -0.577$, $p = 0.008$). However, we didn't find correlation between task-related RMSSD and the functional connectivity between left middle frontal gyrus (−28, 56, −2) and left insula (−35.13, 6.65, 3.44), (−32, 16, −16), (−34, 12, −14) ($r = -0.17, -0.197, -0.115$; $p = 0.306, 0.235, 0.317$).

Resting-State RMSSD Value

A general linear correlation method was used to investigate the relationship between the resting-state RMSSD value and the three above mentioned regional functional connectivity networks in the brain; this analysis showed that the RMSSD value was not correlated with these significant difference brain regions in either the HC group or the MDD group (for HC group: $r = 0.225, 0.173, 0.166$; $p = 0.369, 0.493, 0.511$; for MDD group: $r = -0.205, -0.008, -0.99$; $p = 0.495, 0.855, 0.532$).

Correlation Analysis Between the HAMD Value and Significant Difference Functional Connectivity Networks or HRV Indices in the MDD Group

By Pearson correlation analysis, the HAMD scores in the MDD group were positively correlated with the functional connectivity between the left middle frontal gyrus (−28, 56, −2) and right superior frontal gyrus (42, 60, 2) ($r = 0.516$, $p = 0.020$); the HAMD scores in the MDD group were negatively correlated with HRV indices (for task-related RMSSD: $r = -0.555$, $p = 0.011$; for task-related SDANN: $r = -0.559$, $p = 0.010$; for resting-state RMSSD: $r = -0.497$, $p = 0.026$).

DISCUSSION

This study is the first to employ brain MEG functional connectivity analysis with a go/no-go task, by combining HRV indices, to uncover the neural mechanism of interactions between the ANS and inhibitory and control function in MDD patients. Additionally, this study is the first to confirm that task-related HRV can be used as an index of the association between MDD and autonomic dysregulation.

ANS, which is generally regarded made of sympathetic system and parasympathetic system, is one of the most important factors that are associated with a wide range of somatic and mental disease. Although pacemaker tissues play an important role in cardiac automaticity, heart rate, and rhythm largely depended on the neurotransmitters (acetylcholine, epinephrine, and norepinephrine) secreted by sympathetic nervous system and parasympathetic nervous system. HRV, which represent the rhythm of heart, has been used as an indicator of central–peripheral neural feedback (40). SDANN and RMSSD are two important indices in HRV which reflect sympathetic nervous system and parasympathetic nervous system respectively. There are growing studies to discover the relationship between ANS and central nervous system (CNS) based on neurovisceral integration model, and investigators have identified functional units within the CNS (such as PFC) which are related to several cognitive functions such as executive function, memory, attention, etc. (41). Notably, PFC also plays an important role in inhibition and control function, and there are several researches to find vagally mediated HRV is associated with inhibition and control function.

Consistent with previous studies (22, 42–44), MDD patients present inhibitory and control dysfunction and decreased

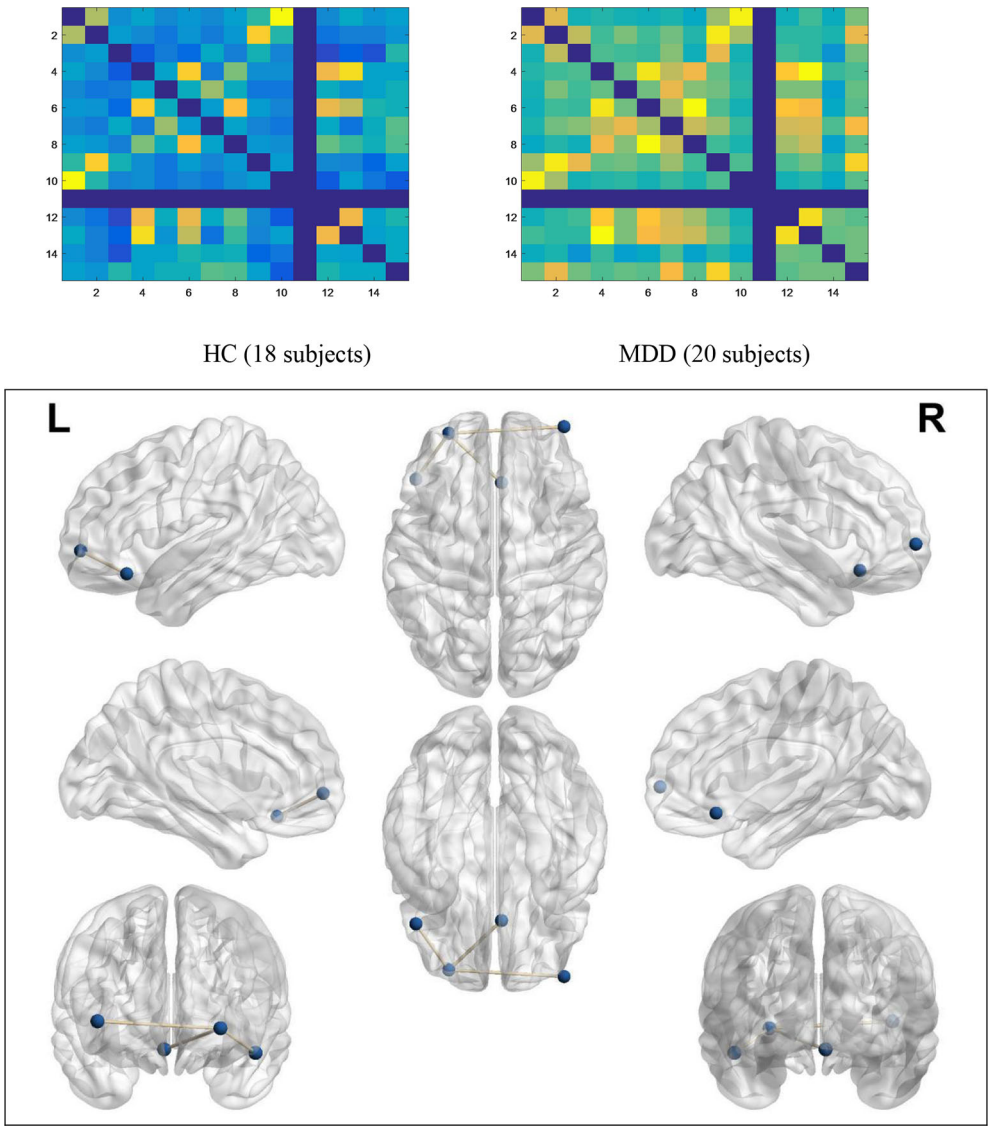

FIGURE 3 | Functional connectivity networks of significant differences. In the no-go trials, the average activity of functional connectivity networks within PFC in the MDD group (20 subjects) was higher than that in the HC group (18 subjects), which means that MDD patients have to activate more connections than HCs to control their behavior.

resting-state RMSSD values. Compared to the task-related state, all participants displayed lower resting-state HRV values. Additionally, MDD patients showed lower HRV indices (SDANN and RMSSD values) than HCs in both the resting state and the task-related state. Furthermore, in MDD patients, both the resting-state and the task-related RMSSD value were related to inhibitory and control dysfunction. A brain MEG functional connectivity analysis in MDD patients revealed that four brain regions within the PFC had significant difference functional connectivity networks. Meanwhile, task-related RMSSD values in HCs were related to the functional connectivity between the left middle frontal gyrus and the anterior cingulate cortex (ACC), while in MDD patients, this measure was not related to the above mentioned functionally connected regions but was instead related to the functional connectivity between the left middle frontal gyrus and insula. However, the resting-state RMSSD value was not related to significant difference functional connectivity networks in all participants.

Our results also support that resting-state HRV can be used as a biomarker of inhibitory and control function in MDD patients. A previous study indicated that task-related HRV may reflect inhibitory and control function at the peripheral level (32). Our results support the theory that the decreased vagus nerve function might be the mechanism of the decreased HRV indices in MDD patients. In addition, comparing HRV indices in the resting state with those during the task (the go/no-go task),

the RMSSD value was closely related to the vagus function and, thus, might be a better marker to index impaired inhibitory and control function than that of the SDANN value, which is associated with the sympathetic nervous system in MDD patients. Our results also confirm that the task-related HRV may reflect the association between the flexibility of cognition and ANS function.

The fundamentals of the PFC function are the "inhibition" of the ordinary and stereotyped responses in order to pursue the novelty "execution". Although PFC plays an important role in so many functions (such as inhibitory, work memory, regulation of visceral feeling, etc.), in this study, the function of inhibitory was highlighted. The PFC plays a critical role in inhibitory and control function, which can be projected to BA8, 9, 10, 11, 12, 13, 44, 45, 46, and 47 Brodmann areas (7, 8). The left middle frontal gyrus (BA10) and right superior frontal gyrus (BA47), seen in this study, belong to the PFC. It is widely recognized that the PFC plays an important role in the regulation of HRV (44–47). A previous study has shown that the middle frontal gyrus and superior frontal gyrus are sensitive brain regions related to inhibitory and control function (48–51). In addition, a study reported that the right superior frontal gyrus is one of the targets of erythropoietin treatment, which can effectively improve the executive function of MDD patients (52). As an important part of the limbic system, the anterior cingulate cortex (ACC) is not only associated with the regulation of inhibitory and control function but also with the regulation of breathing and heart rate. The reduction in dopamine D2 receptors in the ACC is an important pathological mechanism of MDD, and increasing ACC dopamine D2 receptor levels can effectively improve executive function in MDD patients (53). In the go/no-go task, abnormal regional functional connectivity networks in the brain are the neural mechanism of cognitive dysfunction (inhibitory control dysfunction) in MDD. The appearance of "visceral brain" components suggest that decreased HRV indices resulting from the sympathetic-vagus nerve balance disorder are associated with inhibitory and control dysfunction.

Unlike in HCs, HRV indices are not associated with the functional connectivity between the left middle frontal gyrus and anterior cingulate cortex in MDD patients. We suggest that MDD patients have abnormal activation in regional brain functional connectivity, decreasing the regulation of sympathetic-vagus nerve function by the ACC. Namely, this abnormal activation decreases the regulation HRV indices by the ACC; however, to compensate for the decreased regulation of HRV indices by the ACC, as the regulation of the vital center of the body, the insula strengthens the regulation of sympathetic-vagus nerve function. In addition, the functional connectivity networks between insula (no matter in right hemisphere or left hemisphere) and PFC were higher in MDD patients than that in HCs, which supported our idea that the functional connectivity between insula and PFC could compensate for abnormal functional connectivity networks within PFC. However, it is worth noting that, we only took insula into consideration as an auxiliary brain region to explain our results in that there was still controversy about discovering the function about deep brain regions with MEG.

LIMITATIONS

There are some limitations to this study. Firstly, because of the small sample size, our results are preliminary. Secondly, although MEG data integrated with task-related HRV indices has verified that task-related HRV is a characteristic biological marker of MDD in this study, whether task-related HRV can be used as a genuine diagnostic indicator for MDD depends on multidimensional research. Future studies should integrate MEG with other technologies, such as genetic and immunohistochemical techniques, to further confirm the relationship between task-related HRV indices and MDD. Finally, our study only investigated the neural mechanism of interactions between ANS and inhibitory and control function in MDD with MEG measurements. Because inhibitory and control function was only one of neurocognitive functions, other aspects of neurocognitive such as working memory, sustained attention, etc. should be conducted in the future study.

CONCLUSIONS

In conclusion, the decreased task-related HRV is associated with inhibitory control dysfunction through functional inter-region connectivity in the PFC in major depressive disorder, and the task-related HRV be used as an index of the association between MDD and autonomic dysregulation.

Our findings have important implications for understanding the pathophysiology of MDD and task-related HRV could be used to predict abnormal inhibitory and control function in MDD patients. In addition, integrated with task-related HRV, MEG may provide an image-guided tool for intervention.

DATA AVAILABILITY STATEMENT

The raw data supporting the conclusions of this manuscript will be made available by the authors, without undue reservation, to any qualified researcher.

ETHICS STATEMENT

The studies involving human participants were reviewed and approved by the Ethics Committee on Human Studies, Affiliated Nanjing Brain Hospital of Nanjing Medical University, Nanjing, People's Republic of China. The patients/participants provided their written informed consent to participate in this study.

AUTHOR CONTRIBUTIONS

HZ: data curation, formal analysis, methodology, writing original draft, writing review and editing. LH, HJ, ZD, ST, YH, PL, HW: data curation, formal analysis, methodology. QL, ZY: data curation, formal analysis, methodology, writing review and editing.

FUNDING

This work was supported by the National Natural Science Foundation of China [grant number 81871066 and 81571639]; the Jiangsu Provincial Medical Innovation Team of the Project of Invigorating Health Care Through Science, Technology and Education [grant number CXTDC2016004]; and the Jiangsu Provincial Key Research and Development Program [grant number BE2018609]. The funders had no role in study design, data collection and interpretation, or the decision to submit the work for publication.

ACKNOWLEDGMENTS

We thank the editors and reviewers of this manuscript for the many helpful suggestions.

REFERENCES

1. Ferrari AJ, Somerville AJ, Baxter AJ, Norman R, Patten SB, Vos T, et al. Global variation in the prevalence and incidence of major depressive disorder: a systematic review of the epidemiological literature. *Psychol Med* (2013) 43:471–81. doi: 10.1017/S0033291712001511
2. Papakostas GI. Cognitive symptoms in patients with major depressive disorder and their implications for clinical practice. *J Clin Psychiatry* (2014) 75:8–14. doi: 10.4088/JCP.13r08710
3. Wesse JR. Prepotent motor activity and inhibitory control demands in different variants of the go/no-go paradigm. *Psychophysiology* (2018) 55(3): e12871. doi: 10.1111/psyp.12871
4. Ottaviani C. Brain-heart interaction in perseverative cognition. *Psychophysiology* (2018) 55:e13082. doi: 10.1111/psyp.13082
5. Fuster JM, Bressler SL. Past makes future: role of PFC in prediction. *Cogn Neurosci* (2015) 27:639–54. doi: 10.1162/jocn_a_00746
6. Barbas H, García-Cabezas MÁ. How the prefrontal executive got its stripes. *Curr Opin Neurobiol* (2016) 40:125–34. doi: 10.1016/j.conb.2016.07.003
7. Barbier EL, Marrett S, Danek A, Vortmeyer A, van Gelderen P, Duyn J, et al. Imaging cortical anatomy by high-resolution MR at 3.0T: detection of the stripe of Gennari in visual area 17. *Magn Reson Med* (2002) 48:735–8. doi: 10.1002/mrm.10255
8. Zilles K, Amunts K. Centenary of Brodmann's map mdash conception and fate. *Nat Rev Neurosci* (2010) 11:139–45. doi: 10.1038/nrn2776
9. Criaud M, Boulinguez P. Have we been asking the right questions when assessing response inhibition in go/no-go tasks with fMRI? A meta-analysis and critical review. *Neurosci Biobehav Rev* (2013) 37:11–23. doi: 10.1016/j.neubiorev.2012.11.003
10. Krypotos AM, Jahfari S, van Ast VA, Kindt M, Forstmann BU. Individual differences in heart rate variability predict the degree of slowing during response inhibition and initiation in the presence of emotional stimuli. *Front Psychol* (2011) 2:278. doi: 10.3389/fpsyg.2011.00278
11. Robinson LJ, Gallagher P, Watson S, Pearce R, Finkelmeyer A, Maclachlan L, et al. Impairments in cognitive performance in chronic fatigue syndrome are common, not related to co-morbid depression but do associate with autonomic dysfunction. *PloS One* (2019) 14:e0210394. doi: 10.1371/journal.pone.0210394
12. Alamian G, Hincapié AS, Pascarella A, Thiery CE, Saive AL, et al. Measuring alterations in oscillatory brain networks in schizophrenia with resting state MEG: State-of-the-art and methodological challenges. *Clin Neurophysiol* (2017) 128:1719–36. doi: 10.1016/j.clinph.2017.06.246
13. Yamashita M, Yoshihara Y, Hashimoto R, Yahata N, Ichikawa N, Sakai Y, et al. A prediction model of working memory across health and psychiatric disease using whole-brain functional connectivity. *eLife* (2018) 7:e38844. doi: 10.7554/eLife.38844
14. Nugent AC, Robinson SE, Coppola R, Furey ML, Zarate CA Jr. Group differences in megica derived resting state networks: application to major depressive disorder. *Neuroimage* (2015) 118:1–12. doi: 10.1016/j.neuroimage.2015.05.051
15. Jalife J, Michaels DC. Neural control of sinoatrial pacemaker activity. In: Levy MN, Schwartz PJ, editors. *Vagal Control of The Heart: Experimental Basis And Clinical Implications*. Futura: Armonk (1994). p. 173–205.
16. Yeh TC, Kao LC, Tzeng NS, Kuo TB, Huang SY, Chang CC, et al. Heart rate variability in major depressive disorder and after antidepressant treatment with agomelatine and paroxetine: Findings from the Taiwan Study of Depression and Anxiety (TAISDA). *Prog Neuropsychopharmacol Biol Psychiatry* (2016) 64:60–7. doi: 10.1016/j.pnpbp.2015.07.007
17. Terhardt J, Lederbogen F, Feuerhack A, Hamann-Weber B, Gilles M, Schilling C, et al. Heart rate variability during antidepressant treatment with venlafaxine and mirtazapine. *Clin Neuropharmacol* (2013) 36:198–202. doi: 10.1097/WNF.0b013e3182a76fbb
18. Brunoni AR, Kemp AH, Dantas EM, Goulart AC, Nunes MA, Boggio PS, et al. Heart rate variability is a trait marker of major depressive disorder: evidence from the sertraline vs. electric current therapy to treat depression clinical study. *Int J Neuropsychopharmacol* (2013) 16:1937–49. doi: 10.1017/S1461145713000497
19. Thayer JF, Lane RD. A model of neurovisceral integration in emotion regulation and dysregulation. *J Affect Disord* (2000) 61:201–16. doi: 10.1016/s0165-0327(00)00338-4
20. Haapaniemi TH, Pursiainen V, Korpelainen JT, Huikuri HV, Sotaniemi KA, Myllyla VV. Ambulatory ECG and analysis of heart rate variability in Parkinson's disease. *J Neurol Neurosurg Psychiatry* (2001) 70:305–10. doi: 10.1136/jnnp.70.3.305
21. Jandackova VK, Britton A, Malik M. Heart rate variability and depressive symptoms: a cross-lagged analysis over a 10-year period in the White hall II study. *Psychol Med* (2016) 46:2121–31. doi: 10.1017/S003329171600060X
22. Huang C, Gevirtz RN, Onton J. Investigation of vagal afferent functioning using the heartbeat event related potential. *Int J Psychophysiol* (2017) 2017: S0167876017301095. doi: 10.1016/j.ijpsycho.2017.06.007
23. Hartmann R, Schmidt FM, Sander C, Hegerl U. Heart rate variability as indicator of clinical state in depression. *Front Psychiatry* (2018) 9:735. doi: 10.3389/fpsyt.2018.00735
24. Ottaviani C, Shahabi L, Tarvainen M, Cook I, Abrams M, Shapiro D. Cognitive, behavioral, and autonomic correlates of mind wandering and perseverative cognition in major depression. *Front Neurosci* (2014) 8:433. doi: 10.3389/fnins.2014.00433
25. Meister K, Juckel G. A systematic review of mechanisms of change in body-oriented yoga in major depressive disorders. *Pharmacopsychiatry* (2018) 51:73–81. doi: 10.1055/s-0043-111013
26. Caldwell YT, Steffen PR. Adding HRV biofeedback to psychotherapy increases heart rate variability and improves the treatment of major depressive disorder. *Int J Psychophysiol* (2018) 131:96–101. doi: 10.1016/j.ijpsycho.2018.01.001
27. Lin IM, Fan SY, Yen CF, Yeh YC, Tang TC, Huang MF, et al. Heart rate variability biofeedback increased autonomic activation and improved symptoms of depression and insomnia among patients with major depression disorder. *Clin Psychopharmacol Neurosci* (2019) 17:222–32. doi: 10.9758/cpn.2019.17.2.222
28. Pinter A, Szatmari S, Horvath T, Penzlin AI, Barlinn K, Siepmann M, et al. Cardiac dysautonomia in depression—heart rate variability biofeedback as a potential add-on therapy. *Neuropsychiatr Dis Treat* (2019) 15:1287–310. doi: 10.2147/NDT.S200360
29. Windthorst P, Mazurak N, Kuske M, Hipp Giel KE, Enck P, et al. Heart rate variability biofeedback therapy and graded exercise training in management of chronic fatigue syndrome: An exploratory pilot study. *J Psychosom Res* (2017) 93:6–13. doi: 10.1016/j.jpsychores.2016.11.014
30. Jester DJ, Rozek EK. Heart rate variability biofeedback: implications for cognitive and psychiatric effects in older adults. *Aging Ment Health* (2019) 23:574–80. doi: 10.1080/13607863.2018.1432031

31. Ha JH, Park S, Yoon D, Kim B. Short-term heart rate variability in older patients with newly diagnosed depression. *Psychiatry Res* (2015) 226:484–8. doi: 10.1016/j.psychres.2015.02.005
32. Moses ZB, Luecken LJ, Eason JC. Measuring task-related changes in heart rate variability. *Conf Proc IEEE Eng Med Biol Soc* (2007) 2007:644–7. doi: 10.1109/IEMBS.2007.4352372
33. Hauk O. Keep it simple: a case for using classical minimum norm estimation in the analysis of EEG and MEG data. *Neuroimage* (2004) 21:1612–21. doi: 10.1016/j.neuroimage.2003.12.018
34. Sakaki M, Yoo HJ, Nga L, Lee TH, Thayer JF, Mather M. Heart rate variability is associated with amygdala functional connectivity with MPFC across younger and older adults. *Neuroimage* (2016) 139:44–52. doi: 10.1016/j.neuroimage.2016.05.076
35. Wang Q, Tian S, Tang H, Liu X, Yan R, Hua L, et al. Identification of major depressive disorder and prediction of treatment response using functional connectivity between the prefrontal cortices and subgenual anterior cingulate: a real-world study. *J effect Disord* (2019) 252:365–72. doi: 10.1016/j.jad.2019.04.046
36. Garg P, Davenport E, Murugesan G, Wagner B, Whitlow C, Maldjian J, et al. Automatic 1d convolutional neural network-based detection of artifacts in MEG acquired without electrooculography or electrocardiography. *Int Workshop Pattern Recognit Neuroimaging* (2017) 2017:1–10. doi: 10.1109/PRNI.2017.7981506
37. Udupa K, Thirthalli J, Sathyaprabha TN, Kishore KR, Raju TR, Gangadhar BN. Differential actions of antidepressant treatments on cardiac autonomic alterations in depression: a prospective comparison. *Asian J Psychiatr* (2011) 4:100–6. doi: 10.1016/j.ajp.2011.02.006
38. Camm AJ, Malik M, Bigger JT, Breithardt G, Cerutti S, Cohen RJ. Heart rate variability: standards of measurement, physiological interpretation and clinical use. task force of the European society of cardiology and the North American society of pacing and electrophysiology. *Eur Heart J* (1996) 17:354–81. doi: 10.1111/j.1542-474X.1996.tb00275.x
39. Storey JD. The positive false discovery rate: a bayesian interpretation and the q-value. *Ann Stat* (2003) 31:2013–35. doi: 10.1214/aos/1074290335
40. Thayer JF, Lane RD. Claude Bernard and the heart-brain connection: further elaboration of a model of neurovisceral integration. *Neurosci Biobehav Rev* (2009) 33:81–8. doi: 10.1016/j.neubiorev.2008.08.004
41. Forte G, Favieri F. Heart rate variability and cognitive function: a systematic review. *Front Neurosci* (2019) 13:710. doi: 10.3389/fnins.2019.00710
42. Erickson K, Drevets WC, Clark L, Cannon DM, Bain EE, CA Zarate Jr, et al. Mood-congruent bias in affective go/no-go performance of unmedicated patients with major depressive disorder. *Am J Psychiatry* (2005) 162:2171–3. doi: 10.1176/appi.ajp.162.11.2171
43. Bermpohl F, Fregni F, Boggio PS, Thut G, Northoff G, Otachi PT, et al. Effect of low-frequency transcranial magnetic stimulation on an affective go/no-go task in patients with major depression: role of stimulation site and depression severity. *Psychiatry Res* (2006) 141:1–13. doi: 10.1016/j.psychres.2005.07.018
44. Huang M, Frantz J, Moralez G, Sabo T, Davis PF, Davis SL, et al. Reduced resting and increased elevation of heart rate variability with cognitive task performance in concussed athletes. *J Head Trauma Rehabil* (2019) 34:45–51. doi: 10.1097/HTR.0000000000000409
45. Chang WH, Lee IH, Chi MH, Lin SH, Chen KC, Chen PS, et al. Prefrontal cortex modulates the correlations between brain-derived neurotrophic factor level, serotonin, and the autonomic nervous system. *Sci Rep* (2018) 8:2558. doi: 10.1038/s41598-018-20923-y
46. Silva WQAD, Fontes EB, Forti RM, Lima ZL, Elsangedy HM. Affect during incremental exercise: the role of inhibitory cognition, autonomic cardiac function, and cerebral oxygenation. *PloS One* (2017) 12:e0186926. doi: 10.1371/journal.pone.0186926
47. Wendt J, Neubert J, Koenig J, Thayer JF, Hamm AO. Resting heart rate variability is associated with inhibition of conditioned fear. *Psychophysiology* (2015) 52:1161–6. doi: 10.1111/psyp.12456
48. Lavagnino L, Mwangi B, Bauer IE, Cao B, Selvaraj S, Prossin A, et al. Reduced inhibitory control mediates the relationship between cortical thickness in the right superior frontal gyrus and body mass index. *Neuropsychopharmacology* (2016) 41:2275–82. doi: 10.1038/npp.2016.26
49. Kleerekooper I, Van Rooij SH, Van d WWPM, de Leeuw M, Kahn RS, Vink M. The effect of aging on fronto-striatal reactive and proactive inhibitory control. *NeuroImage* (2016) 132:51–8. doi: 10.1016/j.neuroimage.2016.02.031
50. Faul L, Fogleman ND, Mattingly KM, Depue BE. Inhibitory control mediates a negative relationship between body mass index and intelligence: a neurocognitive investigation. *Cognit Affect Behav Neurosci* (2019) 19:392–408. doi: 10.3758/s13415-019-00695-2
51. Xu H, Liu L, Tian Y, Wang J, Li J, Zheng J, et al. A disinhibitory microcircuit mediates conditioned social fear in the prefrontal cortex. *Neuron* (2019) 102:668–82. doi: 10.1016/j.neuron.2019.02.026
52. Miskowiak KW, Vinberg M, Glerup L, Paulson O, Knudsen GM, Ehrenreich H, et al. Neural correlates of improved executive function following erythropoietin treatment in mood disorders. *Psychol Med* (2016) 46:1679–91. doi: 10.1017/S0033291716000209
53. Larisch R, Klimke A, Vosberg H, Löffler S, Gaebel W, Müller-Gärtner HW. In Vivo evidence for the involvement of Dopamine-D2 receptors in striatum and anterior cingulate gyrus in major depression. *Neuroimage* (1997) 5:251–60. doi: 10.1006/nimg.1997.0267

Conflict of Interest: The authors declare that the research was conducted in the absence of any commercial or financial relationships that could be construed as a potential conflict of interest.

frontiers in Psychiatry

ORIGINAL RESEARCH
published: 24 June 2020
doi: 10.3389/fpsyt.2020.00597

Frequency-Specific Resting Connectome in Bipolar Disorder: An MEG Study

Masakazu Sunaga[1], Yuichi Takei[1], Yutaka Kato[1,2], Minami Tagawa[1,3], Tomohiro Suto[3], Naruhito Hironaga[4], Takefumi Ohki[5], Yumiko Takahashi[1], Kazuyuki Fujihara[6], Noriko Sakurai[1], Koichi Ujita[7], Yoshito Tsushima[7] and Masato Fukuda[1]*

[1] Department of Psychiatry and Neuroscience, Gunma University Graduate School of Medicine, Maebashi, Japan, [2] Tsutsuji Mental Hospital, Tatebayashi, Japan, [3] Gunma Prefectural Psychiatric Medical Center, Isesaki, Japan, [4] Brain Center, Faculty of Medicine, Kyushu University, Fukuoka, Japan, [5] Department of Neurosurgery, Osaka University Medical School, Suita, Japan, [6] Department of Genetic and Behavioral Neuroscience, Gunma University Graduate School of Medicine, Maebashi, Japan, [7] Department of Diagnostic Radiology and Nuclear Medicine, Gunma University Graduate School of Medicine, Maebashi, Japan

OPEN ACCESS

Edited by:
Peter Uhlhaas, University of Glasgow, United Kingdom

Reviewed by:
Gianluca Serafini, San Martino Hospital (IRCCS), Italy
Takefumi Ueno, Hizen Psychiatric Center (NHO), Japan

***Correspondence:**
Yuichi Takei
tyuichi@gunma-u.ac.jp

Specialty section:
This article was submitted to Neuroimaging and Stimulation, a section of the journal Frontiers in Psychiatry

Received: *03 April 2020*
Accepted: *09 June 2020*
Published: *24 June 2020*

Citation:
Sunaga M, Takei Y, Kato Y, Tagawa M, Suto T, Hironaga N, Ohki T, Takahashi Y, Fujihara K, Sakurai N, Ujita K, Tsushima Y and Fukuda M (2020) Frequency-Specific Resting Connectome in Bipolar Disorder: An MEG Study. Front. Psychiatry 11:597. doi: 10.3389/fpsyt.2020.00597

Background: Bipolar disorder (BD) is a serious psychiatric disorder that is associated with a high suicide rate, and for which no clinical biomarker has yet been identified. To address this issue, we investigated the use of magnetoencephalography (MEG) as a new prospective tool. MEG has been used to evaluate frequency-specific connectivity between brain regions; however, no previous study has investigated the frequency-specific resting-state connectome in patients with BD. This resting-state MEG study explored the oscillatory representations of clinical symptoms of BD *via* graph analysis.

Methods: In this prospective case-control study, 17 patients with BD and 22 healthy controls (HCs) underwent resting-state MEG and evaluations for depressive and manic symptoms. After estimating the source current distribution, orthogonalized envelope correlations between multiple brain regions were evaluated for each frequency band. We separated regions-of-interest into seven left and right network modules, including the frontoparietal network (FPN), limbic network (LM), salience network (SAL), and default mode network (DMN), to compare the intra- and inter-community edges between the two groups.

Results: In the BD group, we found significantly increased inter-community edges of the right LM–right DMN at the gamma band, and decreased inter-community edges of the right SAL–right FPN at the delta band and the left SAL–right SAL at the theta band. Intra-community edges in the left LM at the high beta band were significantly higher in the BD group than in the HC group. The number of connections in the left LM at the high beta band showed positive correlations with the subjective and objective depressive symptoms in the BD group.

Conclusion: We introduced graph theory into resting-state MEG studies to investigate the functional connectivity in patients with BD. To the best of our knowledge, this is a novel approach that may be beneficial in the diagnosis of BD. This study describes the

spontaneous oscillatory brain networks that compensate for the time-domain issues associated with functional magnetic resonance imaging. These findings suggest that the connectivity of the LM at the beta band may be a good objective biological biomarker of the depressive symptoms associated with BD.

Keywords: magnetoencephalography, bipolar disorder, resting-state network, graph theory, salience network, limbic network, depressive symptoms

INTRODUCTION

Bipolar disorder (BD) affects up to 60 million individuals globally (1). BD can lead to cognitive and functional impairments (2) and is associated with a high mortality rate, particularly as a result of suicide (3). Although suicide attempts can be triggered by stressful life events such as bereavement (4) and biological abnormalities (5), the presence of a psychiatric disorder is the most consistent risk factor for suicidal behavior (6). Therefore, it is important to diagnose BD in the early clinical stage. However, it is difficult to diagnose BD quickly and accurately in clinical practice because its onset is most commonly characterized by a depressive episode, which often resembles unipolar depression (7). The efficacy of pharmacological interventions in the treatment of BD depends on an accurate and early diagnosis (8); however, a diagnostic biomarker has yet to be identified (9). Accordingly, for the accurate and timely diagnosis of BD, there is an urgent need to establish objective clinical biomarkers that are based on a better understanding of BD neuropathology. Studies investigating the resting-state functional connectivity have revealed intrinsic properties of brain disorders (10–13) and are expected to help identify such biomarkers.

Until recently, most studies investigating the functional connectivity in psychiatric patients have used functional magnetic resonance imaging (fMRI) (14). Although fMRI has a high spatial resolution, it measures an indirect neural activity and can only investigate slow oscillations in brain activity (< 0.1 Hz) (15). Compared to fMRI, a major advantage of magnetoencephalography (MEG) is its high temporal and spatial resolution, which enables synchronizations of the local and long-range neural activities to be assessed (16). In addition, the source reconstruction approach using MEG provides valuable spatial information that characterizes neural network modulations (14). Although MEG has many advantages, to our knowledge, there have been no studies of resting-state MEG for evaluating functional connectivity in patients with BD.

Unfortunately, a lack of established methodologies has prevented its widespread use for brain resting-state connectivity studies. In recent years, however, two British groups have developed methodological approaches to evaluate the frequency-specific resting-state connectivity using MEG (17, 18). These advances have enabled the investigation of frequency-specific alterations of resting-state networks *via* graph theory in autism (19) and age-related changes in these networks (20).

Simultaneously, graph theory analysis has been applied to explore brain network connectivity in psychiatric patients (21–25). Graphs are defined as sets of nodes and edges that represent system components and their mutual relationships (26). Using graph theory, brain networks can be represented as graphs that consist of nodes (which correspond to brain regions) and edges (which represent their connections) (27, 28). Therefore, graph theory is ideally suited for investigating complex networks such as human brain networks (26) and may be a potential tool for investigating the network characteristics of psychiatric disorders that alter connectivity within brain networks (29).

The main objective of this study was to investigate the resting-state frequency-specific functional connectivity to glean deeper insights into the pathophysiology of BD and help identify objective clinical biomarkers for the disorder. Here, we describe a novel MEG analysis that explores the resting-state functional connectivity using graph analysis in patients with BD. We hypothesized that resting-state MEG studies would provide important information about the spontaneous oscillatory brain networks, thereby representing an advantage over the sole use of fMRI-based resting-state investigations. We believed that this approach could also help identify clinical objective biomarkers for psychiatric disorders. To achieve this goal, we explored oscillatory representations of subjective and objective depressive symptoms in patients with BD using graph analysis.

MATERIALS AND METHODS

Participants

Seventeen patients with BD and 22 healthy controls (HCs) participated in this prospective case-control study. All patients with BD were recruited from the Gunma University Hospital in Gunma Prefecture, Japan (**Table 1**). All enrolled participants were right-handed, as assessed using the Edinburgh Handedness Inventory (30). To diagnose BD and to exclude participants with a history of psychiatric disorders from the HCs, we administered the Structured Clinical Interview of the Diagnostic and Statistical Manual of Mental Disorders, Fourth Edition for Axis I (31) and Axis II Disorders (32). Subjective and objective depressive and manic symptoms were assessed using the Beck Depression Inventory—Second Edition (BDI-II), Altman Self-Rating Mania (ASRM) scale, 17-item Hamilton Depression Rating (HAMD-17) scale, and Young Mania Rating Scale (YMRS). Patients older than 60 years were excluded to rule out the possible interference of additional pathophysiological factors, such as aging and cerebrovascular changes. Most of the patients with BD (14/17) were using medications, including antipsychotics, mood stabilizers, antidepressants, anxiolytics, hypnotics, and/or antiparkinsonian drugs. The equivalent doses of antidepressants (imipramine equivalent dose in mg/day), antipsychotics (chlorpromazine

TABLE 1 | Detailed demographics, clinical, and medication information of this study.

	HC (n = 22)		BD (n = 17)		t (χ^2)	p
	M	F	M	F		
Sex	11	11	8	9	0.0198	0.888
	Mean	SD	Mean	SD		
Age (years)	44.5	5	47.1	6.1	-1.4643	0.152
JART score	110.2	9.1	111.4	11.5	-0.3467	0.731
GAF score	82.3	4.7	60.6	9.8	9.1539	0.000
BDI-II score	5.6	5.4	18.5	15.5	-3.6594	0.0008
ASRM score	3.7	2.6	3.5	4.2	0.1944	0.8469
HAMD-17 score	–		6.9	4.8	–	
YMRS score	–		0.5	1.5	–	
Antidepressants (mg/day)	–		56.2	97.9	–	
Antipsychotics (mg/day)	–		78.7	134.4	–	
Anxiolytics (mg/day)	–		19.9	32.9	–	
Hypnotics (mg/day)	–		0.5	1.1	–	
Lithium (mg/day)	–		164.7	247.3	–	
Lamotrigine (mg/day)	–		29.4	98.5	–	
Valproate (mg/day)	–		211.7	286.9	–	
Carbamazepine (mg/day)	–		82.3	187.8	–	

Antidepressants, imipramine equivalent dose; Antipsychotics, chlorpromazine equivalent dose; Anxiolytics, diazepam equivalent dose; Hypnotics, flunitrazepam equivalent dose; M, male; F, female; BD, patients with bipolar disorder; HC, healthy controls; JART, Japanese Adult Reading Test; GAF, Global Assessment of Functioning; BDI-II, Beck Depression Inventory–Second Edition; ASRM, Altman Self-Rating Mania Scale; HAMD-17, 17-item Hamilton Depression Rating Scale; YMRS, Young Mania Rating Scale.

equivalent dose in mg/day), anxiolytics (diazepam equivalent dose in mg/day), and hypnotics (flunitrazepam equivalent dose in mg/day) were calculated for each patient (33). HCs had no history of major psychiatric or physical illnesses and medication use. The exclusion criteria for both groups included a clear abnormality in brain magnetic resonance imaging (MRI) findings, neurological illness, traumatic brain injury with a known cognitive consequence or loss of consciousness for more than 5 min, substance use or addiction, and the presence of hearing or vision impairment. The study protocol was approved by the Ethics Committee of the Gunma University Graduate School of Medicine, Japan. All participants provided written informed consent before the study. This study was carried out in accordance with the latest version of the Declaration of Helsinki.

MEG Data Acquisition and Preprocessing

For each participant, we acquired the MEG data for 7 min. A crosshair was presented as a fixation point in front of the participants. The only instruction provided to participants was to keep their eyes open, to relax, and remain awake. To confirm the awareness level and evaluate the extent of sleepiness during MEG acquisition, we used the Stanford Sleepiness Scale (34).

During the experiment, participants sat in an upright position. The neuromagnetic signals were acquired inside a magnetically shielded room (JFE Mechanical Co., Tokyo, Japan) using a whole-head Elekta Neuromag Vector View system (Oy, Helsinki, Finland), which was composed of 306 sensors arranged as 102 triplets (each unit consisting of two orthogonal planar gradiometers and one magnetometer). First, the locations of three fiduciary points (the nasion, and left and right auricular points) defining the head frame coordinate system and a set of head surface points (approximately 150–200 points) (35), as well as those of four head position indicator coils, were digitized using an Isotrak three-dimensional digitizer (Polhemus™, Colchester, VT, USA). During acquisition, the sampling rate was 1000 Hz, and the signals were bandpass filtered between 0.1 and 200 Hz. All off-line analyses were conducted using continuous raw data.

The current source estimate was carried out as follows. For noise suppression, we applied the "oversampled temporal projection" method to improve the sensor noise levels (36). Subsequently, the data were spatially filtered using the signal space separation method (37, 38) with Maxfilter (Elekta, Stockholm, Sweden) to suppress the noise generated by sources outside the brain. A notch filter was used to eliminate noise from the power line (50 Hz) and its harmonics (100 and 150 Hz). We eliminated heartbeat- and eye movement-related artifacts from the raw data using independent component analysis (ICA). The ICA was applied to the MEG sensor signals, and the eye movement signals were isolated based on the hybrid approach of component discrimination using the time (signal waveform) and space (topology) (39).

MRI

Brain MRI scans were acquired using a Siemens 3 T Trio scanner with a 12-channel head coil (Siemens, Erlangen, Munich, Germany) at the Gunma University Hospital and Josai Clinic (Philips Medical Systems, Best, Netherlands). High-resolution T1-weighted anatomical images were acquired using magnetization-prepared rapid acquisition with a gradient-echo sequence. Imaging parameters at the Gunma University Hospital were as follows: repetition time (TR) = 2000 ms, echo time (TE) = 2 ms, inversion time = 990 ms, flip angle = 9 degrees, field of view = 256 × 256 mm^2, matrix size = 256 × 256, and voxel size = 1 × 1 × 1 mm^3. Imaging parameters at the Josai Clinic were as follows: repetition time (TR) = 6.2 ms, echo time (TE) = 2.8 ms, flip angle = 9 degrees, field of view = 256 × 256 × 211 mm (anterior to posterior: AP × foot to head: FH × right to left: RL), matrix size = 256 × 256, and voxel size = 1 × 1 × 1 mm^3. For

anatomical segmentation and brain surface images, we first applied the FreeSurfer reconstruction process to the individual MRI data. Cortical reconstructions and parcellations for each participant were generated from T1-weighed MRI (40–42).

MEG Source Imaging

For the MEG source localization analysis, we used the minimum norm estimates (MNE) suite and MNE python (43). We employed the boundary-element method, with a single compartment bound by the inner surface of the skull for the forward head modeling (44). The source current distribution was estimated using the noise-normalized dynamic statistical parameter mapping (dSPM) method (45, 46). The noise covariance matrix was computed from the empty room acquisition data. To reduce the bias of the estimated source locations towards the superficial currents, we incorporated the depth-weighting parameter (depth = 0.8) by adjusting the source covariance matrix (47).

Data Analysis Procedure for Resting-State Networks

Schematic images of the data analysis procedure used in this study are illustrated in **Figure 1**. We started with MEG sensor detection level analysis and then evaluated the source distribution as described in subsection *MEG Data Acquisition and Preprocessing* (**Figure 1A**). Subsequently, we imported the commonly employed cortex segmentation (Destrieux Atlas) from the FreeSurfer software, which automatically divided the cortex into 150 regions (48). After discarding the "Unknown" regions, the regions were further subdivided into a total of 446 cortical labels (20) (**Figure 1B**), such that each label covered almost identical areas through all the individual and standard brains. We employed this high-resolution parcellation because the cortical surface was convoluted, and the estimated source data were averaged across a large label, which crosses multiple sulci and gyri and possibly results in signal cancellation across the parcel (20). We first applied the above process to the standard brain (Montreal National Institute 305; provided by FreeSurfer software) (49), and then projected this onto each of the individual brains. Source leakage correction was essential for the evaluation of long-range correlations with MEG (50) and was determined in this study as described below.

As shown in **Figure 1C**, we applied the orthogonal correlations to compute the connectivity metrics involved in handling source leakages using the "envelope_correlation" function in MNE (17, 20) at delta (1–4 Hz), theta (4–8 Hz), alpha (8–12 Hz), low beta (13–20 Hz), high beta (20–30 Hz), and gamma (30–80 Hz) bands (17). The "envelope_correlation" obtains the correlation values according to the following calculation flow. We started with $x(t)$ and $y(t)$ as the extracted source waveforms from specific ROI, where t denotes time stamps. First, the extracted source waveforms $x(t)$ and $y(t)$ were bandpass filtered at each frequency band and acquired $x(t,f)$ and $y(t,f)$. For each step-frequency band, the complex signal, $x(t,f)$ and $y(t,f)$, was generated with the Hilbert transform from $x(t,f)$ and $y(t,f)$. The connectivity between the two complex signals $x(t,f)$ and $y(t,f)$ was calculated by orthogonalizing one signal with respect to the other $Y_{\perp X}(t,f)$.

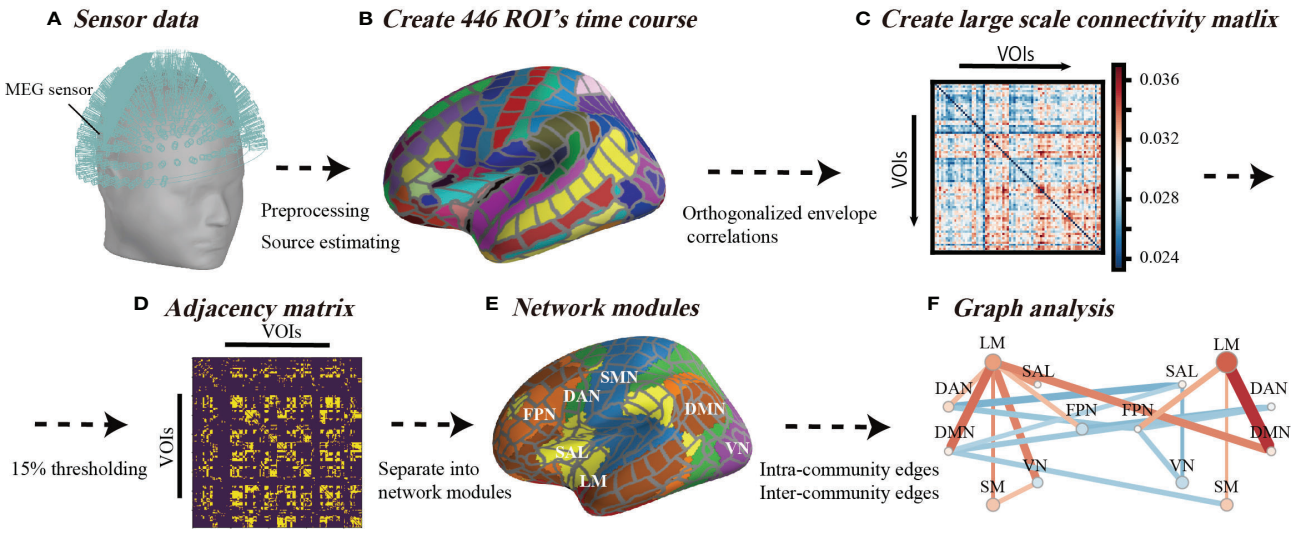

FIGURE 1 | Schematic view of analysis flow. **(A)** Sensor data from 306-channel magnetoencephalography (MEG) and the application of preliminary filtering and noise elimination. **(B)** The source distribution image was estimated using minimum norm estimates, and source waveforms were extracted from 446 regions of interest. **(C)** Analysis flow of orthogonalized correlation. The correlation analysis of the power envelopes from the regions of interest source waveforms. **(D)** The threshold of the correlation matrix was held at the top 15% to ensure that the density or number of connections of the network was equal across all individuals. **(E)** A total of 446 regions of interest were classified for seven networks in each hemisphere. **(F)** The inter-community edges and intra-community edges were calculated from connections separated into seven networks.

$$Y_{\perp X}(t,f) = Im\left(Y(t,f)\frac{X(t,f)^*}{|X(t,f)|}\right) \quad (1)$$

The superscript * denotes the conjecture of the complex value, and "*Im*" denotes the imaginary part of the complex value. The power envelopes $Env_X(t,f)$ were subsequently determined by computation of the absolute value of $X(t,f)$, as follows:

$$Env_X(t,f) = |X(t,f)| = \sqrt{X(t,f)X(t,f)^*} \quad (2)$$

Similarly, $Env_{Y_{\perp X}}(t,f)$ was obtained from $Y_{\perp X}(t,f)$. We calculated the linear correlation between $Env_{Y_{\perp X}}(t,f)$ and $Env_{Y_{\perp X}}(t,f)$. Given the slow time course of these envelopes, and to ensure that enough independent samples were available in the correlation window (17), we calculated the orthogonal correlation using an overlapping sliding window of 30 s with a stride of 1/6 of the window size. Finally, we calculated the median values of sliding correlation values and applied the graph-theoretical analysis to these median correlation values (**Figure 1C**) as described below.

Graph Analysis

We used the graph-theoretical measures (intra-community edges and inter-community edges) to quantify the basic property of resting-state networks (RSNs). We used the connectivity matrix that contained the orthogonal correlations between all N × N node pairs for each frequency band and acquired a connectivity array with the dimensions of $N_{Nodes} \times N_{Nodes} \times N_{Bands}$ for each subject. Thresholding and binarizing the connectivity matrices resulted in adjacency matrix A (**Figure 1D**). We used a threshold proportional scheme to retain a given proportion of the strongest connectivity matrix entries in the connectivity matrix. As there is no rationale for using a cost threshold, we compared the graph network properties for a wide range of costs and used a thresholding range of 5% to 30% at increments of 5%. There was no significant difference among thresholding values (**Figure S1**), therefore, we set a threshold at the top 15% to ensure that the number of network connections (14,851 connections among all regions of interest) was the same across all individuals.

We investigated the changes of RSNs in BD from the existing network understanding framework provided by previous fMRI studies. According to the network template, we separated network modules into seven left and right network modules, including the frontoparietal network (FPN), limbic network (LM), salience network (SAL), dorsal attention network (DAN), default mode network (DMN), somatomotor network (SMN), and visual network (VN) (51) (**Figures 1E** and **2**). In this way, we investigated differences in the connection patterns of intra- and inter-networks community between BD and HC groups. These network templates do not contain sub-cortical regions. We subsequently subdivided all edges into intra-community edges, which connect regions within each network, and inter-community edges, which connect inter-network regions, and measured the number of intra-community and inter-community edges for each frequency band (**Figure 1F**).

We compared the numbers of inter-community and intra-community edges for each frequency band between the HC and BD groups using an independent *t*-test in SciPy (52). Group differences were considered to be statistically significant at a *p*-value of less than 5%. We examined the relationship between significantly different edges (*p*-value less than 1% significance level) in patients with BD and clinical measures (the HAMD-17, BDI-II, ASRMS, and YMRS) using Spearman's rank correlation analysis. The correlation values were determined at a significance level less than 5%.

RESULTS

Sample Characteristics

Table 1 summarizes the demographic characteristics of the sample. Age and sex ratios were not significantly different between the two groups (t = -1.4643, p = 0.152; chi-square = 0.0198, p = 0.888). At the time of the study, the patients with BD

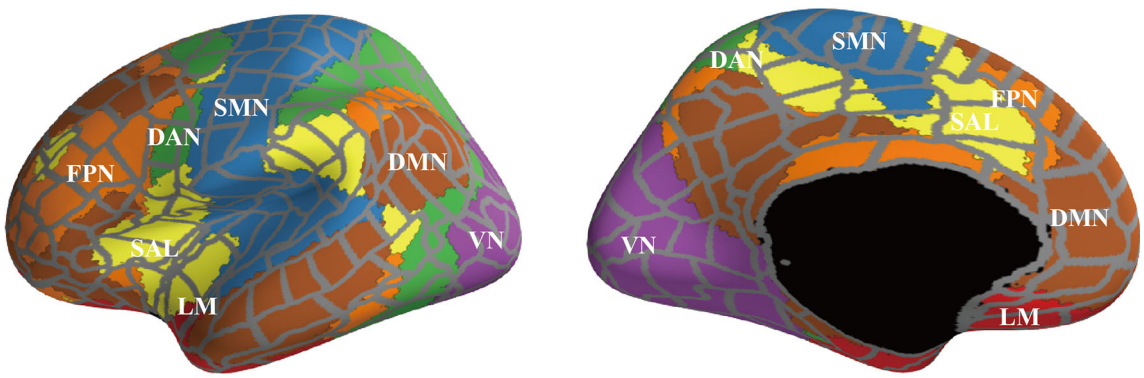

FIGURE 2 | The surface areas of each network module. We separated regions of interest into seven left and right network modules [FPN, frontoparietal network (orange); LM, limbic network (light green); SAL, salience network (yellow); DAN, dorsal attention network (green); DMN, default mode network (brown); SMN, somatomotor network (sky blue); and VN, visual network (deep purple)], according to the network template.

were euthymic or depressive as indicated by their HAMD-17 and YMRS scores.

Inter- and Intra-Community Edges

Figure 3 shows the results of the graph theory analysis, in which the number of inter- and intra-community edges were measured. **Figure 3A** depicts the summarized degrees of inter- and intra-community edges in six frequency band ranges (delta, theta, alpha, low beta, high beta, and gamma), including the plot box bars at a significance level < 1% (**Figure 3B**). We compared the number of edges between HC and BD using an independent *t*-test (**Figure 3A**, left).

In the delta band range, we found lower inter-community edges among the FPN and other network modules in the right FPN–right SAL (t = -2.808, p = 0.007), right FPN–left SAL (t =-2.079, p = 0.046), right FPN–left FPN (t = -2.423, p = 0.020), left FPN–left DMN (t = -2.043, p = 0.048), and left FPN–right SAL (t = -2.230, p = 0.027). The right LM showed higher inter-community levels involving three domains on the right LM–left VN (t = 2.621, p = 0.013), right LM–right DMN (t = 2.038, p = 0.049), and intra-community edges on the left LM (t = 2.261, p = 0.0300) (**Figure 3A**, upper left). In the theta band range, a decreased connectivity between the left and right SAL (t = -2.722, p = 0.009) was found in the BD group (**Figure 3A**, upper middle). Interestingly, almost all inter- and intra-community edges in the alpha band ranges were quite similar in both groups (**Figure 3A**, upper right). In the low beta band range, positive higher community edges were mainly increased in the left hemisphere, and inter-community edges were higher between the left VN–left LM (t = 2.281, p = 0.0284), left VN–left DMN (t = 2.391, p = 0.022), and left DAN–left LM (t = 2.100, p = 0.043), and higher intra-community edges on the left VN (t = 2.273, p = 0.029) (**Figure 3A**, lower left). We paid special attention to the results in the high beta band range and found increased community edges mainly in the LM. Higher inter-community edges were observed, as expected, in the left LM–right FPN (t = 2.094, p = 0.0431), left LM–left DMN (t = 2.038, p = 0.049), and right LM–right DMN (t = 2.201, p = 0.034), and higher intra-community edges on the left LM (t = 2.981, p = 0.005) and left RM (t = 2.480, p = 0.018) (**Figure 3A**, lower middle). Interestingly, the gamma band range also demonstrated higher inter-community edges in both the left and right LMs in this band range, especially for the right LM–right DMN (t = 2.899, p = 0.006) and left LM–left DMN (t = 2.205, p = 0.034), and higher intra-community edges on the right LM (t = 2.356, p = 0.024) (**Figure 3A**, lower right).

To summarize, among the six frequency band ranges, the LM exhibited higher community edges irrespective of the

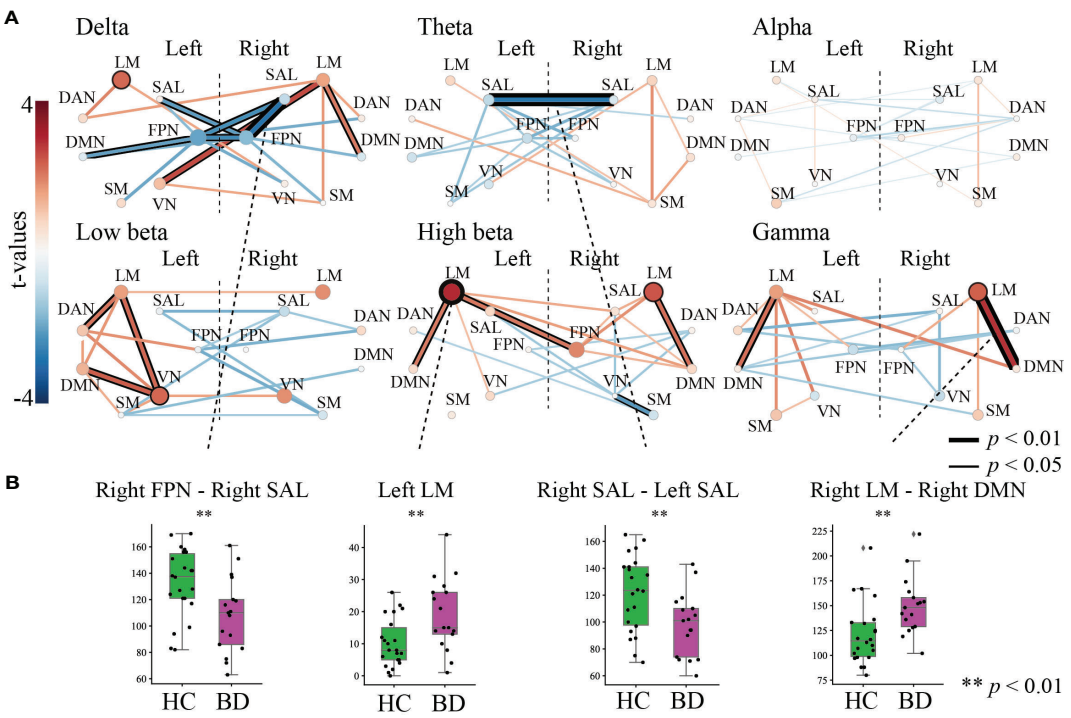

FIGURE 3 | The results of the graph theory analysis for inter- and intra-community edges. **(A)** Graph theory was applied to six frequency band ranges. The left-most bar indicates the color scale of the t-value. All figures in **(A)** indicate *t*-values of results that compared inter-community edges (line thickness and color) and intra-community edges (circle size and color) between healthy controls and patients with bipolar disorder (BD) at each frequency band. Thicker and deeper lines indicate higher inter-community edges, and larger circles indicate higher intra-community edges in patients with BD. If the *p*-value of the inter- or the intra-community edges was below the threshold for significance, the circles or lines are bordered by a thick line ($p < 0.01$) or thin line ($p < 0.05$). **(B)** The results of further statistical analysis for stage **(A)**. The green boxplot shows the results from the HC group, and the purple boxplot shows the results from the BD group. Each vertical boxplot bar indicates the standard error.

hemispheric differences, while the SAL and FPN exhibited a lower community edge among lower frequency band ranges. In particular, the number of inter- and intra-community edges were significantly different between the following groups at each frequency band (all, $p < 0.01$): the right FPN–right SAL at the delta, left SAL–right SAL at the theta (HC > BD), left LM at high beta, and right LM–right DMN at gamma (HC < BD) (**Figure 3B**).

Relationship Between Characteristics of Graph Indices and Clinical Symptoms

We further evaluated the clinical interpretations and relationships *via* commonly used approaches in psychiatric diagnosis. A Spearman's rank correlation analysis was used to assess the relationship between significantly different graph indices (inter- and intra-community edges) and clinical measures (BDI-II, HAMD-17, ASRM, and YMRS scores). **Figure 4** shows the relationship between graph indices and depressive symptoms. The Spearman's rank correlation analysis showed that the number of intra-community edges in the left LM at the high beta band was positively correlated with the HAMD-17 ($r = 0.519$, $p = 0.032$; **Figure 4**, left) and BDI-II ($r = 0.522$, $p = 0.031$) scores within the BD group (**Figure 4**, right). In contrast, age, drug dosages, and the JART, GAF, ASRM, and YMRS scores had no significant relationship with the graph indices.

DISCUSSION

In this study, we performed an analysis using graph theory and observed frequency-specific alterations of RSNs in patients with BD compared to HCs. We observed higher LM community edges at higher frequency band ranges, especially inter-community edges of the right LM–right DMN at the gamma band, and intra-community edges of the left LM at the high beta band, in the BD group. We also observed decreased inter-community edges at lower frequency band ranges, especially in those of the right SAL–right FPN at the delta band and the left SAL–right SAL at the theta band, in the BD group (**Figure 3**). The increase in the number of connections in the left LM at the high beta band was positively correlated with subjective and objective depressive symptoms in the BD group (**Figure 4**).

Several fMRI studies investigating the resting-state functional connectivity in the BD population have shown altered connectivity between parts of the DMN and the limbic system (14, 22, 53–58). The hyper-connectivity between the right LM and the right DMN of the BD group in the present study supports these previous findings and may indicate that alterations in resting-state functional connectivity between the LM and DMN are the essential elements associated with BD. The LM deals with emotional regulation/processing and memory, and previous studies have reported that patients with BD showed increased functional connectivity in the mesoparalimbic network (59, 60). The DMN is thought to be involved in self-referential activities such as inner speech, mental images, remembering past events, and planning future events (61, 62). The higher inter-community edges of LM–DMN suggest that self-referential activity tends to be affected by emotional activity, and we speculate that this tendency induces ruminative thoughts in patients with BD.

We also observed attenuation of the number of inter-community edges of the SAL–FPN at the delta band (**Figure 3A**, top left) and left SAL–right SAL at the theta band

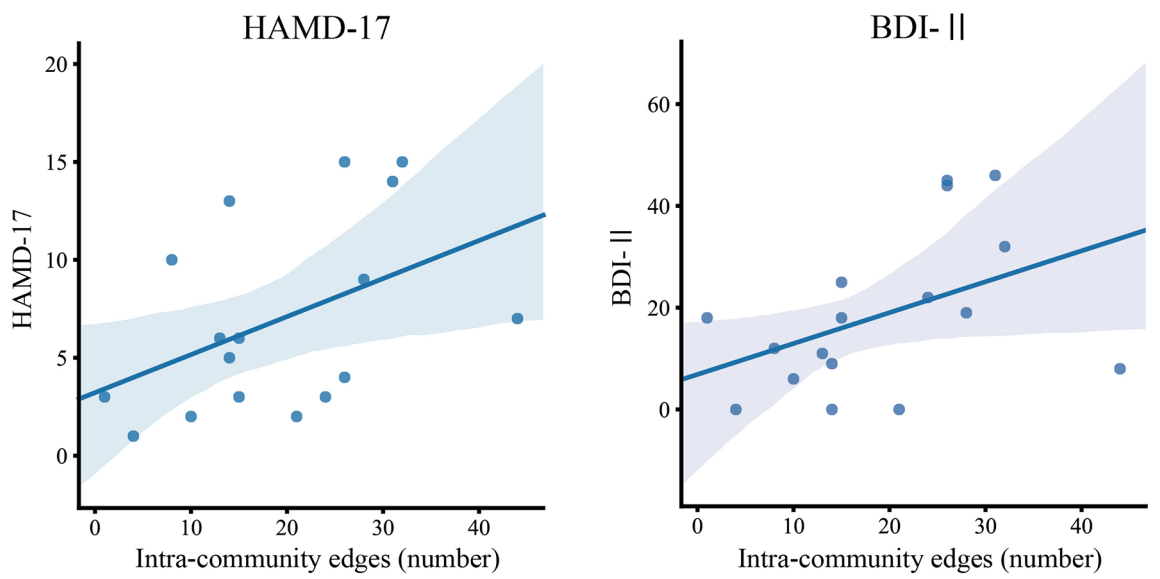

FIGURE 4 | The relationship between intra-community edges and depressive symptoms. The scatter plot of the number of intra-community edges in the left limbic network at the high beta band, and the scores of the Beck Depression Inventory–Second Edition (BDI-II) and 17-item Hamilton Depression Rating Scale (HAMD) in patients with BD. Color-matched transparent areas represent the standard errors of the mean.

(**Figure 3A**, top middle) in the BD group. A previous study also reported a significantly altered functional connectivity between the bilateral dorsal anterior insula and the left inferior parietal lobe in patients with BD (63). The SAL has been implicated in playing an important role in switching between the central executive network and DMN (64). Furthermore, the SAL activates the central executive network to manipulate information stored in working memory, while suppressing the DMN to keep attention focused on task-relevant goals. The hypoconnectivity between the SAL-FPN and left SAL-right SAL may contribute to the difficulty in maintaining a cognitive set and to the focusing of attention on task-relevant goals in patients with BD.

Remarkably, we found that the number of connections in the left LM at the high beta band (**Figure 3A**, lower middle) had positive correlations with the subjective and objective depressive symptoms in the BD group. This finding is consistent with previous reports that alterations in connectivity in the beta band are associated with depressive symptoms in major depressive disorder (65, 66), which demonstrates that excessive connectivity of the LM in the beta band is associated with depressive symptoms. Salvadore et al. investigated the patterns of the anterior cingulate cortex (ACC) and amygdala activity in patients undergoing antidepressant treatment with ketamine using the task of fearful faces (65) and found that pretreatment amygdala activity was negatively correlated with changes in depressive symptoms. These results suggest that LM activity increases with an increase in the severity of depressive symptoms and that the connectivity of the LM in the beta band may be a good objective biological biomarker of the depressive symptoms.

A resting-state EEG study in a BD population found frequency-specific alterations of the network topologies (67). Although no resting-state MEG study investigating functional connectivity has been reported so far, frequency-specific inter-community edges, including the SAL change in the delta and theta bands in patients with BD, were clearly demonstrated in our study. These differences in inter-community edges in the SAL were observed as changes in the low-frequency bands such as delta and theta. A recent study reported that greater theta band connectivity between the right ACC and right anterior insula, a key region within the SAL, predicted a greater reduction in the severity of depression (68). Altered networks at the theta and delta bands have been reported to be associated with pain control and auditory hyperacusis (69, 70). Parker reported that patients with BD exhibited various suprasensory changes experienced during manic/hypomanic "high" states, which generally attenuate or disappear during depressive and euthymic periods (71). Network alternations at the theta band in the SAL may be related to the altered sensory perception of BD. Furthermore, patients with BD experience significantly increased levels of pain, particularly chronic pain and migraine. Difficulty in controlling pain in patients with BD may be related to a slow change in the oscillatory network in the SAL. In future studies, we aim to investigate the relationship between symptom formation and frequency-specific networks in BD.

LIMITATIONS

Unfortunately, statistical analysis with a multiple comparison correction was not possible due to the insufficient number of subjects. Patients with BD in a hypomanic or manic state were not included; therefore, an investigation of the relationship between the manic symptoms and the connectome was not performed. Accordingly, large-scale prospective studies using MEG measurements in patients with BD are needed.

CONCLUSION

In conclusion, we observed frequency-specific alterations of RSNs in patients with BD *via* MEG analysis using graph theory. To the best of our knowledge, this is the first resting-state MEG study investigating functional connectivity using graph theory in a BD population. We show that frequency-specific alterations in the inter-community and intra-community edges in the BD group, and the intra-community edges in the left LM in the high beta band were significantly positively correlated with subjective and objective depressive symptoms in the BD group. We suggest that the connectivity of the LM in the beta band may be a good objective biological biomarker of depressive symptoms in patients with BD. Also, the higher inter-community edges of LM–DMN suggest that self-referential activity tends to be affected by emotional activity in patients with BD. Moreover, the hypoconnectivity between the SAL-FPN and left SAL-right SAL may contribute to the difficulty in maintaining a cognitive set and to the focusing of attention on task-relevant goals in the BD group, and may be related to the altered sensory perception of BD. Further studies based on MEG analysis using graph theory would help elucidate the frequency-specific alterations of RSNs in psychiatric patients and identify biological biomarkers for psychiatric disorders.

DATA AVAILABILITY STATEMENT

The raw data supporting the conclusions of this article will be made available by the authors, without undue reservation.

ETHICS STATEMENT

The studies involving human participants were reviewed and approved by Ethics Committee of the Gunma University Graduate School of Medicine, Japan. The patients/participants provided their written informed consent to participate in this study.

AUTHOR CONTRIBUTIONS

MT, MF, and YuiT designed the study. MS wrote the initial draft of the manuscript. YK, MT, and NH contributed to the analysis and interpretation of data and assisted in the preparation of the manuscript. All authors contributed to the article and approved the submitted version.

FUNDING

This work was supported by the Grants-in-Aid for Scientific Research from the Ministry of Education, Culture, Sports, Science, and Technology; Grant-in-Aid for Young Scientists (B) (No. 16K19748); Grant-in-Aid for Scientific Research (C) (No. 19K08038): Grant-in-Aid for Scientific Research on Innovative Areas (No. 16H06397); and Novartis Research Grant 2018 and 2019.

The authors declare that this study received funding from Novartis. The funder was not involved in the study design, collection, analysis, interpretation of data, the writing of this article, or the decision to submit it for publication.

ACKNOWLEDGMENTS

We are deeply grateful to the subjects and medical staff involved in this project.

SUPPLEMENTARY MATERIAL

The Supplementary Material for this article can be found online at: https://www.frontiersin.org/articles/10.3389/fpsyt.2020.00597/full#supplementary-material

REFERENCES

1. Alonso J, Petukhova M, Vilagut G, Chatterji S, Heeringa S, Üstün TB, et al. Days out of role due to common physical and mental conditions: results from the WHO World Mental Health surveys. *Mol Psychiatry* (2011) 16(12):1234–46. doi: 10.1038/mp.2010.101
2. Martinez-Aran A, Vieta E, Torrent C, Sanchez-Moreno J, Goikolea JM, Salamero M, et al. Functional outcome in bipolar disorder: the role of clinical and cognitive factors. *Bipolar Disord* (2007) 9(1-2):103–13. doi: 10.1111/j.1399-5618.2007.00327.x
3. Schaffer A, Isometsä ET, Tondo L, H Moreno D, Turecki G, Reis C, et al. International Society for Bipolar Disorders Task Force on Suicide: meta-analyses and meta-regression of correlates of suicide attempts and suicide deaths in bipolar disorder. *Bipolar Disord* (2015) 17(1):1–16. doi: 10.1111/bdi.12271
4. Pompili M, Shrivastava A, Serafini G, Innamorati M, Milelli M, Erbuto D, et al. Bereavement after the suicide of a significant other. *Indian J Psychiatry* (2013) 55(3):256–63. doi: 10.4103/0019-5545.117145
5. Pompili M, Gibiino S, Innamorati M, Serafini G, Del Casale A, De Risio L, et al. Prolactin and thyroid hormone levels are associated with suicide attempts in psychiatric patients. *Psychiatry Res* (2012) 200(2-3):389–94. doi: 10.1016/j.psychres.2012.05.010
6. Cavanagh JT, Carson AJ, Sharpe M, Lawrie SM. Psychological autopsy studies of suicide: a systematic review. *Psychol Med* (2003) 33(3):395–405. doi: 10.1017/s0033291702006943
7. Grande I, Berk M, Birmaher B, Vieta E. Bipolar disorder. *Lancet* (2016) 387 (10027):1561–72. doi: 10.1016/S0140-6736(15)00241-X
8. Goodwin GM. Psychopharmacology CGotBAf. Evidence-based guidelines for treating bipolar disorder: revised second edition–recommendations from the British Association for Psychopharmacology. *J Psychopharmacol* (2009) 23 (4):346–88. doi: 10.1177/0269881109102919
9. Vieta E, Phillips ML. Deconstructing bipolar disorder: a critical review of its diagnostic validity and a proposal for DSM-V and ICD-11. *Schizophr Bull* (2007) 33(4):886–92. doi: 10.1093/schbul/sbm057
10. Broyd SJ, Demanuele C, Debener S, Helps SK, James CJ, Sonuga-Barke EJ. Default-mode brain dysfunction in mental disorders: a systematic review. *Neurosci Biobehav Rev* (2009) 33(3):279–96. doi: 10.1016/j.neubiorev.2008.09.002
11. Greicius M. Resting-state functional connectivity in neuropsychiatric disorders. *Curr Opin Neurol* (2008) 21(4):424–30. doi: 10.1097/WCO.0b013e328306f2c5
12. Fox MD, Greicius M. Clinical applications of resting state functional connectivity. *Front Syst Neurosci* (2010) 4:19. doi: 10.3389/fnsys.2010.00019
13. Raichle ME, MacLeod AM, Snyder AZ, Powers WJ, Gusnard DA, Shulman GL. A default mode of brain function. *Proc Natl Acad Sci U S A* (2001) 98 (2):676–82. doi: 10.1073/pnas.98.2.676
14. Alamian G, Hincapie AS, Combrisson E, Thiery T, Martel V, Althukov D, et al. Alterations of Intrinsic Brain Connectivity Patterns in Depression and Bipolar Disorders: A Critical Assessment of Magnetoencephalography-Based Evidence. *Front Psychiatry* (2017) 8:41. doi: 10.3389/fpsyt.2017.00041
15. Jiang H, Dai Z, Lu Q, Yao Z. Magnetoencephalography resting-state spectral fingerprints distinguish bipolar depression and unipolar depression. *Bipolar Disord* (2019). doi: 10.1111/bdi.12871
16. Buzsaki G, Draguhn A. Neuronal oscillations in cortical networks. *Science* (2004) 304(5679):1926–9. doi: 10.1126/science.1099745
17. Hipp JF, Hawellek DJ, Corbetta M, Siegel M, Engel AK. Large-scale cortical correlation structure of spontaneous oscillatory activity. *Nat Neurosci* (2012) 15(6):884–90. doi: 10.1038/nn.3101
18. Brookes MJ, Woolrich M, Luckhoo H, Price D, Hale JR, Stephenson MC, et al. Investigating the electrophysiological basis of resting state networks using magnetoencephalography. *Proc Natl Acad Sci U S A* (2011) 108(40):16783–8. doi: 10.1073/pnas.1112685108
19. Kitzbichler MG, Khan S, Ganesan S, Vangel MG, Herbert MR, Hamalainen MS, et al. Altered Development and Multifaceted Band-Specific Abnormalities of Resting State Networks in Autism. *Biol Psychiatry* (2014) 77(9):794–804. doi: 10.1016/j.biopsych.2014.05.012
20. Khan S, Hashmi JA, Mamashli F, Michmizos K, Kitzbichler MG, Bharadwaj H, et al. Maturation trajectories of cortical resting-state networks depend on the mediating frequency band. *Neuroimage* (2018) 174:57–68. doi: 10.1016/j.neuroimage.2018.02.018
21. Bassett DS, Bullmore ET. Human brain networks in health and disease. *Curr Opin Neurol* (2009) 22(4):340–7. doi: 10.1097/WCO.0b013e32832d93dd
22. He H, Yu Q, Du Y, Vergara V, Victor TA, Drevets WC, et al. Resting-state functional network connectivity in prefrontal regions differs between unmedicated patients with bipolar and major depressive disorders. *J Affect Disord* (2016) 190:483–93. doi: 10.1016/j.jad.2015.10.042
23. Manelis A, Almeida JR, Stiffler R, Lockovich JC, Aslam HA, Phillips ML. Anticipation-related brain connectivity in bipolar and unipolar depression: a graph theory approach. *Brain* (2016) 139(Pt 9):2554–66. doi: 10.1093/brain/aww157
24. Wang Y, Wang J, Jia Y, Zhong S, Niu M, Sun Y, et al. Shared and Specific Intrinsic Functional Connectivity Patterns in Unmedicated Bipolar Disorder and Major Depressive Disorder. *Sci Rep* (2017) 7(1):3570. doi: 10.1038/s41598-017-03777-8
25. Wang Y, Wang J, Jia Y, Zhong S, Zhong M, Sun Y, et al. Topologically convergent and divergent functional connectivity patterns in unmedicated unipolar depression and bipolar disorder. *Transl Psychiatry* (2017) 7(7):e1165. doi: 10.1038/tp.2017.117

26. Fornito A, Zalesky A, Breakspear M. Graph analysis of the human connectome: promise, progress, and pitfalls. *Neuroimage* (2013) 80:426–44. doi: 10.1016/j.neuroimage.2013.04.087
27. Bassett DS, Bullmore E. Small-world brain networks. *Neuroscientist* (2006) 12 (6):512–23. doi: 10.1177/1073858406293182
28. Bassett DS, Bullmore ET. Small-World Brain Networks Revisited. *Neuroscientist* (2017) 23(5):499–516. doi: 10.1177/1073858416667720
29. Catani M. ffytche DH. The rises and falls of disconnection syndromes. *Brain* (2005) 128(Pt 10):2224–39. doi: 10.1093/brain/awh622
30. Oldfield RC. The assessment and analysis of handedness: the Edinburgh inventory. *Neuropsychologia* (1971) 9(1):97–113. doi: 10.1016/0028-3932(71) 90067-4
31. First MB SR, Gibbon M, Williams JBW. *Structured Clinical Interview for DSM-IV Axis I Disorders, Clinician Version 2.0*. New York: New York State Psychiatric Institute (1996).
32. First MB GM, Spitzer RL, Williams JBW, Benjamin LS. *Structured Clinical Interview for DSM-IV Axis II Personality Disorders (SCID-II) User"s Guide and Interview*. Washington DC: American Psychiatric Press (1997).
33. Inada T, Inagaki A. Psychotropic dose equivalence in Japan. *Psychiatry Clin Neurosci* (2015) 69(8):440–7. doi: 10.1111/pcn.12275
34. Hoddes E DW, Zarcone V. The history and use of the Stanford sleepiness scale. *Psychophysiology* (1971) 9:150. doi: 10.1037/t07116-000
35. Hironaga N, Hagiwara K, Ogata K, Hayamizu M, Urakawa T, Tobimatsu S. Proposal for a new MEG-MRI co-registration: a 3D laser scanner system. *Clin Neurophysiol* (2014) 125(12):2404–12. doi: 10.1016/j.clinph.2014.03.029
36. Larson E, Taulu S. Reducing Sensor Noise in MEG and EEG Recordings Using Oversampled Temporal Projection. *IEEE Trans bio-med Eng* (2018) 65 (5):1002–13. doi: 10.1109/TBME.2017.2734641
37. Taulu S, Simola J. Spatiotemporal signal space separation method for rejecting nearby interference in MEG measurements. *Phys Med Biol* (2006) 51(7):1759–68. doi: 10.1088/0031-9155/51/7/008
38. Taulu S, Kajola M, Simola J. Suppression of interference and artifacts by the Signal Space Separation Method. *Brain Topogr* (2004) 16(4):269–75. doi: 10.1023/B:BRAT.0000032864.93890.f9
39. Hironaga N, Ioannides AA. Localization of individual area neuronal activity. *Neuroimage* (2007) 34(4):1519–34. doi: 10.1016/j.neuroimage.2006.10.030
40. Dale AM, Fischl B, Sereno MI. Cortical surface-based analysis. I. Segmentation and surface reconstruction. *Neuroimage* (1999) 9(2):179–94. doi: 10.1006/nimg.1998.0395
41. Fischl B, Sereno MI, Dale AM. Cortical surface-based analysis. II: Inflation, flattening, and a surface-based coordinate system. *Neuroimage* (1999) 9 (2):195–207. doi: 10.1006/nimg.1998.0396
42. Reuter M, Schmansky NJ, Rosas HD, Fischl B. Within-subject template estimation for unbiased longitudinal image analysis. *Neuroimage* (2012) 61 (4):1402–18. doi: 10.1016/j.neuroimage.2012.02.084
43. Gramfort A, Luessi M, Larson E, Engemann DA, Strohmeier D, Brodbeck C, et al. MNE software for processing MEG and EEG data. *Neuroimage* (2014) 86:446–60. doi: 10.1016/j.neuroimage.2013.10.027
44. Hamalainen MS, Sarvas J. Realistic conductivity geometry model of the human head for interpretation of neuromagnetic data. *IEEE Trans bio-med Eng* (1989) 36(2):165–71. doi: 10.1109/10.16463
45. Hashizume A, Hironaga N. Principles of Magnetoencephalography. In: Tobimatsu S, Kakigi R, editors. *Clinical Applications of Magnetoencephalography*. Tokyo: Springer Japan (2016). p. 3–32.
46. Hayamizu M, Hagiwara K, Hironaga N, Ogata K, Hoka S, Tobimatsu S. A spatiotemporal signature of cortical pain relief by tactile stimulation: An MEG study. *Neuroimage* (2016) 130:175–83. doi: 10.1016/j.neuroimage.2016.01.065
47. Lin FH, Witzel T, Ahlfors SP, Stufflebeam SM, Belliveau JW, Hamalainen MS. Assessing and improving the spatial accuracy in MEG source localization by depth-weighted minimum-norm estimates. *Neuroimage* (2006) 31(1):160–71. doi: 10.1016/j.neuroimage.2005.11.054
48. Fischl B, van der Kouwe A, Destrieux C, Halgren E, Segonne F, Salat DH, et al. Automatically parcellating the human cerebral cortex. *Cereb Cortex* (2004) 14 (1):11–22. doi: 10.1093/cercor/bhg087
49. Collins DL, Neelin P, Peters TM, Evans AC. Automatic 3D intersubject registration of MR volumetric data in standardized Talairach space. *J Comput assisted tomogr* (1994) 18(2):192–205. doi: 10.1097/00004728-199403000-00005
50. O'Neill GC, Barratt EL, Hunt BA, Tewarie PK, Brookes MJ. Measuring electrophysiological connectivity by power envelope correlation: a technical review on MEG methods. *Phys Med Biol* (2015) 60(21):R271–95. doi: 10.1088/0031-9155/60/21/R271
51. Yeo BT, Krienen FM, Sepulcre J, Sabuncu MR, Lashkari D, Hollinshead M, et al. The organization of the human cerebral cortex estimated by intrinsic functional connectivity. *J Neurophysiol* (2011) 106(3):1125–65. doi: 10.1152/jn.00338.2011
52. Jones E, Oliphant T, Peterson P. SciPy: Open Source Scientific Tools for Python. (2001).
53. Vargas C, Lopez-Jaramillo C, Vieta E. A systematic literature review of resting state network–functional MRI in bipolar disorder. *J Affect Disord* (2013) 150 (3):727–35. doi: 10.1016/j.jad.2013.05.083
54. Chase HW, Phillips ML. Elucidating neural network functional connectivity abnormalities in bipolar disorder: toward a harmonized methodological approach. *Biol Psychiatry Cognit Neurosci Neuroimaging* (2016) 1(3):288–98. doi: 10.1016/j.bpsc.2015.12.006
55. Chai XJ, Whitfield-Gabrieli S, Shinn AK, Gabrieli JDE, Nieto Castañón A, McCarthy JM, et al. Abnormal Medial Prefrontal Cortex Resting-State Connectivity in Bipolar Disorder and Schizophrenia. *Neuropsychopharmacology* (2011) 36:2009–17. doi: 10.1038/npp.2011.88
56. Houenou J, d'Albis MA, Vederine FE, Henry C, Leboyer M, Wessa M. Neuroimaging biomarkers in bipolar disorder. *Front Biosci (Elite Ed)* (2012) 4:593–606. doi: 10.2741/402
57. Phillips ML, Swartz HA. A critical appraisal of neuroimaging studies of bipolar disorder: toward a new conceptualization of underlying neural circuitry and a road map for future research. *Am J Psychiatry* (2014) 171 (8):829–43. doi: 10.1176/appi.ajp.2014.13081008
58. Strakowski SM, Adler CM, Almeida J, Altshuler LL, Blumberg HP, Chang KD, et al. The functional neuroanatomy of bipolar disorder: a consensus model. *Bipolar Disord* (2012) 14(4):313–25. doi: 10.1111/j.1399-5618.2012.01022.x
59. Khadka S, Meda SA, Stevens MC, Glahn DC, Calhoun VD, Sweeney JA, et al. Is aberrant functional connectivity a psychosis endophenotype? A resting state functional magnetic resonance imaging study. *Biol Psychiatry* (2013) 74 (6):458–66. doi: 10.1016/j.biopsych.2013.04.024
60. Lois G, Linke J, Wessa M. Altered functional connectivity between emotional and cognitive resting state networks in euthymic bipolar I disorder patients. *PloS One* (2014) 9(10):e107829. doi: 10.1371/journal.pone.0107829
61. Greicius MD, Krasnow B, Reiss AL, Menon V. Functional connectivity in the resting brain: a network analysis of the default mode hypothesis. *Proc Natl Acad Sci U S A* (2003) 100(1):253–8. doi: 10.1073/pnas.0135058100
62. Mazoyer B, Zago L, Mellet E, Bricogne S, Etard O, Houde O, et al. Cortical networks for working memory and executive functions sustain the conscious resting state in man. *Brain Res Bull* (2001) 54(3):287–98. doi: 10.1016/s0361-9230(00)00437-8
63. Ellard KK, Zimmerman JP, Kaur N, Van Dijk KRA, Roffman JL, Nierenberg AA, et al. Functional Connectivity Between Anterior Insula and Key Nodes of Frontoparietal Executive Control and Salience Networks Distinguish Bipolar Depression From Unipolar Depression and Healthy Control Subjects. *Biol Psychiatry Cognit Neurosci Neuroimaging* (2018) 3(5):473–84. doi: 10.1016/j.bpsc.2018.01.013
64. Menon V. Salience Network. *Brain Mapp* (2015) 2:597–611. doi: 10.1016/B978-0-12-397025-1.00052-X
65. Salvadore G, Cornwell BR, Sambataro F, Latov D, Colon-Rosario V, Carver F, et al. Anterior cingulate desynchronization and functional connectivity with the amygdala during a working memory task predict rapid antidepressant response to ketamine. *Neuropsychopharmacology* (2010) 35(7):1415–22. doi: 10.1038/npp.2010.24
66. Nugent AC, Robinson SE, Coppola R, Furey ML, Zarate CAJr. Group differences in MEG-ICA derived resting state networks: Application to major depressive disorder. *Neuroimage* (2015) 118:1–12. doi: 10.1016/j.neuroimage.2015.05.051
67. Kim DJ, Bolbecker AR, Howell J, Rass O, Sporns O, Hetrick WP, et al. Disturbed resting state EEG synchronization in bipolar disorder: A graph-

theoretic analysis. *NeuroImage Clin* (2013) 2:414–23. doi: 10.1016/j.nicl.2013.03.007

68. Whitton AE, Webb CA, Dillon DG, Kayser J, Rutherford A, Goer F, et al. Pretreatment Rostral Anterior Cingulate Cortex Connectivity With Salience Network Predicts Depression Recovery: Findings From the EMBARC Randomized Clinical Trial. *Biol Psychiatry* (2019) 85 (10):872–80. doi: 10.1016/j.biopsych.2018.12.007
69. Taesler P, Rose M. Prestimulus Theta Oscillations and Connectivity Modulate Pain Perception. *J Neurosci* (2016) 36(18):5026–33. doi: 10.1523/JNEUROSCI.3325-15.2016
70. Han JJ, Jang JH, Ridder D, Vanneste S, Koo JW, Song JJ. Increased parietal circuit-breaker activity in delta frequency band and abnormal delta/theta band connectivity in salience network in hyperacusis subjects. *PloS One* (2018) 13(1):e0191858. doi: 10.1371/journal.pone.0191858
71. Parker G. The suprasensory world of bipolar II disorder. *Am J Psychiatry* (2014) 171(6):614–5. doi: 10.1176/appi.ajp.2014.13121570

Conflict of Interest: The authors declare that the research was conducted in the absence of any commercial or financial relationships that could be construed as a potential conflict of interest.

frontiers in Psychiatry

ORIGINAL RESEARCH
published: 22 July 2020
doi: 10.3389/fpsyt.2020.00683

Alterations of Heartbeat Evoked Magnetic Fields Induced by Sounds of Disgust

Yutaka Kato[1,2]*, *Yuichi Takei*[2], *Satoshi Umeda*[3], *Masaru Mimura*[4] and *Masato Fukuda*[2]

[1] Tsutsuji Mental Hospital, Gunma, Japan, [2] Department of Psychiatry and Neuroscience, Gunma University Graduate School of Medicine, Maebashi, Japan, [3] Department of Psychology, Keio University, Tokyo, Japan, [4] Department of Neuropsychiatry, Keio University School of Medicine, Tokyo, Japan

The majority of the models of emotional processing attribute subjective emotional feelings to physiological changes in the internal milieu, which are sensed by the interoceptive system. These physiological reactions evoked by emotional phenomena occur *via* the autonomic nervous system, and give rise to alterations in body-mind interactions that are characterized by heartbeat evoked magnetic fields (HEFs) involving brain regions associated with emotional perception. The current study used magnetoencephalography (MEG) to examine regional cortical activity and connectivity changes in HEFs provoked by the emotion of disgust. MEG results from 39 healthy subjects (22 female) revealed that passively listening to sounds of disgust elicited right insular cortical activity and enhancement of cortical connectivity between the right anterior ventral insular cortex and left ventromedial prefrontal cortex, demonstrated by phase lag indexes in the beta frequency range. Furthermore, inter-trial coherence significantly increased at 19 Hz and 23 Hz, and decreased at 14 Hz, which highlights the involvement of low beta oscillations in emotional processing. As these results were based on spontaneously triggered bioelectrical signals, more indigenous and induced signals were extracted with a block designed experiment. The insular cortices play an important role in emotional regulation and perception as the main cortical target for signals with interoceptive information, providing direct substrates of emotional feelings. The current results provide a novel insight into frequency properties of emotional processing, and suggest that emotional arousal evoked by listening to sounds of disgust partially impact the autonomic nervous system, altering HEFs *via* connectivity changes in the right anterior ventral insular cortex and left ventromedial prefrontal cortex.

Keywords: MEG (magnetoencephalography), insular cortices, emotion, heartbeat evoked magnetic fields, cortical connectivity, oscillation

OPEN ACCESS

Edited by:
Peter Uhlhaas,
University of Glasgow,
United Kingdom

Reviewed by:
Hugo Critchley,
Brighton and Sussex Medical School,
United Kingdom
Yasuo Terao,
Kyorin University, Japan

***Correspondence:**
Yutaka Kato
yutaka.kt@gmail.com

Specialty section:
This article was submitted to Neuroimaging and Stimulation, a section of the journal Frontiers in Psychiatry

Received: *14 May 2020*
Accepted: *30 June 2020*
Published: *22 July 2020*

Citation:
Kato Y, Takei Y, Umeda S, Mimura M and Fukuda M (2020) Alterations of Heartbeat Evoked Magnetic Fields Induced by Sounds of Disgust. Front. Psychiatry 11:683. doi: 10.3389/fpsyt.2020.00683

INTRODUCTION

The majority of the models of emotional processing attribute subjective emotional feelings to physiological changes in the internal milieu, including the skeletomuscular, neuroendocrine, and autonomic nervous systems (1–3). These changes are often triggered by external events as well as the homeostatic changes of inner bodily status, and can affect body-mind interactions (4–6). Indeed,

affective experiences initially give rise to specific physiological changes in the body, which are bidirectionally associated with the perception of one's emotions (7, 8). Central representations of the bodily responses caused by external emotive stimuli are perceived as emotions; i.e., automatically generated bodily responses *via* the autonomic nervous system can result in subjective emotional feelings (9). Derived from this theory is the notion that the relative ability to perceive internal body status influences measures of subjective affective experience, which highlights the fundamental importance of the body in emotional phenomena.

The ability to self-monitor one's own internal body status is a key feature of the body-mind interaction in emotional awareness. Interoception, which is the sensitivity to visceral sensations (10), refers to the current homeostatic conditions of the entire body (11) and the ability of this information to reach conscious awareness (12). Interoception derives not only from musculoskeletal, circulating, and humoral signals within the body, but also from afferent information *via* autonomic nervous reflexes and higher levels of autonomic regulation originating from visceral organs and vascular systems (13). Two distinct neural pathways convey interoceptive information. The lamina I spinothalamocortical pathway carries information regarding the internal milieu, such as muscle contractions in vessel walls, peripheral blood flow, temperature, pain, tissue injury, and levels of O2 and CO2, while the vagal nerve carries visceral signals regarding the cardiovascular, respiratory, gastrointestinal, and genito-urinary systems (14). The crosstalk between these two pathways within the projections of the brainstem to the insular and somatosensory cortices facilitates the organization of topographical maps of bodily status within structures (3). Namely, interoceptive information originates from multiple organs *via* corresponding conduits and is gathered and successively processed in the structures of the brain, providing topographically organized somatic maps. Among these, the sensitivity to one's own heartbeat is closely associated with interoceptive awareness (14, 15) and the intensity of experienced emotions (16–18). The accuracy of heartbeat counts has been found to be positively correlated with the sensitivity of emotional traits, such as tendencies for general anxiety (19, 20).

To investigate the cortical activation related to interoception, both heartbeat evoked potentials (HEPs) and heartbeat evoked magnetic fields (HEFs), which are measured using electroencephalography (EEG) and magnetoencephalography (MEG), respectively, serve as useful indexes of interoceptive processing, and reflect the sensitivity to ones' own internal body states (21–23). HEPs/HEFs are computed by averaging the neural signals with time-locked triggers of individual R peaks of electrocardiography (ECG), which emerge after 200 to 300 ms and are mainly derived from fronto-central regions of the brain (24–29). Thus far, HEPs/HEFs have been associated with cardiovascular arousal (30), heartbeat awareness (31–33), visual awareness (34), self-consciousness (35, 36), self-face recognition (37), pain perception (38), empathy (39), sleep states (40), and psychiatric disorders, including depression (41), depersonalization (42), and borderline personality disorder (43).

Aside from this accumulating evidence, the precise mechanisms of HEPs/HEFs on emotional experiences are still unclear. As most studies have used EEG to measure the effects on interoceptive awareness, poor spatial resolution has obscured elucidation of these physiological features. We hypothesized that the subjective experience of emotions would elicit the peripheral physiological responses initially, then affect the emotion related cortical activities. Particularly, we anticipated that disgust feeling of emotion will impact either myocardial or gastric functions, thus give rise to the alteration of HEFs reflecting these changes of bodily status. To assess our hypothesis that spontaneous heartbeat movements evoke cortical activities and connectivity changes related to emotional processing, we conducted MEG, which has a high temporal and spatial resolution. In this way, we investigated alterations in HEFs that are mediated by disgusting experiences to clarify the precise cortical activity, connectivity, and frequency properties to better understand brain-mind interactions.

MATERIALS AND METHODS

Subjects

Thirty-nine healthy volunteers participated in the experiment (22 female, mean age: 39.3 years ± 8.55 years, range: 20–58 years). One additional participant was excluded because of technical artifacts during the MEG recording. All participants had normal or corrected-to-normal vision and no hearing difficulties, and all were right-handed according to the Edinburgh Handedness Scale (44). No participants reported any history of neurological or major psychiatric conditions, and no participants were on medications, including mood stabilizers, antidepressants, antipsychotics, anxiolytics, or hypnotics. Before the experiment, all subjects were fully informed about the MEG recording, and they all provided written informed consent. The experimental procedures were approved by the Ethics Committee of Gunma University Graduate School of Medicine in concordance with the Code of Ethics of the World Medical Association (Declaration of Helsinki).

Stimuli

Subjects passively listened to auditory sounds of disgust and control sounds selected from the International Affective Digital Sounds (IADS-2) (45) with their eyes open and focused on a fixation point projected on a screen during the presentations. The experiment consisted of four blocks of 3 min each, in which two different types of sound sets were alternatively presented; the entire experiment therefore took 12 min in total (**Figure 1**). The auditory stimuli of disgust consisted of a 6-second stereo audio recording of scenic events that effectively provoked the affective scenery (successively presented twice: 12 s) with 15 sets of sounds (one session forming blocks with 3 min of stimuli each), which were randomly selected from 10 different sound sets. The 10

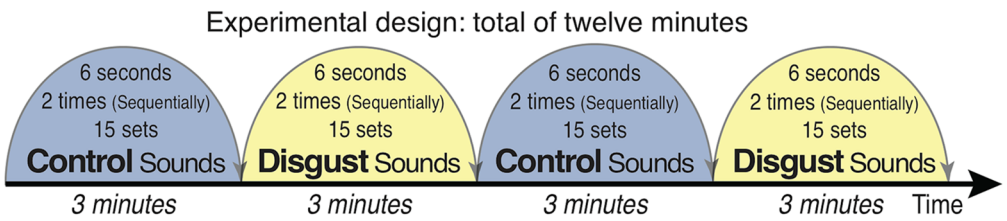

FIGURE 1 | Schema of the experimental design. Auditory stimuli were presented in a shielded room *via* earphones bilaterally while participants fixated on a cross. Ten types of disgust/control sounds were presented from the International Affective Digital Sounds (including human vomiting/cow moos, human fighting with a stomach being hit/digging a hole with a shovel, and child abuse/cheers in a baseball stadium). Each of the 15 stimuli (6 s) was presented twice (12 s), with 3 min of stimulus presentation per block. The blocks were alternatively presented, and the experiment lasted for a total of 12 min.

sounds of disgust were as follows: (1) Male Cough (IADS-2 sound No. 241; a man having a coughing fit), (2) Female Cough (No. 242; a woman having a coughing fit), (3) Hiccups (No. 245; a man with sustained hiccups), (4) Vomiting (No. 255; a man vomiting), (5) Screaming (No. 275; a man screaming), (6) FemScream2 (No. 276; a female screaming for help), (7) Child Abuse (No. 278; a baby screaming after the sound of being hit by a man using abusive language), (8) Attack3 (No. 281; sounds of domestic violence indicating that a woman is being hit), (9) Fight3 (No. 283; a fight between two men as indicated by sounds of abdominal hitting), and (10) Belch (No. 702; a man belching).

Control sounds were selected with the same sound set structure as that of the sounds of disgust. The 10 control sounds were as follows: (1) Baby (IADS-2 sound file No. 110; a baby laughing), (2) Music Box (No. 111; a baby laughing with music box sounds), (3) Kids1 (No. 112; voices of pleasure of children in the park), (4) Cows (No. 113; a cow mooing similar to the sound of vomiting), (5) Pig (No. 130; barks of pigs similar to belching sounds), (6) Glowl2 (No. 133; the bark of an elephant), (7) Brook (No. 172; the sound of water flowing), (8) Kids2 (No. 224; the sounds of playing children in the park), (9) Baseball (No. 353; cheering sounds in a baseball stadium followed by the sound of something being hit, similar to the sound of child abuse), and (10) Shovel (No. 382; the sound of digging a hole with a shovel, similar to the sound of abdominal hitting).

After the experiment, subjects were requested to rate the strengths of emotions they had felt (maximum 100; minimum 0) during the disgust and control blocks, respectively, regarding six elements of emotions – fear, sadness, anger, disgust, happiness, and love (46). Statistical analysis was performed by scaling the independent components of emotions according to the disgust/control conditions.

MEG Recording

MEG was recorded in a magnetically shielded room (JFE Mechanical Co., Tokyo, Japan) with a 306-channel whole-head system (Elekta Neuromag, Helsinki, Finland). The system had 102 sensor-triplets, each of which contained a magnetometer, a longitudinal gradiometer, and a latitudinal gradiometer. Silver cup electrodes were located at six sites of the body to measure individual ECGs and exclude noise from the ECG and EOG. The locations of three fiduciary points (nasion and left and right auricular points) defining the head frame coordinate system, a set of head surface points, and the locations of the four head position indicator coils were digitized using an Isotrak three-dimensional digitizer (Polhemus™, Colchester, VT, USA). MEG and EOG signals were simultaneously recorded during stimuli presentation at a sampling rate of 1,000 Hz. All off-line analyses were based on the saved continuous raw data. Sleepiness scores at the time of the MEG examination were assessed using the Stanford Sleepiness Scale (47) before and after each task.

Preprocessing and Epoching

Initially, all off-line analyses were based on the saved continuous raw data. For noise suppression and motion correction, the data were spatially filtered using the signal space separation method (48, 49) with Elekta Neuromag Maxfilter software, which suppresses noise generated by sources outside the brain. A notch filter was applied to eliminate noise from the power line (50 Hz) and its harmonics (100 Hz and 150 Hz). We eliminated eye movement- and body movements- related artifacts from the raw data using independent component analysis (ICA). The ICA was applied to the MEG sensor signals, and the eye movement and body movement signals were isolated based on visual inspection by two expert researchers. MEG data were then divided into two epochs, disgust and control conditions, with simultaneously recorded ECG signals, which resulted in two different data sets of 6 min each per condition.

Data Analysis

HEFs were calculated by MEG signals locked to the R peaks of the ECG separately for the two conditions. We detected R peaks using the "find_ecg_events" function in MNE-python. We acquired epochs of 800 ms, which included a pre-R peak baseline of 200 ms, triggered with ECG R peaks at a latency of 0 ms. According to the rate of the subjects' heartbeat, an averaging of 410 to 570 times provided two different data sets corresponding to the conditions (disgust or control). Subtracted waveforms derived from the subtraction of the control condition from the disgust condition were calculated for every subject. Epochs were rejected if the peak-to-peak amplitude during the target epoching period exceeded 400 fT and 4,000 fT/cm in any of the magnetometer and gradiometer channels, respectively. Using the data of individual ECG, the standard deviation of the

averaged normal-to-normal (NN) beat intervals, with both standard deviation of all NN intervals (SDNN) representing sympathetic function, and root mean square of successive differences of successive NN intervals (RMSSD) representing parasympathetic functions, were calculated.

To obtain anatomical segmentation and brain surface images, we first applied the FreeSurfer reconstruction process to each participant's MRI data. Cortical reconstructions and parcellations for each subject were generated from a T1-weighted MRI (50, 51). After correcting the topological defects, cortical surfaces were triangulated using dense meshes with ~130,000 vertices in each hemisphere.

The dense triangulation of the folded cortical surface provided by FreeSurfer was decimated to a grid of 10,242 dipoles per hemisphere, corresponding to a spacing of approximately 3 mm between adjacent source locations. To compute the forward solution, the boundary-element method with a single compartment bounded by the inner surface of the skull was used (52). The watershed algorithm in FreeSurfer was used to generate the inner skull surface triangulations from the anatomical MRI images of each participant. The source current distribution was estimated using the minimum norm estimates (MNE) suite and MNE python, which are widely used distributed source models for MEG analysis (http://www.martinos.org/mne/) (53). We employed the boundary-element method, with a single compartment bound by the inner surface of the skull for the forward head modeling (52). The source current distribution was estimated using the noise-normalized dynamic statistical parameter mapping (dSPM) method (54, 55). The noise covariance matrix was computed from the empty room acquisition data. To reduce the bias of the estimated source locations toward the superficial currents, we incorporated a depth weighting parameter (depth = 0.8) by adjusting the source covariance matrix to evaluate the current (56).

Next, we imported commonly used cortex segmentation from the FreeSurfer software. We used the Desikan-Killiany Atlas (aparc) for cortical parcellation (57, 58). We found prominent activity in the insular cortices, and so parcellated this structure into three sub-regions (anterior ventral, anterior dorsal, and posterior insular cortices) according to a previous study (59). We acquired 72 source waveforms for each participant.

Induced power (Power) and inter-trial coherence (ITC) estimation were acquired using "source_induced_power" function in mne-python (60). Inter-trial coherence (ITC) was indexed by summation of phase angles of all epochs demonstrating as the following formula:

$$ITC(f,t) = \frac{1}{n}\sum_{k=1}^{n}\frac{F_k(f,t)}{|F_k(f,t)|}$$

The $F_k(f,t)$ denotes the spectral estimate of trial k at frequency f and time, n is the number of trials, || represents the complex norm. The ITC measure takes values between 0 and 1. The Morlet wavelet transform was set to single epochs in time courses in the 8–24 Hz frequency range for a duration of -200 to 600 ms under the arousal and control conditions. Data for Power and ITC in each condition were then normalized against the baseline power between the latencies of 200 ms and 400 ms obtained from the right anterior ventral insular cortices in the control condition.

The phase lag index (PLI) was calculated based on the time series of six insula seed sub-regions between 200 ms and 500 ms at 8–13 Hz for the alpha band and at 14–24 Hz for the beta band (61). Connectivity strength at each region of interest (ROI) was estimated using Fisher's Z-transformed PLI values between that ROI and all other ROIs.

Statistical comparisons were made using Scipy (62) by using statistical parametric maps obtained from MEG data to calculate the source-evoked time courses and ITC across all subjects. Independent t-tests were applied to the source-evoked time courses to compare the two conditions (disgust/control) between -100 and 500 ms. We first normalized the ITC of all insular sub-regions by calculating Z-values using the mean and standard deviations of the ITC in the right anterior ventral insular sub-regions between the 200 and 600 ms latency window and 8 and 24 Hz frequency range (**Figure 3** lower panel). Then, we compared the normalized ITC between the two conditions (disgust/control) using independent t-tests. We considered statistical significance to be indicated by p-values under 1% (enclosed area with white line in **Figure 3**, lower panel; distribution of significance). Next, we compared the averaged values of distribution of significance in each frequency band using independent t-tests. In addition, we compared the PLI of the right anterior ventral insular cortices as the seed region using Mann-Whitney U tests. We masked p-values under 5%, and converted p-values to z-values, as seen in **Figure 5**.

Data and Code Availability Statement

The raw data supporting the conclusions of this article will be made available by the authors, without undue reservation.

RESULTS

Subjective Emotions Evoked by Stimuli

Subjects independently rated their emotional experiences during control/disgust blocks from 0 (minimum) to 100 (maximum) regarding the six elements of emotion (i.e., fear, sadness, anger, disgust, happiness, and love). During disgust conditions, the strengths of emotions such as disgust (average +81.7 ± 25.3), fear (average +40.8 ± 29.3), sadness (average +37.0 ± 35.4), and anger (average +32.2 ± 30.5) were higher. On the contrary, the strengths of happiness (average -43.0 ± 33.5) and love (average -39.7 ± 31.7) were lower. The most dominant emotion evoked by stimuli sounds was disgust, followed by the decreased emotion of happiness.

Heart Rate Variability

In order to estimate the time-domain measures of heart rate variability, we calculated heart rates, and normal-to-normal beat (NN) intervals to obtain standard deviations for all NN intervals (SDNN), which represent sympathetic function, and the root mean square of successive differences of successive NN intervals (RMSSD), representing parasympathetic function. No significant

differences between conditions were found in heart rate (disgust = 66.63 [SD = 8.92], control = 66.67 [SD = 8.95]; p = 0.79), SDNN (disgust = 42.64 [SD = 28.35]; control = 43.87 [SD = 29.47]; p = 0.42), or RMSSD (disgust = 35.06 [SD = 24.93]; control = 35.64 [SD = 23.00]; p = 0.37).

Source Current Distribution

Using MNE analysis (53), cortical strained minimum norm source currents were estimated according to cortical activities during the designated time points throughout the whole averaged latencies. All subjects exhibited cortical activity in both conditions; however, the most prominent findings were derived from the subtracted distributions between the disgust and control conditions, whereby subtracted activity was mainly elicited in the bilateral insular cortices and the right inferior frontal gyrus. Using averaged data across all subjects, we observed increased activity in the bilateral insular cortices and the right inferior frontal gyrus between 270 ms and 300 ms in the disgust condition relative to the control condition. **Figure 2** depicts the subtracted distributions of source current estimation across all subjects at the latencies of 291.8 ms of the right, anterior, and left surfaces order from right to left; the resulting images indicate that the bilateral insular cortices (right dominantly) and the right inferior frontal gyrus were simultaneously activated.

Source-Evoked Time Courses and Inter-Trial Coherences of Insular Cortical Sub-Regions

To characterize the insular cortical activity, we evaluated the source-evoked time courses from the insular cortices, which were divided into three sub-regions according to previous studies (59, 63, 64); these sub-regions were the anterior dorsal, anterior ventral, and posterior insular cortices. The mean coordinates of the insular sub-regions were as follows: left anterior dorsal insula (x = -38, y = 6, z = 2), right anterior dorsal insula (x = 35, y = 7, z = 3), left anterior ventral insula (x = -33, y = 13, z = -7), right anterior ventral insula (x = 32, y = 10, z = -6), left posterior insula (x = -38, y = -6, z = 5), and right posterior insula (x = 35, y = -11, z = 6). **Figure 3** (upper right panel) depicts the schema of three insular cortical sub-regions in the right hemisphere. **Figure 3** (upper left panel) depicts the source-evoked time courses of both hemispheres. Although five sub-regions of the insular cortices demonstrated similar activation during whole time course at all frequency ranges, there was a non-significant amplification of activity in the right anterior ventral insular cortices between 160 ms and 260 ms in the disgust conditions (p = 0.274). All six sub-regions of the insular cortices had peak amplitudes at around 250 ms between the 200 ms and 300 ms latency, which suggests that the bilateral insular cortices were similarly activated after the ECG R peaks in both conditions. No significant between-condition differences were found in any of the six sub-regions.

To investigate the frequency properties of these responses, we calculated the inter-trial coherence (ITC) from the regional source power analysis in 12 different distributions (six regions by two conditions) according to the insular sub-regions. Statistical comparisons of each ITC between the two conditions (disgust/control) were made at the frequency range of 8 to 24 Hz in the 0 ms to 600 ms latency window by normalizing the baseline power between the 200 ms and 600 ms latency obtained from the right anterior ventral insular cortices of the control conditions, shown by the t-values between conditions in **Figure 3** (lower panel). Significant differences between the control and disgust conditions were found at five distributions (distributions of significances) in only right anterior ventral insular sub-region responses; there were significant increases in four distributions at the frequencies of 19 Hz at around 400 ms, 500 ms, and 550 ms, and 23 Hz at around 525 ms (t-value = 4.064, p = 0.00012; disgust mean = 1.380 [SD = 2.38]/control mean = -0.294 [SD = 0.97]). There was a significant decrease in one distribution at 14 Hz at around 300 ms (t-value = -2.676, p = 0.00912; disgust mean = -6.131 [SD = 14.43]/control mean = 0.0632 [SD = 0.83]), highlighted by surrounding white rectangles in **Figure 3** at the panel of right anterior ventral insular cortices. There were no significant differences between conditions in the other insular sub-regions at any frequency range or latency. The individual averaged ITCs of two low beta bands (14 Hz; 19 and 23 Hz) in five significantly different distributions (distributions of significances) of each condition are shown in **Figure 4** for a total of 39 subjects. The left panel represents the averaged ITC of the frequency range of 14 Hz individually (disgust mean = -6.13 [SD = 14.4]/control mean = 0.063 [SD = 0.83]), whereas the right panel shows a frequency range of 19 and 23 Hz (disgust mean = 1.38 [SD = 2.38]/control mean = -0.29 [SD = 0.97]); in both frequencies, there were significant differences between the conditions according to the statistical significances

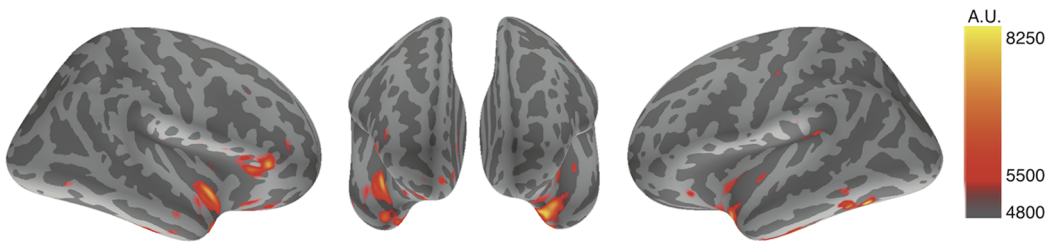

FIGURE 2 | Source current estimation. The source current estimation demonstrated activity in bilateral insular cortices and the right inferior frontal gyrus at the latency of 291.8 ms after the R peak of ECG in the disgust condition. This is illustrated by the source current distributions of disgust minus control conditions of the right, anterior, and left surfaces. The color bar indicates the arbitrary unit (A.U.) defined by mne analyze.

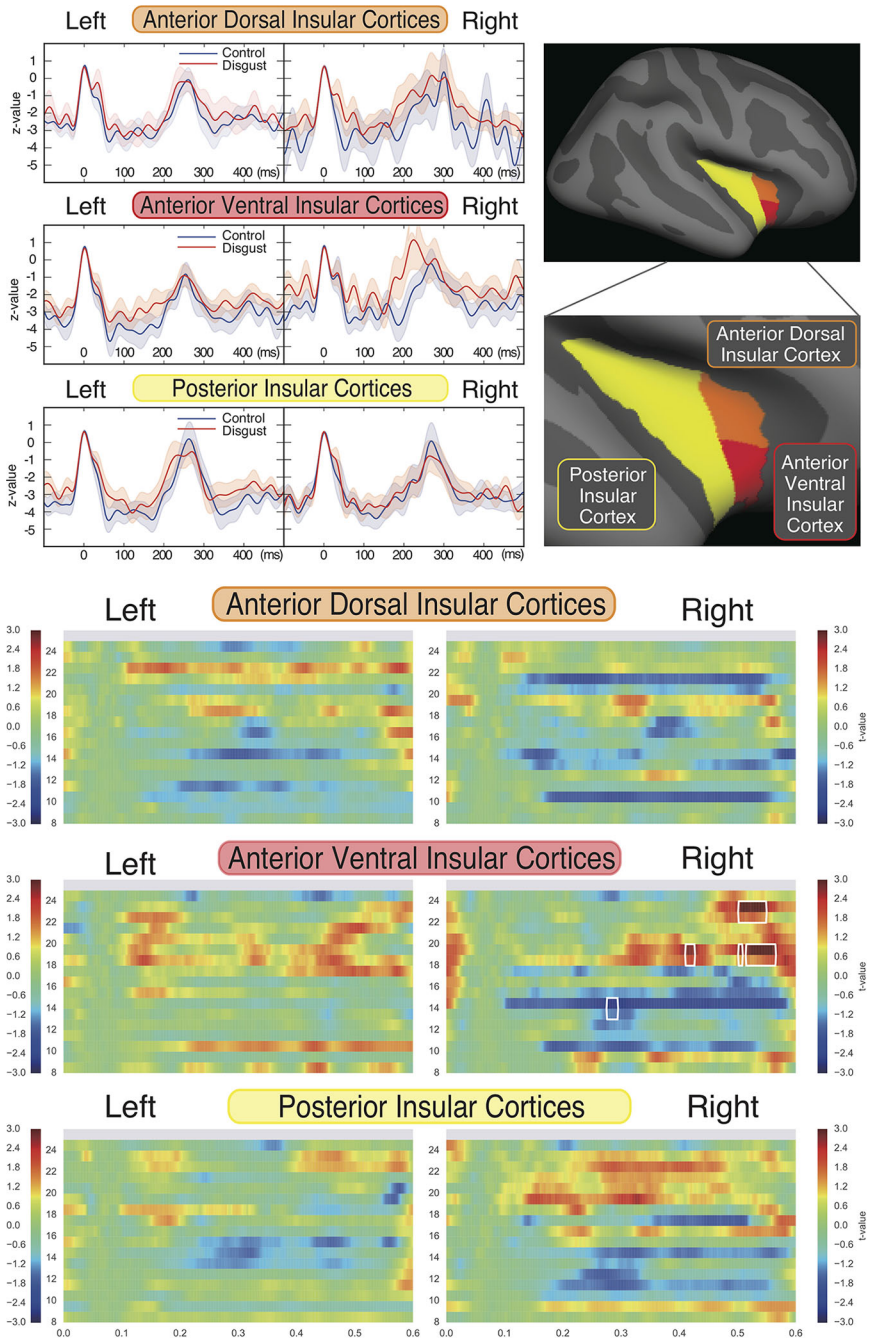

FIGURE 3 | Source strengths of insular sub-regions represented by source-evoked time courses and inter-trial coherences. Insular cortices were divided into three sub-regions, as the anterior ventral, anterior dorsal, and posterior regions of each hemisphere (upper right panel). The source-evoked time courses (upper left panel) were estimated from three sub-regions of the insular cortices of both hemispheres. The X-axis shows the latencies from -100 ms to 500 ms, and the Y-axis shows the Z-value of evoked source activities. The red and blue lines represent the disgust and control conditions, respectively. Z-values were similar at five insular sub-regions; however, the right anterior ventral sub-region demonstrated a trend towards amplification of z-value between 160 ms and 260 ms in the disgust condition. Although no significant differences were found between conditions of all sub-regions, all insular sub-regions exhibited peak amplitudes in both conditions between 250 ms and 300 ms after ECG R peaks. The comparison of inter-trial coherences (ITCs) of the sub-regions (lower panel) between conditions revealed a significant increase of z-value at the frequencies of 19 and 23 Hz and a significant decrease at 14 Hz, only at the right anterior ventral insular sub-regions (highlighted by surrounding rectangles drawn by white line; distributions of significances). The X-axis shows the latencies from 0 ms to 600 ms, the Y-axis shows frequencies from 8 Hz to 24 Hz, and the color bar indicates t-values (+ 3 to - 3) between conditions of each frequency and latency of the responses calculated by t-tests applied for between-condition comparisons (disgust vs. control).

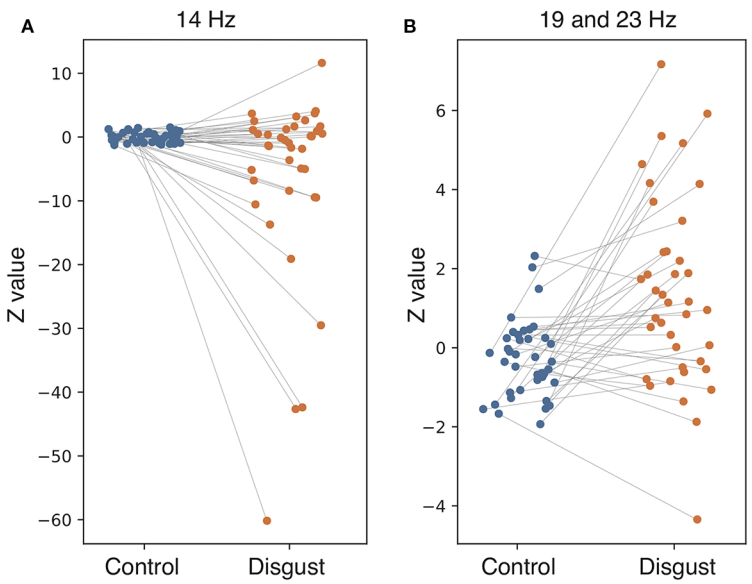

FIGURE 4 | Individual averaged inter-trial coherence (ITC) of distributions of significances. Individual averaged ITCs were plotted for subjects in both conditions (blue plot: control condition; orange plot: disgust condition; line: individual changes between conditions). The **(A)** represents the distributions at 14 Hz, and the **(B)** shows distributions at 19 and 23 Hz. Each plot indicates the Z-value of individual averaged ITC in both conditions corresponding to the individual changes.

of the averaged ITC. These individual averaged ITC were not correlated to z-scores of visual analog scales statistically of each emotion, that subjects felt during stimuli presentations.

Phase Lag Index

Based on the source-evoked time courses and ITC results, which indicated the importance of the beta frequency range, particularly at the right anterior ventral insular sub-region, we calculated the phase lag indexes (PLIs) between right anterior ventral insular cortical sub-regions and other cortical regions of the 68 vertexes across the whole brain at beta frequency bands (14–24 Hz) across all subjects. To clarify the significant correlation of PLI to other brain regions, we excluded PLIs with p-values exceeding 0.05 according to the Mann-Whitney U test. **Figure 5** shows the subtracted PLI between the disgust and control conditions at the beta frequency range between the right anterior ventral insular cortices and other brain regions. Significant connectivity changes were found at the contralateral (left) ventromedial prefrontal cortex (VMPFC) in concordance with the right anterior ventral region of the insular cortices at the beta frequency range when comparing the two conditions using the PLI result (Mann-Whitney U = 284.0, p = 0.0072, disgust mean = 0.0656 [SD = 0.0441]/control mean = 0.0450 [SD = 0.0323]). Significant increases in PLI compared to the anterior ventral insular cortices were also found in the left pars opercularis (Mann-Whitney U = 328.0, p = 0.03622, disgust mean = 0.0469 [SD = 0.0282]/control mean = 0.0603 [SD = 0.0336]), right posterior cingulate (Mann-Whitney U = 333.0, p = 0.04250, disgust mean = 0.0673 [SD = 0.0525]/control mean = 0.0518 [SD = 0.0535]), and the left bank of the superior temporal sulcus (Mann-Whitney U = 314.0, p = 0.02257, disgust mean = 0.0601 [SD = 0.0648]/control mean = 0.0630 [SD = 0.0286]).

DISCUSSION

The current study revealed that listening to sounds of disgust induces changes in HEFs. Behavioral data indicated that the sound stimuli affected the subjective emotional state by increasing disgust emotion as well as decreasing happiness. As the source current estimation by subtracting disgust minus control conditions revealed the activation, not the suppression, of bilateral insular cortices and inferior frontal cortices, the main effect provoked by the current stimuli was associated with the evoked disgust emotions than the suppressed happiness. Since several studies have reported there to be a relationship between disgust and insular cortical activity (65, 66), the most prominent locus affecting the alteration of HEFs was insular activities evoked by the subjective experience of disgust. In addition, the physiological result on the heart rate variability could not demonstrate the statistical differences in the peripheral cardiac effects such as heart rate, SDNN, and RMSSD on the contrary to our hypothesis. Since our study did not utilize the other indices, such as gastrointestinal information, it would be difficult to further evaluate the initial peripheral effect by means of these physiological data alone. Taken together, the psychophysiological results indicated the alteration of HEFs found in the current study were affected by subjective feeling of disgust, without significant changes in tonic myocardial activities detected by the heart rate variability analysis.

Besides the neural transfer relating to the myocardial activities, there assumed to be alternative conduit such as the humoral pathways involving circulating cytokines, and direct involvement *via* immune cells from the periphery. In addition, interoceptive processing is modulated by respiratory (67), gastrointestinal (68),

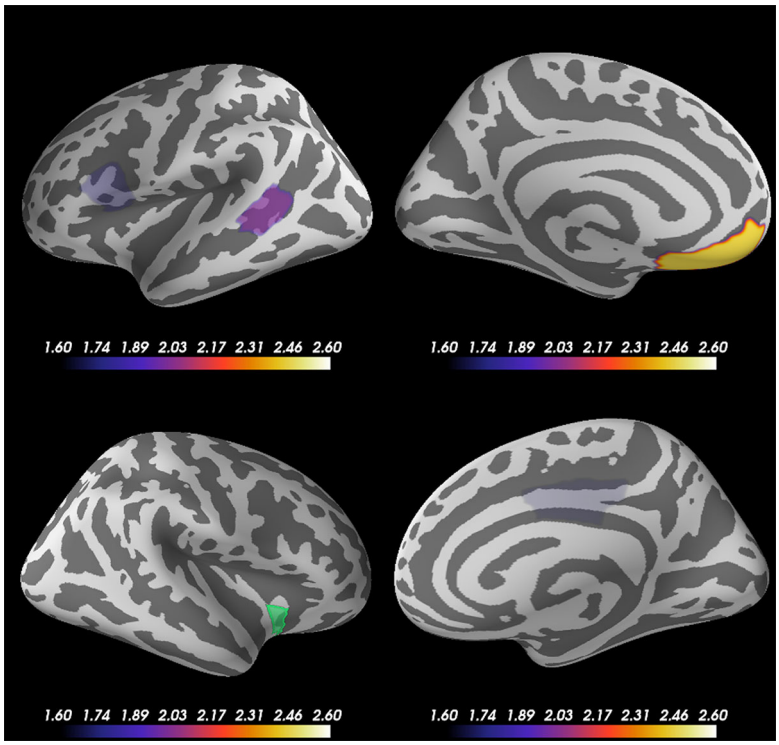

FIGURE 5 | Cortical regions showing significant changes in the phase lag index (PLI) between the right anterior ventral insular cortices. Statistical comparison between the two conditions (disgust/control) of the right anterior ventral sub-region of insular cortices and other brain regions (68 vertexes) using phase lag indexes (PLI) demonstrated significant increases between the right anterior ventral region of the insular cortices (green) and left ventromedial prefrontal cortex (VMPFC) at the beta frequency range of 14 Hz to 24 Hz. The other brain regions that exhibited significant changes of PLI between the right anterior ventral insular cortices were the left pars opercularis, right posterior cingulate, and left bank of the superior temporal sulcus. The color bar indicates the z-value determined using the Mann-Whitney U test of PLI between the right anterior ventral insular cortex and other cortical regions by conditions.

and genito-urinary information, in addition to the cardiovascular status. Given the nature of interoception, alternative analysis by measuring spontaneous activity towards other organs may reveal the different characteristics of interoceptive processing; however, the temporal advantages of utilizing MEG would be the most efficient for analyzing relatively highly frequent and periodic responses, i.e., myocardial activity, based on rather accumulating evidence. Since the current study utilized disgust emotion mainly affecting the insular cortices, the afferent information was delivered by either autonomic or somatosensory pathway. The former was mainly carried *via* the parasympathetic vagal nerve, which projects mainly to the anterior ventral insular cortices, whereas the latter partially projected directly through the posterior insular cortices. In order to investigate the evoked responses as a carrier signal from periphery, and representing cortical/subcortical patterns of activity, we have estimated the source-evoked time courses and ITCs by dividing the insular cortices in each hemisphere into three sub-regions (anterior dorsal, anterior ventral, and posterior insular cortices). No significant between-condition changes in source-evoked time courses were found, however, the significant differences in ITC—increasing at 19 and 23 Hz and decreasing at 14 Hz—were found only at the right anterior ventral insular sub-region. In addition, statistical analysis of PLIs using the Mann-Whitney U test revealed a significant connectivity change between the right anterior ventral insular cortex and left VMPFC. Since the current results were calculated by averaging the MEG signals triggered by spontaneously delivered bioelectrical cues directly from living organs (individual heartbeats), not by externally supplied cues, the averaged responses reflect more indigenous and induced activities. The current results support our hypothesis that spontaneous heartbeats evoke cortical activity that is associated with the perceptive consequences of inner bodily states according to emotional states. In particular, when subjects felt disgust, brain activity in the right insular cortices and connectivity of beta frequency between the right anterior ventral insular cortices and VMPFC increased. These results suggest that the insular cortices are core regions that mediate the physiological changes modulated by emotional state, and closely associated with the VMPFC in the processing and propagation of information to other brain regions. Although previous studies (69–71) have suggested that the processing of somatic information was performed with low beta frequency (14 to 24 Hz), our results provide additional information of the frequency property within the low beta frequency range both for suppression of 14 Hz and amplification of 19 and 23 Hz when people experience emotions as a consequence of their inner bodily state.

Beyond cortico-cortical networks in the brain, Harrison et al. (68) have reported there to be a relationship between cerebral blood flow and peripheral bodily status. The authors evaluated this correlation using both cardiac and gastric response, which were measured using a combination of functional magnetic resonance imaging (fMRI) and simultaneous recording of multiorgan physiological responses while observing motion pictures of disgust. The authors used two distinct forms of disgust that are defined using functionally different domains (72), i.e., "core disgust" and "body-boundary-violation (BBV) disgust" (73), which elicited two independent patterns of peripheral physiological responses as well as cortical activation. "Core disgust" refers to the feeling related to protecting the body from disease or infection (74–77), is usually provoked by images of the ingestion of spoiled food or vomit, and elicits changes in gastric and right dorsal insular activities. In contrast, "BBV disgust" is related to the denial of mortality, is usually induced by images of body mutilation, blood, and venesection, and evokes changes in cardiac power and left dorsal anterior insular cortex activity. Indeed, "core disgust" induces feelings of nausea, retching, and rapid-gastric activities (78–80), whereas "BBV disgust" evokes feelings of dizziness and lightheadedness, affects cardiovascular responses, and in extreme forms can manifest as vasovagal syncope for 3%–4% of the population (81). Interestingly, both types of disgust stimuli have been found to evoke similar activity in the anterior insula; "core disgust" elicited more activity in the ventral mid-anterior region, while "BBV disgust" activated the primary sensorimotor cortices and superior parietal region (82). Thus, the insular cortices may be the regions in which emotions are embodied, whereby inner bodily states are projected to the brain to perceive and regulate the subjective experience of emotions. Interoceptive afferent signals are conveyed to the dorsal posterior insular cortices, where a highly resolved and somatotopically organized cortical representation of the physiological condition of all bodily tissues is provided (83). Emotionally salient information is replicated repeatedly along regions spanning the anterior to posterior insular cortices, which enables progressive incorporation with multimodal information. The anterior insular cortices are connected to the amygdala, cingulate, ventral striatum, prefrontal, and multimodal sensory regions (84). These connections integrate homeostatic conditions (85) according to motivational, hedonic, cognitive, and social signals, which ultimately form the corresponding emotional state. Our results support these concepts and suggest that listening to sounds of disgust affects activity in the right anterior insular cortices, thereby forming the subjective experience of emotion.

The insular cortices have been identified as the main cortical target of the interoceptive information by organizing topographical bodily maps documented in contemporary neuroscience (5, 14, 83, 84, 86). Afferent feedback from bodily states will eventually be represented in the specific brain network that supply neural substrates of visceral feeling and interoceptive status. The VMPFC is also involved in this network as the trigger region to re-activate somatic patterns, and also as the endpoint where bodily changes in response to brain activity are referred back *via* the somatosensory and insular cortices (87). In addition, recent functional neuroimaging studies have also implicated the insular cortices in both interoceptive processing and emotional feelings (8, 9, 66) in collaborating with somatosensory cortices, such as SI and SII (29, 33), as well as the specific cortical network of default mode (34). Abnormal activity of cortical network implicated in these regions, i.e. high resting-state activity in the insular and limbic/subcortical regions as well as the hypoactivity in higher-level cortical regions, are associated to the clinical conditions of depressive state, including anhedonia, hopelessness, apathy, and particularly dysphoria (88), in extremely forms manifesting, e.g., Cotard syndrome (89). The insular cortices play a key role in executing these functions by representing and projecting information from the sensory feedback of inner bodily status (3, 90).

This study has several limitations that should be mentioned. First, it is unclear whether R or T of ECG triggering were suitable for averaging the HEFs. Although several reports have used T trigger averaging (34, 91), our alternative analysis using T peaks did not clearly identify major components as reported in previous studies. Given the nature of ECG characteristics, the R peak is more prominent than T triggers; averaging using R enables more robust, stable, and technically easier applications without any jittering. Therefore, the HEF components in our study may have been contaminated by ECG T wave components, as the T wave follows the R peak by approximately 400 ms. More convenient and reliable methods for averaging with the T peak should be evaluated. Future studies should examine whether utilizing R or T in individual ECG is superior for obtaining HEFs. The second limitation is related to individual differences in the strength of HEFs. The variations of interoceptive awareness mean that the strength of HEFs thereby vary considerably (18). These variations could be influential distracters in grand-averaging across subjects. Given the premise that one subject may have a greater influence in grand-averaging, an individual with greater responses would more strongly affect the tendency. As our results may contain individual differences, grand-averaged data could reflect unequal contributions among subjects. The third limitation is that our stimuli induce "core" disgust, which mainly results in a feeling of dysphoria in the stomach, without any quantifications of gastrointestinal activity. By excluding BBV disgust, such as bleeding or body mutilation, the stimuli may still have been insufficient for induction of pure "core" disgust due to the limited selection from IADS. As we could not fully evaluate the peripheral effects on interoceptive processing, including cardiovascular as well as gastrointestinal activity, the whole picture of interoceptive carrier and the interpretations on cortical or subcortical reflections still remain uncertain. In fact, gastrointestinal information was also carried regarding the chemical and inflammatory environment as well as the composition of gut bacteria and endocrine responses, is known to modify emotional function (92, 93). Indeed, the responses evoked by the current study may contain all the consequences resulting from presentation of the stimuli, thus future study is required to clarify the characteristics of interoceptive afferent information not only within the regional carrier but also beyond the cortical or subcortical activity constituting brain network, by supporting with the reinforced

findings both on behavioral and physiological data; here, the nature of information propagation may help our understanding of further forms of interoception associating to the clinical conditions with aberrant interoceptive processing.

Despite these limitations, the neuromagnetic dynamics demonstrated in the current study revealed HEF-evoked alterations in both activity and connectivity that were affected by emotional experiences. These results provide insights into the frequency properties of information propagation that occurs in the specific beta frequency. This novel method used heartbeat rhythms originating internally, i.e., spontaneous activity of a living organ and not using external stimuli, to determine how indigenous and induced brain activity develop. Moreover, this made it possible to adopt a block design, which is frequently used in fMRI and other brain imaging studies in translational research. Emotional experiences evoked by passive listening to sounds of disgust modulate the autonomic system, which can potentially give rise to alterations in HEFs *via* changes in activity of the right insular cortices and connectivity changes to the VMPFC.

CONCLUSION

The alteration of HEFs was investigated in 39 healthy volunteers in association with the subjective feeling of disgust, which evoked right insular cortical activity and the enhancement of cortical connectivity, within the beta frequency range, between the right anterior ventral insular cortex and the left ventromedial prefrontal cortex. Furthermore, the inter-trial coherence in the right anterior insular cortices increased at 19 Hz and 23 Hz, and decreased at 14 Hz, which highlights the involvement of low beta oscillations in emotional processing. The corticolimbic network, particularly involving the insular cortices, plays an important role in emotional regulation and perception. The current results provide a novel insight into the frequency properties of emotional processing, and suggest that emotional arousal impacts the autonomic nervous system, thus giving rise to the alteration of HEFs *via* connectivity changes in the anterior ventral insular cortex and ventromedial prefrontal cortex.

DATA AVAILABILITY STATEMENT

The raw data supporting the conclusions of this article will be made available by the authors, without undue reservation.

ETHICS STATEMENT

The studies involving human participants were reviewed and approved by Ethics Committee of Gunma University Graduate School of Medicine. The patients/participants provided their written informed consent to participate in this study.

AUTHOR CONTRIBUTIONS

YK and YT conceptualized, designed, and conducted the study. SU supported data analysis and interpretation. MM and MF supported the interpretations. YK and all co-authors corrected the manuscript. All authors contributed to the article and approved the submitted version.

FUNDING

This work was supported by the Japan Society for the Promotion of Science (Grant-in-Aid for Scientific Research on Innovative Areas; Science of personalized value development through adolescence: integration of brain, real-world, and life-course approaches), area B01 (16H06397), and Grants-in-Aid for Scientific Research B (15H04890, 16K19748). This work was also partially supported by the Japan Agency for Medical Research and Development, AMED (Strategic Research Program for Brain Sciences, Integrative Research on Depression, Dementia and Development Disorders [IR3D]; Development of diagnostic and therapeutic methods for depressive symptoms based on mesocorticolimbic system).

ACKNOWLEDGMENTS

We thank our volunteers for participating in this study. We also thank Itsuko Nishimura and Shinobu Nagai for their help with data acquisition.

SUPPLEMENTARY MATERIAL

The Supplementary Material for this article can be found online at: https://www.frontiersin.org/articles/10.3389/fpsyt.2020.00683/full#supplementary-material

REFERENCES

1. James W. What is an emotion? *Mind* (1884) 9:188–205. doi: 10.1093/mind/os-IX.34.188
2. Lange CG. *The emotions: a psychophysiological study*. Baltimore: Williams and Wilkins (1885).
3. Damasio A, Carvalho GB. The nature of feelings: evolutionary and neurobiological origins. *Nat Rev Neurosci* (2013) 14(2):143–52. doi: 10.1038/nrn3403
4. Schachter S, Singer JE. Cognitive, social, and physiological determinants of emotional state. *Psychol Rev* (1962) 69:379–99. doi: 10.1037/h0046234
5. Damasio AR. *Descartes" Error: Emotion, Reason, and the Human Brain*. New York: Grosset/Putnam (1994).
6. Cameron OG. Interoception: the inside story–a model for psychosomatic processes. *Psychosom Med* (2001) 63:697–710. doi: 10.1097/00006842-200109000-00001
7. Lane RD, McRae K, Reiman EM, Chen K, Ahern GL, Thayer JF. Neural correlates of heart rate variability during emotion. *Neuroimage* (2009) 44:213–22. doi: 10.1016/j.neuroimage.2008.07.056
8. Craig AD. How do you feel–now? The anterior insula and human awareness. *Nat Rev Neurosci* (2009) 10:59–70. doi: 10.1038/nrn2555

9. Critchley HD, Wiens S, Rotshtein P, Ohman A, Dolan RJ. Neural systems supporting interoceptive awareness. *Nat Neurosci* (2004) 7:189–95. doi: 10.1038/nn1176
10. Sherrington CS. *The integrative action of the nervous system*. New Haven, CT: Yale University Press (1906).
11. Gu X, FitzGerald TH. Interoceptive inference: homeostasis and decision-making. *Trends Cogn Sci* (2014) 18:269–70. doi: 10.1016/j.tics.2014.02.001
12. Craig AD. Interoception: the sense of the physiological condition of the body. *Curr Opin Neurobiol* (2003) 13:500–5. doi: 10.1016/s0959-4388(03)00090-4
13. Garfinkel SN, Critchley HD. Interoception, emotion and brain: new insights link internal physiology to social behaviour. Commentary on: "Anterior insular cortex mediates bodily sensibility and social anxiety" by Terasawa et al. (2012). *Soc Cogn Affect Neurosci* (2013) 8:231–4. doi: 10.1093/scan/nss140
14. Craig AD. How do you feel? Interoception: the sense of the physiological condition of the body. *Nat Rev Neurosci* (2002) 3:655–66. doi: 10.1038/nrn894
15. Wiens S. Interoception in emotional experience. *Curr Opin Neurol* (2005) 18:442–7. doi: 10.1097/01.wco.0000168079.92106.99
16. Herbert BM, Pollatos O, Schandry R. Interoceptive sensitivity and emotion processing: an EEG study. *Int J Psychophysiol* (2007) 65:214–27. doi: 10.1016/j.ijpsycho.2007.04.007
17. Pollatos O, Traut-Mattausch E, Schroeder H, Schandry R. Interoceptive awareness mediates the relationship between anxiety and the intensity of unpleasant feelings. *J Anxiety Disord* (2007) 21:931–43. doi: 10.1016/j.janxdis.2006.12.004
18. Terasawa Y, Moriguchi Y, Tochizawa S, Umeda S. Interoceptive sensitivity predicts sensitivity to the emotions of others. *Cogn Emot* (2014) 28:1435–48. doi: 10.1080/02699931.2014.888988
19. Stewart SH, Buffett-Jerrott SE, Kokaram R. Heartbeat awareness and heart rate reactivity in anxiety sensitivity: a further investigation. *J Anxiety Disord* (2001) 15:535–53. doi: 10.1016/s0887-6185(01)00080-9
20. Pollatos O, Traut-Mattausch E, Schandry R. Differential effects of anxiety and depression on interoceptive accuracy. *Depress Anxiety* (2009) 26:167–73. doi: 10.1002/da.20504
21. Schandry R. Heart beat perception and emotional experience. *Psychophysiol* (1981) 18:483–8. doi: 10.1111/j.1469-8986.1981.tb02486.x
22. Van der Does AJ, Van Dyck R, Spinhoven P. Accurate heartbeat perception in panic disorder: fact and artefact. *J Affect Disord* (1997) 43:121–30. doi: 10.1016/s0165-0327(96)01414-0
23. Mussgay L, Klinkenberg N, Rüddel H. Heart beat perception in patients with depressive, somatoform and personality disorders. *J Psychophysiol* (1999) 13:27–36. doi: 10.1027//0269-8803.13.1.27
24. Riordan H, Squires NK, Brener J. Cardio-cortical potentials: electrophysiological evidence for visceral perception. *Psychophysiology* (1990) 27:S59. doi: 10.1111/j.1469-8986.1990.tb02374.x
25. Montoya P, Schandry R, Müller A. Heartbeat evoked potentials (HEP): topography and influence of cardiac awareness and focus of attention. *Electroencephalogr Clin Neurophysiol* (1993) 88:163–72. doi: 10.1016/0168-5597(93)90001-6
26. Schandry R, Montoya P. Event-related brain potentials and the processing of cardiac activity. *Biol Psychol* (1996) 42:75–85. doi: 10.1016/0301-0511(95)05147-3
27. Dirlich G, Dietl T, Vogl L, Strian F. Topography and morphology of heart action-related EEG potentials. *Electroencephalogr Clin Neurophysiol* (1998) 108:299–305. doi: 10.1016/s0168-5597(98)00003-3
28. Leopold C, Schandry R. The heartbeat-evoked brain potential in patients suffering from diabetic neuropathy and in healthy control persons. *Clin Neurophysiol* (2001) 112:674–82. doi: 10.1016/s1388-2457(01)00480-1
29. Pollatos O, Kirsch W, Schandry R. Brain structures involved in interoceptive awareness and cardioafferent signal processing: a dipole source localization study. *Hum Brain Mapp* (2005) 26:54–64. doi: 10.1002/hbm.20121
30. Gray MA, Taggart P, Sutton PM, Groves D, Holdright DR, Bradbury D, et al. A cortical potential reflecting cardiac function. *Proc Natl Acad Sci USA* (2007) 104:6818–23. doi: 10.1073/pnas.0609509104
31. Schandry R, Sparrer B, Weitkunat R. From the heart to the brain: a study of heartbeat contingent scalp potentials. *Int J Neurosci* (1986) 30:261–75. doi: 10.3109/00207458608985677
32. Pollatos O, Schandry R. Accuracy of heartbeat perception is reflected in the amplitude of the heartbeat-evoked brain potential. *Psychophysiology* (2004) 41:476–82. doi: 10.1111/1469-8986.2004.00170.x
33. Canales-Johnson A, Silva C, Huepe D, Rivera-Rei Á., Noreika V, Garcia Mdel C, et al. Auditory feedback differentially modulates behavioral and neural markers of objective and subjective performance when tapping to your heartbeat. *Cereb Cortex* (2016) 25:4490–503. doi: 10.1093/cercor/bhv076
34. Park HD, Correia S, Ducorps A, Tallon-Baudry C. Spontaneous fluctuations in neural responses to heartbeats predict visual detection. *Nat Neurosci* (2014) 17:612–8. doi: 10.1038/nn.3671
35. Babo-Rebelo M, Wolpert N, Adam C, Hasboun D, Tallon-Baudry C. Is the cardiac monitoring function related to the self in both the default network and right anterior insula? *Philos Trans R Soc Lond B Biol Sci* (2017) 371:20160004. doi: 10.1098/rstb.2016.0004
36. Park HD, Bernasconi F, Bello-Ruiz J, Pfeiffer C, Salomon R, Blanke O. Transient modulations of neural responses to heartbeats covary with bodily self-consciousness. *J Neurosci* (2016) 36:8453–60. doi: 10.1523/JNEUROSCI.0311-16.2016
37. Sel A, Azevedo RT, Tsakiris M. Heartfelt self: cardio-visual integration affects self-face recognition and interoceptive cortical processing. *Cereb Cortex* (2017) 27:5144–55. doi: 10.1093/cercor/bhw296
38. Shao S, Shen K, Wilder-Smith EP, Li X. Effect of pain perception on the heartbeat evoked potential. *Clin Neurophysiol* (2011) 122:1838–45. doi: 10.1016/j.clinph.2011.02.014
39. Fukushima H, Terasawa Y, Umeda S. Association between interoception and empathy: evidence from heartbeat-evoked brain potential. *Int J Psychophysiol* (2011) 79:259–65. doi: 10.1016/j.ijpsycho.2010.10.015
40. Lechinger J, Heib DP, Gruber W, Schabus M, Klimesch W. Heartbeat-related EEG amplitude and phase modulations from wakefulness to deep sleep: Interactions with sleep spindles and slow oscillations. *Psychophysiology* (2015) 52:1441–50. doi: 10.1111/psyp.12508
41. Terhaar J, Viola FC, Bär KJ, Debener S. Heartbeat evoked potentials mirror altered body perception in depressed patients. *Clin Neurophysiol* (2012) 123:1950–7. doi: 10.1016/j.clinph.2012.02.086
42. Schulz A, Köster S, Beutel ME, Schächinger H, Vögele C, Rost S, et al. Altered patterns of heartbeat-evoked potentials in depersonalization/derealization disorder: neurophysiological evidence for impaired cortical representation of bodily signals. *Psychosom Med* (2015) 77:506–16. doi: 10.1097/PSY.0000000000000195
43. Müller LE, Schulz A, Andermann M, Gäbel A, Gescher DM, Spohn A, et al. Cortical representation of afferent bodily signals in borderline personality disorder: neural correlates and relationship to emotional dysregulation. *JAMA Psychiat* (2015) 72:1077–86. doi: 10.1001/jamapsychiatry.2015.1252
44. Oldfield RC. The assessment and analysis of handedness: the Edinburgh inventory. *Neuropsychologia* (1971) 9:97–113. doi: 10.1016/0028-3932(71)90067-4
45. Bradley MM. *The International Affective Digitized Sounds (2nd edition; IADS-2): affective ratings of sounds and instruction manual (Tech. Rep. B-3)*. Gainesville, FL: University of Florida (2007).
46. Darwin CR. *The Expression of Emotions in Man and Animals*. London: John Murray (1872).
47. Hoddes E, Zarcone V, Smythe H, Phillips R, Dement WC. Quantification of sleepiness: a new approach. *Psychophysiology* (1973) 10:431–6. doi: 10.1111/j.1469-8986.1973.tb00801.x
48. Taulu S, Kajola M, Simola J. Suppression of interference and artifacts by the Signal Space Separation Method. *Brain Topogr* (2004) 16:269–75. doi: 10.1023/b:brat.0000032864.93890.f9
49. Taulu S, Simola J. Spatiotemporal signal space separation method for rejecting nearby interference in MEG measurements. *Phys Med Biol* (2006) 51:1759–68. doi: 10.1088/0031-9155/51/7/008
50. Dale AM, Fischl B, Sereno MI. Cortical surface-based analysis. I. Segmentation and surface reconstruction. *Neuroimage* (1999) 9:179–94. doi: 10.1006/nimg.1998.0395
51. Fischl B, Sereno MI, Dale AM. Cortical surface-based analysis: II: Inflation, flattening, and a surface-based coordinate system. *Neuroimage* (1999) 9:195–207. doi: 10.1006/nimg.1998.0396

52. Hämäläinen MS, Sarvas J. Realistic conductivity geometry model of the human head for interpretation of neuromagnetic data. *IEEE Trans Biomed Eng* (1989) 36:165–71. doi: 10.1109/10.16463
53. Gramfort A, Luessi M, Larson E, Engemann DA, Strohmeier D, Brodbeck C, et al. MNE software for processing MEG and EEG data. *Neuroimage* (2014) 86:446–60. doi: 10.1016/j.neuroimage.2013.10.027
54. Hashizume A, Hironaga N. Principles of Magnetoencephalography. In: Tobimatsu S, Kakigi R, editors. *Clinical Applications of Magnetoencephalography*. Tokyo: Springer Japan (2016). p. 3–32.
55. Hayamizu M, Hagiwara K, Hironaga N, Ogata K, Hoka S, Tobimatsu S. A spatiotemporal signature of cortical pain relief by tactile stimulation: An MEG study. *Neuroimage* (2016) 130:175–83. doi: 10.1016/j.neuroimage.2016.01.065
56. Lin FH, Witzel T, Ahlfors SP, Stufflebeam SM, Belliveau JW, Hämäläinen MS. Assessing and improving the spatial accuracy in MEG source localization by depth-weighted minimum-norm estimates. *Neuroimage* (2006) 31:160–71. doi: 10.1016/j.neuroimage.2005.11.054
57. Desikan RS, Ségonne F, Fischl B, Quinn BT, Dickerson BC, Blacker D, et al. An automated labeling system for subdividing the human cerebral cortex on MRI scans into gyral based regions of interest. *Neuroimage* (2006) 31:968–80. doi: 10.1016/j.neuroimage.2006.01.021
58. Destrieux C, Fischl B, Dale A, Halgren E. Automatic parcellation of human cortical gyri and sulci using standard anatomical nomenclature. *Neuroimage* (2010) 53:1–15. doi: 10.1016/j.neuroimage.2010.06.010
59. Chang LJ, Yarkoni T, Khaw MW, Sanfey AG. Decoding the role of the insula in human cognition: functional parcellation and large-scale reverse inference. *Cereb Cortex* (2013) 23:739–49. doi: 10.1093/cercor/bhs065
60. Gramfort A, Luessi M, Larson E, Engemann DA, Strohmeier D, Brodbeck C, et al. MEG and EEG data analysis with MNE-Python. *Front Neurosci* (2013) 7:267. doi: 10.3389/fnins.2013.00267
61. Stam CJ, Nolte G, Daffertshofer A. Phase lag index: assessment of functional connectivity from multi channel EEG and MEG with diminished bias from common sources. *Hum Brain Mapp* (2007) 28:1178–93. doi: 10.1002/hbm.20346
62. Jones E, Oliphant E, Peterson P. (2001). *SciPy: Open Source Scientific Tools for Python*. http://www.scipy.org.
63. Deen B, Pitskel NB, Pelphrey KA. Three systems of insular functional connectivity identified with cluster analysis. *Cereb Cortex* (2011) 21:1498–506. doi: 10.1093/cercor/bhq186
64. Klein TA, Ullsperger M, Danielmeier C. Error awareness and the insula: links to neurological and psychiatric diseases. *Front Hum Neurosci* (2013) 7:14. doi: 10.3389/fnhum.2013.00014
65. Wicker B, Keysers C, Plailly J, Royet JP, Gallese V, Rizzolatti G. Both of us disgusted in My insula: the common neural basis of seeing and feeling disgust. *Neuron* (2003) 40:655–64. doi: 10.1016/s0896-6273(03)00679-2
66. Singer T, Seymour B, O'Doherty J, Kaube H, Dolan RJ, Frith CD. Empathy for pain involves the affective but not sensory components of pain. *Science* (2004) 303:1157–62. doi: 10.1126/science.1093535
67. Garfinkel SN, Manassei MF, Hamilton-Fletcher G, In den Bosch Y, Critchley HD, Engels M. Interoceptive dimensions across cardiac and respiratory axes. *Philos Trans R Soc B* (2016) 371:20160014. doi: 10.1098/rstb.2016.0014
68. Harrison NA, Gray MA, Gianaros PJ, Critchley HD. The embodiment of emotional feelings in the brain. *J Neurosci* (2010) 30:12878–84. doi: 10.1523/JNEUROSCI.1725-10.2010
69. Hari R, Salmelin R. Human cortical oscillations: a neuromagnetic view through the skull. *Trends Neurosci* (1997) 20:44–9. doi: 10.1016/S0166-2236(96)10065-5
70. Farmer SF. Rhythmicity, synchronization and binding in human and primate motor systems. *J Physiol* (1998) 509:3–14. doi: 10.1111/j.1469-7793.1998.003bo.x
71. Jensen O, Goel P, Kopell N, Pohja M, Hari R, Ermentrout B. On the human sensorimotor-cortex beta rhythm: sources and modeling. *Neuroimage* (2005) 26:347–55. doi: 10.1016/j.neuroimage.2005.02.008
72. Tybur JM, Lieberman D, Kurzban R, DeScioli P. Disgust: evolved function and structure. *Psychol Rev* (2013) 120:65–84. doi: 10.1037/a0030778
73. Rozin P, Lowery L, Ebert R. Varieties of disgust faces and the structure of disgust. *J Pers Soc Psychol* (1994) 66:870–81. doi: 10.1037//0022-3514.66.5.870
74. Haidt J, McCauley C, Rozin P. Individual differences in sensitivity to disgust: A scale sampling seven domains of disgust elicitors. *Pers Indiv Differ* (1994) 16:701–13. doi: 10.1016/0191-8869(94)90212-7
75. Haidt J, Rozin P, McCauley C, Imada S. Body, psyche, and culture: The relationship of disgust to morality. *Psychol Dev Soc* (1997) 9:107–31. doi: 10.1177/097133369700900105
76. Rozin P, Haidt J, McCauley CR. Disgust. In: Lewis M, Haviland-Jones JM, Barrett LF editors. *Handbook of emotions, 3rd ed.* New York, NY: Guilford Press (2008). p. 757–76.
77. Rozin P, Haidt J, McCauley CR. Disgust: The body and soul emotion in the 21st century. In: McKay D, Olatunji O, editors. *Disgust and its disorders*. Washington, DC: American Psychological Association (2009). p. 9–29.
78. Stern RM, Crawford HE, Stewart WR, Vasey MW, Koch KL. Sham feeding. Cephalic-vagal influences on gastric myoelectric activity. *Dig Dis Sci* (1989) 34:521–7. doi: 10.1007/bf01536327
79. Stern RM, Jokerst MD, Levine ME, Koch KL. The stomach's response to unappetizing food: cephalic-vagal effects on gastric myoelectric activity. *Neurogastroenterol Motil* (2001) 13:151–4. doi: 10.1046/j.1365-2982.2001.00250.x
80. Gianaros PJ, Quigley KS, Mordkoff JT, Stern RM. Gastric myoelectrical and autonomic cardiac reactivity to laboratory stressors. *Psychophysiology* (2001) 38:642– 652. doi: 10.1111/1469-8986.3840642
81. Accurso V, Winnicki M, Shamsuzzaman AS, Wenzel A, Johnson AK, Somers VK. Predisposition to vasovagal syncope in subjects with blood/injury phobia. *Circulation* (2001) 104:903–7. doi: 10.1161/hc3301.094910
82. Wright P, He G, Shapira NA, Goodman WK, Liu Y. Disgust and the insula: fMRI responses to pictures of mutilation and contamination. *Neuroreport* (2004) 15:2347–51. doi: 10.1097/00001756-200410250-00009
83. Damasio AR, Grabowski TJ, Bechara A, Damasio H, Ponto LL, Parvizi J, et al. Subcortical and cortical brain activity during the feeling of self-generated emotions. *Nat Neurosci* (2000) 3:1049–56. doi: 10.1038/79871
84. Mufson EJ, Mesulam MM. Insula of the old-world monkey. II: Afferent cortical input and comments on the claustrum. *J Comp Neurol* (1982) 212:23–37. doi: 10.1002/cne.902120103
85. Andrew D, Craig AD. Spinothalamic lamina I neurons selectively responsive to cutaneous warming in cats. *J Physiol* (2001) 537:489–95. doi: 10.1111/j.1469-7793.2001.00489.x
86. Damasio AR. The somatic marker hypothesis and the possible functions of the prefrontal cortex. *Philos Trans R Soc Lond B Biol Sci* (1996) 351:1413–20. doi: 10.1098/rstb.1996.0125
87. Bechara A. The role of emotion in decision-making: evidence from neurological patients with orbitofrontal damage. *Brain Cogn* (2004) 55:30–40. doi: 10.1016/j.bandc.2003.04.001
88. Northoff G, Wiebking C, Feinberg T, Panksepp J. The 'resting-state hypothesis' of major depressive disorder–A translational subcortical–cortical framework for a system disorder. *Neurosci Biobehav Rev* (2011) 35:1929–45. doi: 10.1016/j.neubiorev.2010.12.007
89. Seth AK. Interoceptive inference, emotion, and the embodied self. *Trends Cognit Sci* (2013) 17(11):565–73. doi: 10.1016/j.tics.2013.09.007
90. Bechara A, Damasio AR. The somatic marker hypothesis: a neural theory of economic decision. *Games Econ Behav* (2005) 52:336–72. doi: 10.1016/j.geb.2004.06.010
91. Babo-Rebelo M, Richter CG, Tallon-Baudry C. Neural responses to heartbeats in the default network encode the self in spontaneous thoughts. *J Neurosci* (2016) 36:7829–40. doi: 10.1523/JNEUROSCI.0262-16.2016
92. Mayer EA. Gut feelings: the emerging biology of gut-brain communication. *Nat Rev Neurosci* (2011) 12:453–66. doi: 10.1038/nrn3071
93. Mayer EA, Knight R, Mazmanian SK, Cryan JF, Tillisch K. Gut microbes and the brain: paradigm shift in neuroscience. *J Neurosci* (2014) 34:15490–6. doi: 10.1523/JNEUROSCI.3299-14.2014

Conflict of Interest: The authors declare that the research was conducted in the absence of any commercial or financial relationships that could be construed as a potential conflict of interest.

frontiers in Psychiatry

ORIGINAL RESEARCH
published: 04 August 2020
doi: 10.3389/fpsyt.2020.00743

Reduced Dorsal Visual Oscillatory Activity During Working Memory Maintenance in the First-Episode Schizophrenia Spectrum

*Brian A. Coffman[1], Gretchen Haas[2], Carl Olson[3], Raymond Cho[2,4], Avniel Singh Ghuman[5] and Dean F. Salisbury[1]**

[1] Clinical Neurophysiology Research Laboratory, Western Psychiatric Hospital of UPMC, Department of Psychiatry, University of Pittsburgh School of Medicine, Pittsburgh, PA, United States, [2] Western Psychiatric Hospital of UPMC, Department of Psychiatry, University of Pittsburgh School of Medicine, Pittsburgh, PA, United States, [3] Center for Neural Basis of Cognition, Carnegie Mellon University, Pittsburgh, PA, United States, [4] Department of Psychiatry and Behavioral Sciences, Baylor College of Medicine, Houston, TX, United States, [5] Laboratory of Cognitive Neurodynamics, Department of Neurosurgery, Presbyterian Hospital, University of Pittsburgh School of Medicine, Pittsburgh, PA, United States

OPEN ACCESS

Edited by:
Peter Uhlhaas,
University of Glasgow,
United Kingdom

Reviewed by:
Till R Schneider,
University of Hamburg, Germany
Tineke Grent-'T-Jong,
University of Glasgow,
United Kingdom

***Correspondence:**
Dean F. Salisbury
SalisburyD@upmc.edu

Specialty section:
This article was submitted to Neuroimaging and Stimulation, a section of the journal Frontiers in Psychiatry

Received: 07 April 2020
Accepted: 16 July 2020
Published: 04 August 2020

Citation:
Coffman BA, Haas G, Olson C, Cho R, Ghuman AS and Salisbury DF (2020) Reduced Dorsal Visual Oscillatory Activity During Working Memory Maintenance in the First-Episode Schizophrenia Spectrum. Front. Psychiatry 11:743. doi: 10.3389/fpsyt.2020.00743

Cognitive deficits in people with schizophrenia are among the hardest to treat and strongly predict functional outcome. The ability to maintain sensory precepts in memory over a short delay is impacted early in the progression of schizophrenia and has been linked to reliable neurophysiological markers. Yet, little is known about the mechanisms of these deficits. Here, we investigated possible neurophysiological mechanisms of impaired visual short-term memory (vSTM, aka working memory maintenance) in the first-episode schizophrenia spectrum (FESz) using magnetoencephalography (MEG). Twenty-eight FESz and 25 matched controls performed a lateralized change detection task where they were cued to selectively attend and remember colors of circles presented in either the left or right peripheral visual field over a 1 s delay. Contralateral alpha suppression (CAS) during the delay period was used to assess selective attention to cued visual hemifields held in vSTM. Delay-period CAS was compared between FESz and controls and between trials presenting one vs three items per visual hemifield. CAS in dorsal visual cortex was reduced in FESz compared to controls in high-load trials, but not low-load trials. Group differences in CAS were found beginning 100 ms after the disappearance of the memory set, suggesting deficits were not due to the initial deployment of attention to the cued visual hemifield prior to stimulus presentation. CAS was not greater for high-load vs low-load trials in FESz subjects, although this effect was prominent in controls. Further, lateralized gamma (34–40 Hz) power emerged in dorsal visual cortex prior to the onset of CAS in controls but not FESz. Gamma power in this cluster differed between groups at both high and low load. CAS deficits observed in FESz were correlated with change detection accuracy, working memory function, estimated IQ, and negative symptoms. Our results implicate deficits in CAS in trials requiring broad, but not narrow, focus of attention to spatially distributed objects maintained in vSTM in FESz, possibly due to reduced ability to broadly distribute visuospatial attention (alpha) or disruption of

object-location binding (gamma) during encoding/consolidation. This early pathophysiology may shed light upon mechanisms of emerging working memory deficits that are intrinsic to schizophrenia.

Keywords: first-episode schizophrenia, magnetoencephalography, visual short-term memory, working memory, alpha, gamma

INTRODUCTION

People with schizophrenia have reduced capacity to maintain visual information in the focus of attention and working memory over short periods of time (1, 2). This deficit in visual short-term memory (vSTM), otherwise known as visual working memory maintenance (3, 4), may contribute to a variety of cognitive impairments in schizophrenia (5, 6). Working memory impairment is observable even at the first episode of psychosis (7, 8), and has been linked to functional outcome (9, 10). Neurophysiologically, people with schizophrenia show reduced activity during the delay between encoding and retrieval in frontal (11, 12) and parieto-occipital cortical areas (13, 14) when multiple items are held in vSTM. The mechanism of these impairments, however, remains unclear. Some have proposed that inefficiency of specific aspects of working memory performance, such as selective attention or consolidation, may account for observed vSTM deficits (13, 15). Although psychomotor processing speed is generally reduced in schizophrenia (16), covert attentional orienting/selection of stimuli during encoding is not delayed or reduced (17), ruling out problems in initial processing. Similarly, duration of the maintenance period does not seem to impact schizophrenia-related deficits in performance beyond about 1 s for visual stimuli (8, 18, 19), ruling out interference from distraction or increased decay of the percept. Thus, vSTM impairments in schizophrenia likely occur early in maintenance, possibly during consolidation of the percept.

A common method for assessing vSTM is visual change detection. In a typical change detection task, subjects maintain an image in working memory over a short delay period and indicate whether any item(s) in a later probe image has/have changed. The number of items presented (memory load) is manipulated and performance (e.g. *K*, an estimate of the number of items stored in memory) is compared between trials of varying load (3, 20). Although the task is quite simple, the outcome (*K*) depends on multiple factors. Poor performance could stem from errors during encoding, maintenance, or retrieval and could be related to poor orienting, feature selection/analysis, consolidation, accelerated decay of representations in working memory, interference from other sources of information, problems with executing an appropriate behavioral response, or any combination thereof. By directing attention to specific visual fields, some of these factors can be separated. In the lateralized change detection task, stimuli are presented peripherally, and participants are asked to remember the items from one visual hemifield while ignoring the other. This results in lateralized perceptual representations in posterior cortical areas not only during encoding, but also throughout the delay period, and concomitant lateralized neurophysiological responses measurable with magnetoencephalography (MEG). This enables comparison of neurophysiology between cortical hemispheres, providing a powerful within-subject control condition for measurement of group differences.

Contralateral alpha suppression (CAS) is the reduction from baseline of alpha band (8–12 Hz) spectral power contralateral to the focus of visual attention. CAS reflects the spatial focus of selective attention to external stimuli and to internally-generated perceptual representations (21, 22), making CAS a prime candidate for investigating selective attention during vSTM maintenance. Alpha oscillations in posterior cortex generally index the inhibition of ongoing neural activity (23), and may have a causal role in perceptual attention, with increased alpha in areas with inhibited processing of distractor stimuli, and reduced alpha activity in areas representing to-be-remembered perceptual activity. When applied externally *via* transcranial magnetic stimulation, perturbations in parieto-occipital alpha-band oscillations (but not beta- or theta-band) alter neural excitability, with diminished visual perceptual ability in visual field contralateral to the stimulated hemisphere, and increased ability in the ipsilateral visual field (24). In contrast, prior research on visual stimulus evoked oscillations suggests that low-frequency (LF) gamma band (30–40 Hz) spectral power these represents local excitatory/inhibitory network activity. Further, parieto-occipital LF gamma power perturbations contralateral to the attended visual stimulus are thought to index attentional perceptual mechanisms such as feature binding, scene segmentation, and/or stimulus representation (25). It is unknown if contralateral LF gamma power modulation can be identified within cortical generators of CAS or whether these phenomena are correlated. Gamma deficits in schizophrenia have been observed in a variety of contexts, including auditory (26, 27) and visual (28) sensation, and in frontal areas during working memory updating (29). However, effects of schizophrenia on contralateral parieto-occipital LF gamma power modulation during vSTM have not been investigated previously.

Reduced CAS during covert visual attention (30) and reduced (non-lateralized) alpha suppression during vSTM maintenance (22) have been reported in long-term schizophrenia. However, schizophrenia-related deficits in CAS have not been assessed during vSTM maintenance, and CAS deficits have not been reported early in the disease course. Here we used MEG to investigate CAS as a possible neurophysiological mechanism of vSTM impairment in people at first episode of schizophrenia-spectrum psychosis (FESz). This population is ideal for investigating cognitive deficits in early-stage schizophrenia, as medication effects have not yet become a confound for assessment of behavioral and neurophysiological responses. Further, to investigate whether cortical generators of CAS show

co-localized and concomitant LF gamma power modulation, and given the long history and wide literature base showing deficits in selective attention (31–33) as well as disruptions in LF gamma oscillatory responses in both first-episode and long-term schizophrenia (27, 34–36), we examined broader spectral power differences in parieto-occipital sources of CAS.

METHODS

Participants

Twenty-eight individuals with FESz and 25 HC participants were included in the study. Subjects were screened for colorblindness using pseudoisochromatic plates and had at least nine years of schooling as well as an estimated IQ over 85. None of the participants had: a) history of concussion or head injury with sequelae, b) history of alcohol or drug addiction or detox in the last five years, or c) presence of neurological disease or disorder. Participants provided voluntary informed consent and were compensated for participation. Procedures were approved by the University of Pittsburgh Institutional Review Board (IRB).

All participants completed the MATRICS Cognitive Consensus Battery (MCCB) (37), the Hollingshead Index of Socioeconomic Status (SES) (38) and the Wechsler Abbreviated Scale of Intelligence (WASI-I) (39). See **Table 1** for demographic measures. Research diagnoses were based on a consensus conference of baseline research assessment and confirmed 6 months after initial clinical assessment based on all longitudinal data at the 6-month follow-up assessment. Diagnostic status for all FESz and HC participants was based on findings from the Structured Clinical Interview for DSM-IV (SCID-IV) and consensus conference review. One FESz participant was lost to follow-up and therefore remains with the diagnosis of Schizophreniform Disorder (Provisional). Symptoms were rated using the Positive and Negative Symptom Scale (PANSS), Scale for Assessment of Positive Symptoms (SAPS), and Scale for Assessment of Negative Symptoms (SANS). All interviews and tests were conducted by an expert (Masters'- or PhD-level) clinical assessor (see **Table 2** for clinical measures). Of the 28 FESz participants, 18 received diagnoses of schizophrenia (paranoid: n=8; undifferentiated: n=8; residual: n=2), 4 of schizoaffective disorder (depressed subtype), and 6 of psychotic disorder not otherwise specified (NOS). All FESz participated within their first episode of psychosis and had less than 2 months of lifetime antipsychotic medication exposure. Eleven FESz (39.2%) were medication-naive.

Procedures

Participants performed a lateralized change detection task (**Figure 1**). They were cued to covertly attend one visual hemifield (direction cue, 1.5° visual angle, 500 ms duration). An array of 1 (low-load) or 3 (high-load) filled colored circles was then presented in each hemifield (memory array) for 200 ms. One second later, another array was presented (probe) and participants indicated by button press with the right pointer or middle finger whether one of the circles in the attended hemifield had chane per hemifield). Participants were instructed to ignore changes in the unattended hemifield. The mapping of buttons (pointer/middle) to responses (change/no-change) was counterbalanced across participants. The following trial categories were equiprobable: no change, attended hemifield change, unattended hemifield change, or change in both hemifields. Thus, target responses (change/no-change) were also equiprobable. Participants had 2,000 ms to respond before the next trial. Circles could be one of 6 colors selected for equivalent luminance and color contrast. Circles subtended 0.65° and spatial locations were randomly selected from a 3° x 7° grid presented 1.5° to the left/right of central fixation. Stimuli

TABLE 1 | Participant Demographics and Neuropsychological Scores.

	Mean ± SD		t/χ^2	p
	FESz	HC		
Sociodemographic data				
Age (years)	23.0 ± 4.8	21.6 ± 4.5	1.1	0.268
Sex (M/F)	18/10	16/9	0.1	0.983
Participant SES	29.6 ± 13.1	33.9 ± 15.2	−1.0	0.303
Parental SES	41.9 ± 13.6	47.9 ± 12.9	−1.6	0.117
Education (years)	12.6 ± 2.5	13.8 ± 3.1	−1.5	0.136
Neuropsychological Tests				
WASI IQ	107.9 ± 16.9	107.1 ± 9.4	−0.2	0.829
MCCB—Processing speed	42.5 ± 15.3	51.6 ± 8.3	2.7	**0.009**
MCCB—Attention	40.8 ± 11.5	46.2 ± 9	1.9	0.063
MCCB—Working memory	41.9 ± 14.5	46.8 ± 8.7	1.5	0.138
MCCB—Verbal learning	44.5 ± 11.2	51.1 ± 8.7	2.4	**0.020**
MCCB—Visual learning	40.6 ± 13	44.9 ± 8.1	1.4	0.157
MCCB—Reasoning	44.7 ± 12	50.9 ± 8	2.2	**0.030**
MCCB—Social cognition	45.6 ± 13.7	54.5 ± 9.1	2.8	**0.008**
MCCB—Total	38.6 ± 14.8	49.1 ± 6.7	3.3	**0.002**

Descriptive and inferential statistics are reported for first-episode schizophrenia subjects (FESz) and healthy controls (HC). Significant p-values are bolded. All other differences are non-significant ($p > 0.05$).

FES, first-episode schizophrenia; HC, healthy control; SES, Socioeconomic Status; WASI, Wechsler Abbreviated Scale.

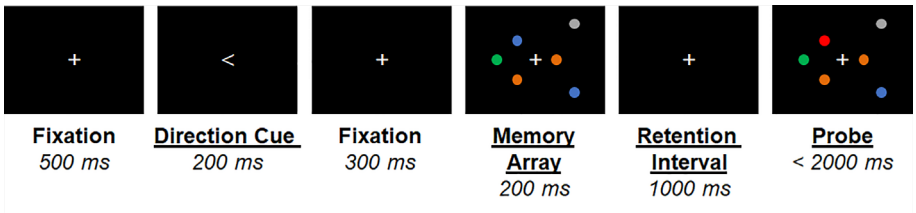

FIGURE 1 | Graphical depiction of the lateralized visual short-term memory (vSTM) task. An example trial is shown for the attend-right high memory load condition. Timing of stimuli presented is shown below each stimulus.

were presented in five blocks of 75 trials, with short (~2 min) breaks between trials. The direction cue orientation, trial category, number of circles presented (low or high load), and spatial locations of the circles within the 3° x 7° grid were all randomly selected at the start of each trial.

MEG

MEG data were obtained in a magnetically shielded room (Imedco AG, Hägendorf, Switzerland) using a a 306-channel whole-head MEG system (Elekta Neuromag) with a sampling rate of 1,000 Hz (online half-power band pass filter = 0.1–330 Hz). Bipolar leads were placed above and below the left eye (VEOG) and lateral to the outer canthi of both eyes (HEOG). Bipolar ECG leads were placed just below the left and right clavicle. Four head position indicator (HPI) coils were placed on the head and locations (relative to the nasion and preauricular points) were recorded using a 3D-digitizer (ISOTRAK; Polhemus, Inc., Colchester, VT). Head position was tracked continuously throughout the experiment.

Structural MRI

Structural MRIs were obtained for use in MEG source modeling. Sagittal T1-weighted anatomical MR images were obtained using a Siemens TIM Trio 3 Tesla MRI system with a multi-echo 3D MPRAGE sequence [relaxation time/echo time/inversion time = 2530/1.74, 3.6, 5.46, 7.32/1260 ms, flip angle = 7°, field of view (FOV) = 220 x 220 mm, 1 mm isotropic voxel size, 176 slices, GRAPPA acceleration factor = 2].

MEG Signal Preprocessing

The temporal extension of the Signal Space Separation method (40, 41) was used to remove noise sources outside of the MEG helmet and MEG sensor data were corrected for head motion using the Neuromag MaxFilter software (40). Using the MATLAB-based EEGLAB Toolbox (42), channels/segments with excessive noise or transient muscle artefacts were removed *via* visual inspection and a high-pass filter (0.5 Hz; 12 dB/oct) was applied. Adaptive Mixture ICA (AMICA) (43–45) was then performed to detect and remove one eye-blink and a maximum of 2 ECG components (representing pulsation and/or QRS artefacts) for each subject. Some subjects (N=5) did not present detectable ECG artefacts in the MEG signal. Components were identified based on their topography and temporal dynamics. All removed components were well-isolated (i.e. no additional blink/pulsation/QRS component was identified).

MEG Analysis

The MEG sensor locations were registered to structural images using MRIlab (Elekta-Neuromag Oy, Helsinki, Finland). The locations of possible dipole sources were constrained to the gray/white matter boundary segmented from the structural MRI data using Freesurfer (http://www.surfer.nmr.mgh.harvard.edu) (46–48). This boundary was tessellated into an icosohedron with 5 mm spacing between vertices, resulting in a source model with ~5,000 current locations per hemisphere. A forward solution was modeled as a single-shell (homogenous tissue) boundary-element model. The noise covariance matrix (calculated from the baseline interval of each trial) and forward solution were then used to create a linear inverse operator using a loose orientation constraint of 0.4 (0=current dipoles must be normal to the cortex; 1=no constraint) (49), with depth weighting applied. Continuous MEG data were filtered (100 Hz low-pass; 24 dB/oct) and source activity was then estimated from 204 planar gradiometer channels using MNE (50). After source modeling, correct trials were segmented from 300 ms before direction cue onset (i.e. 800 ms prior to memory array onset) to 500 ms after probe stimulus onset (i.e. 1,700 ms prior to memory array onset), and trials were rejected in which the magnetic field in any gradiometer exceeded 5 pT difference from baseline or eye movements were detected. Eye movements were detected in the HEOG channel using a step function, with a moving window or 200 ms duration with rejection criterion of +25 μV (51). Morlet wavelet deconvolution was then applied using 5 cycles at 1 Hz increments from 3 to 40 Hz, and event-related spectral perturbation was calculated as the relative change from baseline for each frequency measured. ROI analyses were performed on these native-space data, while vertex-wise analyses were performed on data morphed into a common space (fsaverage/MNI-305) with 10 mm smoothing.

Analysis of source-level time-frequency data then proceeded in a two-step analysis. First, to identify the generators of CAS, mean 8–12 Hz frequency power during vSTM maintenance (averaged from 200 to 1,200 ms after memory set onset) was assessed with vertex-wise one-sample t-tests across all subjects, separately for remember-left and remember-right trials. Parametric maps were corrected for multiple comparisons using spatial-cluster-based permutation testing with 1,000 iterations, using a cluster-forming threshold of $p<0.05$ and minimum cluster size of eight vertices (52). Regional labels corresponding to clusters of significant differences between

TABLE 2 | Patient Characteristics.

Symptoms	
PANSS—General	39.7 ± 6.8
PANSS—Negative	17.9 ± 4.9
PANSS—Positive	21.1 ± 5.1
PANSS—Total	78.7 ± 13.7
Medication data	
Cpz. equivalent dose (mg)*	218.6 ± 142.9
Medicated**/unmedicated	17/11

Descriptive statistics (mean ± SD) are reported for clinical variables and medication status for first-episode schizophrenia subjects.
*** Of the 17 medicated participants, 13 were prescribed Risperidone, 5 were prescribed Olanzapine, and 2 were prescribed Aripriprazole (3 participants were prescribed two medications).*
**Cpz equivalent dose is calculated only for medicated participants*
PANSS, Positive and Negative Symptom Scale.

high- and low-load were then identified from the Destrieux atlas implemented in Freesurfer. In the second step, average time-frequency maps were generated for each ROI, separately for each cortical hemisphere and stimulus condition. ROI-averaged time-frequency data ipsilateral to the attended hemifield were subtracted from those contralateral, and contralateral-ipsilateral difference spectra in high and low load conditions were compared between groups across the 3–40 Hz frequency spectrum and 200–1,200 ms retention interval time window using two separate time-frequency-cluster-based permutation tests (1,000 iterations, cluster-forming threshold of $p<0.05$, minimum cluster size of 8 contiguous time-frequency data points). Power within group-difference lateralized time/frequency cluster were then compared using separate 2 (group: HC vs. FESz) x 2 (load: high vs low) repeated-measures ANOVAs to identify possible group X load interactions.

Demographic, Clinical, and Behavioral Data Analysis

Demographics and neurocognitive measures were compared between groups using independent samples t-tests and chi-square tests where appropriate. Task behavioral data including vSTM capacity (*K*) and reaction time (correct trials only) were subjected to a 2 (group: HC vs. FESz) x 2 (load: high vs low) repeated-measures ANOVA. *K* was calculated according to Rouder et al. (53) as the number of items to be remembered (*S*), multiplied by the ratio of the difference between hit rate (H) and false alarm rate (FA) to the correct rejection rate (1-FA), expressed as $K=S*(H-FA)/(1-FA)$. Pearson correlations were computed separately for HC and FESz to explore relationships between behavioral and neurophysiological measures of working memory (K, RT, and contralateral-ipsilateral differential alpha/LF gamma power in high and low load conditions), and clinical/cognitive variables.

RESULTS

Behavior

vSTM capacity (*K*) was lower in FESz than HC ($F_{(1,50)}=7.5$; $p=0.008$; **Table 3**). An interaction between group and memory load ($F_{(1,50)}=4.7$; $p=0.035$) was driven by greater vSTM capacity differences across groups at high memory load (t_{50} = 2.61; $p=0.002$) as compared to low load (t_{50} = 2.97; $p=0.005$). Differences between conditions were significant within both groups (p's<0.001).

Response times were significantly slower for FESz compared to HC ($F_{(1,50)}=7.7$; $p=0.008$), and for high memory load compared to low load ($F_{(1,50)}=99.3$; $p<0.001$). Further, an interaction was found ($F_{(1,50)}=8.2$; $p=0.006$), where differences between FESz and HC were greater at low ($t_{(50)}=3.3$, $p=0.002$) than high ($t_{(50)}=2.2$, $p=0.03$) memory load. The simple memory load effect was significant within both groups (p's<0.001).

Alpha Power

Mean alpha power during working memory maintenance was significantly reduced from baseline within dorsal lateral occipital cortex in both high and low memory load (**Figure 2**), with the most pronounced suppression in visual regions contralateral to the attended visual hemifield at high memory load. ROIs were generated in each hemisphere for the cortical vertices spanning the middle occipital sulcus, sulcus lunatus, superior occipital gyrus, superior occipital sulcus, and transverse occipital sulcus. Within average contralateral-ipsilateral difference spectra, only one time-frequency cluster was identified in the alpha band for high-load trials, spanning 7–11 Hz and 320–1,016 ms after onset of the memory array (**Figure 3**). No clusters were identified for low-load trials. Mixed methods ANOVA confirmed an interaction between group and memory load ($F_{(1,51)}=4.1$; $p=0.048$; **Table 4**), which was driven by greater CAS in HC than FESz in high ($t_{(51)}=3.3$, $p=0.002$), but not low load trials ($p>0.1$). Further, CAS was greater in high load than low load trials for HC ($t_{(24)}=2.5$, $p=0.021$), but not FESz ($t_{(51)}=-0.1$, *n.s.*).

LF Gamma Power Within CAS Clusters

A time-frequency cluster was identified in the LF gamma band spanning 34–40 and 276–600 ms after sample stimulus onset in high load trials, where contralateral LF gamma power increased from baseline in HC, but not FESz (**Figure 3**). No clusters were identified in low-load trials. ANOVA results did not indicate a group x memory load interaction ($p>0.1$). Rather, a trend-level main effect of group was found ($F_{(1,51)}=3.6$; $p=0.063$; **Table 4**), indicating greater lateralized LF gamma power in HC vs FESz across memory load conditions. The main effect of memory load was not significant ($p>0.1$).

Neurocognitive and Clinical Relationships

No significant correlations were found between oscillatory responses and reaction times; however, accuracy (*K*) was

TABLE 3 | Descriptive statistics for behavioral and neurophysiological effects.

	HC	FESz
K		
Low Load	0.95 ± 0.01	0.85 ± 0.03
High Load	2.19 ± 0.09	1.77 ± 0.13
Reaction time (ms)		
Low Load	725 ± 27	863 ± 30
High Load	822 ± 27	916 ± 31

Descriptive statistics (mean ± SEM) are reported for first-episode schizophrenia subjects (FESz) and healthy controls (HC).

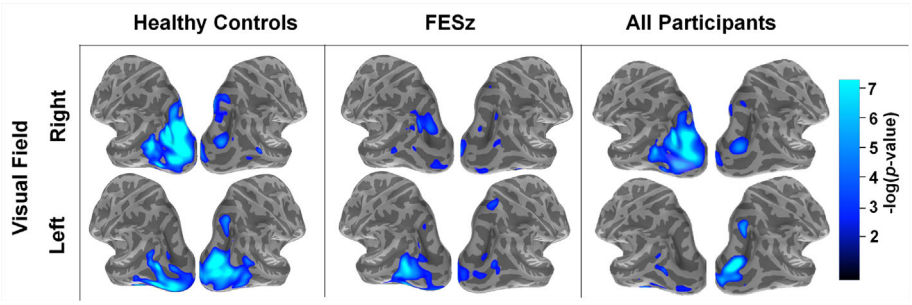

FIGURE 2 | Spatial distribution of source-resolved contralateral alpha suppression (CAS) in high-load trials in healthy controls, first-episode schizophrenia (FESz), and all participants. Source-resolved activity is shown for stimuli presented in the right (upper) and left (lower) visual field. These images represent average alpha power between 8–12 Hz and 200–1,200 ms after the onset of the memory set stimulus, which was done as an initial analysis step prior to time-frequency cluster analysis (see **Figure 3**).

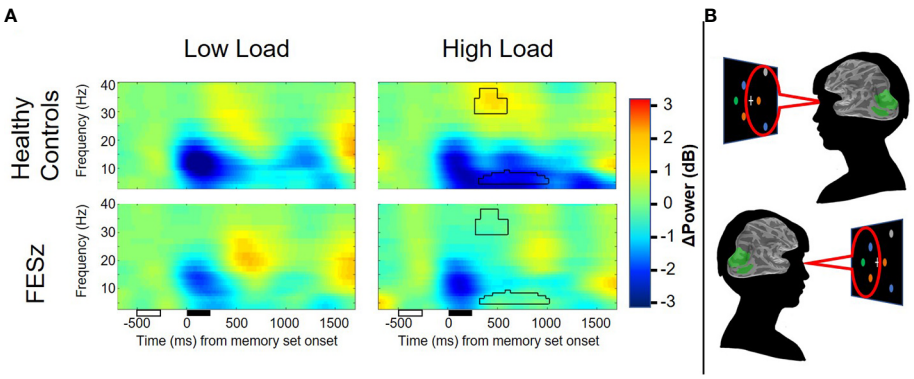

FIGURE 3 | Average contralateral minus ipsilateral time-frequency spectra from dorsal occipital ROIs. Lateralized suppression of alpha and enhancement of gamma power during the maintenance period is evident in healthy controls, but not first episode schizophrenia patients. Unfilled and filled boxes below the x-axis represent onsets/durations of the attention cue and memory set stimuli, respectively. Power values are shown as relative change from baseline in decibels (dB). Time-frequency clusters surviving correction for multiple comparisons are depicted by black outline.

TABLE 4 | Descriptive statistics for spectral effects.

	CAS (dB)		Gamma Power (dB)	
	HC	FESz	HC	FESz
Low Load	−0.41 ± 0.59	0.03 ± 0.64	0.53 ± 0.35	0.68 ± 0.29
Left Visual Field				
Right Visual Field	−1.94 ± 0.55	−1.07 ± 0.76	0.11 ± 0.33	−0.22 ± 0.31
High Load	−2.09 ± 0.66	−0.48 ± 0.56	0.29 ± 0.39	0.37 ± 0.32
Left Visual Field				
Right Visual Field	−2.22 ± 0.61	−0.47 ± 0.57	0.73 ± 0.44	−1.17 ± 0.35

Descriptive statistics (mean ± SEM) are reported for first-episode schizophrenia subjects (FESz) and healthy controls (HC).
FES, first-episode schizophrenia; HC, healthy controls.

moderately correlated with CAS within high load trials in HC (r = −0.35; p=0.097) and FESz (r = −0.32; p=0.093). Additional correlations were detected only within FESz. Greater WASI IQ was significantly correlated with greater CAS in FESz (r = −0.41; p=0.028). Similarly, greater MCCB working memory scores were related to greater CAS in FESz for both high-load (r = −0.49; p=0.008) and low-load (r = −0.41; p=0.032) trials. The same was true for the reasoning and problem-solving scale (high-load: r = −0.42; p=0.025; low-load: r = −0.42; p=0.025). Among FESz, greater negative symptom severity (as measured by the PANSS) was related to reduced alpha for both high-load (r = 0.53; p=0.007) and low-load (r = 0.49; p=0.015) trials. After controlling for WASI IQ, these correlations remained significant except for correlations between CAS and MCCB

reasoning/problem-solving scale, where magnitudes of *r*-values for low and high load trials were reduced to −0.35 and −0.39, respectively. No correlations were identified between CAS and LF gamma power, nor was LF gamma modulation correlated with any other variable (*p*'s>0.1).

Medication Effects

As nearly half of our FESz sample was unmedicated, we compared behavioral performance (*K*, RT) and neurophysiological measures (CAS and lateralized LF gamma power) between medicated and unmedicated FESz participants to investigate the effects of medication. There were no significant differences between medicated and nonmedicated FESz on any of these measures, nor were any of these measures correlated with chlorpromazine-equivalent dosages in medicated patients (*p*'s>0.1).

DISCUSSION

Attentional control is fundamental to nearly all aspects of cognition, from learning and memory to social cognition and complex decision making (54–57). This is perhaps most evident in the link between attention and working memory. Attention and working memory are so tightly intertwined that some have even argued against a short-term memory storage system that exists separately from attention and long-term memory, suggesting that what we call working memory is actually a combination of attentional selection, rehearsal, and consolidation/off-loading to activated long term memory (56, 58, 59). Many others assert that attention cannot sufficiently explain all working memory phenomena observed and a separate system is needed for working memory, but still acknowledge the role of attention in controlling the processes of working memory (60, 61). In the current study, we examined the effects of schizophrenia on attentional control during working memory maintenance by investigating CAS, a robust and objective neurophysiological marker of the focus of attention.

Our results show reduced CAS in dorsal occipital cortex in FESz when multiple items are maintained in lateralized vSTM. CAS differences between groups begin ~300 ms after onset of the memory array and persist throughout the delay period in healthy subjects, but not FESz. This extends upon previous findings of reduced CAS during visual attention in long-term schizophrenia (30), and has strong implications for previous findings of reduced delay period activity, despite no difference in encoding and orienting of attention. Visual objects maintained in vSTM are quickly bound with their spatial locations into an internalized visual scene after sensation (~100–200 ms) and attention selection/orienting (~250–400 ms) (62). In this way, contextual aspects of the individual items can be registered and linked to representations in long-term memory (63, 64). During vSTM maintenance, this global context is assembled from the individual items held in working memory and itself maintained throughout the delay period. vSTM is facilitated when global patterns exist, suggesting that scene assembly during vSTM is adaptive (65). Delay-period CAS represents the focus of attention in this maintained visual scene (66). Our results suggest that something has gone awry with deployment of attention to multiple items during maintenance in schizophrenia. Indeed, individuals with schizophrenia are impaired in the ability to simultaneously attend to multiple locations (67), although the ability to narrowly focus attention to a single location is preserved (17) if not enhanced (68, 69). Deficits are observed in the shift of attention from global to local spatial context as well (70). Thus, individuals with schizophrenia-spectrum psychotic disorders may have limited access to global representations of objects maintained in vSTM due to reduced ability to distribute attention broadly, or due to disruption of object-location binding.

We also found that manipulating the number of items maintained in vSTM resulted in LF gamma-band oscillatory response in contralateral dorsal visual cortex, where LF gamma power increased for multi-object arrays in healthy controls. Interestingly, this LF gamma burst onsets before CAS, and shortly after attentional orienting. LF gamma power increase in dorsal occipital areas may indicate consolidation of visual objects in working memory and construction of internal scenes. Reported evidence of occipitoparietal LF gamma increases with unconscious learning of visual search arrays has similar timing to the effects observed here (71). LF gamma responses were absent in FESz at both low and high load here. Thus, we propose that FESz may have reduced ability to form visual scenes that can be searched in vSTM. This is concordant with previous findings of deficits in the allocation of spatial attention to multiple items (68, 72), as well as findings of reduced ability to shift between local and global context in visual scenes (70, 73, 74). However, it is important to note that we did not find that CAS was statistically correlated with LF gamma power modulation in this sample. It is also possible that gamma power increases spanned higher frequencies than those investigated here; however, we decided to focus on LF gamma power here following prior studies which have investigated wider-band frequency spectra in similar contexts (25, 71)

Although our results are consistent with literature showing reduced ability to focus broadly in individuals with schizophrenia compared to healthy controls, there are some inconsistencies between results observed in the low load condition here and what has been described in previous research. Specifically, Leanard, Luck, and colleagues (14) have shown larger responses in people with long-term schizophrenia compared to healthy controls in low memory load conditions, which has been interpreted as hyperfocusing on individual items during encoding and maintenance (68, 69). We did not find evidence of hyperfocusing here. It is possible that hyperfocusing may arise with progression beyond the early stage of the illness—we have investigated individuals at first episode of psychosis here and cannot speak to this hypothesis. Longitudinal studies are needed to determine the validity of this statement. Further, the study by Leonard et al. did not utilize the spatial cuing approach used here. Rather than using a directional cue to orient the participants prior to encoding, they used different shapes on either side of fixation. The spatial cue used in the current design may have given the opportunity for the control group to focus spatial attention before memory display onset more intensely than they would in a design without that forewarning. Indeed,

deficits in cued redirection of covert spatial attention have been reported in long-term schizophrenia (75, 76), and controls here were more accurate than FESz at low load, which has not been reported previously.

In conclusion, our results show reduced lateralization of the focus of attention during vSTM, possibly due to impairment in the ability to broadly distribute spatial attention or reduced object-location binding. Forming hierarchical scene-based representations using visual information, semantic information, and objects is useful for organizing and summarizing information held in working memory. Healthy observers do this naturally in visual arrays, even when they do not explicitly contain patterns (65). Problems with the formation and/or utilization of scenes in vSTM could impact multiple aspects of schizophrenia, including visual learning, the ability to detect visual patterns (real or illusory), and the guidance of attention during social interaction. Deficits in the ability to represent high-level conceptual information along with object representations in working memory may prove fruitful for explaining complex aspects of working memory dysfunction that are hallmark of schizophrenia.

DATA AVAILABILITY STATEMENT

The raw data supporting the conclusions of this article will be made available by the authors, without undue reservation.

ETHICS STATEMENT

The studies involving human participants were reviewed and approved by the University of Pittsburgh Institutional Review Board. Written informed consent to participate in this study was provided by the participants' legal guardian/next of kin.

AUTHOR CONTRIBUTIONS

DS, RC, and CO designed the study and wrote the protocol. GH performed clinical evaluations. AG consulted on MEG source analysis. BC collected data and performed the data reduction and statistical analyses. BC and DS interpreted findings. BC wrote the first draft of the paper. All authors contributed to the article and approved the submitted version.

FUNDING

This research was supported by funding from the National Institute of Health (P50 MH103204).

ACKNOWLEDGMENTS

We thank the faculty and staff of the WPH Psychosis Recruitment and Assessment Core, the Conte Center for Translational Mental Health Research (P50 MH103204, David Lewis, MD, Director) and the University of Pittsburgh Clinical Translational Science Institute (UL1 RR024153, Steven E. Reis, MD) for their assistance in recruitment, diagnostic and psychopathological assessments, and neuropsychological evaluations. We also thank P. Jolicoeur and E. Vogel for their help with study design, and Timothy K. Murphy, M. Ward, J. Leiter-McBeth, K. Ward, and S. Haigh for assistance with data collection.

REFERENCES

1. Gold JM, Wilk CM, McMahon RP, Buchanan RW, Luck SJ. Working memory for visual features and conjunctions in schizophrenia. *J Abnorm Psychol* (2003) 112:61–71. doi: 10.1037/0021-843X.112.1.61
2. Lee J, Park S. Working Memory Impairments in Schizophrenia: A Meta-Analysis. *J Abnormal Psychol* (2005) 114:599–611. doi: 10.1037/0021-843X.114.4.599
3. Cowan N. The magical number 4 in short-term memory: a reconsideration of mental storage capacity. *Behav Brain Sci* (2001) 24:87–114. doi: 10.1017/S0140525X01003922
4. Miller GA. The magical number seven, plus or minus two: some limits on our capacity for processing information. *psychol Rev* (1956) 63:81–97. doi: 10.1037/h0043158
5. Hill SK, Griffin GB, Miura TK, Herbener ES, Sweeney JA. Salience of working-memory maintenance and manipulation deficits in schizophrenia. *psychol Med* (2010) 40:1979–86. doi: 10.1017/S003329171000019X
6. Johnson MK, McMahon RP, Robinson BM, Harvey AN, Hahn B, Leonard CJ, et al. The relationship between working memory capacity and broad measures of cognitive ability in healthy adults and people with schizophrenia. *Neuropsychology* (2013) 27:220–9. doi: 10.1037/a0032060
7. Schneider F, Habel U, Reske M, Kellermann T, Stöcker T, Shah NJ, et al. Neural correlates of working memory dysfunction in first-episode schizophrenia patients: An fMRI multi-center study. *Schizophr Res* (2007) 89:198–210. doi: 10.1016/j.schres.2006.07.021
8. Zanello A, Curtis L, Badan Bâ M, Merlo MCG. Working memory impairments in first-episode psychosis and chronic schizophrenia. *Psychiatry Res* (2009) 165:10–8. doi: 10.1016/j.psychres.2007.10.006
9. Dickinson D, Coursey RD. Independence and overlap among neurocognitive correlates of community functioning in schizophrenia. *Schizophr Res* (2002) 56:161–70. doi: 10.1016/S0920-9964(01)00229-8
10. Milev P, Ho B-C, Arndt S, Andreasen NC. Predictive Values of Neurocognition and Negative Symptoms on Functional Outcome in Schizophrenia: A Longitudinal First-Episode Study With 7-Year Follow-Up. *AJP* (2005) 162:495–506. doi: 10.1176/appi.ajp.162.3.495
11. Glahn DC, Ragland JD, Abramoff A, Barrett J, Laird AR, Bearden CE, et al. Beyond hypofrontality: a quantitative meta-analysis of functional neuroimaging studies of working memory in schizophrenia. *Hum Brain Mapp* (2005) 25:60–9. doi: 10.1002/hbm.20138
12. Van Snellenberg JX, Girgis RR, Horga G, van de Giessen E, Slifstein M, Ojeil N, et al. Mechanisms of Working Memory Impairment in Schizophrenia. *Biol Psychiatry* (2016) 80:617–26. doi: 10.1016/j.biopsych.2016.02.017
13. Bachman P, Kim J, Yee CM, Therman S, Manninen M, Lönnqvist J, et al. Efficiency of working memory encoding in twins discordant for schizophrenia. *Psychiatry Res: Neuroimaging* (2009) 174:97–104. doi: 10.1016/j.pscychresns.2009.04.010
14. Leonard CJ, Kaiser ST, Robinson BM, Kappenman ES, Hahn B, Gold JM, et al. Toward the Neural Mechanisms of Reduced Working Memory Capacity in Schizophrenia. *Cereb Cortex* (2013) 23:1582–92. doi: 10.1093/cercor/bhs148
15. Schlösser RG, Koch K, Wagner G, Nenadic I, Roebel M, Schachtzabel C, et al. Inefficient executive cognitive control in schizophrenia is preceded by altered

functional activation during information encoding: an fMRI study. *Neuropsychologia* (2008) 46:336–47. doi: 10.1016/j.neuropsychologia.2007.07.006
16. Morrens M, Hulstijn W, Sabbe B. Psychomotor slowing in schizophrenia. *Schizophr Bull* (2007) 33:1038–53. doi: 10.1093/schbul/sbl051
17. Luck SJ, Fuller, Braun EL, Robinson B, Summerfelt A, Gold JM. The speed of visual attention in schizophrenia: electrophysiological and behavioral evidence. *Schizophr Res* (2006) 85:174–95. doi: 10.1016/j.schres.2006.03.040
18. Lee J, Park S. Working memory impairments in schizophrenia: A meta-analysis. *J Abnormal Psychol* (2005) 114:599–611. doi: 10.1037/0021-843X.114.4.599
19. Salisbury DF. Semantic activation and verbal working memory maintenance in schizophrenic thought disorder: insights from electrophysiology and lexical ambiguity. *Clin EEG Neurosci* (2008) 39:103–7. doi: 10.1177/155005940803900217
20. Pashler H. Familiarity and visual change detection. *Percept Psychophysics* (1988) 44:369–78. doi: 10.3758/BF03210419
21. Bacigalupo F, Luck SJ. Lateralized Suppression of Alpha-Band EEG Activity As a Mechanism of Target Processing. *J Neurosci* (2019) 39:900. doi: 10.1523/JNEUROSCI.0183-18.2018
22. Erickson M, Albrecht M, Robinson B, Luck S, Gold J. Impaired Suppression of Delay-Period Alpha and Beta Is Associated With Impaired Working Memory in Schizophrenia. *Biol Psychiatry: Cogn Neurosci Neuroimaging* (2016) 2:272–9. doi: 10.1016/j.bpsc.2016.09.003
23. Mathewson KE, Lleras A, Beck DM, Fabiani M, Ro T, Gratton G. Pulsed out of awareness: EEG alpha oscillations represent a pulsed-inhibition of ongoing cortical processing. *Front Psychol* (2011) 2:99. doi: 10.3389/fpsyg.2011.00099
24. Romei V, Gross J, Thut G. On the role of prestimulus alpha rhythms over occipito-parietal areas in visual input regulation: correlation or causation? *J Neurosci* (2010) 30:8692–7. doi: 10.1523/JNEUROSCI.0160-10.2010
25. Muller MM, Gruber T, Keil A. Modulation of induced gamma band activity in the human EEG by attention and visual information processing. *Int J Psychophysiol* (2000) 38:283–99. doi: 10.1016/S0167-8760(00)00171-9
26. Hirano Y, Oribe N, Kanba S, Onitsuka T, Nestor PG, Spencer KM. Spontaneous Gamma Activity in Schizophrenia. *JAMA Psychiatry* (2015) 72:813–21. doi: 10.1001/jamapsychiatry.2014.2642
27. Oribe N, Hirano Y, del Re E, Seidman LJ, Mesholam-Gately RI, Woodberry KA, et al. Progressive reduction of auditory evoked gamma in first episode schizophrenia but not clinical high risk individuals. *Schizophr Res* (2019) 208:145–52. doi: 10.1016/j.schres.2019.03.025
28. Spencer KM, Niznikiewicz MA, Shenton ME, McCarley RW. Sensory-Evoked Gamma Oscillations in Chronic Schizophrenia. *Biol Psychiatry* (2008) 63:744–7. doi: 10.1016/j.biopsych.2007.10.017
29. Barr MS, Rajji TK, Zomorrodi R, Radhu N, George TP, Blumberger DM, et al. Impaired theta-gamma coupling during working memory performance in schizophrenia. *Schizophr Res* (2017) 189:104–10. doi: 10.1016/j.schres.2017.01.044
30. Kustermann T, Rockstroh B, Kienle J, Miller GA, Popov T. Deficient attention modulation of lateralized alpha power in schizophrenia. *Psychophysiology* (2016) 53:776–85. doi: 10.1111/psyp.12626
31. Carter CS, Mintun M, Nichols T, Cohen JD. Anterior cingulate gyrus dysfunction and selective attention deficits in schizophrenia:[15O] H2O PET study during single-trial Stroop task performance. *Am J Psychiatry* (1997) 154:1670–5. doi: 10.1176/ajp.154.12.1670
32. Brébion G, Smith MJ, Gorman JM, Malaspina D, Sharif Z, Amador X. Memory and schizophrenia: Differential link of processing speed and selective attention with two levels of encoding. *J Psychiatr Res* (2000) 34:121–7. doi: 10.1016/S0022-3956(99)00050-3
33. Everett J, Laplante L, Thomas J. The selective attention deficit in schizophrenia: limited resources or cognitive fatigue? *J Nervous Ment Dis* (1989) 177(12):735–8. doi: 10.1097/00005053-198912000-00004
34. Shin Y-W, O'Donnell BF, Youn S, Kwon JS. Gamma oscillation in schizophrenia. *Psychiatry Invest* (2011) 8:288–96. doi: 10.4306/pi.2011.8.4.288
35. Spencer KM, Nestor PG, Perlmutter R, Niznikiewicz MA, Klump MC, Frumin M, et al. Neural synchrony indexes disordered perception and cognition in schizophrenia. *Proc Natl Acad Sci USA* (2004) 101:17288. doi: 10.1073/pnas.0406074101
36. Newson JJ, Thiagarajan TC. EEG frequency bands in psychiatric disorders: a review of resting state studies. *Front Hum Neurosci* (2019) 12:521. doi: 10.3389/fnhum.2018.00521
37. Nuechterlein KH, Green MF. MATRICS consensus cognitive battery manual. *Los Angeles CA: MATRICS Assess Inc* (2006).
38. Hollingshead AB. Four factor index of social status. (1975).
39. Axelrod BN. Validity of the Wechsler abbreviated scale of intelligence and other very short forms of estimating intellectual functioning. *Assessment* (2002) 9:17–23. doi: 10.1177/1073191102009001003
40. Taulu S, Simola J. Spatiotemporal signal space separation method for rejecting nearby interference in MEG measurements. *Phys Med Biol* (2006) 51:1759–68. doi: 10.1088/0031-9155/51/7/008
41. Taulu S, Kajola M, Simola J. Suppression of interference and artifacts by the signal space separation method. *Brain Topography* (2004) 16:269–75. doi: 10.1023/B:BRAT.0000032864.93890.f9
42. Delorme A, Makeig S. EEGLAB: an open source toolbox for analysis of single-trial EEG dynamics including independent component analysis. *J Neurosci Methods* (2004) 134:9–21. doi: 10.1016/j.jneumeth.2003.10.009
43. Delorme A, Palmer J, Onton J, Oostenveld R, Makeig S. Independent EEG Sources Are Dipolar. *PloS One* (2012) 7:e30135. doi: 10.1371/journal.pone.0030135
44. Hsu S-H, Pion-Tonachini L, Palmer J, Miyakoshi M, Makeig S, Jung T-P. Modeling brain dynamic state changes with adaptive mixture independent component analysis. *NeuroImage* (2018) 183:47–61. doi: 10.1016/j.neuroimage.2018.08.001
45. Palmer JA, Makeig S, Kreutz-Delgado K, Rao BD. Newton method for the ICA mixture model. In: *2008 IEEE International Conference on Acoustics, Speech and Signal Processing*. New York: IEEE (2008). p. 1805–8.
46. Dale AM, Fischl B, Sereno MI. Cortical Surface-Based Analysis: I. Segmentation and Surface Reconstruction. *NeuroImage* (1999) 9:179–94. doi: 10.1006/nimg.1998.0395
47. Fischl B, Liu A, Dale AM. Automated manifold surgery: constructing geometrically accurate and topologically correct models of the human cerebral cortex. *IEEE Trans Med Imaging* (2001) 20:70–80. doi: 10.1109/42.906426
48. Fischl B, Sereno MI, Tootell RB, Dale AM. High-resolution intersubject averaging and a coordinate system for the cortical surface. *Hum Brain Mapp* (1999) 8:272–84. doi: 10.1002/(SICI)1097-0193(1999)8:4<272::AID-HBM10>3.0.CO;2-4
49. Lin F, Belliveau JW, Dale AM, Hämäläinen MS. Distributed current estimates using cortical orientation constraints. *Hum Brain Mapp* (2006) 27:1–13. doi: 10.1002/hbm.20155
50. Gramfort A, Luessi M, Larson E, Engemann DA, Strohmeier D, Brodbeck C, et al. MNE software for processing MEG and EEG data. *Neuroimage* (2014) 86:446–60. doi: 10.1016/j.neuroimage.2013.10.027
51. Luck SJ. *An Introduction to the Event-Related Potential Technique*. Cambridge, MA: MIT press (2014).
52. Maris E, Oostenveld R. Nonparametric statistical testing of EEG-and MEG-data. *J Neurosci Methods* (2007) 164:177–90. doi: 10.1016/j.jneumeth.2007.03.024
53. Rouder JN, Morey RD, Morey CC, Cowan N. How to measure working memory capacity in the change detection paradigm. *Psychonomic Bull Rev* (2011) 18:324–30. doi: 10.3758/s13423-011-0055-3
54. Ford JM, Mathalon DH, Heinks T, Kalba S, Faustman WO, Roth WT. Neurophysiological evidence of corollary discharge dysfunction in schizophrenia. *Am J Psychiatry* (2001) 158:2069–71. doi: 10.1176/appi.ajp.158.12.2069
55. De Martino B, Kumaran D, Seymour B, Dolan RJ. Frames, Biases, and Rational Decision-Making in the Human Brain. *Science* (2006) 313:684. doi: 10.1126/science.1128356
56. Engle RW. Working memory capacity as executive attention. *Curr Dir psychol Sci* (2002) 11:19–23. doi: 10.1111/1467-8721.00160
57. Parasuraman R, Manzey DH. Complacency and bias in human use of automation: An attentional integration. *Hum Factors* (2010) 52:381–410. doi: 10.1177/0018720810376055
58. Cowan N. Short-term memory based on activated long-term memory: A review in response to Norris (2017). *Psychol Bull* (2019) 145:822–47. doi: 10.1037/bul0000199

59. Rhodes S, Cowan N. Attention in working memory: attention is needed but it yearns to be free. *Ann New Y Acad Sci* (2018) 1424:52. doi: 10.1111/nyas.13652
60. Norris D. Even an activated long-term memory system still needs a separate short-term store: A reply to Cowan (2019). *Psychol Bull* (2019) 145(8):848–53. doi: 10.1037/bul0000204
61. Norris D. Short-term memory and long-term memory are still different. *psychol Bull* (2017) 143:992. doi: 10.1037/bul0000108
62. Grent-'t-Jong T, Woldorff MG. Timing and sequence of brain activity in top-down control of visual-spatial attention. *PloS Biol* (2007) 5:e12–2. doi: 10.1371/journal.pbio.0050012
63. Droll J, Hayhoe MM, Triesch J, Sullivan BT. Working memory for object features is influenced by scene context. *J Vision* (2004) 4:152–2. doi: 10.1167/4.8.152
64. Hollingworth A, Rasmussen IP. Binding objects to locations: The relationship between object files and visual working memory. *J Exp Psychol: Hum Percept Perform* (2010) 36:543. doi: 10.1037/a0017836
65. Brady TF, Tenenbaum JB. A probabilistic model of visual working memory: Incorporating higher order regularities into working memory capacity estimates. *psychol Rev* (2013) 120:85. doi: 10.1037/a0030779
66. Günseli E, Fahrenfort JJ, van Moorselaar D, Daoultzis KC, Meeter M, Olivers CNL. EEG dynamics reveal a dissociation between storage and selective attention within working memory. *Sci Rep* (2019) 9:13499. doi: 10.1038/s41598-019-49577-0
67. Hahn B, Robinson BM, Harvey AN, Kaiser ST, Leonard CJ, Luck SJ, et al. Visuospatial attention in schizophrenia: deficits in broad monitoring. *J Abnorm Psychol* (2012) 121:119–28. doi: 10.1037/a0023938
68. Kreither J, Lopez-Calderon J, Leonard CJ, Robinson BM, Ruffle A, Hahn B, et al. Electrophysiological Evidence for Hyperfocusing of Spatial Attention in Schizophrenia. *J Neurosci* (2017) 37:3813. doi: 10.1523/JNEUROSCI.3221-16.2017
69. Luck SJ, McClenon C, Beck VM, Hollingworth A, Leonard CJ, Hahn B, et al. Hyperfocusing in schizophrenia: Evidence from interactions between working memory and eye movements. *J Abnormal Psychol* (2014) 123:783. doi: 10.1037/abn0000003
70. Coleman MJ, Cestnick L, Krastoshevsky O, Krause V, Huang Z, Mendell NR, et al. Schizophrenia Patients Show Deficits in Shifts of Attention to Different Levels of Global-Local Stimuli: Evidence for Magnocellular Dysfunction. *Schizophr Bull* (2009) 35:1108–16. doi: 10.1093/schbul/sbp090
71. Chaumon M, Schwartz D, Tallon-Baudry C. Unconscious learning versus visual perception: dissociable roles for gamma oscillations revealed in MEG. *J Cogn Neurosci* (2009) 21:2287–99. doi: 10.1162/jocn.2008.21155
72. Luck SJ, Hahn B, Leonard CJ, Gold JM. The hyperfocusing hypothesis: A new account of cognitive dysfunction in Schizophrenia. *Schizophr Bull* (2019) 45:991–1000. doi: 10.1093/schbul/sbz063
73. Granholm E, Perry W, Filoteo JV, Braff D. Hemispheric and attentional contributions to perceptual organization deficits on the global-local task in schizophrenia. *Neuropsychology* (1999) 13:271. doi: 10.1037/0894-4105.13.2.271
74. Bellgrove MA, Vance A, Bradshaw JL. Local–global processing in early-onset schizophrenia: Evidence for an impairment in shifting the spatial scale of attention. *Brain Cogn* (2003) 51:48–65. doi: 10.1016/S0278-2626(02)00509-2
75. Gooding DC, Braun JG, Studer JA. Attentional network task performance in patients with schizophrenia–spectrum disorders: evidence of a specific deficit. *Schizophr Res* (2006) 88:169–78. doi: 10.1016/j.schres.2006.07.009
76. Maruff P, Pantelis C, Danckert J, Smith D, Currie J. Deficits in the endogenous redirection of covert visual attention in chronic schizophrenia. *Neuropsychologia* (1996) 34:1079–84. doi: 10.1016/0028-3932(96)00035-8

Conflict of Interest: The authors declare that the research was conducted in the absence of any commercial or financial relationships that could be construed as a potential conflict of interest.

frontiers in Psychiatry

PERSPECTIVE
published: 21 August 2020
doi: 10.3389/fpsyt.2020.00863

Prospects for Future Methodological Development and Application of Magnetoencephalography Devices in Psychiatry

Naruhito Hironaga[1]*, *Yuichi Takei*[2], *Takako Mitsudo*[3], *Takahiro Kimura*[4] and *Yoji Hirano*[3]

[1] Brain Center, Faculty of Medicine, Kyushu University, Fukuoka, Japan, [2] Department of Psychiatry and Neuroscience, Gunma University Graduate School of Medicine, Maebashi, Japan, [3] Department of Neuropsychiatry, Graduate School of Medical Sciences, Kyushu University, Fukuoka, Japan, [4] Institute of Liberal Arts and Science, Kanazawa University, Kanazawa, Japan

Magnetoencephalography (MEG) is a functional neuroimaging tool that can record activity from the entire cortex on the order of milliseconds. MEG has been used to investigate numerous psychiatric disorders, such as schizophrenia, bipolar disorder, major depression, dementia, and autism spectrum disorder. Although several review papers on the subject have been published, perspectives and opinions regarding the use of MEG in psychiatric research have primarily been discussed from a psychiatric research point of view. Owing to a newly developed MEG sensor, the use of MEG devices will soon enter a critical period, and now is a good time to discuss the future of MEG use in psychiatric research. In this paper, we will discuss MEG devices from a methodological point of view. We will first introduce the utilization of MEG in psychiatric research and the development of its technology. Then, we will describe the principle theory of MEG and common algorithms, which are useful for applying MEG tools to psychiatric research. Next, we will consider three topics—child psychiatry, resting-state networks, and cortico-subcortical networks—and address the future use of MEG in psychiatry from a broader perspective. Finally, we will introduce the newly developed device, the optically-pumped magnetometer, and discuss its future use in MEG systems in psychiatric research from a methodological point of view. We believe that state-of-the-art electrophysiological tools, such as this new MEG system, will further contribute to our understanding of the core pathology in various psychiatric disorders and translational research.

Keywords: magnetencephalography, psychiatry, resting state networks, cortico-subcortical networks, optically-pumped magnetometers

OPEN ACCESS

Edited by:
Jun Soo Kwon,
Seoul National University, South Korea

Reviewed by:
Remko van Lutterveld,
UMC Utrecht Brain Center, Netherlands
June Sic Kim,
Seoul National University, South Korea

***Correspondence:**
Naruhito Hironaga
hironaga@med.kyushu-u.ac.jp

Specialty section:
This article was submitted to Neuroimaging and Stimulation, a section of the journal Frontiers in Psychiatry

Received: *14 May 2020*
Accepted: *07 August 2020*
Published: *21 August 2020*

Citation:
Hironaga N, Takei Y, Mitsudo T, Kimura T and Hirano Y (2020) Prospects for Future Methodological Development and Application of Magnetoencephalography Devices in Psychiatry. Front. Psychiatry 11:863. doi: 10.3389/fpsyt.2020.00863

INTRODUCTION

Numerous research studies in the field of psychiatry have made use of magnetoencephalography (MEG) systems. Schizophrenia (SZ), major depression, autism spectrum disorders (ASD), child psychiatry, attention deficit hyperactivity disorder (ADHD), obsessive-compulsive disorder (OCD), dementia, and other conditions have been investigated using MEG either alone or in combination

with multiple neuroimaging modalities. Such studies have commonly used auditory stimulation owing to the strong relationship between auditory system abnormalities and psychiatric disorders [e.g., auditory hallucinations in SZ (1)]. In particular, the auditory steady-state response (ASSR) and mismatch negativity (MMN) response are representative markers used to indicate auditory processing abnormalities in neurophysiological studies in psychiatry (2–7). Recently, research into resting-state networks (RSNs) has received much attention in both neuroscience and psychiatric research because RSNs play a key role in the baseline or default mode of normal and disordered brains. In psychiatric studies, evaluation of whole-brain dynamics would be of more interest than a functional localization-based approach (8, 9). Thus, time-frequency analysis, which is used to evaluate whole-brain activity, is frequently used in this field. The main advantage of MEG is its high temporal resolution and adequate spatial resolution.

Historically, detecting electromagnetic brain activity has been a topic of interest since the mid-20th century. Hans Berger, who invented electroencephalography (EEG), was a pioneer in methods of recording electrical brain activity. Subsequently, 30 years later, Baule and McFee successfully detected the heartbeat *via* magnetic field detection (10). Then, the superconducting quantum interference device (SQUID)-type magnetometer integrated with shield technology successfully achieved the detection of very small magnetic fields from the human brain (11). In the 1970s, the gradient-type magnetometer was developed (12) and multi-channel recording came into use in clinical settings in the 1980s. In the 1990s, whole-head-type MEG was developed by several vendors. At the beginning of the 21st century, no notable hardware development was taking place; however, the last decade has seen the development of new technologies. Thus, it is now pertinent to consider how new MEG technologies will contribute to psychiatry research. We first briefly summarize the basic principle of MEG and its use in psychiatric research. Next, we will describe the use of MEG in child psychiatry, the study of RSNs, and the study of cortico-subcortical networks. We also present schematic images comparing the current (**Figure 1**) and new MEG systems (**Figure 2**). Then, we will discuss the potential for these new MEG technologies to be used in future psychiatric research.

MEG AND OTHER NEUROIMAGING MODALITIES

In humans, several functional brain measurement techniques are now available. For example, functional magnetic resonance imaging (fMRI), near-infrared spectroscopy (NIRS), EEG, and MEG. Here, we will briefly describe the pros and cons of each technique when applied to psychiatric research. An advantage of MEG is notably its non-invasiveness, which is critical for psychiatric patients, while the strong magnetic field generated during fMRI recordings is questionably invasive especially for children and infants. Using blood oxygenation level-dependent signal changes, fMRI provides high spatial resolution if participants remain still but with a lower temporal resolution that limits its functional estimations. Moreover, artificial sound noise generated by the MRI device causes problem for auditory experiments, which are a major focus in psychiatric research. EEG exhibits high temporal resolution, equivalent to MEG, yet its spatial resolution is disputed due to distorted detection through several tissues with different conductivities. In psychiatric experiments, rapid and comfortable recordings that are related to preliminary processes and limitation of motions are ideal for patients. Preparation of EEG (i.e., fixing many electrodes) is time consuming. Alternatively, NIRS does not require a complex preparation process and is relatively robust to the problem of body movements, but it has less spatial and time resolution compared with EEG/MEG. Although the spatial resolution of MEG is disputed because of its ill-posed inverse solution, MEG can provide high temporal resolution under certain spatial resolution, enabling almost the whole cortex to be covered by any measurement in a single system. Indeed, being non-invasive, fast, and comfortable, MEG measurements offer several advantages for brain response recordings from psychiatric patients.

MEG ANALYSIS AND FUNDAMENTAL FRAMEWORKS

MEG Analysis for Psychiatric Research

MEG sensors detect magnetic field changes in neuronal electric currents that are sensitive to the currents perpendicular to the sulci or fissures over the cortex. MEG source reconstruction accuracy depends on factors such as the forward and inverse problems, the signal-to-noise ratio (S/N) including the number of trials for averaging, and MEG-magnetic resonance imaging (MRI) co-registration issues. The first factor, the inverse problem, has been extensively addressed; however, other factors are crucial in practice. The patented methods of noise cancellation are applied as necessary, which include gradient formation (16) and the offline Maxfilter (17), which can help to achieve a higher S/N ratio. As a preliminary step, a band pass filter is applied to the frequency range of interest. Furthermore, independent component analysis (ICA) is a powerful tool for extracting target components or eliminating artifacts (18). We must then consider the MEG source reconstruction process. Given the widespread use of MRI, the co-registration process is now crucial for MEG, EEG, and even for transcranial magnetic stimulation (19). Stylus magnetic-field digitizers are commonly used. However, these are less accurate and more time-consuming than photogrammetry-based systems, 3D laser/structured-light scanners, or 3D printers, which are reliable alternatives for measuring head shape (13, 20–22). Once MEG-MRI alignment is fixed, forward computation needs to be considered. Currently, a realistic model utilizing the boundary element method (23) or the finite element method (24) is a popular and accurate approach. Following the lead field computation, the inverse solution should be applied to obtain a source activation map. Typically, we distinguish two groups of algorithms; one is the equivalent current dipole (ECD) (25), and the other is distributed source analysis. Currently, the minimum norm-based approach or an adaptive beam-former is common algorithms for the latter case (26, 27). Minimum norm estimates (MNE) is a

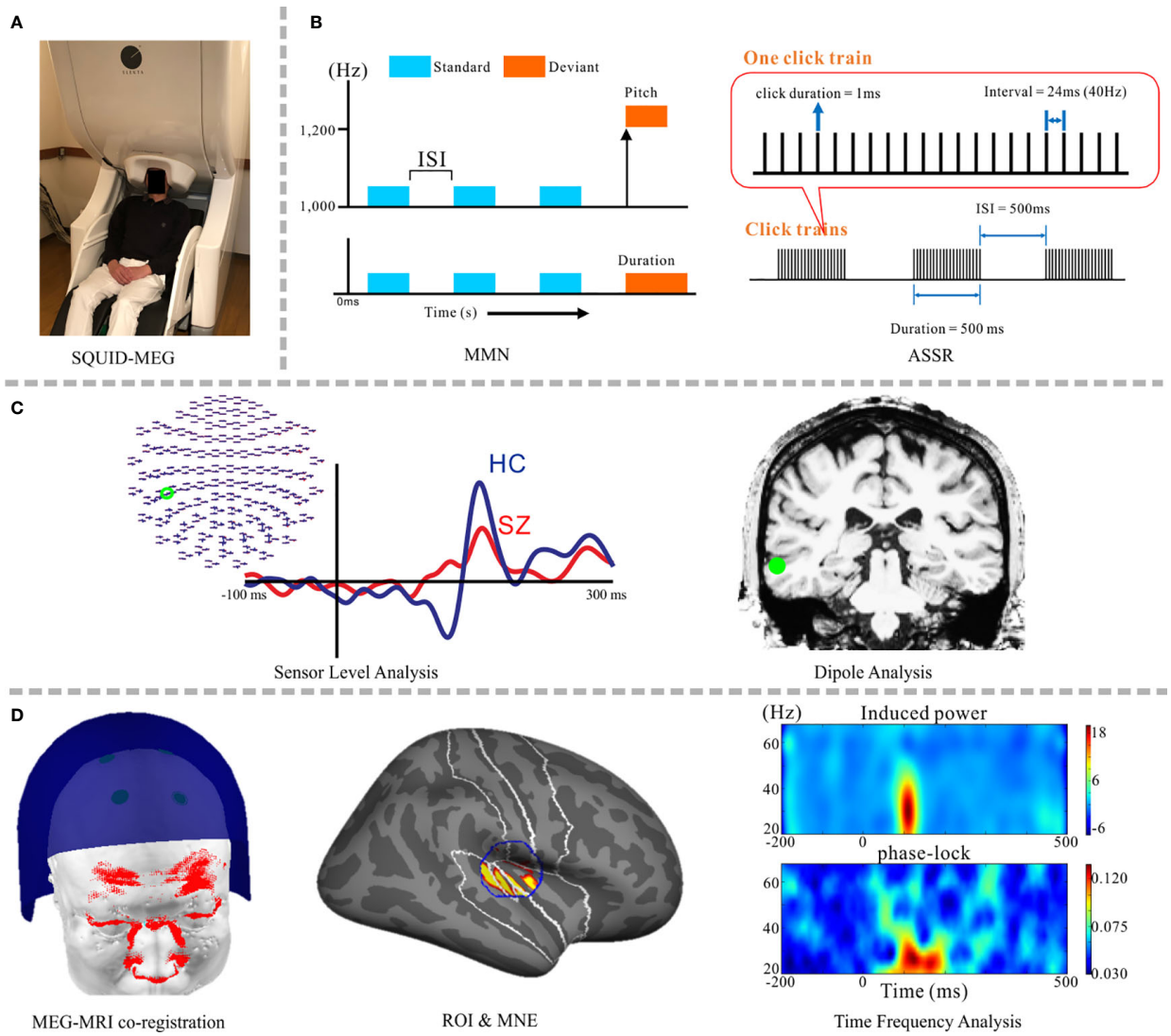

FIGURE 1 | Schematic images from psychiatric research implementing the SQUID-MEG system. **(A)** SQUID-MEG system: the brain is covered by fixed positional sensors in the dewar helmet. **(B)** A representative, frequently-employed auditory stimulation paradigm for MEG diagnosis, including the MMN (left) and ASSR (right) responses. **(C)** Orthodox MEG analysis: a sensor-level analysis making a comparison between patients with SZ (red) and HC (blue) (left) and dipole analysis (right). **(D)** The current method used in MEG psychiatric research, from right side: accurate MEG-MRI co-registration using a 3D laser scanner (13), specified ROI and source reconstruction results using MNE, and time-frequency analysis using source waveforms; induced power (upper) and the phase-locking factor (lower). SQUID, superconducting quantum interference device; SZ, schizophrenia; HC, healthy control; MMN, mismatch negativity; ASSR, auditory steady-state response; ROI, region of interest; MNE, minimum norm estimates.

technique that uses pre-fixed source points over the brain to minimize the total current of all nodes. Furthermore, a noise normalization technique is frequently applied using the pre-trigger period or entire raw data (28). Then, time frequency analysis should be applied using signals extracted from target regions. In psychiatric research, oscillatory analysis enables us to detect abnormal fast and varied neural activities, hence, time-frequency analysis and connective analysis including coherence, phase synchrony, and envelope correlation *via* wavelet transform, are commonly performed (29, 30). Recently, cross-frequency coupling, such as phase-amplitude coupling between low and high frequency oscillatory components, has also been discussed (31–34).

Fundamental Frameworks

Figure 1 depicts a schematic image of psychiatric research using SQUID-MEG. Sensors are fixed in the dewar (**Figure 1A**). Components elicited in response to auditory stimuli, the MMN and ASSR, are frequently used to detect auditory sensory deficits in psychiatric disorders (**Figure 1B**). Combination studies with sensor-level and dipole analysis have been popular (**Figure 1C**) (35–38). Hirano and colleagues demonstrated oscillatory deficits in response

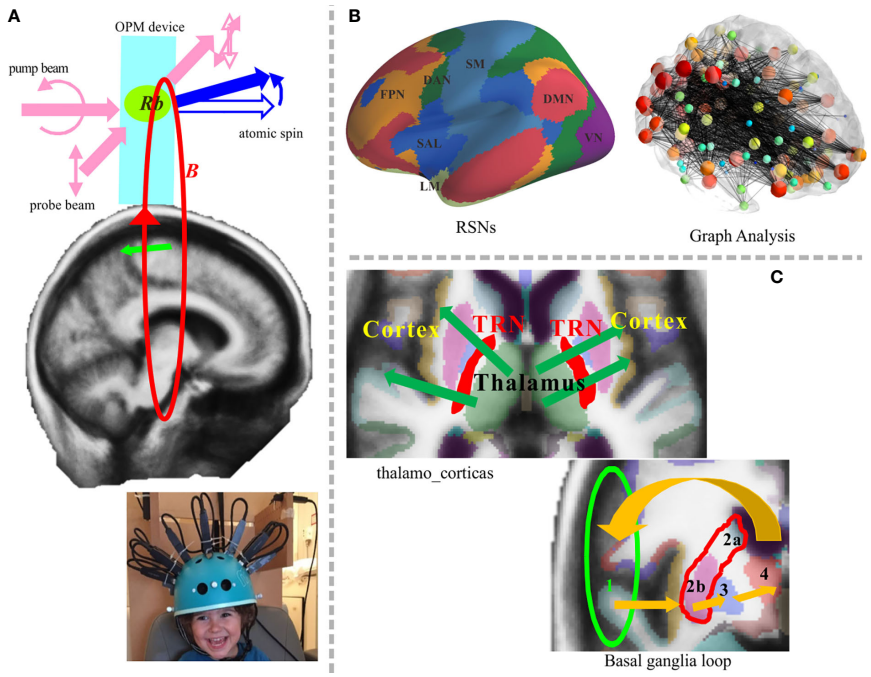

FIGURE 2 | Potential application of the OPM-MEG system in future work. **(A)** Newly developed system and principle of atom magnetometer (upper panel). Two laser beams are arranged orthogonally; one is the pump beam that polarizes the vaporized atomic electron spin, and the other is the probe beam that measures the state of spin evolving in the magnetic field *B*. Rb denotes rubidium atom. The lower sub-figure presents a pediatric OPM-MEG system adapted from Hill et al. (14). **(B)** RSN analysis will involve deep brain structures. Representative RSNs (left) and an image showing graph theory analysis (right) (15). **(C)** The cortico-subcortical network could be targeted in future work. Thalamocortical communication (upper left) and the basal ganglia loop, 1. cortex→2. striatum (a. caudate nucleus orb. putamen)→3. pallidum→4. thalamus→1.cortex (lower right). OPM, optically pumped magnetometers; TRN, thalamic reticular nucleus.

to speech sounds in SZ (39) and bipolar disorder (40), ASSR gamma oscillatory abnormalities in SZ (41) and mood disorders (42), and MMN deficits in major depressive disorder (43). Given the relatively high spatial resolution, distributed source analysis has become the main method for analyzing MEG data (**Figure 1D**) [e.g., MNE (44–46), the beamforming (47)]. At present, one state-of-the-art technique is applying wavelet transform and connected analysis to the extracted source waveforms *via* a combination of distributed source analysis and ICA (48, 49).

SPECIFIC MEG APPLICATIONS FOR PSYCHIATRIC DISORDERS

Here we describe three specific MEG applications in psychiatric disorders since we consider that these will be the key roles of the coming psychiatric study using MEG.

Child Psychiatry

Owing to its completely non-invasive approach, MEG is one of the most suitable technologies in child psychiatry. Indeed, ASD and ADHD in child psychiatry have been well investigated using MEG (50–54). Although infant MEG systems are commercially available (55), only a few institutions possess these systems. The main obstacle to MEG use in babies and children is head and body movements. The simplest way to deal with this issue is to discard the data from when patients make large movements. Another way to overcome these issues is the use of continuous head localization; however, the use of strong magnetic field generation during the measurement in children is controversial. MRI scanning in younger children is problematic, but the use of standard brains from a series of age-matched infant MRIs can help to reduce the problem. Dipole methods with a spherical model are still the dominant approach in children; hence, the accuracy level in children is not comparable to that in adult cases.

Resting-State Networks

Brain activity occurs not only during cognitive processes, but also during sleep or rest (56, 57), which is when RSN activity can be recorded. RSNs involve key network domains that are known to underlie the pathophysiology of many psychiatric disorders (58, 59), such as the default mode network, central executive network, and saliency network. Several RSN studies utilizing MEG for psychiatric researches have been reported (60–67). A common way of making use of the strengths of MEG is to investigate RSNs on the basis of a source reconstruction technique in various frequency bands. Analyzing frequency-specific RSNs involving deeper brain such as limbic regions can reveal pathophysiology of psychiatric disorders as network failure.

Thalamocortical Communication and the Basal Ganglia Loop in Psychiatric Disorders

Recently, aberrant oscillatory activity has been reported in various psychiatric disorders. Functional interactions within the cortico-subcortical network are considered to contribute to abnormal oscillation *via* alterations in neurotransmitters and receptors in psychiatric disorders. We argue that there are relationships among the cortico-subcortical network (including the limbic system, thalamus, and basal ganglia) and related networks, which form functional loops that are of interest in psychiatric research. Although the ability of MEG to detect the activity of deep brain structures is still disputed, there are a few credible reports under current SQUID-MEG system (68, 69). Schulman et al. hypothesized that the generation of abnormal recurrent neuronal activation in neuropsychiatric disorders occurred through aberrant thalamocortical rhythm epiphenomena (70). Patients with OCD usually recognize that obsessions and compulsions are not logical, but they are not under their control; thus, it is important to investigate whether cognitive changes in OCD may be caused by abnormal neural circuits. The basal ganglia loops not only underlie sensorimotor control but also cognitive functions associated with limbic control and motivated behavior (71); hence, recent work on OCD has been focused on the contribution of the basal ganglia loops. fMRI studies have suggested that OCD involves abnormal functioning in specific frontal-subcortical brain circuits (72). Enhanced activity within the basal ganglia loop is clearly seen in OCD even at resting state (73). However, the temporal dynamic of these loops has not been sufficiently addressed in humans. The new MEG could help to elucidate the contribution of altered basal ganglia loops to OCD.

LIMITATIONS OF THE CURRENT SQUID-MEG SYSTEM

MEG is a very attractive tool for psychiatric research, including in the diagnosis of psychoses. However, the penetration rate of MEG is generally very low compared with fMRI, EEG, and transcranial magnetic stimulation (58). In general, an MEG laboratory is expensive to set up and maintain. Further, despite MEG being simple to measure, it requires a complex data analysis. The source reconstruction analysis *via* a mathematically ill-posed problem requires a complex knowledge of physics, mathematics, and computational issues. Current practical limitations of SQUID-MEG include its poor sensitivity to deep brain activities and its sensitivity to head motion artifacts. These problems are not solvable in principle because they depend on the hardware design and configuration. The main hardware limitations of the SQUID-MEG system relate to the fixed location and orientation of the detection coils (sensors). The fixed coil position within the dewar limits the distance between the brain and the sensors to approximately 2–3 cm and the gradiometers (axial or planar) are designed to increase the sensitivity of the cortical responses. Indeed, using the current SQUID-MEG system, it is difficult to detect activity in the thalamus and basal ganglia accurately because of their depth and anatomical structure. Additionally, the fixed coil location requires the subject to lie still during measurement. As such, the system is sensitive to head movement. These limitations of the current SQUID-MEG system reduce its utility in child psychiatry and analysis of cortico-subcortical networks. Thus, there is increasing interest in the development of new MEG systems, as described below.

NEWLY DEVELOPED MEG SENSORS

Until the 20st century, low temperature SQUID-MEGs were the only choice of device for MEG sensors; however, current technologies have meant that new MEG devices are now available. In particular, the development of optically-pumped magnetometers (OPM; also termed 'on-scalp MEG') has accelerated in recent years. The development of the atomic magnetometer began earlier, but because of their poor sensitivity, their use was not emphasized. Drastic changes have occurred since the development of a new spin-exchange relaxation-free condition, which has led to sensitivities up to the femtotesla range (74). **Figure 2** shows potential uses of OPM-MEG in future research. **Figure 2A** (upper) depicts a schematic image of the fundamental principle of an atomic magnetometer embedded in an OPM device. Studies using this new technology have reported results that are relevant to psychiatric research, such as phase-locked evoked responses generated by auditory stimuli (75) and the detection of induced changes in the frequency domain (76). One of the most important issues when considering the newly developed OPM is the wearable-type system, which increases the flexibility of sensor location and orientation. The on-scalp MEG system can reduce the distance between the sensors and the brain, allowing detectors to be placed several millimeters above the scalp surface. The flexible position and orientation indicate that this system could be used to measure activity of not only the cerebral cortex but also subcortical brain areas. The S/N ratio will be drastically improved which is not comparable to SQUID-MEG. A study from 2017 reported that the S/N ratio was four times higher than the SQUID-type MEG in general, and eight times higher on surface areas (77). By using flexible-type sensors, it is possible to freely orientate the sensors according to the target brain structure. When using wearable-type sensors, MEG-MRI co-registration is crucial because of non-fixed flexible sensor locations and orientations, but some proposals have been made for the use of OPM with 3D printers or 3D-structured light scanners (21, 22, 77). The higher S/N ratio and the orientation-free design of the system allows the detection of deeper brain signals. The accuracy of source localization-based time-frequency analysis also ameliorated along with the hardware development. Another advantage of wearable-type sensors relates to the reduced influence of head movements during measurement. Notably, the maintenance cost of MEG will be drastically reduced because the new sensor works at room temperature. We strongly believe that this non-pyrogenic MEG device will increase the penetration rate of MEG.

UTILIZATION OF OPM-MEG FOR PSYCHIATRIC RESEARCH

The OPM-MEG could be a better, more accurate alternative method for recording neuromagnetic signals from infants and children since the wearable sensors reduce the problem of head movement compensation (**Figure 2A**, lower). A higher S/N ratio would also allow single-trial analyses to be performed, which is beneficial to detecting the dynamic changes in the brain. For example, MMN experiments generally consist of standard and deviant stimuli, and the number of deviant stimuli is lower than the number of standard stimuli. As such, there is an incongruence in the number of averaged trials between the two conditions. Thus, the interest around single-trial analysis of OPM-MEG data in MMN research is increasing. Oscillatory whole-brain analyses in milliseconds resolution is a good tool for RSN analysis (**Figure 2B**). Covering the whole cortex is crucial in psychiatric research because the RSNs and recurrent loops are likely to be important in psychiatric diseases, as described in the previous subsections. The possibility of using OPM to detect the activity of deep brain structures has not yet been examined systematically. Nevertheless, OPM was suggested to detect deeper source signals because of its higher S/N ratio and orientation-free system. Indeed, a recent OPM-MEG study reported that the detection accuracy for deeper source signals is almost twofold that of SQUID-MEG and even allowed for detection in the spinal cord (77). However, further advances are required for assessment of cortico-subcortical networks. In recent years, there have been systematic advances in the SQUID-MEG system. With respect to hardware, developments in gradiometers, magnetometers, and reference channels have improved the detection of both shallow and deep sources, which may be useful for cortico-subcortical network analysis. From a theoretical viewpoint, an optimized weighted lead field matrix for deeper source detection, and integration of signal separation methods such as ICA, would also aid in cortico-subcortical network analysis. However, the practical development of such sophisticated subcortical-level network analyses for the new MEG system will take a little more time. Thus, it may be better to initially focus on the shallow source activity because these subcortical networks involve cortical signals. Then, we can shift to the measurement of deeper brain signals and development of more sophisticated tools and devices. Finally, advanced task configuration and experimental design should be considered for reliable measurement of activity in deeper brain networks. Although OPM-MEG can detect activity in deeper brain regions, its credit level is not identical to fMRI. Nonetheless, OPM-MEG provides valuable temporal information. At any rate, the possibility of deep-brain recordings would represent a considerable advancement compared with the current scenario. Detection of deeper brain structures using OPM-MEG enables measurement of thalamocortical communication and the basal ganglia loop, which are of great interest in psychiatric research (**Figure 2C**). Given the importance of temporal information and the limitations of fMRI, RSN analyses will be extended to the wider brain area, with the possibility of exciting temporal information.

CONCLUSION

We addressed the limitations of the current SQUID-MEG system, the expectations of the newly developed MEG system, and how this system should be utilized in psychiatric research. Using MEG, investigation of brain dynamics with high temporal resolution will be invaluable for psychiatric research. Ideally, future investigations will incorporate data on the order of milliseconds that can be used to better understand the role of complex brain networks in psychiatry, such as those involving the cerebrum, cerebellum, limbic system, thalamus, basal ganglia, and their related networks. The development of sensors should provide new insights in child psychiatry and entire brain networks involving deeper structures. Although multimodal analyses are more powerful in principle, the newly developed OPM-MEG neurophysiological device will be very useful and accurate for psychiatric research, even as a standalone single system, because OPM-MEG has both higher temporal and spatial resolution. Note that development of such state-of-the-art functional neuroimaging systems will provide further advances in the fields of neuroscience and psychiatric research. Identifying novel biomarkers for detection of psychiatric disorders is a key goal of psychiatric research (2, 3, 9). We believe that continued MEG advancement will open new doors for establishing neurophysiological biomarkers for psychiatric disorders in the near future.

DATA AVAILABILITY STATEMENT

All datasets presented in this study are included in the article/supplementary material.

ETHICS STATEMENT

The studies involving human participants were reviewed and approved by Ethics Committee of the Graduate School of Medical Sciences, Kyushu University. The patients/participants provided their written informed consent to participate in this study. Written informed consent was obtained from the individual(s) for the publication of any potentially identifiable images or data included in this article.

AUTHOR CONTRIBUTIONS

All authors, NH, YT, TM, TK, and YH, have contributed to writing the manuscript.

FUNDING

This work was supported by Scientific Research from the Ministry of Education, Culture, Sports, Science, and Technology; Grant-in-Aid for Young Scientists (B) (no. JP16K19748) and for Scientific

Research (A) (no. JP19H00630), (B) (nos. JP17H02624 and JP19H03579) and (C) (nos. JP19K08038, JP18K07604, and JP20K12572); AMED under grant (no. JP20dm0207069); and SIRS Research Fund Award (YH) from Schizophrenia International Research Society.

ACKNOWLEDGMENTS

We thank Yuka Egashira, Mariko Hayamizu, and Nami Taniguchi for their comments and discussions. We thank Edanz Group for editing a draft of this manuscript.

REFERENCES

1. Hirano S, Spencer KM, Onitsuka T, Hirano Y. Language-related neurophysiological deficits in schizophrenia. *Clin EEG Neurosci* (2020) 51 (4):222–33. doi: 10.1177/1550059419886686
2. Javitt DC, Siegel SJ, Spencer KM, Mathalon DH, Hong LE, Martinez A, et al. A roadmap for development of neuro-oscillations as translational biomarkers for treatment development in neuropsychopharmacology. *Neuropsychopharmacol* (2020) 45(9):1411–22. doi: 10.1038/s41386-020-0697-9
3. Hirano Y, Oribe N, Kanba S, Onitsuka T, Nestor PG, Spencer KM. Spontaneous gamma activity in schizophrenia. *JAMA Psychiatry* (2015) 72 (8):813–21. doi: 10.1001/jamapsychiatry.2014.2642
4. Thuné H, Recasens M, Uhlhaas PJ. The 40-Hz auditory steady-state response in patients with schizophrenia: a meta-analysis. *JAMA Psychiatry* (2016) 73 (11):1145–53. doi: 10.1001/jamapsychiatry.2016.2619
5. Hirano Y, Oribe N, Onitsuka T, Kanba S, Nestor PG, Hosokawa T, et al. Auditory cortex volume and gamma oscillation abnormalities in schizophrenia. *Clin EEG Neurosci* (2020) 51(4):244–51. doi: 10.1177/1550059420914201
6. Edgar JC. Identifying electrophysiological markers of autism spectrum disorder and schizophrenia against a backdrop of normal brain development. *Psychiatry Clin Neurosci* (2020) 74(1):1–11. doi: 10.1111/pcn.12927
7. Ono Y, Kudoh K, Ikeda T, Takahashi T, Yoshimura Y, Minabe Y, et al. Auditory steady-state response at 20 Hz and 40 Hz in young typically developing children and children with autism spectrum disorder. *Psychiatry Clin Neurosci* (2020) 74(6):354–61. doi: 10.1111/pcn.12998
8. Sunaga M, Takei Y, Kato Y, Tagawa M, Suto T, Hironaga N, et al. Frequency-specific resting connectome in bipolar disorder: an MEG study. *Front Psychiatry* (2020) 11:597. doi: 10.3389/fpsyt.2020.00597
9. Ohki T, Takei Y. Neural mechanisms of mental schema: a triplet of delta, low beta/spindle and ripple oscillations. *Eur J Neurosci* (2018) 48(7):2416–30. doi: 10.1111/ejn.13844
10. Baule G, McFee R. Detection of the magnetic field of the heart. *Am Heart J* (1963) 66(1):95–6. doi: 10.1016/0002-8703(63)90075-9
11. Cohen D. Magnetoencephalography: detection of the brain's electrical activity with a superconducting magnetometer. *Science* (1972) 175(4022):664–6. doi: 10.1126/science.175.4022.664
12. Zimmerman JE, Thiene P, Harding JT. Design and operation of stable rf-biased superconducting point-contact quantum devices, and a note on the properties of perfectly clean metal contacts. *J Appl Phys* (1970) 41:1572. doi: 10.1063/1.1659074
13. Hironaga N, Hagiwara K, Ogata K, Hayamizu M, Urakawa T, Tobimatsu S. Proposal for a new MEG-MRI co-registration: A 3D laser scanner system. *Clin Neurophysiol* (2014) 125:2404–12. doi: 10.1016/j.clinph.2014.03.029
14. Hill RM, Boto E, Holmes N, Hartley C, Seedat ZA, Leggett J, et al. A tool for functional brain imaging with lifespan compliance. *Nat Commun* (2019) 10 (1):4785. doi: 10.1038/s41467-019-12486-x
15. Yeo BT, Krienen FM, Sepulcre J, Sabuncu MR, Lashkari D, Hollinshead M, et al. The organization of the human cerebral cortex estimated by intrinsic functional connectivity. *J Neurophysiol* (2011) 106(3):1125–65. doi: 10.1152/jn.00338.2011
16. Vrba J, Fife AA, Burbank MB, Weinberg H, Brickett PA. Spatial discrimination in SQUID gradiometers and 3rd order gradiometer performance. *Can J Phys* (2011) 60(7):1060–73. doi: 10.1139/p82-144
17. Taulu S, Kajola M, Simola J. Suppression of interference and artifacts by the signal space separation method. *Brain Topogr* (2004) 16(4):269–75. doi: 10.1023/b:brat.0000032864.93890.f9
18. Hironaga N, Ioannides AA. Localization of individual area neuronal activity. *NeuroImage* (2007) 34:1519–34. doi: 10.1016/j.neuroimage.2006.10.030
19. Hironaga N, Kimura T, Mitsudo T, Gunji A, Iwata M. Proposal for an accurate TMS-MRI co-registration process via 3D laser scanning. *Neurosci Res* (2019) 144:30–9. doi: 10.1016/j.neures.2018.08.012
20. Qian S, Sheng Y. A single camera photogrammetry system for multi-anglefast localization of EEG electrodes. *Ann Biomed Eng* (2011) 39:2844–56. doi: 10.1007/s10439-011-0374-6
21. Meyer SS, Bonaiuto J, Lim M, Rossiter H, Waters S, Bradbury D, et al. Flexible head-casts for high spatial precision MEG. *J Neurosci Methods* (2017) 276:38–45. doi: 10.1016/j.jneumeth.2016.11.009
22. Zetter R, Iivanainen J, Parkkonen L. Optical co-registration of MRI and on-scalp MEG. *Sci Rep* (2019) 9:5490. doi: 10.1038/s41598-019-41763-4
23. Mosher JC, Leahy RM, Lewis PS. EEG and MEG: Forward solutions for inverse methods. *IEEE Trans Biomed Eng* (1999) 46:245–59. doi: 10.1109/10.748978
24. Piastra MC, Nüßing A, Vorwerk J, Bornfleth H, Oostenveld R, Engwer C, et al. The Discontinuous Galerkin Finite Element Method for Solving the MEG and the Combined MEG/EEG Forward Problem. *Front Neurosci* (2018) 12:30:30. doi: 10.3389/fnins.2018.00030
25. Sarvas J. Basic mathematical and electromagnetic concepts of the biomagnetic inverse problem. *Phys Med Biol* (1987) 32(1):11–22. doi: 10.1088/0031-9155/32/1/004
26. Hämäläinen M, Hari R, Ilmoniemi RJ, Knuutila J, Lounasmaa OV. Magnetoencephalography - theory, instrumentation, and applications to noninvasive studies of the working human brain. *Rev Mod Phys* (1993) 65:413–97. doi: 10.1103/RevModPhys.65.413
27. Hashizume A, Hironaga N. Principles of magnetoencephalography. In: Tobimatsu S, Kakigi R, editors. *Clinical applications of magnetoencephalography*. Tokyo: Springer Japan (2016) p. 3–32. doi: 10.1007/978-4-431-55729-6_1
28. Dale AM, Liu AK, Fischl BR, Buckner RL, Belliveau JW, Lewine JD, et al. Dynamic statistical parametric mapping: combining fMRI and MEG for high-resolution imaging of cortical activity. *Neuron* (2000) 26:55–67. doi: 10.1016/s0896-6273(00)81138-1
29. Grent-'t-Jong T, Gajwani R, Gross J, Gumley AI, Krishnadas R, Lawrie SM, et al. Association of magnetoencephalographically measured high-frequency oscillations in visual cortex with circuit dysfunctions in local and large-scale networks during emerging psychosis. *JAMA Psychiatry* (2020) 77(8):1–75. doi: 10.1001/jamapsychiatry.2020.0284
30. Takei Y, Fujihara K, Tagawa M, Hironaga N, Near J, Kasagi M, et al. The inhibition/excitation ratio related to task-induced oscillatory modulations during a working memory task: a multtimodal-imaging study using MEG and MRS. *NeuroImage* (2016) 128:302–15. doi: 10.1016/j.neuroimage.2015.12.057
31. Hirano S, Nakhnikian A, Hirano Y, Oribe N, Kanba S, Onitsuka T, et al. Phase-amplitude coupling of the electroencephalogram in the auditory cortex in schizophrenia. *Biol Psychiatry Cogn Neurosci Neuroimaging* (2018) 3 (1):69–76. doi: 10.1016/j.bpsc.2017.09.001
32. Khan S, Gramfort A, Shetty NR, Kitzbichler MG, Ganesan S, Moran JM, et al. Local and long-range functional connectivity is reduced in concert in autism spectrum disorders. *PNAS* (2013) 110(8):3107–12. doi: 10.1073/pnas.1214533110
33. Ohki T, Matsuda T, Gunji A, Takei Y, Sakuma R, Kaneko Y, et al. Timing of phase-amplitude coupling is essential for neuronal and functional maturation of audiovisual integration in adolescents. *Brain Behav* (2020) 10(6):e01635. doi: 10.1002/brb3.1635
34. Ohki T, Gunji A, Takei Y, Takahashi H, Kaneko Y, Kita Y, et al. Neural oscillations in the temporal pole for a temporally congruent audio-visual speech detection task. *Sci Rep* (2016) 6:37973. doi: 10.1038/srep37973
35. Hirano Y, Hirano S, Maekawa T, Obayashi C, Oribe N, Monji A, et al. Auditory gating deficit to human voices in schizophrenia: A MEG study. *Schizophr Res* (2010) 117(1):61–7. doi: 10.1016/j.schres.2009.09.003
36. Takei Y, Kumano S, Hattori S, Uehara T, Kawakubo Y, Kasai K, et al. Preattentive dysfunction in major depression: a magnetoencephalography study using auditory mismatch negativity. *Psychophysiology* (2009) 46(1):52–61. doi: 10.1111/j.1469-8986.2008.00748.x

37. Takei Y, Kumano S, Maki Y, Hattori S, Kawakubo Y, Kasai K, et al. Preattentive dysfunction in bipolar disorder: a MEG study using auditory mismatch negativity. *Prog Neuropsychopharmacol Biol Psychiatry* (2010) 34 (6):903–12. doi: 10.1016/j.pnpbp.2010.04.014
38. Shimano S, Onitsuka T, Oribe N, Maekawa T, Tsuchimoto R, Hirano S, et al. Preattentive dysfunction in patients with bipolar disorder as revealed by the pitch-mismatch negativity: a magnetoencephalography (MEG) study. *Bipolar Disord* (2014) 16(6):592–9. doi: 10.1111/bdi.12208
39. Hirano S, Hirano Y, Maekawa T, Obayashi C, Oribe N, Kuroki T, et al. Abnormal neural oscillatory activity to speech sounds in schizophrenia: a magnetoencephalography study. *J Neurosci* (2008) 28(19):4897–903. doi: 10.1523/JNEUROSCI.5031-07.2008
40. Oribe N, Onitsuka T, Hirano S, Hirano Y, Maekawa T, Obayashi C, et al. Differentiation between bipolar disorder and schizophrenia revealed by neural oscillation to speech sounds: an MEG study. *Bipolar Disord* (2010) 12(8):804–12. doi: 10.1111/j.1399-5618.2010.00876.x
41. Tsuchimoto R, Kanba S, Hirano S, Oribe N, Ueno T, Hirano Y, et al. Reduced high and low frequency gamma synchronization in patients with chronic schizophrenia. *Schizophr Res* (2011) 133:99–105. doi: 10.1016/j.schres.2011.07.020
42. Isomura S, Onitsuka T, Tsuchimoto R, Nakamura I, Hirano S, Oda Y, et al. Differentiation between major depressive disorder and bipolar disorder by auditory steady-state responses. *J Affect Disord* (2016) 190:800–6. doi: 10.1016/j.jad.2015.11.034
43. Hirakawa N, Hirano Y, Nakamura I, Hirano S, Sato J, Oribe N, et al. Right hemisphere pitch-mismatch negativity reduction in patients with major depression: an MEG study. *J Affect Disord* (2017) 215:225–9. doi: 10.1016/j.jad.2017.03.046
44. Matz K, Junghöfer M, Elbert T, Weber K, Wienbruch C, Rockstroh B. Adverse experiences in childhood influence brain responses to emotional stimuli in adult psychiatric patients. *Int J Psychophysiol* (2010) 75(3):277–86. doi: 10.1016/j.ijpsycho.2009.12.010
45. Sanfratello L, Aine C, Stephen J. Neuroimaging investigations of dorsal stream processing and effects of stimulus synchrony in schizophrenia. *Psychiatry Res Neuroimaging* (2018) 278:56–64. doi: 10.1016/j.pscychresns.2018.05.005
46. Recasens M, Gross J, Uhlhaas PJ. Low-frequency oscillatory correlates of auditory predictive processing in cortical-subcortical networks: a MEG-study. *Sci Rep* (2018) 8(1):14007. doi: 10.1038/s41598-018-32385-3
47. Britton JC, Bar-Haim Y, Carver FW, Holroyd T, Norcross MA, Detloff A, et al. Isolating neural components of threat bias in pediatric anxiety. *J Child Psychol Psychiatry* (2012) 53(6):678–86. doi: 10.1111/j.1469-7610.2011.02503.x
48. Sanfratello L, Houck JM, Calhoun VD. Dynamic functional network connectivity in schizophrenia with magnetoencephalography and functional magnetic resonance imaging: Do different timescales tell a different story? *Brain Connect* (2019) 9(3):251–62. doi: 10.1089/brain.2018.0608
49. Hirvonen J, Wibral M, Palva JM, Singer W, Uhlhaas P, Palva S. Whole-brain source-reconstructed MEG-data reveal reduced long-range synchronization in chronic schizophrenia. *eNEURO* (2017) 4(5):ENEURO.0338-17.2017. doi: 10.1523/ENEURO.0338-17.2017.0338-17
50. Rojas DC, Wilson LB. γ-band abnormalities as markers of autism spectrum disorders. *Biomark Med* (2014) 8(3):353–68. doi: 10.2217/bmm.14.15
51. Cornew L, Roberts TP, Blaskey L, Edgar JC. Resting-state oscillatory activity in autism spectrum disorders. *J Autism Dev Disord* (2012) 42(9):1884–94. doi: 10.1007/s10803-011-1431-6
52. Rojas DC, Maharajh K, Teale P, Rogers SJ. Reduced neural synchronization of gamma-band MEG oscillations in first-degree relatives of children with autism. *BMC Psychiatry* (2008) 8:66. doi: 10.1186/1471-244X-8-66
53. Mulas F, Capilla A, Fernández S, Etchepareborda MC, Campo P, Maestú F, et al. Shifting-related brain magnetic activity in attention-deficit/hyperactivity disorder. *Biol Psychiatry* (2006) 59(4):373–9. doi: 10.1016/j.biopsych.2005.06.031
54. Muthuraman M, Moliadze V, Boecher L, Siemann J, Freitag CM, Groppa S, et al. Multimodal alterations of directed connectivity profiles in patients with attention-deficit/hyperactivity disorders. *Sci Rep* (2019) 9(1):20028. doi: 10.1038/s41598-019-56398-8
55. Chen YH, Saby J, Kuschner E, Gaetz W, Edgar JC, Roberts TPL. Magnetoencephalography and the infant brain. *NeuroImage* (2019) 189:445–58. doi: 10.1016/j.neuroimage.2019.01.059
56. Horovitz SG, Braun AR, Carr WS, Picchioni D, Balkin TJ, Fukunaga M. Decoupling of the brain's default mode network during deep sleep. *PNAS* (2009) 106(27):11376–81. doi: 10.1073/pnas.0901435106
57. Raichle ME, MacLeod AM, Snyder AZ, Powers WJ, Gusnard DA, Shulman GL. A default mode of brain function. *PNAS* (2001) 98(2):676–82. doi: 10.1073/pnas.98.2.676
58. Uhlhaas PJ, Liddle P, Linden DEJ, Nobre AC, Singh KD, Gross J. Magnetoencephalography as a tool in psychiatric research: current status and perspective. *Biol Psychiatry Cogn Neurosci Neuroimaging* (2017) 2 (3):235–44. doi: 10.1016/j.bpsc.2017.01.005
59. Menon V. Large-scale brain networks and psychopathology: a unifying triple network model. *Trends Cognit Sci* (2011) 15(10):483–506. doi: 10.1016/j.tics.2011.08.003
60. Hinkley LB, Vinogradov S, Guggisberg AG, Fisher M, Findlay AM, Nagarajan SS. Clinical symptoms and alpha band resting-state functional connectivity imaging in patients with schizophrenia: implications for novel approaches to treatment. *Biol Psychiatry* (2011) 70(12):1134–42. doi: 10.1016/j.biopsych.2011.06.029
61. Rutter L, Carver FW, Holroyd T, Nadar SR, Mitchell-Francis J, Apud J, et al. Magnetoencephalographic gamma power reduction in patients with schizophrenia during resting condition. *Hum Brain Mapp* (2009) 30:3254–64. doi: 10.1002/hbm.20746
62. Kim JS, Shin KS, Jung WH, Kim SN, Kwon JS, Chung CK. Power spectral aspects of the default mode network in schizophrenia: an MEG study. *BMC Neurosci* (2014) 15:104. doi: 10.1186/1471-2202-15-104
63. Datko M, Gougelet R, Huang MX, Pineda JA. Resting state functional connectivity MRI among spectral MEG current sources in children on the autism spectrum. *Front Neurosci* (2016) 10:258:258. doi: 10.3389/fnins.2016.00258
64. Lajiness-O'Neill R, Brennan JR, Moran JE, Richard AE, Flores AM, Swick C, et al. Patterns of altered neural synchrony in the default mode network in autism spectrum disorder revealed with magnetoencephalography (MEG): relationship to clinical symptomatology. *Autism Res* (2018) 11(3):434–49. doi: 10.1002/aur.1908
65. Brodski-Guerniero A, Naumer MJ, Moliadze V, Chan J, Althen H, Ferreira-Santos F, et al. Predictable information in neural signals during resting state is reduced in autism spectrum disorder. *Hum Brain Mapp* (2018) 39(8):3327–40. doi: 10.1002/hbm.24072
66. Khan S, Hashmi JA, Mamashli F, Michmizos K, Kitzbichler MG, Bharadwaj H, et al. Maturation trajectories of cortical resting-state networks depend on the mediating frequency band. *NeuroImage* (2018) 174:57–68. doi: 10.1016/j.neuroimage.2018.02.018
67. Wilson TW, Franzen JD, Heinrichs-Graham E, White ML, Knott NL, Wetzel MW. Broadband neurophysiological abnormalities in the medial prefrontal region of the default-mode network in adults with ADHD. *Hum Brain Mapp* (2013) 34(3):566–74. doi: 10.1002/hbm.21459
68. Papadelis C, Leonardelli E, Staudt M, Braun C. Can magnetoencephalography track the afferent information flow along white matter thalamo-cortical fibers? *NeuroImage* (2012) 60(2):1092–105. doi: 10.1016/j.neuroimage.2012.01.054
69. Roux F, Wibral M, Singer W, Aru J, Uhlhaas PJ. The phase of thalamic alpha activity modulates cortical gamma-band activity: evidence from resting-state MEG recordings. *J Neurosci* (2013) 33(45):17827–35. doi: 10.1523/JNEUROSCI.5778-12.2013
70. Schulman JJ, Cancro R, Lowe S, Lu F, Walton KD, Llinás RR. Imaging of thalamocortical dysrhythmia in neuropsychiatry. *Front Hum Neurosci* (2011) 5:69. doi: 10.3389/fnhum.2011.00069
71. Macpherson T, Hikida T. Role of basal ganglia neurocircuitry in the pathology of psychiatric disorders. *Psychiatry Clin Neurosci* (2019) 3(6):289–301. doi: 10.1111/pcn.12830
72. Saxena S, Brody AL, Schwartz JM, Baxter LR. Neuroimaging and frontal-subcortical circuitry in obsessive-compulsive disorder. *Br J Psychiatry Suppl* (1998) 35:26–37. doi: 10.1192/S0007125000297870
73. Graybiel AM, Rauch SL. Toward a neurobiology of obsessive-compulsive disorder. *Neuron* (2000) 28(2):343–7. doi: 10.1016/s0896-6273(00)00113-6
74. Kominis IK, Kornack TW, Allred JC, Romalis MV. A subfemtotesla multichannel atomic magnetometer. *Nature* (2003) 422(6932):596–9. doi: 10.1038/nature01484

75. Johnson CN, Schwindt PDD, Weisend M. Magnetoencephalography with a two-color pump-probe, fiber-coupled atomic magnetometer. *Appl Phys Lett* (2010) 97(24):1–3. 243703. doi: 10.1063/1.3522648
76. Kamada K, Sato D, Ito Y, Natsukawa H, Okano K, Mizutani N, et al. Human magnetoencephalogram measurements using newly developed compact module of high-sensitivity atomic magnetometer. *Jpn J Appl Phys* (2015) 54:26601. doi: 10.7567/JJAP.54.026601
77. Boto E, Meyer SS, Shah V, Alem O, Knappe S, Kruger P, et al. A new generation of magnetoencephalography: room temperature measurements using optically-pumped magnetometers. *NeuroImage* (2017) 149:404–14. doi: 10.1016/j.neuroimage.2017.01.034

Conflict of Interest: The authors declare that the research was conducted in the absence of any commercial or financial relationships that could be construed as a potential conflict of interest.

frontiers in Psychiatry

ORIGINAL RESEARCH
published: 03 September 2020
doi: 10.3389/fpsyt.2020.554844

Neurophysiological Face Processing Deficits in Patients With Chronic Schizophrenia: An MEG Study

Naotoshi Ohara[1,2], Yoji Hirano[1,3], Naoya Oribe[1,4], Shunsuke Tamura[1], Itta Nakamura[1], Shogo Hirano[1], Rikako Tsuchimoto[1,5], Takefumi Ueno[1,4], Osamu Togao[6], Akio Hiwatashi[7], Tomohiro Nakao[1] and Toshiaki Onitsuka[1]**

[1] Department of Neuropsychiatry, Graduate School of Medical Sciences, Kyushu University, Fukuoka, Japan, [2] Medical Corporation Seiryokai, Mimamigaoka Hospital, Fukuoka, Japan, [3] Department of Psychiatry, Harvard Medical School, Boston, MA, United States, [4] Division of Clinical Research, National Hospital Organization, Hizen Psychiatric Medical Center, Saga, Japan, [5] Center for Health Sciences and Counseling, Kyushu University, Fukuoka, Japan, [6] Department of Molecular Imaging and Diagnosis, Graduate School of Medical Sciences, Kyushu University, Fukuoka, Japan, [7] Department of Clinical Radiology, Graduate School of Medical Sciences, Kyushu University, Fukuoka, Japan

OPEN ACCESS

Edited by:
André Schmidt,
University of Basel, Switzerland

Reviewed by:
Kiyoto Kasai,
University of Tokyo, Japan
Thomas Whitford,
University of New South Wales, Australia
Toshihiko Maekawa,
Kyushu University, Japan

***Correspondence:**
Yoji Hirano
yhouji@mac.com
Toshiaki Onitsuka
onitsuka.toshiaki.939@m.kyushu-u.ac.jp

Specialty section:
This article was submitted to Neuroimaging and Stimulation, a section of the journal Frontiers in Psychiatry

Received: 23 April 2020
Accepted: 19 August 2020
Published: 03 September 2020

Citation:
Ohara N, Hirano Y, Oribe N, Tamura S, Nakamura I, Hirano S, Tsuchimoto R, Ueno T, Togao O, Hiwatashi A, Nakao T and Onitsuka T (2020) Neurophysiological Face Processing Deficits in Patients With Chronic Schizophrenia: An MEG Study. Front. Psychiatry 11:554844. doi: 10.3389/fpsyt.2020.554844

Background: Neuropsychological studies have revealed that patients with schizophrenia (SZ) have facial recognition difficulties and a reduced visual evoked N170 response to human faces. However, detailed neurophysiological evidence of this face processing deficit in SZ with a higher spatial resolution has yet to be acquired. In this study, we recorded visual evoked magnetoencephalography (MEG) and examined whether M170 (a magnetic counterpart of the N170) activity deficits are specific to faces in patients with chronic SZ.

Methods: Participants were 26 patients with SZ and 26 healthy controls (HC). The M170 responses to faces and cars were recorded from whole-head MEG, and global field power over each temporal cortex was analyzed. The distributed M170 sources were also localized using a minimum-norm estimation (MNE) method. Correlational analyses between M170 responses and demographics/symptoms were performed.

Results: As expected, the M170 was significantly smaller in the SZ compared with the HC group in response to faces, but not to cars (faces: $p = 0.01$; cars: $p = 0.55$). The MNE analysis demonstrated that while the M170 was localized over the fusiform face area (FFA) in the HC group, visual-related brain regions other than the FFA were strongly activated in the SZ group in both stimulus conditions. The severity of negative symptoms was negatively correlated with M170 power (rho = –0.47, $p = 0.01$) in SZ. Within HC, there was a significant correlation between age and the M170 responses to faces averaged for both hemispheres (rho = 0.60, $p = 0.001$), while such a relationship was not observed in patients with SZ (rho = 0.09, $p = 0.67$).

Conclusion: The present study showed specific reductions in the M170 response to human faces in patients with SZ. Our findings could suggest that SZ is characterized by face processing deficits that are associated with the severity of negative symptoms. Thus,

we suggest that social cognition impairments in SZ might, at least in part, be caused by this functional face processing deficit.

Keywords: schizophrenia, magnetoencephalography, M170, human faces, fusiform gyrus

INTRODUCTION

Social deficits caused by psychiatric disorders can be quite severe. Patients with schizophrenia (SZ) suffer from severe psychosocial dysfunctions and the substantial burden of the disease affects patients worldwide (1). The employment rate is low for patients with SZ (2), and social exclusion is commonly experienced (3). These dysfunctions could be attributed to impairments in social cognition, which is, at least in part, caused by face processing deficits (4). Therefore, it is important to investigate the neural basis of face recognition deficits in patients with SZ.

Neuropsychological studies have revealed that patients with SZ have facial recognition difficulties (e.g., 5–7). Neurophysiological approaches have also detected facial recognition deficits in SZ. The visually evoked N170 component is a negative potential recorded using electroencephalography (EEG) at occipitotemporal electrodes at around 170 ms after stimulus onset and reflects the early phase of face processing (8). A face-sensitive N170 reduction has been repeatedly reported in patients with SZ (9–11). Moreover, it has been suggested that this reduction in the face-sensitive N170 is significantly associated with social dysfunction in patients with SZ (12, 13). To date, only one face recognition study in patients with SZ has used magnetoencephalography (MEG). Rivolta et al. (14) reported significantly increased magnetic M170 (a magnetic counterpart of the N170) responses during the perception of Mooney faces in antipsychotic-naïve first-episode patients with SZ; the authors concluded that this effect may indicate aberrant glutamatergic neurotransmission at illness onset (15). However, to our knowledge, no study has examined the specific face-sensitive M170 response in patients with chronic SZ. It has been suggested that reductions in glutamate levels observed in patients with SZ are caused by excitotoxicity during the acute phase of the illness, and that this may have a huge impact on patients' brain function during recurrences throughout the course of the illness (15). Indeed, Tsai et al. (16) found decreased glutamate levels in the postmortem brains of patients with chronic SZ. Thus, given this evidence, we hypothesized that patients with chronic SZ would show reduced face-sensitive M170 responses that reflect altered glutamatergic neurotransmission in the chronic state.

MEG offers a higher spatial resolution than EEG, which allows the source of neuronal activity to be more accurately located. Furthermore, MEG waveforms cannot be deformed by conductivity affecting volume currents, which makes it more suitable for assessing the laterality of neural activity. In healthy subjects, it has been reported that the M170 is generated in the fusiform gyrus, which is a crucial region for facial recognition (17). However, Pierce et al. (18) reported that patients with autism process human faces outside the fusiform gyrus.

The present study examined, for the first time, the M170 response to faces in patients with chronic SZ, which can offer insights as to whether the fusiform gyrus is the center of face recognition in patients with chronic SZ. Given that patients with SZ have been reported to exhibit a bilateral N170 reduction that is specific to faces, we also investigated the M170 response to cars (see, for example, 13, 19). This work allows us to better understand whether the face recognition process is specifically impaired in chronic SZ. The present study was designed to test the hypothesis that patients with chronic SZ show less activation in early visual processing for faces than healthy subjects, as measured by the M170 response to faces.

MATERIALS AND METHODS

Subjects

A total of 26 patients with SZ (13 male) and 26 healthy controls (HC; 16 male) aged between 20 and 65 years participated in the study. All participants were right-handed and had normal or corrected-to-normal visual acuity. After receiving a complete explanation of the study, all subjects signed an informed consent form according to the regulations of the Research Ethics Committee of the Graduate School of Medical Sciences, Kyushu University. For both groups, the exclusion criteria were as follows: 1) major head trauma; 2) neurological illness; 3) history of electroconvulsive therapy; 4) drug or alcohol dependence; 5) drug or alcohol abuse within the past five years; and/or 6) a verbal intelligence quotient below 75. The HC participants were screened using the Structured Clinical Interview (SCID) non-patient edition (20), which confirmed that no HC participants, or their first-degree relatives, had an Axis-I psychiatric disorder.

All patients were recruited from Kyushu University Hospital, the Japan Self-Defense Forces Fukuoka Hospital, and an affiliated private clinic (Kouno Clinic), and had been diagnosed with SZ based on medical records and the SCID-DSM IV (21). The patients' symptoms were evaluated on the Scale for the Assessment of Positive Symptoms (SAPS) (22) and the Scale for the Assessment of Negative Symptoms (SANS) (23). **Table 1** shows the demographic data for all participants. All patients were receiving neuroleptic medication [typical neuroleptics (1/26 patients), atypical (20/26), or both (5/26)], with a mean daily dose equivalent to 398 ± 292 mg/day of chlorpromazine (24).

Visual Stimuli and Experimental Procedures

The stimuli were two colored pictures of emotionally neutral faces (1 male and 1 female Asian faces), two pictures of cars, and one picture of a butterfly. Stimuli were presented using Stim2 software (Compumedics Neuroscan) video projector that was placed outside the magnetically shielded room in which the

TABLE 1 | Demographic and clinical characteristics of the subjects.

	HC	SZ	df	t or x^2	p
Sex, M/F, No	16/10	13/13	1	0.70	0.40
Age (years)	40.4 ± 14.0	40.0 ± 10.8	50	0.12	0.90
Handedness	96.4 ± 10.3	99.4 ± 2.1	50	−1.32	0.20
SES	2.6 ± 0.9	3.3 ± 1.0	50	−2.53	0.02*
Parental SES	3.1 ± 0.8	2.8 ± 1.0	50	1.41	0.17
Medication dose (CPZ equiv., mg)		398 ± 292			
Symptom onset (years)		25.7 ± 9.0			
Duration of illness (years)		14.1 ± 9.9			
SAPS		33.2 ± 31.4			
SANS		54.4 ± 31.6			
GAF		56.5 ± 14.0			

The data are given as mean ± SD. HC, healthy controls; SZ, patients with schizophrenia. Asterisks indicate statistically significant results. SZ showed significantly lower SES than HC.

experiment was conducted. All images were 24 × 24 cm in size and the distance between the subjects' eyes and the screen was 100 cm. During the experiment, the two faces and two cars were presented 60 times each, and the butterfly target was presented 30 times. Stimuli were presented in a pseudo-random order. The images appeared in the center of the screen for 500 ms, each preceded by a 200 ms interval during which a fixation point was presented in the middle of the screen at which subjects were asked to maintain their gaze, followed by a 200-ms interval during which the screen was blank. The interstimulus interval was 1,900 ms. Subjects were instructed to click a mouse button with their right hand as soon as they saw the target picture (butterfly). A no-response was recorded if the response time exceeded 1,500 ms.

Data Collection and Processing

Magnetic signals were acquired using a 306-channel sensor array whole-head MEG system (Vectorview; ELEKTA Neuromag, Finland). The sampling rate was set to 1 kHz and the recording band-pass filter was set to 0.01–330 Hz. All data sets were filtered using Maxfilter to eliminate noise originating from outside of the brain (25). We analyzed data recorded using 204-sensor, planar-type gradiometers. Before the recording, four head position indicator (HPI) coils were attached to the scalp, and a three-dimensional digitizer was used to determine the anatomical landmarks of the head with regard to the HPI coils. The accurate location of the head with regard to the sensor array was measured using the HPI coils.

Magnetic Global Field Power of the M170

The event-related field was calculated in each gradiometer by averaging artifact-free epochs (epochs larger than 2000 ft/cm were rejected) within a latency window of −100 to 700 ms, with 0 ms corresponding to the visual stimulus onset. The averaged waveforms were digitally filtered from 1 to 20 Hz using a band-pass Butterworth filter and then amplitude-baselined relative to the pre-stimulus period of −100 to 0 ms. To analyze the M170, we selected 10 pairs of sensors (20 sensors) around one gradiometer coil that showed the largest amplitude within 120–250 ms after stimuli onset in each temporal hemisphere (**Figure 1**), because signals are strongest when the sensors are located just above local cerebral sources (26). The magnetic counterpart of the global field power (mGFP) was obtained separately for each hemisphere using the root mean square (RMS) values across the selected 10 sensors. The peak amplitude of the M170 was defined as the largest amplitude of the individual mGFP within 120–250 ms after stimulus onset, and the M170 peak latency was defined as the time of the peak amplitude of M170 from stimulus onset.

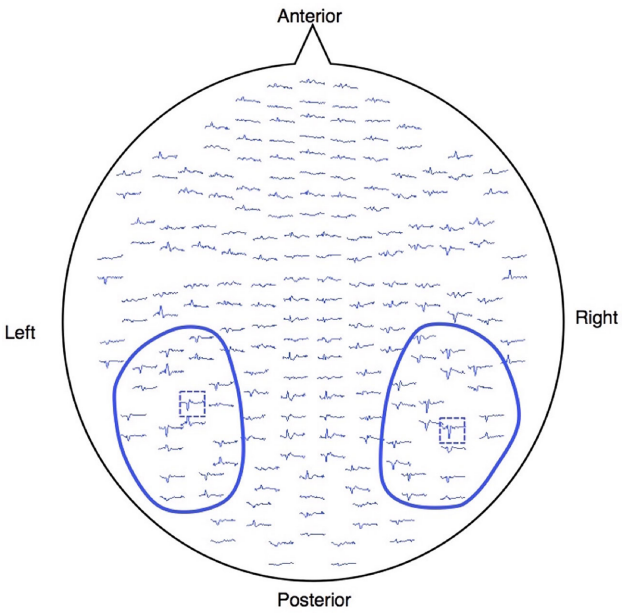

FIGURE 1 | Waveforms of one healthy subject projected onto the measured 204 gradiometers. The MEG signals were acquired using a whole-head, 306-channel sensor array that comprised 102 identical triple-sensor elements. Each sensor consisted of two orthogonal planar-type gradiometers and one magnetometer. Circled waveforms with blue lines indicate the sensors used for the analysis. The blue dashed boxes are the sensors, which showed the largest response between 120 and 250 ms after the stimulus onset for each hemisphere.

Source Localization Analysis

To investigate the distributed source of the M170, source localization analysis was performed for the averaged waveform before baseline correction using a minimum-norm estimation (27). We first conducted a co-registration between MEG data and a template MRI (MNI-305, 28) based on the head position data obtained through the HPI coils and 3-D digitizer (we excluded data from 6 HC and 8 SZ subjects from further source analysis because the co-registration accuracy was poor). We then computed the forward solutions for all source locations (mesh-patterned 8,196 dipole locations were marked in the standard brain) using a single-compartment boundary-element model. A noise covariance matrix was created using the pre-stimulus period epoch data. The noise-normalized source activity [dynamical statistical parametric mapping (dSPM); 29] at each source location was estimated from each time point of the averaged waveform using an MNE inverse operator computed from the forward solution and the noise covariance matrix. To

visualize the distributed source of the M170 in each stimulus condition (faces or cars), we calculated the time-averaged dSPM values within 120–250 ms at each source location.

Statistical Analysis

Student's t-tests were used to assess between-group differences in age, handedness score, education years, SES, parental SES, and sleeping scale. The mGFP peak latencies and M170 amplitudes were analyzed using a repeated-measures analysis of variance (rmANOVA), with group (SZ or HC) as a between-subjects factor, and hemisphere (left or right) and stimulus type (faces or cars) as within-subjects factors. Degrees of freedom were adjusted using the Huynh-Feldt epsilon for factors with more than two levels. The associations between the clinical symptoms and the mGFP peak latencies and powers of the M170 and dipole moments were investigated using Spearman's rho. All results were considered significant at $p \leq 0.05$.

RESULTS

Demographics

There were no significant between-group differences in age, handedness, education years, or sleeping scale. The SZ group had a significantly lower SES and parental SES than the HC group. The SZ group had a significantly longer mean reaction time than the HC group ($t[50] = -2.94$, $p = 0.05$), but there were no between-group group differences in the accuracy of target responses (SZ, 97.7%; HC, 97.1%; $t[50] = -0.39$, $p = 0.70$).

Magnetic Global Field Power of the M170

The rmANOVA revealed a significant main effect of group [$F(1,50) = 7.1$, $p = 0.01$] and stimulus [$F(1,50) = 31.3$, $p < 0.001$] on the mGFP value of the M170 (**Figure 2**). There was also a significant stimulus-by-group interaction effect [$F(1,50) = 14.6$, $p < 0.001$]. There was no main effect of hemisphere on the mGFP value of the M170 [$F(1,50) = 0.9$, $p = 0.36$] and no interactions related to group ($0.56 \leq p \leq 1.00$). To delineate the significant stimulus-by-group interaction, stimulus differences and group differences were compared using t-tests using the average power of M170 of both hemispheres. In the HC group, the M170 power in response to face stimuli was significantly greater than that in response to cars ($t[25] = 5.3$, $p < 0.001$), but the SZ group showed no such significant differences ($t[25] = 0.9$, $p = 0.38$). The SZ group showed a significant M170 power reduction in response to faces compared to the HC group ($t[50] = 3.7$, $p = 0.01$). However, there were no significant between-group differences in response to cars ($t[50] = 0.6$, $p = 0.55$). These results suggest that the SZ group showed an M170 reduction that was specific to faces.

Latency of the M170

Table 2 shows the latencies of the M170. The rmANOVA revealed a significant main effect of stimulus on M170 latency [$F(1,50) = 35.6$, $p < 0.001$]. There was no main effect of group and no group-related interactions.

Source Distribution of the M170

Figure 3 shows group-averaged source distribution maps of the M170 in responses to faces and cars. In the HC group, strong activations were observed near or within the fusiform face area (FFA) of the right hemisphere in both stimulus conditions. In contrast, source activity spread broadly throughout visual-related brain regions other than the FFA in the SZ group.

Correlations Between M170 Power and Clinical Measurements

In the SZ group, we calculated the correlation between the face-evoked M170 power averaged across both hemispheres, as well as

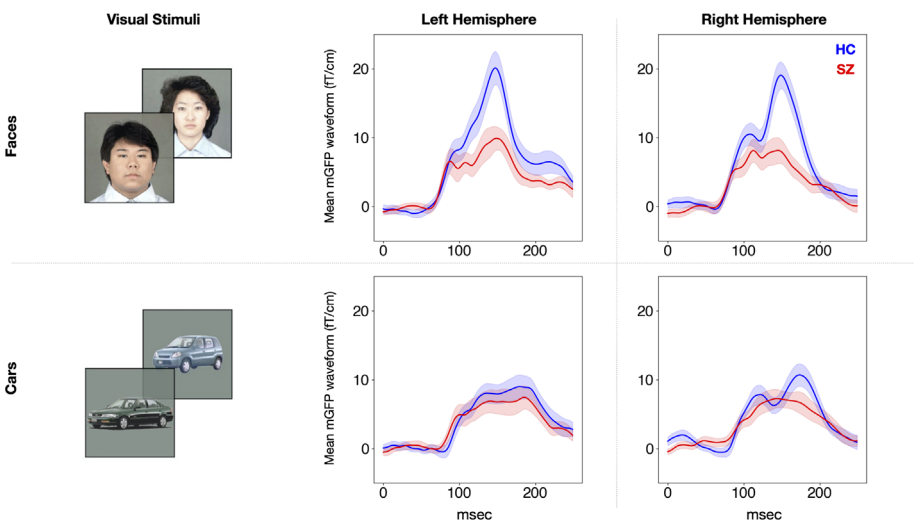

FIGURE 2 | Group average M170 waveforms in response to faces and cars for each hemisphere. The waveforms of the SZ group (n = 26) are shown in red and those of the HC group (n = 26) are shown in blue. The SEM is plotted semitransparent. SZ, patients with schizophrenia; HC, healthy control.

TABLE 2 | Mean M170 power and latencies averaged in healthy controls (N = 26) and patients with schizophrenia (N = 26).

	Face					Car				
	HC	SZ	df	t	p	HC	SZ	df	t	p
Amplitude (fT/cm)										
Right	23.2 ± 10.4	13.3 ± 9.6	50	3.5	0.001	13.4 ± 7.3	12.6 ± 8.2	50	0.33	0.74
Left	24.6 ± 12.6	15.6 ± 10.5	50	2.8	0.008	14.2 ± 8.0	12.6 ± 9.5	50	0.65	0.52
Latency (ms)										
Right	149.7 ± 11.9	156.5 ± 20.7	50	−1.4	0.16	168.9 ± 19.0	169.4 ± 21.4	50	−0.10	0.92
Left	155.7 ± 21.5	161.9 ± 22.2	50	−1.0	0.31	170.8 ± 24.8	172.1 ± 24.0	50	−0.19	0.85

The data are shown as mean ± SD.
HC, healthy controls; SZ, individuals with schizophrenia.

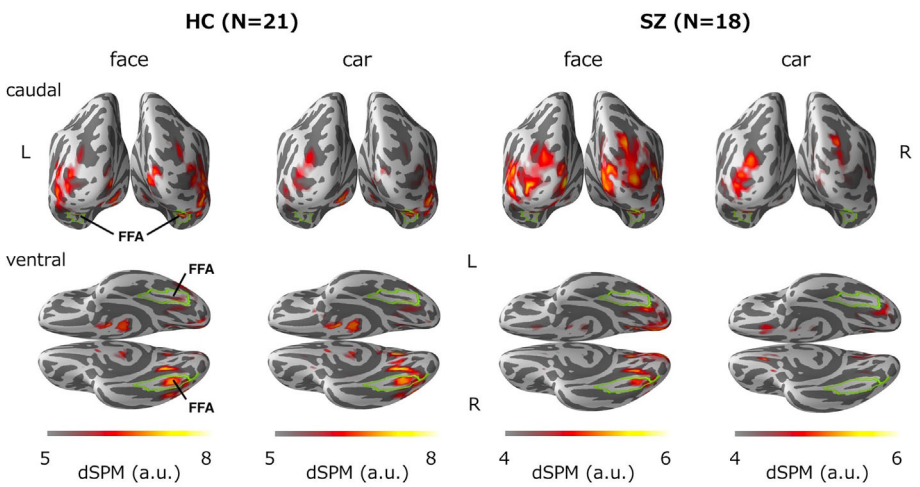

FIGURE 3 | Group-averaged source distribution maps of the M170 in response to faces and cars. The upper and lower panels show the distribution maps from the caudal and ventral views, respectively. The horizontal bars at the bottom indicate the colored threshold levels of the distribution maps. The fusiform gyrus is outlined in green. FFA, fusiform face area.

within the left and right hemispheres, and the clinical symptom scores. The M170 power was significantly correlated with the SANS total score (averaged: rho = −0.47, p = 0.01; left: rho = −0.46, p = 0.02; right: rho = −0.42, p = 0.04; **Figure 4**). There were no significant correlations between demographic or symptom scores and M170 variables in response to any stimuli (−0.37 ≤ rho ≤ 0.30, 0.06 ≤ p ≤ 0.93). There were no significant correlations between chlorpromazine-equivalent doses and the value of the M170 in response to any stimuli (−0.19 ≤ rho ≤ 0.28, 0.19 ≤ p ≤ 0.94).

Within the HC group, there was a significant correlation between age and the M170 global field power to faces averaged for both hemispheres (rho = 0.60, p = 0.001), while such a relationship was not observed in the chronic SZ group (rho = 0.09, p = 0.67; **Figure 5**).

DISCUSSION

The major findings of this study were as follows: 1) the power of the M170 was significantly smaller in SZ group than in the HC group, specifically in response to human faces, 2) there was no significant between-group difference in the dipole locations of the M170, which were estimated to originate from the fusiform gyrus, 3) SANS scores were negatively correlated with M170 power to faces, and 4) for the HC group, there was a significant correlation between age and the M170 power to faces, while such a relationship was not observed in the chronic SZ group.

Our finding of an M170 reduction in response to faces in patients with chronic SZ is consistent with the face-sensitive N170 attenuations reported in a meta-analysis (10) and a recent systematic review (30). The meta-analysis reported that the effect size of the face-sensitive N170 reduction was 0.64 (10). For first-episode or drug-naïve patients with SZ, the small number of studies that have investigated the N170 or M170 response to faces have reported mixed findings. For example, Rivolta et al. (14) reported a significantly increased magnetic face-sensitive M170 to pictures of moony faces in antipsychotic-naïve, first-episode patients with SZ. Yang et al. (31) reported no N170 reduction in response to emotional faces in first-episode/early course (<3 years of illness) patients with SZ. However, Salisbury et al. (32) showed a significant

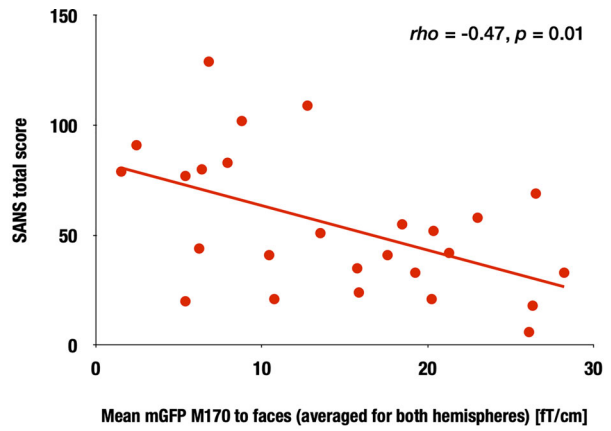

FIGURE 4 | Correlation between the M170 response to faces and SANS total scores in the SZ group. Scattergram showing the relationship between the M170 response to faces averaged for both hemispheres and the SANS total scores in the SZ group.

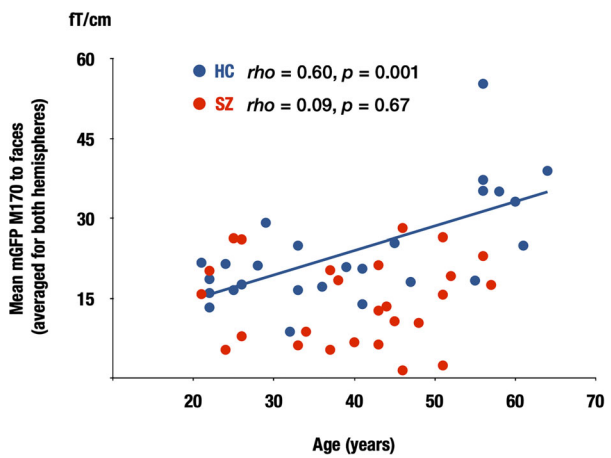

FIGURE 5 | Correlation between the M170 response to faces and age in both groups. Scattergrams showing the relationship between the M170 response to faces averaged for both hemispheres and age in the HC and SZ groups. SZ: patients with schizophrenia (red), HC, healthy control (blue).

N170 attenuation in response to neutral faces and cars in first-hospitalized patients with SZ. Tsunoda et al. (13) found a significant N170 reduction in response to neutral faces in the early course of SZ (the average duration of illness: 6.4 months). The samples of Salisbury et al. (32) and Tsunoda et al. (13) were medication managed. Therefore, the effects of acute psychosis and medication on face processing should be further examined.

Although it is not yet clear whether the face-sensitive M170 is altered in acute drug-naïve patients, the previous and the current findings indicate that the face-sensitive M170 is decreased in patients with chronic medicated SZ. Rivolta et al. (14) have suggested that a shift of the excitation/inhibition balance toward excitation could lead to face-sensitive M170 abnormalities. Reduced face-sensitive M170 responses found in the current study might be associated with altered glutamatergic neurotransmission in the chronic state, with possible progressive pathophysiological changes after the onset of SZ.

It is not yet clear why face-sensitive N170 and M170 responses are specifically impaired in chronic SZ compared to the processing of other visual objects. In social communication, people need to distinguish human faces instantaneously. It may be possible that sophisticated processes such as face recognition may be more vulnerable to abnormal neuronal excitation, while general visual processing deficits progress slowly after the onset of SZ. Salisbury et al. (32) reported significant N170 reductions in response to faces and cars in SZ. They argued that their sample size was large in comparison with previous studies and suggested that possible power issues partially allowed them to detect overall N170 reduction in SZ. A comprehensive review has pointed out that, at the behavioral level, visual perception deficits in SZ may not be specific to faces, are often present when the cognitive and perceptual demands of a task are high, and are likely to worsen with the progression of the illness (33). Thus, further research is required to clarify our findings at both the behavioral and neurophysiological levels.

The present study found that a face-sensitive M170 reduction is associated with dysfunction of the fusiform gyrus in chronic SZ. Onitsuka et al. (19) found a significant association between face-sensitive N170 attenuation and gray matter reduction of the fusiform gyrus in the right hemisphere of patients with chronic SZ. Thus, both structural and functional deficits could underlie this face-sensitive attenuation in SZ. At the cellular level, the face-sensitive M170 deficit identified in our study may involve progressive dendritic spine alterations (34), which is the strongest source of evoked responses (35). Furthermore, in terms of the source distribution of M170, the MNE analysis demonstrated that while the M170 was localized over the FFA in the HC group, visual-related brain regions other than the FFA were strongly activated in the SZ group in both stimulus conditions (**Figure 3**). Thus, it is likely that face-sensitive M170 abnormality could arise from inefficient neural network activities during visual face processing in SZ.

We found a shorter M170 latency for faces than for cars in both groups, which was compatible with our previous findings (e.g., 13). The N170/M170 are known to show larger and earlier peak activity in response to face stimuli than to non-face stimuli (36–38). Hence, our results suggest that while face-sensitive M170 power is decreased, its processing speed remains normal in SZ.

We found that patients with chronic SZ with more severe negative symptoms had smaller face-sensitive M170 responses, which is generally consistent with the literature. However, it should be noted that the sample size for our correlational analyses may not be sufficient, which needs to be replicated in more extensive sample studies. One recent systematic review (30) reported a tendency for an association between a face-sensitive N170 reduction and higher severity of positive and negative symptoms. The authors suggested that the face-sensitive N170 may be useful for evaluating social functioning and rehabilitation efficacy. In patients with temporal lobe epilepsy, one study found

that socioeconomic status was significantly correlated with the N170 amplitudes to faces (39). The present study did not demonstrate specificity to schizophrenic psychosis, as we did not include another psychosis group. Therefore, the M170 in other psychoses or neuropsychiatric diseases should be further examined. Moreover, given that longitudinal studies have highlighted the use of EEG/MEG indices as biomarkers for detecting the onset and risk of SZ (40–43), it could be important to evaluate the longitudinal face-specific M170/N170 changes during the early phase of SZ in future studies. Further, long-term test-retest reliability studies (44) may confirm the robustness of the M170/N170 index as a biomarker. Since face and language processing deficits (45) in SZ may interact with each other, it is vital to investigate the neural integration mechanism during simultaneous voice-face information processing (46) in patients with SZ in future. Investigating the association between neurophysiological deficits and structural deficits (e.g., 19, 47) may also shed light on the underlying mechanism of this face processing abnormality.

In the present study, there was a significant association between age and the M170 power to faces in the HC group. It has been reported that the N170 amplitudes in response to faces were larger in older than in young healthy participants (48–52), and the current result is consistent with previous findings. For patients with chronic SZ, such a relationship was not observed. These findings suggest that the normal aging process may not occur in patients with SZ.

CONCLUSION

In summary, the present study showed specific M170 reductions in response to human faces in patients with chronic SZ, and SZ may be characterized by face processing deficits associated with the severity of negative symptoms. We suggest that social cognition impairments in SZ might, at least in part, be caused by functional face processing deficits. Thus, face-specific M170 activity could be a useful biological index to evaluate social cognition abnormalities in SZ.

DATA AVAILABILITY STATEMENT

The raw data supporting the conclusions of this article will be made available by the authors, without undue reservation.

ETHICS STATEMENT

The studies involving human participants were reviewed and approved by The Ethics Committee of the Graduate School of Medical Sciences, Kyushu University. The patients/participants provided their written informed consent to participate in this study. Written informed consent was also obtained from the individuals for the publication of any potentially identifiable images or data included in this article.

AUTHOR CONTRIBUTIONS

TO and NOh designed the study. NOh, NOr, and IN collected and analyzed the data. NO prepared the first draft of the manuscript. YH, NOr, SH, RT, and ST assisted data analyses and created figures. TU, OT, AH, TN, and ST edited the manuscript. YH and TO critically revised manuscript. All authors contributed to and have approved the final manuscript.

FUNDING

This research was supported, in part, by AMED under Grant Number JP20dm0207069 (TO); Grant-in-Aid for Young Scientists B JP22791129 (YH), JP 15K19735 (NOr), and JP 17K16385 (NOr), a Grant-in-Aid for Scientific Research C: JP 16K10217 (TO), JP 19K08049 (NOr), JP 15K09836 (YH), JP 18K07604 (YH), JP 19H03579 (YH) from the Japanese Ministry of Education, Culture, Sports, Science, and Technology; Medical Research Fund (YH) from Takeda Science Foundation; SIRS Research Fund Award (YH) from Schizophrenia International Research Society. The funding sources had no further role in study design; in the collection, analysis, and interpretation of data; in the writing report; and in the decision to submit the paper for publication.

ACKNOWLEDGMENTS

The authors gratefully acknowledge the administrative support of Motoko Soya.
We thank Nia Cason, PhD, from Edanz Group (https://en-author-services.edanzgroup.com/) for editing a draft of this manuscript.

REFERENCES

1. Charlson FJ, Ferrari AJ, Santomauro DF, Diminic S, Stockings E, Scott JG, et al. Global Epidemiology and Burden of Schizophrenia: Findings from the Global Burden of Disease Study 2016. *Schizophr Bull* (2018) 44:1195–203. doi: 10.1093/schbul/sby058
2. Marwaha S, Johnson S. Schizophrenia and employment - a review. *Soc Psychiatry Psychiatr Epidemiol* (2004) 39:337–49. doi: 10.1007/s00127-004-0762-4
3. Killaspy H, White S, Lalvani N, Berg R, Thachil A, Kallumpuram S, et al. The impact of psychosis on social inclusion and associated factors. *Int J Soc Psychiatry* (2013) 60:148–54. doi: 10.1177/0020764012471918
4. Marwick K, Hall J. Social cognition in schizophrenia: a review of face processing. *Br Med Bull* (2008) 88:43–58. doi: 10.1093/bmb/ldn035
5. Addington J, Addington D. Facial affect recognition and information processing in schizophrenia and bipolar disorder. *Schizophr Res* (1998) 32:171–81. doi: 10.1016/S0920-9964(98)00042-5
6. Evangeli M, Broks ME. Face processing in schizophrenia: parallels with the effects of amygdala damage. *Cognit Neuropsychiatry* (2000) 5:81–104. doi: 10.1080/135468000395754
7. Soria Bauser D, Thoma P, Aizenberg V, Brune M, Juckel G, Daum I. Face and body perception in schizophrenia: a configural processing deficit? *Psychiatry Res* (2012) 195:9–17. doi: 10.1016/j.psychres.2011.07.017

8. Bentin S, Deouell LY. Structural encoding and identification in face processing: erp evidence for separate mechanisms. *Cognit Neuropsychol* (2000) 17:35–55. doi: 10.1080/026432900380472
9. Feuerriegel D, Churches O, Hofmann J, Keage HAD. The N170 and face perception in psychiatric and neurological disorders: A systematic review. *Clin Neurophysiol* (2014) 126:1141–58. doi: 10.1016/j.clinph.2014.09.015
10. Mccleery A, Lee J, Joshi A, Wynn JK, Hellemann GS, Green MF. Meta-analysis of face processing event-related potentials in schizophrenia. *Biol Psychiatry* (2015) 77:116–26. doi: 10.1016/j.biopsych.2014.04.015
11. Onitsuka T, Spencer KM, Nakamura I, Hirano Y, Hirano S, Mccarley RW, et al. Altered P3a Modulations to Emotional Faces in Male Patients with Chronic Schizophrenia. *Clin EEG Neurosci* (2020) 51:215–21. doi: 10.1177/1550059419896723
12. Obayashi C, Nakashima T, Onitsuka T, Maekawa T, Hirano Y, Hirano S, et al. Decreased spatial frequency sensitivities for processing faces in male patients with chronic schizophrenia. *Clin Neurophysiol* (2009) 120:1525–33. doi: 10.1016/j.clinph.2009.06.016
13. Tsunoda T, Kanba S, Ueno T, Hirano Y, Hirano S, Maekawa T, et al. Altered face inversion effect and association between face N170 reduction and social dysfunction in patients with schizophrenia. *Clin Neurophysiol* (2012) 123:1762–8. doi: 10.1016/j.clinph.2012.01.024
14. Rivolta D, Castellanos NP, Stawowsky C, Helbling S, Wibral M, Grützner C, et al. Source-reconstruction of event-related fields reveals hyperfunction and hypofunction of cortical circuits in antipsychotic-naive, first-episode schizophrenia patients during Mooney face processing. *J Neurosci* (2014) 34:5909–17. doi: 10.1523/JNEUROSCI.3752-13.2014
15. Uno Y, Coyle JT. Glutamate hypothesis in schizophrenia. *Psychiatry Clin Neurosci* (2019) 73:204–15. doi: 10.1111/pcn.12823
16. Tsai G, Passani LA, Slusher BS, Carter R, Baer L, Kleinman JE, et al. Abnormal excitatory neurotransmitter metabolism in schizophrenic brains. *Arch Gen Psychiatry* (1995) 52:829–36. doi: 10.1001/archpsyc.1995.03950220039008
17. Watanabe S, Kakigi R, Koyama S, Kirino E. Human face perception traced by magneto- and electro-encephalography. *Brain Res Cognit Brain Res* (1999) 8:125–42. doi: 10.1016/S0926-6410(99)00013-0
18. Pierce K, Müller RA, Ambrose J, Allen G, Courchesne E. Face processing occurs outside the fusiform 'face area' in autism: evidence from functional MRI. *Brain* (2001) 124:2059–73. doi: 10.1093/brain/124.10.2059
19. Onitsuka T, Niznikiewicz MA, Spencer KM, Frumin M, Kuroki N, Lucia LC, et al. Functional and structural deficits in brain regions subserving face perception in schizophrenia. *Am J Psychiatry* (2006) 163:455–62. doi: 10.1176/appi.ajp.163.3.455
20. Spitzer RL, Williams JBW, Gibbson M, First M. *The Structured Clinical Interview for DSM-III-R (SCID-NP)-Non-Patient Edition*. American Psychiatric Association, Washington, DC. American Psychiatric Association: Washington, DC (1990).
21. First MB, Spitzer RL, Gibbon M, Williams JBW. *Structured Clinical Interview for DSM-IV-TR Axis I Disorders, Research Version, Patient Edition. (SCID-I/P)*. Biometrics Research, New York State Psychiatric Institute: New York, NY (2002).
22. Andreasen NC. *Scale for the Assessment of Positive Symptoms (SAPS)*. Department of Psychiatry, University of Iowa College of Medicine: Iowa City, IA (1984).
23. Andreasen NC. *Scale for the Assessment of Negative Symptoms (SANS)*. Department of Psychiatry, University of Iowa College of Medicine: Iowa City, IA (1981).
24. Woods SW. Chlorpromazine equivalent doses for the newer atypical antipsychotics. *J Clin Psychiatry* (2003) 64:663–7. doi: 10.4088/JCP.v64n0607
25. Nenonen J, Nurminen J, Kičić D, Bikmullina R, Lioumis P, Jousmäki V, et al. Validation of head movement correction and spatiotemporal signal space separation in magnetoencephalography. *Clin Neurophysiol* (2012) 123:2180–91. doi: 10.1016/j.clinph.2012.03.080
26. Hämäläinen M, Hari R. *Magnetoencephalographic Characterization of Dynamic Brain Activation: Basic Principles and Methods of Data Collection and Source Analysis*. Amsterdam: Elsevier Inc (2002) p. 227–53.
27. Hämäläinen M, Ilmoniemi R. Interpreting magnetic fields of the brain: minimum norm estimates. *Med Bio Eng Comput* (1994) 32:35–42.
28. Collins DL, Neelin P, Peters TM, Evans AC. Automatic 3D intersubject registration of MR volumetric data in standardized Talairach space. *J Comput Assist Tomogr* (1994) 18:192–205.
29. Dale AM, Liu AK, Fischl BR, Buckner RL, Belliveau JW, Lewine JD, et al. Dynamic statistical parametric mapping: combining fMRI and MEG for high-resolution imaging of cortical activity. *Neuron* (2000) 26:55–67. doi: 10.1016/s0896-6273(00)81138-1
30. Murashko AA, Shmukler A. EEG correlates of face recognition in patients with schizophrenia spectrum disorders: A systematic review. *Clin Neurophysiol* (2019) 130:986–96. doi: 10.1016/j.clinph.2019.03.027
31. Yang C, Zhang T, Li Z, Heeramun-Aubeeluck A, Liu N, Huang N, et al. Changes in event-related potentials in patients with first-episode schizophrenia and their siblings. *BMC Psychiatry* (2017) 17:20–8. doi: 10.1186/s12888-016-1189-7
32. Salisbury DF, Krompinger JW, Lynn SK, Onitsuka T, Mccarley RW. Neutral face and complex object neurophysiological processing deficits in long-term schizophrenia and in first hospitalized schizophrenia-spectrum individuals. *Int J Psychophysiol* (2019) 145:57–64. doi: 10.1016/j.ijpsycho.2019.06.002
33. Bortolon C, Capdevielle D, Raffard S. Face recognition in schizophrenia disorder: A comprehensive review of behavioral, neuroimaging and neurophysiological studies. *Neurosci Biobehav Rev* (2015) 53:79–107. doi: 10.1016/j.neubiorev.2015.03.006
34. Glausier J, Lewis D. Dendritic spine pathology in schizophrenia. *Neuroscience* (2013) 251:90–107. doi: 10.1016/j.neuroscience.2012.04.044
35. Suzuki M, Larkum M. Dendritic calcium spikes are clearly detectable at the cortical surface. *Nat Commun* (2017) 8:276. doi: 10.1038/s41467-017-00282-4
36. Itier RJ, Taylor MJ. N170 or N1? Spatiotemporal differences between object and face processing using ERPs. *Cereb Cortex* (2004) 14:132–42. doi: 10.1093/cercor/bhg111
37. Rossion B, Joyce CA, Cottrell GW, Tarr MJ. Early lateralization and orientation tuning for face, word, and object processing in the visual cortex. *Neuroimage* (2003) 20:1609–24. doi: 10.1016/j.neuroimage.2003.07.010
38. Xu Y, Liu J, Kanwisher N. The M170 is selective for faces, not for expertise. *Neuropsychologia* (2005) 43:588–97. doi: 10.1016/j.neuropsychologia.2004.07.016
39. Mogi T, Tsunoda T, Yoshino A. Altered upright face recognition and presence of face inversion effect in temporal lobe epilepsy: An event-related potential study. *Psychiatry Clin Neurosci* (2019) 73:269–76. doi: 10.1111/pcn.12829
40. Edgar JC. Identifying electrophysiological markers of autism spectrum disorder and schizophrenia against a backdrop of normal brain development. *Psychiatry Clin Neurosci* (2020) 74:1–11. doi: 10.1111/pcn.12927
41. Oribe N, Hirano Y, Kanba S, Del Re E, Seidman L, Mesholam-Gately R, et al. Progressive Reduction of Visual P300 Amplitude in Patients with First-Episode Schizophrenia: An ERP Study. *Schizophr Bull* (2015) 41:460–70. doi: 10.1093/schbul/sbu083
42. Oribe N, Hirano Y, del Re E, Seidman LJ, Mesholam-Gately RI, Woodberry KA, et al. Progressive reduction of auditory evoked gamma in first episode schizophrenia but not clinical high risk individuals. *Schizophr Res* (2019) 208:145–52. doi: 10.1016/j.schres.2019.03.025
43. Oribe N, Hirano Y, del Re E, Mesholam-Gately RI, Woodberry KA, Ueno T, et al. Longitudinal evaluation of visual P300 amplitude in clinical high-risk subjects: An event-related potential study. *Psychiatry Clin Neurosci* (2020). doi: 10.1111/pcn.13083
44. Hirano Y, Nakamura I, Tamura S, Onitsuka T. Long-term Test-retest Reliability of Auditory Gamma Oscillations Between Different Clinical EEG Systems. *Front Psychiatry* (2020). doi: 10.3389/fpsyt.2020.00876
45. Hirano S, Spencer KM, Onitsuka T, Hirano Y. Language-Related Neurophysiological Deficits in Schizophrenia. *Clin EEG Neurosci* (2020) 51:222–33. doi: 10.1177/1550059419886686
46. Nakamura I, Hirano Y, Ohara N, Hirano S, Ueno T, Tsuchimoto R, et al. Early Integration Processing between Faces and Vowel Sounds in Human Brain: An MEG Investigation. *Neuropsychobiology* (2015) 71:187–95. doi: 10.1159/000377680
47. Hirano Y, Oribe N, Onitsuka T, Kanba S, Nestor PG, Hosokawa T, et al. Auditory Cortex Volume and Gamma Oscillation Abnormalities in Schizophrenia. *Clin EEG Neurosci* (2020c) 51:244–51. doi: 10.1177/1550059420914201

48. Chaby L, Jemel B, George N, Renault B, Fiori N. An ERP study of famous face incongruity detection in middle age. *Brain Cognit* (2001) 45:357–77. doi: 10.1006/brcg.2000.1272
49. Pfütze E-M, Sommer W, Schweinberger SR. Age-related slowing in face and name recognition: evidence from event-related brain potentials. *Psychol Aging* (2002) 17:140–60. doi: 10.1037/0882-7974.17.1.140
50. de Fockert JW, Ramchurn A, Van Velzen J, Bergström Z, Bunce D. Behavioral and ERP evidence of greater distractor processing in old age. *Brain Res* (2009) 1282:67–73. doi: 10.1016/j.brainres.2009.05.060
51. Gao L, Xu J, Zhang B, Zhao L, Harel A, Bentin S. Aging effects on early-stage face perception: an ERP study. *Psychophysiology* (2009) 46:970–83. doi: 10.1111/j.1469-8986.2009.00853.x
52. Daniel S, Bentin S. Age-related changes in processing faces from detection to identification: ERP evidence. *Neurobiol Aging* (2012) 33:206.e201–228. doi: 10.1016/j.neurobiolaging.2010.09.001

Conflict of Interest: The authors declare that the research was conducted in the absence of any commercial or financial relationships that could be construed as a potential conflict of interest.

The reviewer, TM, declared a shared affiliation, though no collaboration, with the authors to the handling editor.

frontiers in Psychiatry

ORIGINAL RESEARCH
published: 09 September 2020
doi: 10.3389/fpsyt.2020.551808

Frontoparietal Network Connectivity During an *N*-Back Task in Adults With Autism Spectrum Disorder

Veronica Yuk[1,2,3*], *Charline Urbain*[4,5], *Evdokia Anagnostou*[6,7,8] *and Margot J. Taylor*[1,2,3,9]

[1] Department of Diagnostic Imaging, The Hospital for Sick Children, Toronto, ON, Canada, [2] Neurosciences & Mental Health Program, SickKids Research Institute, The Hospital for Sick Children, Toronto, ON, Canada, [3] Department of Psychology, University of Toronto, Toronto, ON, Canada, [4] Neuropsychology and Functional Neuroimaging Research Group, Center for Research in Cognition & Neurosciences and ULB Neuroscience Institute, Université Libre de Bruxelles (ULB), Brussels, Belgium, [5] Laboratoire de Cartographie Fonctionnelle du Cerveau, Hôpital Erasme, Université Libre de Bruxelles, Brussels, Belgium, [6] Bloorview Research Institute, Holland Bloorview Kids Rehabilitation Hospital, Toronto, ON, Canada, [7] Department of Neurology, The Hospital for Sick Children, Toronto, ON, Canada, [8] Department of Paediatrics, University of Toronto, Toronto, ON, Canada, [9] Department of Medical Imaging, University of Toronto, Toronto, ON, Canada

Background: Short-term and working memory (STM and WM) deficits have been demonstrated in individuals with autism spectrum disorder (ASD) and may emerge through atypical functional activity and connectivity of the frontoparietal network, which exerts top-down control necessary for successful STM and WM processes. Little is known regarding the spectral properties of the frontoparietal network during STM or WM processes in ASD, although certain neural frequencies have been linked to specific neural mechanisms.

Methods: We analysed magnetoencephalographic data from 39 control adults (26 males; 27.15 ± 5.91 years old) and 40 adults with ASD (26 males; 27.17 ± 6.27 years old) during a 1-back condition (STM) of an *n*-back task, and from a subset of this sample during a 2-back condition (WM). We performed seed-based connectivity analyses using regions of the frontoparietal network. Interregional synchrony in theta, alpha, and beta bands was assessed with the phase difference derivative and compared between groups during periods of maintenance and recognition.

Results: During maintenance of newly presented vs. repeated stimuli, the two groups did not differ significantly in theta, alpha, or beta phase synchrony for either condition. Adults with ASD showed alpha-band synchrony in a network containing the right dorsolateral prefrontal cortex, bilateral inferior parietal lobules (IPL), and precuneus in both 1- and 2-back tasks, whereas controls demonstrated alpha-band synchrony in a sparser set of regions, including the left insula and IPL, in only the 1-back task. During recognition of repeated vs. newly presented stimuli, adults with ASD exhibited decreased theta-band connectivity compared to controls in a network with hubs in the right inferior frontal gyrus and left IPL in the 1-back condition. Whilst there were no group differences in connectivity in the 2-back condition, adults with ASD showed no frontoparietal network recruitment during recognition, whilst controls activated networks in the theta and beta bands.

Edited by:
Peter Uhlhaas,
University of Glasgow,
United Kingdom

Reviewed by:
Satu Palva,
University of Helsinki, Finland
Peter G. Enticott,
Deakin University, Australia

****Correspondence:***
Veronica Yuk
veronica.yuk@mail.utoronto.ca

Specialty section:
This article was submitted to Neuroimaging and Stimulation, a section of the journal Frontiers in Psychiatry

Received: *14 April 2020*
Accepted: *13 August 2020*
Published: *09 September 2020*

Citation:
Yuk V, Urbain C, Anagnostou E and Taylor MJ (2020) Frontoparietal Network Connectivity During an N-Back Task in Adults With Autism Spectrum Disorder. Front. Psychiatry 11:551808. doi: 10.3389/fpsyt.2020.551808

Conclusions: Our findings suggest that since adults with ASD performed well on the *n*-back task, their appropriate, but effortful recruitment of alpha-band mechanisms in the frontoparietal network to maintain items in STM and WM may compensate for atypical modulation of this network in the theta band to recognise previously presented items in STM.

Keywords: autism, connectivity, working memory, theta, alpha, maintenance, recognition, MEG

INTRODUCTION

Adults with autism spectrum disorder (ASD) demonstrate difficulties with a variety of executive functions (1–4), one of which is working memory (WM), which refers to the ability to hold and manipulate information in mind (5, 6). WM is related to short-term memory (STM), which involves the mental storage of information for a short period of time (7, 8), and which is also impaired in adults with ASD (9–12). Given their link with each other, and their influence on cognitive capabilities, such as intelligence and academic achievement (13–18), understanding the nuances and the extent of STM and WM impairments in ASD is a crucial first step in improving cognitive outcomes in this population. The current literature points to a more severe deficit in ASD in visual, especially visuospatial, aspects of STM and WM, rather than in verbal STM and WM (10, 19–23), though people with ASD exhibit impairments in both modalities (11, 24). Neuroimaging work has additionally shown that individuals with ASD exhibit atypical neural activity and connectivity during visual STM tasks (25–27) and in both visual and verbal WM tasks (28–32).

Several functional neuroimaging studies of STM and WM have demonstrated activation of a frontoparietal network (33–39) consisting mainly of the dorsolateral prefrontal cortex (dlPFC), which includes the superior and middle frontal gyri (SFG and MFG), and of the inferior parietal lobule (IPL). The frontoparietal network is thought to exercise cognitive control to adapt to rapidly changing goals and demands (40–44) that certainly occur in STM and WM tasks. The IPL has been primarily associated with maintenance (45–51), which entails the temporary storage of information in STM or WM, though the dlPFC has also been implicated (46, 48, 52–56). The dlPFC is additionally involved in recognition of previously presented or repeated stimuli (57–60), a function which encompasses access to or selection of relevant stimulus representations in STM or WM, and it also plays a role in updating or manipulation of information in WM. Much of the STM and WM literature in ASD has utilised paradigms tapping both maintenance and recognition processes; during such tasks, individuals with ASD show differential activation of this frontoparietal network across development, exhibiting increased activity in the dlPFC during childhood (27, 61), but the opposite in adulthood (26, 31, 62). Moreover, they show poor modulation of these frontoparietal regions with increasing cognitive load (30, 63, 64).

More recent work has examined not only the activation of regions in the frontoparietal network, but also how they communicate or synchronise with each other and with other brain areas. These connections are thought to be fundamental for exerting top-down control on other areas and networks for successful task performance (41, 42, 65–70). In the ASD population, studies generally demonstrate that areas in the frontoparietal network are less coupled with each other and with other regions of the brain (26, 29, 31). This reduced functional connectivity suggests impairments in integrating information amongst brain areas during maintenance and recognition, which may contribute to ASD symptomatology (25, 32). These findings echo the current literature on connectivity in ASD, which posits that individuals with ASD show decreased long-range functional connectivity and altered local connectivity across a range of contexts (71–76), suggesting that a deficit in neural communication may account for the cognitive difficulties observed in the ASD population.

Although neural long-range synchrony, especially in the theta and alpha frequency bands, has been linked to STM and WM maintenance and recognition processes (39, 77–85), the specific frequency band(s) in which these connectivity differences occur in individuals with ASD have been less explored. To our knowledge, only one study has demonstrated reduced alpha-band connectivity in children with ASD during a WM task, reflecting inefficient processing during recognition of repeated stimuli that was associated with severity of their ASD symptoms (32). Frequency-specific differences in STM- or WM-related connectivity in adults with ASD and their relation to behaviour have yet to be examined, even though these abilities can impact adaptive behaviours in individuals with ASD (3, 86, 87).

Thus, the present study investigated whether adults with ASD demonstrate connectivity differences when engaging STM and WM processes, and if they are frequency-dependent. Adults with and without ASD performed an *n*-back task, a classic paradigm in which participants view a series of stimuli and are asked to recall whether the current stimulus was also presented *n* trials earlier (88). We measured and compared connectivity between the control and ASD groups during maintenance and recognition of novel visual stimuli for both 1-back and 2-back versions of the task. The 1-back condition involves mainly STM processes, as an individual is only required to maintain and recognise the stimulus shown in the previous trial in mind. On the other hand, the 2-back condition elicits WM processes, as one must continuously monitor and update information stored in and retrieved from memory. Due to their involvement in STM (38, 39, 83, 84, 89–93) and WM mechanisms (77–79, 94–96) as well as long-range interregional communication (97–99), we specifically contrasted phase synchrony in the theta, alpha, and beta frequency bands. We also focused on connections amongst frontoparietal network regions and the rest of the brain, given its known role in STM (37–39, 84) and WM (33, 36, 100, 101), and

since prior work has demonstrated deficits in this network in ASD (25, 27, 31). As individuals with ASD show deficits in tasks involving STM and WM maintenance (11, 20), decreased brain activity during STM recognition (27), and reduced connectivity during WM recognition (32), we predicted that adults with ASD would demonstrate decreased interregional connectivity during both maintenance and recognition of novel stimuli in STM and WM. We further hypothesised that these differences would appear in the alpha band, in line with our previous findings in children with ASD (32), and given its link with STM and WM processes, especially maintenance (77, 85, 102–105).

MATERIALS AND METHODS

Participants

We recruited 92 adults aged 18–40 years, inclusive, for this study, approved by the Research Ethics Board at the Hospital for Sick Children. Individuals were included if they were not born prematurely, had no MRI or MEG contraindications, and demonstrated an IQ ≥ 70, measured using the full-scale, two-subtest version of the Wechsler Abbreviated Scale of Intelligence (WASI or WASI-II) (106, 107). Control adults were additionally screened for any developmental, neurological, or psychological disorders. Adults with ASD had a primary diagnosis of ASD by an experienced clinician, which was confirmed by the Autism Diagnostic Observation Schedule (ADOS-G or ADOS-2) (108, 109). All participants gave informed written consent before taking part in the study.

Participants were excluded if they performed poorly on the task (i.e., ≤50% accuracy on 1-back task or ≥50% false alarm rate), had a low number of correct trials (<40 in each condition) after accounting for artefacts, or poor data quality (e.g., poor head localization in the MEG). We then matched participants in the ASD group with those in the control group on age (within two years) and sex, and subsequently excluded any control participants who could not be matched. As participants tended to perform better on the 1-back than the 2-back version of the task, and as we evaluated the 1- and 2-back data separately, the final samples for these two analyses differed; the sample for the 2-back analysis was a subset of that for the 1-back analysis. For the 1-back task, 39 control adults (26 males; 27.15 ± 5.91 years old) and 40 adults with ASD (26 males; 27.17 ± 6.27 years old) met all inclusion and exclusion criteria. For the 2-back task, 29 control adults (19 males; 26.40 ± 5.79 years old) and 30 adults with ASD (19 males; 26.36 ± 6.26 years old) were included in the analyses. Neither sample differed significantly in age, sex, or IQ, and mean calibrated severity scores on the ADOS for both ASD samples were around 7 (**Table 1**).

TABLE 1 | Demographics for 1-back and 2-back samples.

	Control	ASD	t or X^2	p
	Mean (SD) or Count	**Mean (SD) or Count**		
1-back	$N = 39$	$N = 40$		
Age	27.15 (5.91)	27.17 (6.27)	0.02	0.99
Sex	26 M, 13 F	26 M, 14 F	2.43×10^{-31}	1
IQ	114.34 (11.36)	111.79 (14.37)	0.86	0.39
ADOS CSS	—	6.89 (2.25)	—	—
2-back	$N = 29$	$N = 30$		
Age	26.40 (5.79)	26.36 (6.26)	0.03	0.98
Sex	19 M, 10 F	19 M, 11 F	6.01×10^{-31}	1
IQ	115.45 (11.98)	113.48 (13.04)	0.60	0.55
ADOS CSS	—	7.00 (2.09)	—	—

ADOS, Autism Diagnostic Observation Schedule; CSS, calibrated severity score.

Experimental Design

Questionnaires

To obtain a standardised measure of WM, we asked participants and their informants (e.g., partner or parent) to complete the Behavior Rating Inventory of Executive Function, Adult Version (BRIEF-A) (110). This questionnaire assesses difficulties with a variety of executive functions that an individual may experience in everyday life. It provides t scores reflecting the degree of impairment on a particular executive function scale, as well as composite scores. We used t scores on the WM scale of the BRIEF-A, with higher scores denoting more severe deficits in WM. Participants also filled out the Social Responsiveness Scale, Second Edition (SRS-2) (111). The Total t score was taken to gauge ASD symptom severity.

N-Back MEG Task

Participants performed a visual n-back task with two loads, 1- and 2-back (**Figure 1A**), to elicit STM and WM processes. This task was used in our previous work examining differences in brain activation and functional connectivity between children with and without ASD (27, 32). Our task protocol was similar; stimuli consisted of novel colourful abstract images presented serially for 200 ms each on a black background. During the interstimulus interval, participants saw a white fixation cross for a random duration between 1,050–1,300 ms. Participants pressed a button if the most recently presented stimulus matched that shown n trials previously.

The two loads of the n-back task were run in separate blocks. The l-back load scenario consisted of 285 trials: 190 unique images were presented, and 95 of these were shown again on the subsequent trial. The 2-back load segment of the task contained 330 trials: 220 distinct images were shown, of which 110 were repeated two trials later. Stimuli in the 1- and 2-back loads did not overlap. We refer to trials in which stimuli are presented for the first time as "New," and those in which they are shown again as "Repeat."

All participants first practised both blocks of the task and were given feedback outside of the MEG scanner to ensure they understood the task requirements. Individuals viewed the task on a rear projection screen 80 cm away from the MEG dewar. *Presentation 18.1* software (Neurobehavioral Systems Inc., https://www.neurobs.com/presentation) was used to display the task, as well as record participant responses.

Neuroimaging Data Aquisition

A 151-channel CTF MEG system (Coquitlam, British Columbia, Canada) recorded MEG data at a 600 Hz sampling rate from participants during the task. Adults lay supine with their head in

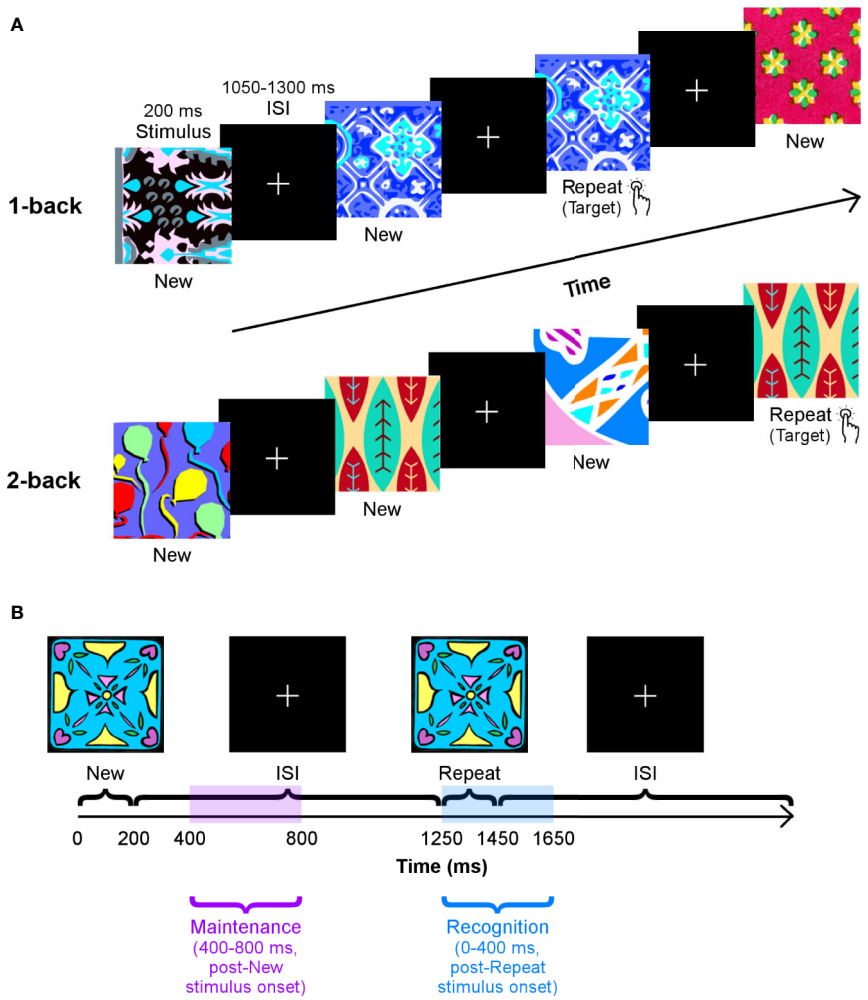

FIGURE 1 | The *n*-back task. **(A)** Participants' performance on two loads of this task — 1-back (top row) and 2-back (bottom row) — were tested in separate blocks. They were instructed to press a button as quickly as possible when they recognised that a stimulus had been repeated one or two trials earlier. Images were presented for 200 ms, and the interstimulus interval varied between 1,050–1,300 ms. **(B)** A schematic of the time windows used to analyse working memory maintenance and recognition processes, with the 1-back load as an example.

the MEG dewar. Head position was tracked continuously through three fiducial coils on the nasion and left and right pre-auricular points. To reduce noise in the data, an anti-aliasing low-pass filter at 150 Hz and a third order spatial gradient were applied.

A 12-channel head coil in a 3T MRI scanner (MAGNETOM, Siemens AG, Erlangen, Germany) recorded T1-weighted MRI data from participants. A sagittal 3D MPRAGE sequence (TR/TE = 2,300/2.96 ms, FA = 9°, FOV = 192×240×256 mm, voxel size = 1.0 mm isotropic) was utilised. Participants were scanned with radio-opaque markers at the MEG fiducial points to allow for coregistration of functional MEG data with structural MRI data.

Statistical Analysis

Behavioural Data

WM capability in everyday life was compared between adults with and without ASD in the 1- and 2-back samples by examining whether there were group (control vs. ASD) or rater (self vs. informant) effects, as well as an interaction between the two, on the WM scale of the BRIEF-A. Performance on the *n*-back task was contrasted between groups by assessing the effect of group (control vs. ASD) on accuracy and median response time (RT) for the 1- and 2-back loads independently. Accuracy was assessed using d-prime (d′); hits were correct Repeat trials, and false alarms were incorrect New trials.

We used linear mixed effects models to investigate the effects on BRIEF-A data and *t* tests for the task performance measures. Analyses were carried out separately for the 1-back and 2-back samples in R 3.5.0 (R Core Team, https://www.r-project.org/). Significant results are reported for $p < 0.05$.

MEG Data

Preprocessing

MEG data preprocessing and analyses were done using the FieldTrip toolbox (112) in MATLAB 2017b (The MathWorks,

www.mathworks.com/products/matlab/). Data were epoched from −1,500–2,000 ms, relative to stimulus onset. Signals were then filtered from 1–150 Hz with a fourth-order Butterworth bandpass filter, with 60 and 120 Hz notch filters. Artefacts from physiological sources (e.g., eyes and heart) were detected and removed with independent component analysis. Trials in which the signal was >2,000 fT or head movement was >5 mm were excluded. Of the remaining trials, only correct New and Repeat trials were used for further analyses.

Forward models based on the single-shell method (113) were created from each participant's T1-weighted MRI data. Inverse models were constructed using the forward model and constrained to the centroids of the 90 regions of the Automated Anatomic Labeling (AAL) atlas (114). Activity at each centroid was taken to represent that respective AAL region. Time series at these sources were estimated using a linearly constrained minimum variance beamformer (115). The covariance matrix was computed on the MEG signal from −400–800 ms, to which 5% regularisation was applied. The neural activity index was calculated to ensure attenuation of centre-of-head noise biases.

Connectivity

As our task involved strong visual and motor responses, we performed seed-based analyses to focus on connectivity between core regions of the frontoparietal network and the rest of the brain to assess phase synchrony directly related to maintenance and recognition of novel visual stimuli. Therefore, we examined the connections amongst six bilateral regions of interest (ROIs) from the AAL atlas, as well as their links to the other AAL regions (except Heschl's gyrus and olfactory cortex, as their roles in audition and olfaction are not involved in our task). Our ROIs were chosen based on meta-analyses of *n*-back studies (33, 35, 36). They consisted of the superior frontal gyri [SFG; (-19, 35, 42) and (20, 31, 44)], medial superior frontal gyri [mSFG; (-6, 49, 31) and (8, 51, 30)], middle frontal gyri [MFG; (-34, 33, 35) and (37, 33, 34)], inferior frontal gyri [IFG; (-47, 30, 14) and (49, 30, 14)], insulae [(-36, 7, 3) and (38, 6, 2)], and inferior parietal lobules [IPL; (-44, -46, 47) and (45, -46, 50)].

Connectivity between each pair of sources was quantified using the phase difference derivative (PDD) (116). Source-estimated data were filtered into our frequency bands of interest with Hamming-windowed FIR bandpass filters at the following passbands: 4–7 Hz (theta), 8–14 Hz (alpha), and 15–30 Hz (beta). The lower and upper stopband frequencies for each filter were at 0.6 and 1.9 times the lower and upper frequency cutoffs of each passband, respectively. To reduce detection of spurious connections due to signal leakage, filtered data were subsequently orthogonalized. The instantaneous phase for each source timeseries in each frequency band was obtained with the Hilbert transform. PDD values were calculated at each time point from −400–800 ms using the method outlined by Tewarie and colleagues (117).

Interregional neural communication during maintenance and recognition of novel visual stimuli was determined by considering phase synchrony values in two time windows: 400–800 ms, after the onset of a New stimulus, and 0–400 ms, following the presentation of a Repeat stimulus, respectively (**Figure 1B**). These windows were established based on average median RTs in both groups, which ranged from ~425–525 ms, across both loads (see Results section). Regarding recognition, we examined a window from 0–400 ms, post-Repeat stimulus onset and just before the lower end of the average median RT, as it would encompass processing related to successful recognition during correct Repeat trials. We compared phase synchrony in this window to that in a similar window of 0–400 ms, post-New stimulus onset (Repeat > New, 0–400 ms, poststimulus onset), as New trials act as a control condition that involves the first occurrence of the stimulus. To investigate maintenance, we evaluated a window from 400–800 ms, post-New stimulus onset, to prevent capturing any perceptual, encoding, and/or identification functions that may occur during early visual processing. Furthermore, we chose this interval to avoid overlap with our recognition analysis and the baseline window. We contrasted connectivity in this time window in New trials with connectivity in an equivalent window of 400–800 ms, post-Repeat stimulus onset in Repeat trials (New > Repeat, 400–800 ms, poststimulus onset). Mean connectivity at all pairwise connections for each participant and each condition in these comparisons was obtained by standardising PDD values in these windows by the baseline period, –400–0 ms, then averaging the resultant *z* scores over the entire time window of interest.

Statistical comparisons of within-group connectivity during maintenance and recognition were conducted as described above for both adults with and without ASD. We then tested for statistically significant group differences in each of these scenarios (e.g., Control vs. ASD, New > Repeat for maintenance; Control vs. ASD, Repeat > New for recognition). All within- and between-group comparisons were performed for the 1- and 2-back samples separately. For both types of contrasts, we performed cluster-based permutation testing, as implemented in the Network-Based Statistic toolbox (118), to find networks demonstrating significant differences between conditions and groups. Essentially, the Network-Based Statistic approach begins by performing *t* tests at each connection and applying a threshold, which we chose to be $t = 2.641$ (1-back) or $t = 2.665$ (2-back), which are equivalent to $p < 0.005$ in their respective samples. The robustness of the largest contiguous network formed from the suprathreshold connections was assessed with permutation testing. A null distribution of maximal network size was obtained by rearranging group labels over 5,000 permutations. This procedure allowed for the calculation of a family-wise error-corrected *p* value (p_{FWE}) of the observed network. Networks were considered significant at $p_{FWE} < 0.05$. We used BrainNet Viewer (119) and code provided by Koelewijn and colleagues (120) to visualise these networks.

Brain-Behaviour Relations

We explored whether mean network connectivity in any of our group comparisons was associated with WM abilities as measured by the BRIEF-A, task performance (accuracy and median RT), and with ASD symptom severity. Thus, for any networks that differed significantly between groups, we performed regressions of each the BRIEF-A WM scale scores,

d′, median RT, and SRS-2 Total scores on mean PDD values in those networks. We report any significant main effects of mean connectivity and/or its interaction with group for $p < 0.05$.

RESULTS

Behaviour

On the WM subscale of the BRIEF-A, adults with ASD demonstrated significantly more WM difficulties than controls (**Figure 2**) in both the 1-back ($F(1,43) = 25.56$, $p < 0.0001$, $d = 0.65$) and 2-back ($F(1,38) = 22.18$, $p < 0.0001$, $d = 0.64$) samples. Adults with ASD, compared to their informants, generally rated themselves higher on the WM scale (1-back: $F(1,43) = 19.38$, $p = 0.0001$, $d = 0.34$; 2-back: $F(1,38) = 14.06$, $p = 0.0006$, $d = 0.32$), indicating a greater number of difficulties with WM.

On the *n*-back task, there were no group differences in accuracy (1-back: $t(76.93) = 0.77$, $p = 0.44$, $d = 0.17$; 2-back: $t(55.30) = 0.51$, $p = 0.61$, $d = 0.13$) in the 1- or 2-back loads (**Figure 3A**). The two groups also had similar median RTs in the 1-back load ($t(76.97) = 1.51$, $p = 0.13$, $d = 0.34$), but their differences in median RT during the 2-back load approached significance ($t(54.71) = 1.93$, $p = 0.058$, $d = 0.50$), such that adults with ASD had slightly longer median RTs than controls (**Figure 3B**).

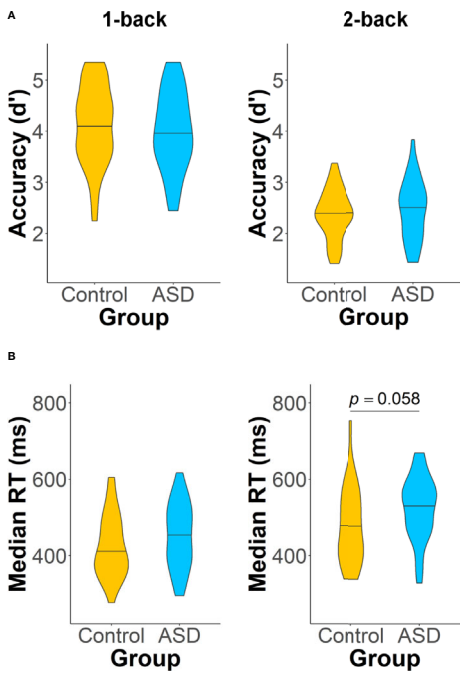

FIGURE 3 | Accuracy **(A)** and median RT **(B)** on the two loads of the *n*-back task: 1-back (left panel) and 2-back (right panel). Adults with autism spectrum disorder (ASD) showed a trend of having longer median RTs than control adults on the 2-back task ($p = 0.058$). Analyses of all other task performance measures did not reveal any significant group differences.

Neuroimaging

Maintenance

For the 1-back task, during the maintenance window, both control adults ($p_{FWE} = 0.048$) and adults with ASD ($p_{FWE} = 0.001$) recruited aspects of the frontoparietal network selectively in the alpha band. In the control group, the network hub with the most (four) connections was the left IPL, which mainly communicated with other left hemisphere regions, such as the left insula (**Figure 4A**). The right IPL and IFG were also involved in this network, though they were each only connected to two other regions. In the ASD group, both the right SFG and MFG were the main hubs with five connections each, linking the right dlPFC with the right IPL and with several left posterior regions, including the left IPL and precuneus (**Figure 4B**). In this network, the right IFG also showed synchrony with the right IPL and precuneus.

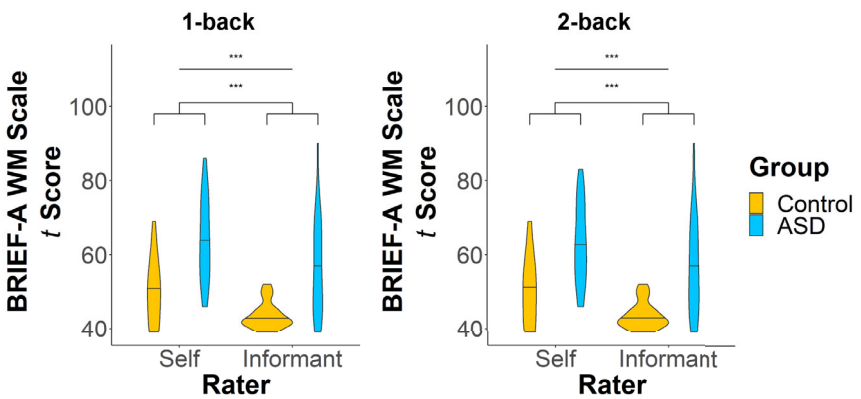

FIGURE 2 | *T* scores on the working memory (WM) scale of the BRIEF-A for the 1-back (left panel) and 2-back (right panel) samples. There were significant main effects of both group and rater on WM scores. ***$p < 0.001$.

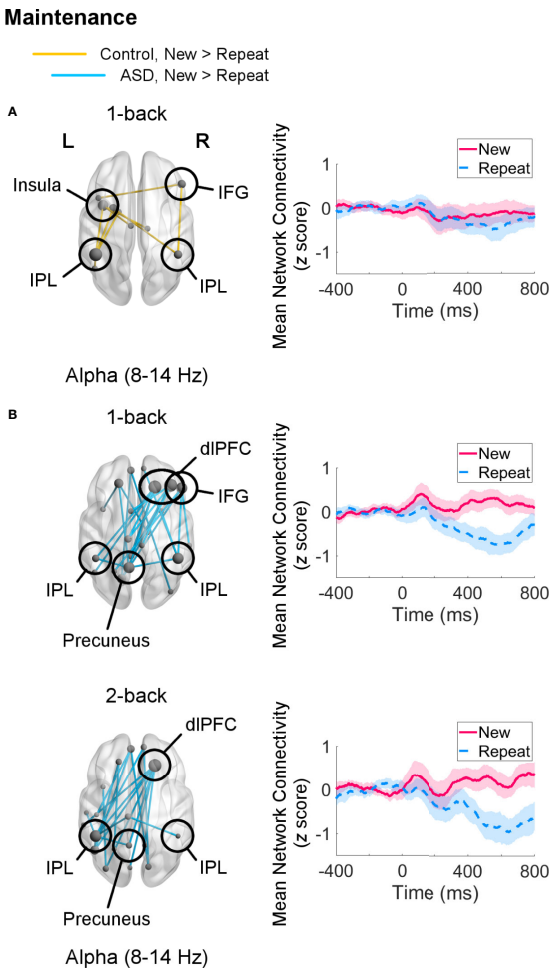

FIGURE 4 | Networks showing increased connectivity during maintenance of novel visual stimuli (New versus Repeat trials, 400–800 ms, poststimulus onset) during the 1-back and 2-back loads (left) and mean connectivity of these networks between –400–800 ms (right). Node size is scaled by number of connections. Connectivity values are given as *z* scores. **(A)** Control adults showed recruitment of a network in the alpha band in the 1-back load (p_{FWE} = 0.048), but not in the 2-back load. **(B)** Adults with autism spectrum disorder (ASD) displayed greater connectivity in a network in the alpha band similar between the 1-back (p_{FWE} = 0.001) and 2-back (p_{FWE} = 0.002) samples.

For the 2-back load, adults with ASD continued to show increased alpha-band connectivity during New versus Repeat trials (p_{FWE} = 0.002) in a right dlPFC-left posterior network linking the right SFG hub with the left IPL and precuneus (**Figure 4B**). Control adults did not exhibit greater engagement of any networks in any frequency band for New compared to Repeat trials for this load. There were no significant group differences in the maintenance interval for either load.

Recognition

Recognition processes in the 1-back load were associated with a trend (p_{FWE} = 0.056) increase in theta-band network connectivity in control adults for Repeat relative to New trials. This network was sparse, consisting mainly of a few connections (two each) amongst the left MFG, right IFG, bilateral IPL, and precuneus (**Figure 5**). Adults with ASD did not show any differential connectivity for Repeat versus New trials in any frequency band. When comparing the two groups, adults with ASD exhibited significantly decreased theta-band connectivity compared to control adults (p_{FWE} = 0.046) in a network of regions in which the right IFG and left IPL were major hubs (**Figure 6**).

Within-group analyses for the 2-back load during recognition revealed organisation of networks in the theta (p_{FWE} = 0.0084) and

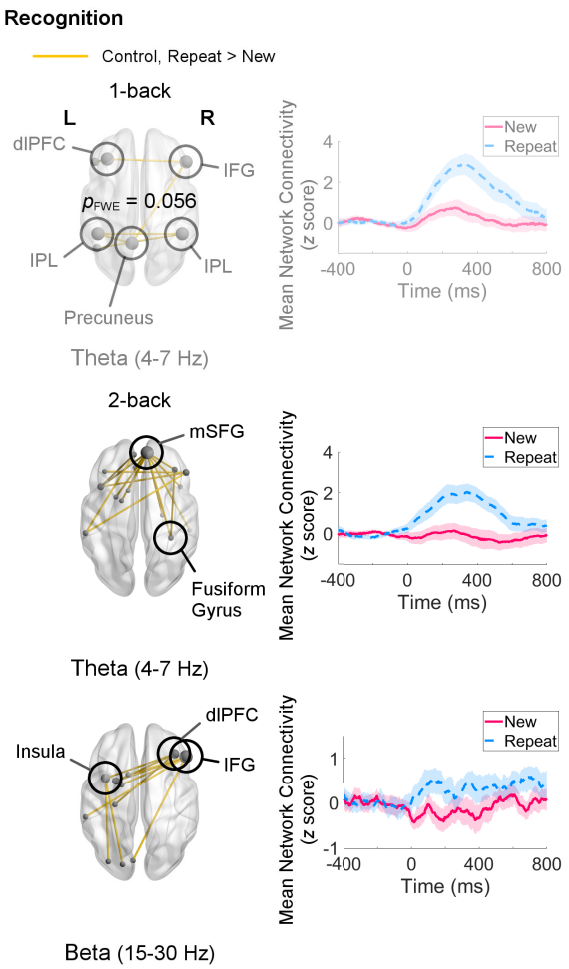

FIGURE 5 | Networks showing increased connectivity during recognition of repeated visual stimuli (Repeat versus New trials, 0–400 ms, poststimulus onset) for the 1-back and 2-back loads in the control group (left) and mean connectivity of these networks between –400–800 ms (right). Node size is scaled by number of connections. Connectivity values are given as *z* scores. In the 1-back load, control adults recruited a theta-band network, but it was only significant at a trend level (p_{FWE} = 0.056). In the 2-back load, they exhibited greater connectivity in networks in the theta (p_{FWE} = 0.0084) and beta (p_{FWE} = 0.015) bands. Adults with autism spectrum disorder (ASD) did not show differential connectivity during recognition.

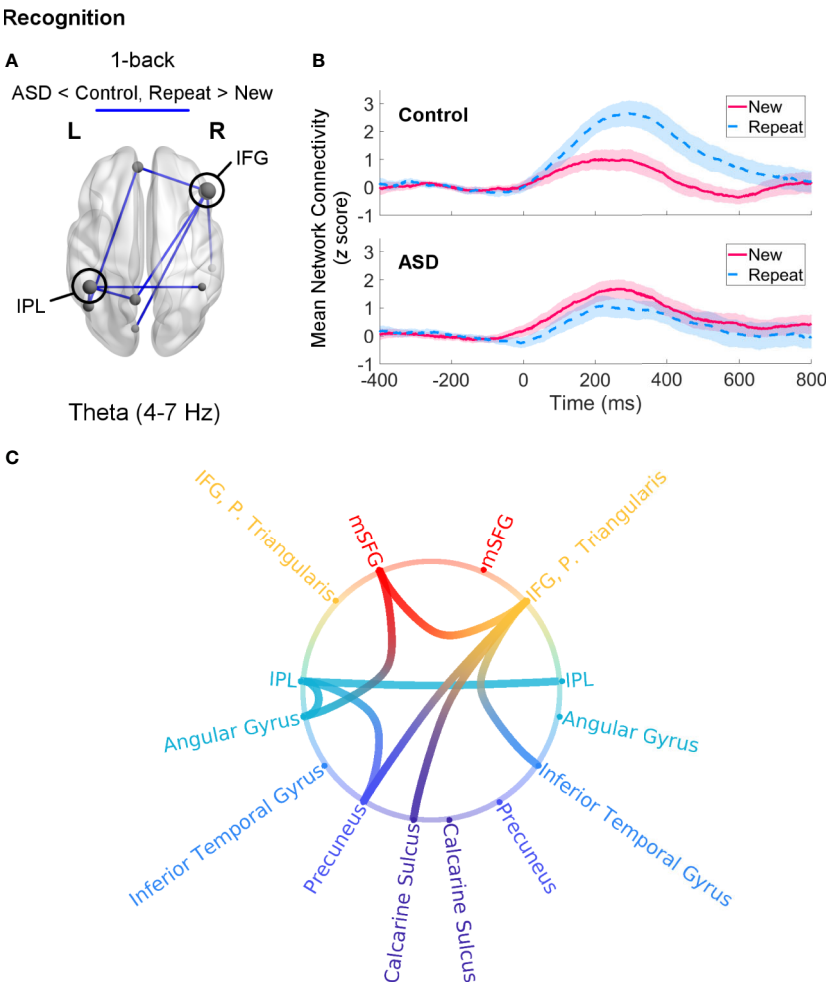

FIGURE 6 | Theta-band connectivity in adults with autism spectrum disorder (ASD) compared to controls during recognition of novel visual stimuli (Repeat versus New trials, 0–400 ms, poststimulus onset) in the 1-back load. **(A)** Adults with ASD showed significantly reduced (p_{FWE} = 0.046) theta-band connectivity in a network with hubs in the right IFG and left IPL. Node size is scaled by number of connections. **(B)** Mean connectivity in this network between −400–800 ms in the control (top) and ASD (bottom) groups. Connectivity values are given as *z* scores. **(C)** Network connectivity represented as a circle plot. Nodes are colour-coded in the following manner, from top to bottom: medial frontal structures (red), frontal areas (orange), parietal regions (turquoise), temporal areas (blue), medial parietal structures (dark blue), occipital areas (purple).

beta (p_{FWE} = 0.015) bands in the control group (**Figure 5**). The theta-band network primarily involved coordination between the mSFG and temporal regions, for example the right fusiform gyrus. The beta-band network displayed a different topography, with the right IFG having the highest (five) number of connections, followed by the right MFG and left insula (three each). Although adults with ASD in this sample also did not show any differential connectivity for this analysis in any frequency band, no significant group differences were found for the 2-back load.

Brain-Behaviour Relations

Mean connectivity in the theta-band network that differed between groups was not associated with any of our behavioural or clinical measures, nor was its interaction with group (all *p*s > 0.05).

DISCUSSION

Our study illustrates the complex distinctions in STM and WM processing between adults with and without ASD on both the behavioural and neural level. In our sample, adults with ASD performed equally as well as control adults on our visual *n*-back task, although there was a tendency for adults with ASD to have longer RTs in the 2-back block, during WM processing. This pattern was also observed by Lever and colleagues (121), who similarly demonstrated that despite being as accurate as controls on an *n*-back task, adults with ASD took significantly longer to respond. Slower RTs may be indicative of slower processing speed, which has also been reported in ASD ((122–127); but see (128, 129)). Whilst it may not affect performance on simple

experimental STM or WM tasks, this trend towards longer responses or processing could have more noticeable effects in complex, everyday behaviours. Since deficits in processing speed and WM have been found in individuals with ASD (19, 86, 130–132), further work is needed to clarify the link between processing speed and WM abilities in ASD, especially as our ASD group reported WM difficulties on the BRIEF-A. Our neuroimaging analyses examined the underlying neural differences in the frontoparietal network responsible for maintenance and recognition of novel visual stimuli that may contribute to these impairments.

Maintenance

During maintenance of novel visual stimuli, we observed that whilst adults with and without ASD did not differ significantly from each other, they exhibited distinct topologies and sizes of the networks they recruited. During the 1-back task, the alpha-band network recruited by controls was fairly left-lateralized, as the left IPL and left insula showed the most connections. The IPL is an integral part of the frontoparietal network involved in *n*-back tasks (33, 35, 36), and it may serve to maintain stimulus information in STM and WM (37, 45–48, 133–136), as well as shift attention to specific items in WM (137, 138). Although the IPL is more commonly associated with spatial STM and WM (e.g., (49, 139–145)), there is evidence that it similarly participates in object or image identity STM and WM (33, 36, 37, 50, 146–149). The insula has also been associated with object STM capacity (150), but its principal function is in recruiting the frontoparietal network when attentional and executive resources are needed (151–153) through its functional connections with the dlPFC (154, 155).

In comparison, adults with ASD demonstrated greater alpha-band interregional synchrony for New versus Repeat trials during the 1- and 2-back loads. The networks recruited in both loads were similar; they had a right frontal-to-left parietal configuration and included the right dlPFC, bilateral IPLs, and precuneus. The dlPFC is a key region in STM and WM processing, employing top-down control to maintain, monitor or update, and manipulate task-relevant information in mind (52, 53, 56, 156–159), by focusing attention to target stimulus representations in the IPL (54, 101, 160, 161). The precuneus mediates several higher-order cognitive functions (162–164), and given its connections with the IPL, it is likely involved in visuospatial processing (165–167) and visual recall (168–170) in this task. The particular involvement of the precuneus in the ASD group may reflect greater mental engagement, as our previous work showed that children with ASD activated the precuneus more with heavier cognitive load (27). Whilst we did not detect any significant group differences, the recruitment of additional STM and WM regions — the dlPFC and precuneus — in ASD group compared to controls, as well as of several other brain regions, may reflect effortful maintenance processes in ASD adults.

The particular arrangement of this right frontal, left posterior network not only mirrors previous work finding atypical functional lateralization in ASD during a WM task (31), but also suggests that maintenance of novel visual information is challenging for adults with ASD. In control adults, increasing task load has been associated with bilateral activation of the IPL (171, 172) and dlPFC (34, 173, 174), with a few demonstrating stronger effects in right dlPFC (175–177). Greater dlPFC-IPL (frontoparietal) connectivity has also been linked to higher task load (77, 178). Therefore, the strong involvement of the right dlPFC and its connection to the left IPL in the ASD group in both the 1- and 2-back loads indicates that holding visual stimuli in mind is mentally taxing for adults with ASD. In both groups, however, brain regions synchronised selectively in the alpha band, which has been implicated in STM and WM maintenance (77, 84, 85, 91, 103, 105, 179). Thus, our findings demonstrate that adults with ASD utilise appropriate neural mechanisms to successfully maintain novel visual stimuli in STM and WM, but it may be effortful for them.

Recognition

During recognition of repeated visual stimuli, adults with ASD exhibited no differential connectivity between Repeat and New trials for either the 1- or 2-back load. Hence, when contrasted with the control group, they showed significantly decreased theta-band synchrony compared to controls during the 1-back load in a network with hubs in the right IFG and left IPL. The ventrolateral PFC, which includes the IFG, is thought to work with the IPL for active retrieval of information (53). Specifically, the right IFG plays a major role in inhibition (180–184) and potentially preventing proactive interference during WM (137, 185–187), whereas the IPL, in addition to storing stimulus representations, may be responsible for retrieval (146). Since the selection of relevant information in STM during recognition may not only involve enhancement of target stimulus representations, but also suppression of irrelevant ones, and given evidence that individuals with ASD experience deficits in interference control ((188–190); but see (191, 192)), the reduced involvement of the IFG and IPL during recognition may reflect a potential breakdown in regulating interference from other stimuli in STM. This possible deficit in inhibiting task-irrelevant stimuli is further corroborated by the fact that these differences occurred in the theta band, as interregional theta-band connectivity is thought to mediate long-range neural communication, top-down control, and integration of distant regions (99, 193–195), especially during retrieval (196).

A similar effect was not found when contrasting the two groups in the 2-back task, which may be attributable to the slightly smaller sample size and therefore less power due to a greater variation in response in this condition. Importantly, the control group showed recruitment of theta-band networks for both loads (and additionally a beta-band network in the 2-back load), whereas the ASD group showed no greater connectivity in either load for Repeat compared to New trials. As the pattern of within-group results was similar across loads, a comparable but subthreshold trend may exist in the 2-back condition.

Taking into account that decreased connectivity has been observed in fMRI in ASD during other *n*-back tasks (25, 29, 31), our findings in the 1-back condition substantiate reports of long-range underconnectivity in ASD (72, 74, 197–199). The specificity of this difference to the theta band is also in line

with prior work emphasising the role of theta oscillations in STM (39, 82, 84) and recognition/retrieval (196, 200–202). This result is in contrast to our previous work (32), where we found that these differences occurred in the alpha band during recognition of repeated visual stimuli in a WM task. However, there are some key distinctions between these two studies. First, the present work observed that connectivity in the fronto*parietal* network was only significantly reduced in the ASD relative to control group in the theta band during the 1-back condition, whilst we previously reported decreased alpha-band synchrony in a fronto*temporal* network in individuals with ASD during the 2-back condition (32). Therefore, it is unclear from our prior work whether frontoparietal network connectivity also differed between individuals with and without ASD in the 2-back condition in either the theta or alpha bands, and whether frontotemporal network connectivity was affected in the current study. Second, our earlier study assessed children with ASD, whereas here we included only adults with ASD; thus, part of this discrepancy may be attributable to maturational processes. As both theta and alpha bands have been associated with STM and WM functions (77, 82–85, 95, 196, 203–205), it may be that connectivity related to recognition strengthens in the alpha band but weakens in the theta band over development in ASD. Whilst global network efficiency in the theta and alpha bands increases with age (206), these longitudinal changes in frequency-specific, long-range neural connectivity have not been characterised in ASD, neither has the frontoparietal network or any other networks related to STM or WM explicitly. Future work into the developmental trajectory of the spectral component of the frontoparietal network and its relation to STM and WM in ASD will be necessary to clarify these distinct findings in children and adults with ASD.

Another important consideration is that mean connectivity in the theta-band network that differed between groups in the 1-back load was not correlated with our behavioural measures. However, as our analyses probed very specific STM (1-back) and WM (2-back) mechanisms, it may be challenging to relate these fine neural differences to overall task performance and more complex behaviours drawing on WM abilities in everyday life. Therefore, it will be valuable for prospective work to evaluate whether these findings persist in more ecologically valid tasks of STM and WM.

Conclusion

Our neuroimaging study revealed unique aspects of STM and WM maintenance and recognition processes in adults with ASD. We demonstrated that whilst adults with ASD appropriately employ alpha-band oscillatory mechanisms to facilitate maintenance of novel visual stimuli in STM and WM, the distinct topology and extent of the recruited networks suggest that these functions are effortful for individuals with ASD. The strong engagement of maintenance processes may offset the observed atypicalities in theta-band connectivity in the ASD group during recognition of previously presented visual stimuli, at least in scenarios tapping STM. Given the spatial and spectral specificity of our findings, we propose that alpha-band connectivity between the dlPFC and IPL in the frontoparietal network enhances the neural representations of target stimuli during maintenance, thereby countering potentially stronger interference effects that occur during recognition due to reduced theta-band synchrony of the IFG and IPL with other regions of the brain.

We are the only study to date to use MEG to detail these maintenance and recognition processes and their spectral properties in the frontoparietal network in ASD. Thus, additional work is needed to independently validate our findings and interpretations in other investigations of STM and WM functions, especially as the distinct connectivity patterns in the control and ASD groups whilst maintaining novel visual stimuli in STM and WM showed only qualitative differences. It would be important to examine maintenance and recognition in other STM and WM tasks that more clearly separate these processes, as in higher loads of *n*-back tasks, participants are required to maintain stimuli from previous trials in WM, even after recognising a repeated stimulus. This constraint may explain why we did not observe differential connectivity in the control group during the maintenance window of the 2-back load when comparing phase synchrony during New and Repeat trials, and perhaps why we did not find any significant group differences in networks recruited for maintenance of novel visual stimuli. Furthermore, since our paradigm only included 1- and 2-back loads, we were unable to robustly assess whether adults with and without ASD show discrepancies in network recruitment with increasing cognitive load. As previous work has suggested that individuals with ASD do not show load-dependent modulation of activity in the frontoparietal network (26, 30, 63, 207), the effect of load on network connectivity in ASD is an important consideration. Finally, future work should explore STM- and WM-related connectivity patterns in broader samples of individuals with ASD, as our study included mainly higher-functioning adults with ASD who were able to perform well on our *n*-back task (though who still reported difficulties with WM in everyday life), and since there may be considerable heterogeneity in network recruitment in the ASD population, which may account for the lack of differential connectivity at the group level during recognition in our ASD sample. Our findings demonstrate, however, atypical frontoparietal network connectivity in adults with ASD when engaging in recognition of repeated visual stimuli, especially in STM, and further research will be essential to uncovering the nuances of these discrepancies.

DATA AVAILABILITY STATEMENT

The raw data supporting the conclusions of this article will be made available by the authors, without undue reservation.

ETHICS STATEMENT

The studies involving human participants were reviewed and approved by the Hospital for Sick Children Research Ethics Board. The patients/participants provided their written informed consent to participate in this study.

AUTHOR CONTRIBUTIONS

MT conceived and designed the study. VY collected and analysed the data, interpreted the findings, and drafted the manuscript. CU, EA and MT contributed significantly to revising the manuscript. All authors contributed to the article and approved the submitted version.

FUNDING

This work was funded by Canadian Institutes of Health Research grants MOP-119541 and MOP-142379 to MT and a Frederick Banting and Charles Best Canada Graduate Scholarships Doctoral Award awarded to VY.

ACKNOWLEDGMENTS

We thank Simeon Wong, Rachel Leung, MyLoi Huynh-Silveira, Julie Lu Patranoiu, Rianne Hastie Adams, Rachael Lyon, Katharine Coons, Marc Lalancette, Tammy Rayner and Ruth Weiss for their help in recruitment, data collection and/or analyses. We are also very grateful to all individuals who participated in this study.

REFERENCES

1. Demetriou EA, Lampit A, Quintana DS, Naismith SL, Song YJC, Pye JE, et al. Autism spectrum disorders: A meta-analysis of executive function. *Mol Psychiatry* (2018) 23:1198–204. doi: 10.1038/mp.2017.75
2. Pellicano E. The development of executive function in autism. *Autism Res Treat* (2012) 2012:146132. doi: 10.1155/2012/146132
3. Wallace GL, Kenworthy L, Pugliese CE, Popal HS, White EI, Brodsky E, et al. Real-world executive functions in adults with autism spectrum disorder: Profiles of impairment and associations with adaptive functioning and co-morbid anxiety and depression. *J Autism Dev Disord* (2016) 46:1071–83. doi: 10.1007/s10803-015-2655-7
4. Hill EL. Executive dysfunction in autism. *Trends Cognit Sci* (2004) 8:26–32. doi: 10.1016/j.tics.2003.11.003
5. Baddeley A. Working memory: Theories, models, and controversies. *Annu Rev Psychol* (2012) 63:1–29. doi: 10.1146/annurev-psych-120710-100422
6. D'Esposito M. From cognitive to neural models of working memory. *Philos Trans R Soc B Biol Sci* (2007) 362:761–72. doi: 10.1098/rstb.2007.2086
7. Aben B, Stapert S, Blokland A. About the distinction between working memory and short-term memory. *Front Psychol* (2012) 3:301. doi: 10.3389/fpsyg.2012.00301
8. Cowan N. What are the differences between long-term, short-term, and working memory? *Prog Brain Res* (2008) 169:323–38. doi: 10.1016/S0079-6123(07)00020-9
9. Bowler DM, Poirier M, Martin JS, Gaigg SB. Nonverbal short-term serial order memory in autism spectrum disorder. *J Abnorm Psychol* (2016) 125:886–93. doi: 10.1037/abn0000203
10. Williams DL, Goldstein G, Minshew NJ. Impaired memory for faces and social scenes in autism: clinical implications of memory dysfunction. *Arch Clin Neuropsychol* (2005) 20:1–15. doi: 10.1016/j.acn.2002.08.001
11. Desaunay P, Briant AR, Bowler DM, Ring M, Gérardin P, Baleyte J-M, et al. Memory in autism spectrum disorder: A meta-analysis of experimental studies. *Psychol Bull* (2020) 146:377–410. doi: 10.1037/bul0000225
12. Poirier M, Martin JS, Gaigg SB, Bowler DM. Short-term memory in autism spectrum disorder. *J Abnorm Psychol* (2011) 120:247–52. doi: 10.1037/a0022298
13. Wilhelm O, Hildebrandt A, Oberauer K. What is working memory capacity, and how can we measure it? *Front Psychol* (2013) 4:433. doi: 10.3389/fpsyg.2013.00433
14. Conway ARA, Kane MJ, Engle RW. Working memory capacity and its relation to general intelligence. *Trends Cognit Sci* (2003) 7:547–52. doi: 10.1016/j.tics.2003.10.005
15. Gathercole SE, Pickering SJ, Knight C, Stegmann Z. Working memory skills and educational attainment: Evidence from national curriculum assessments at 7 and 14 years of age. *Appl Cognit Psychol* (2004) 18:1–16. doi: 10.1002/acp.934
16. Alloway TP, Alloway RG. Investigating the predictive roles of working memory and IQ in academic attainment. *J Exp Child Psychol* (2010) 106:20–9. doi: 10.1016/j.jecp.2009.11.003
17. Bull R, Espy KA, Wiebe SA. Short-Term Memory, Working Memory, and Executive Functioning in Preschoolers: Longitudinal Predictors of Mathematical Achievement at Age 7 Years. *Dev Neuropsychol* (2008) 33:205–28. doi: 10.1080/87565640801982312
18. Murrihy C, Bailey M, Roodenburg J. Psychomotor Ability and Short-term Memory, and Reading and Mathematics Achievement in Children. *Arch Clin Neuropsychol* (2017) 32:618–30. doi: 10.1093/arclin/acx033
19. Tse VWS, Crabtree J, Islam S, Stott J. Comparing intellectual and memory abilities of older autistic adults with typically developing older adults using WAIS-IV and WMS-IV. *J Autism Dev Disord* (2019) 49:4123–33. doi: 10.1007/s10803-019-04122-w
20. Wang Y, Zhang Y, Liu L, Cui J, Wang J, Shum DHK, et al. A meta-analysis of working memory impairments in autism spectrum disorders. *Neuropsychol Rev* (2017) 27:46–61. doi: 10.1007/s11065-016-9336-y
21. Chien Y-L, Gau SS-F, Shang C-Y, Chiu Y-N, Tsai W-C, Wu Y-Y. Visual memory and sustained attention impairment in youths with autism spectrum disorders. *Psychol Med* (2015) 45:2263–73. doi: 10.1017/S0033291714003201
22. Williams DL, Goldstein G, Carpenter PA, Minshew NJ. Verbal and spatial working memory in autism. *J Autism Dev Disord* (2005) 35:747–56. doi: 10.1007/s10803-005-0021-x
23. Zinke K, Fries E, Altgassen M, Kirschbaum C, Dettenborn L, Kliegel M. Visuospatial Short-Term Memory Explains Deficits in Tower Task Planning in High-Functioning Children with Autism Spectrum Disorder. *Child Neuropsychol* (2010) 16:229–41. doi: 10.1080/09297040903559648
24. Habib A, Harris L, Pollick F, Melville C. A meta-analysis of working memory in individuals with autism spectrum disorders. *PloS One* (2019) 14:e0216198. doi: 10.1371/journal.pone.0216198
25. Barendse EM, Schreuder LJ, Thoonen G, Hendriks MPH, Kessels RPC, Backes WH, et al. Working memory network alterations in high-functioning adolescents with an autism spectrum disorder. *Psychiatry Clin Neurosci* (2018) 72:73–83. doi: 10.1111/pcn.12602
26. Koshino H, Kana RK, Keller TA, Cherkassky VL, Minshew NJ, Just MA. fMRI investigation of working memory for faces in autism: Visual coding and underconnectivity with frontal areas. *Cereb Cortex* (2008) 18:289–300. doi: 10.1093/cercor/bhm054
27. Urbain CM, Pang EW, Taylor MJ. Atypical spatiotemporal signatures of working memory brain processes in autism. *Transl Psychiatry* (2015) 5:e617. doi: 10.1038/tp.2015.107
28. Silk TJ, Rinehart N, Bradshaw JL, Tonge B, Egan G, O'Boyle MW, et al. Visuospatial processing and the function of prefrontal-parietal networks in autism spectrum disorders: A functional MRI study. *Am J Psychiatry* (2006) 163:1440–3. doi: 10.1176/ajp.2006.163.8.1440
29. Braden BB, Smith CJ, Thompson A, Glaspy TK, Wood E, Vatsa D, et al. Executive function and functional and structural brain differences in middle-age adults with autism spectrum disorder. *Autism Res* (2017) 10:1945–59. doi: 10.1002/aur.1842
30. Vogan VM, Francis KE, Morgan BR, Smith ML, Taylor MJ. Load matters: Neural correlates of verbal working memory in children with autism spectrum disorder. *J Neurodev Disord* (2018) 10:19. doi: 10.1186/s11689-018-9236-y
31. Koshino H, Carpenter PA, Minshew NJ, Cherkassky VL, Keller TA, Just MA. Functional connectivity in an fMRI working memory task in

high-functioning autism. *Neuroimage* (2005) 24:810–21. doi: 10.1016/j.neuroimage.2004.09.028
32. Urbain C, Vogan VM, Ye AX, Pang EW, Doesburg SM, Taylor MJ. Desynchronization of fronto-temporal networks during working memory processing in autism. *Hum Brain Mapp* (2016) 37:153–64. doi: 10.1002/hbm.23021
33. Owen AM, McMillan KM, Laird AR, Bullmore E. N-back working memory paradigm: A meta-analysis of normative functional neuroimaging studies. *Hum Brain Mapp* (2005) 25:46–59. doi: 10.1002/hbm.20131
34. Rottschy C, Langner R, Dogan I, Reetz K, Laird AR, Schulz JB, et al. Modelling neural correlates of working memory: A coordinate-based meta-analysis. *Neuroimage* (2012) 60:830–46. doi: 10.1016/j.neuroimage.2011.11.050
35. Yaple ZA, Stevens WD, Arsalidou M. Meta-analyses of the n-back working memory task: fMRI evidence of age-related changes in prefrontal cortex involvement across the adult lifespan. *Neuroimage* (2019) 196:16–31. doi: 10.1016/j.neuroimage.2019.03.074
36. Mencarelli L, Neri F, Momi D, Menardi A, Rossi S, Rossi A, et al. Stimuli, presentation modality, and load-specific brain activity patterns during n-back task. *Hum Brain Mapp* (2019) 40:3810–31. doi: 10.1002/hbm.24633
37. Majerus S, D'Argembeau A, Martinez Perez T, Belayachi S, Van der Linden M, Collette F, et al. The Commonality of Neural Networks for Verbal and Visual Short-term Memory. *J Cognit Neurosci* (2010) 22:2570–93. doi: 10.1162/jocn.2009.21378
38. Babiloni C, Babiloni F, Carducci F, Cincotti F, Vecchio F, Cola B, et al. Functional Frontoparietal Connectivity During Short-Term Memory as Revealed by High-Resolution EEG Coherence Analysis. *Behav Neurosci* (2004) 118:687–97. doi: 10.1037/0735-7044.118.4.687
39. Cashdollar N, Malecki U, Rugg-Gunn FJ, Duncan JS, Lavie N, Duzel E. Hippocampus-dependent and -independent theta-networks of active maintenance. *Proc Natl Acad Sci* (2009) 106:20493–8. doi: 10.1073/pnas.0904823106
40. Corbetta M, Shulman GL. Control of goal-directed and stimulus-driven attention in the brain. *Nat Rev Neurosci* (2002) 3:201–15. doi: 10.1038/nrn755
41. Marek S, Dosenbach NUF. The frontoparietal network: Function, electrophysiology, and importance of individual precision mapping. *Dialogues Clin Neurosci* (2018) 20:133–40. doi: 10.31887/DCNS.2018.20.2/smarek
42. Fair DA, Dosenbach NUF, Church JA, Cohen AL, Brahmbhatt S, Miezin FM, et al. Development of distinct control networks through segregation and integration. *Proc Natl Acad Sci U S A* (2007) 104:13507–12. doi: 10.1073/pnas.0705843104
43. Harding IH, Harrison BJ, Breakspear M, Pantelis C, Yücel M. Cortical representations of cognitive control and working memory are dependent yet non-interacting. *Cereb Cortex* (2016) 26:557–65. doi: 10.1093/cercor/bhu208
44. Dosenbach NUF, Fair DA, Miezin FM, Cohen AL, Wenger KK, Dosenbach RAT, et al. Distinct brain networks for adaptive and stable task control in humans. *Proc Natl Acad Sci U S A* (2007) 104:11073–8. doi: 10.1073/pnas.0704320104
45. Becke A, Müller N, Vellage A, Schoenfeld MA, Hopf J-M. Neural sources of visual working memory maintenance in human parietal and ventral extrastriate visual cortex. *Neuroimage* (2015) 110:78–86. doi: 10.1016/j.neuroimage.2015.01.059
46. Gazzaley A, Rissman J, D'Esposito M. Functional connectivity during working memory maintenance. *Cognit Affect Behav Neurosci* (2004) 4:580–99. doi: 10.3758/cabn.4.4.580
47. Jonides J, Schumacher EH, Smith EE, Koeppe RA, Awh E, Reuter-Lorenz PA, et al. The role of parietal cortex in verbal working memory. *J Neurosci* (1998) 18:5026–34. doi: 10.1523/JNEUROSCI.18-13-05026.1998
48. Ragland JD, Turetsky BI, Gur RC, Gunning-Dixon F, Turner T, Schroeder L, et al. Working memory for complex figures: An fMRI comparison of letter and fractal n-back tasks. *Neuropsychology* (2002) 16:370–9. doi: 10.1037/0894-4105.16.3.370
49. Robitaille N, Marois R, Todd J, Grimault S, Cheyne D, Jolicœur P. Distinguishing between lateralized and nonlateralized brain activity associated with visual short-term memory: fMRI, MEG, and EEG evidence from the same observers. *Neuroimage* (2010) 53:1334–45. doi: 10.1016/j.neuroimage.2010.07.027
50. Christophel TB, Hebart MN, Haynes J-D. Decoding the Contents of Visual Short-Term Memory from Human Visual and Parietal Cortex. *J Neurosci* (2012) 32:12983–9. doi: 10.1523/JNEUROSCI.0184-12.2012
51. Todd JJ, Marois R. Capacity limit of visual short-term memory in human posterior parietal cortex. *Nature* (2004) 428:751–4. doi: 10.1038/nature02466
52. Fiez J, Raife E, Balota D, Schwarz J, Raichle M, Petersen S. A positron emission tomography study of the short-term maintenance of verbal information. *J Neurosci* (1996) 16:808–22. doi: 10.1523/JNEUROSCI.16-02-00808.1996
53. Petrides M. Lateral prefrontal cortex: Architectonic and functional organization. *Philos Trans R Soc B Biol Sci* (2005) 360:781–95. doi: 10.1098/rstb.2005.1631
54. Curtis CE, D'Esposito M. Persistent activity in the prefrontal cortex during working memory. *Trends Cognit Sci* (2003) 7:415–23. doi: 10.1016/S1364-6613(03)00197-9
55. Courtney SM, Petit L, Haxby JV, Ungerleider LG. The role of prefrontal cortex in working memory: Examining the contents of consciousness. *Philos Trans R Soc B Biol Sci* (1998) 353:1819–28. doi: 10.1098/rstb.1998.0334
56. Serences JT. Neural mechanisms of information storage in visual short-term memory. *Vision Res* (2016) 128:53–67. doi: 10.1016/j.visres.2016.09.010
57. D'Esposito M, Postle BR, Rypma B. Prefrontal cortical contributions to working memory: Evidence from event-related fMRI studies. *Exp Brain Res* (2000) 133:3–11. doi: 10.1007/s002210000395
58. Ranganath C, Johnson MK, D'Esposito M. Prefrontal activity associated with working memory and episodic long-term memory. *Neuropsychologia* (2003) 41:378–89. doi: 10.1016/s0028-3932(02)00169-0
59. Veltman DJ, Rombouts SARB, Dolan RJ. Maintenance versus manipulation in verbal working memory revisited: An fMRI study. *Neuroimage* (2003) 18:247–56. doi: 10.1016/s1053-8119(02)00049-6
60. Rowe JB, Toni I, Josephs O, Frackowiak RSJ, Passingham RE. The prefrontal cortex: Response selection or maintenance within working memory? *Science* (2000) 288:1656–60. doi: 10.1126/science.288.5471.1656
61. Yeung MK, Lee TL, Chan AS. Right-lateralized frontal activation underlies successful updating of verbal working memory in adolescents with high-functioning autism spectrum disorder. *Biol Psychol* (2019) 148:107743. doi: 10.1016/j.biopsycho.2019.107743
62. Luna B, Minshew NJ, Garver KE, Lazar NA, Thulborn KR, Eddy WF, et al. Neocortical system abnormalities in autism: An fMRI study of spatial working memory. *Neurology* (2002) 59:834–40. doi: 10.1212/WNL.59.6.834
63. Vogan VM, Morgan BR, Lou SM, Taylor MJ. Functional changes during visuo-spatial working memory in autism spectrum disorder: 2-year longitudinal functional magnetic resonance imaging study. *Autism* (2019) 23:639–52. doi: 10.1177/1362361318766572
64. Rahko JS, Vuontela VA, Carlson S, Nikkinen J, Hurtig TM, Kuusikko-Gauffin S, et al. Attention and working memory in adolescents with autism spectrum disorder: A functional MRI study. *Child Psychiatry Hum Dev* (2016) 47:503–17. doi: 10.1007/s10578-015-0583-6
65. Cohen JR, D'Esposito M. The segregation and integration of distinct brain networks and their relationship to cognition. *J Neurosci* (2016) 36:12083–94. doi: 10.1523/JNEUROSCI.2965-15.2016
66. Finc K, Bonna K, Lewandowska M, Wolak T, Nikadon J, Dreszer J, et al. Transition of the functional brain network related to increasing cognitive demands. *Hum Brain Mapp* (2017) 38:3659–74. doi: 10.1002/hbm.23621
67. Cole MW, Reynolds JR, Power JD, Repovs G, Anticevic A, Braver TS. Multi-task connectivity reveals flexible hubs for adaptive task control. *Nat Neurosci* (2013) 16:1348–55. doi: 10.1038/nn.3470
68. Spreng RN, Stevens WD, Chamberlain JP, Gilmore AW, Schacter DL. Default network activity, coupled with the frontoparietal control network, supports goal-directed cognition. *Neuroimage* (2010) 53:303–17. doi: 10.1016/j.neuroimage.2010.06.016
69. Dixon ML, De La Vega A, Mills C, Andrews-Hanna J, Spreng RN, Cole MW, et al. Heterogeneity within the frontoparietal control network and its relationship to the default and dorsal attention networks. *Proc Natl Acad Sci U S A* (2018) 115:E1598–607. doi: 10.1073/pnas.1715766115
70. Cocchi L, Zalesky A, Fornito A, Mattingley JB. Dynamic cooperation and competition between brain systems during cognitive control. *Trends Cognit Sci* (2013) 17:493–501. doi: 10.1016/j.tics.2013.08.006

71. Belmonte MK, Allen G, Beckel-Mitchener A, Boulanger LM, Carper RA, Webb SJ. Autism and abnormal development of brain connectivity. *J Neurosci* (2004) 24:9228–31. doi: 10.1523/JNEUROSCI.3340-04.2004
72. O'Reilly C, Lewis JD, Elsabbagh M. Is functional brain connectivity atypical in autism? A systematic review of EEG and MEG studies. *PloS One* (2017) 12:e0175870. doi: 10.1371/journal.pone.0175870
73. Kessler K, Seymour RA, Rippon G. Brain oscillations and connectivity in autism spectrum disorders (ASD): New approaches to methodology, measurement and modelling. *Neurosci Biobehav Rev* (2016) 71:601–20. doi: 10.1016/j.neubiorev.2016.10.002
74. Di Martino A, Yan C-G, Li Q, Denio E, Castellanos FX, Alaerts K, et al. The autism brain imaging data exchange: Towards a large-scale evaluation of the intrinsic brain architecture in autism. *Mol Psychiatry* (2014) 19:659–67. doi: 10.1038/mp.2013.78
75. Kana RK, Libero LE, Moore MS. Disrupted cortical connectivity theory as an explanatory model for autism spectrum disorders. *Phys Life Rev* (2011) 8:410–37. doi: 10.1016/j.plrev.2011.10.001
76. Geschwind DH, Levitt P. Autism spectrum disorders: Developmental disconnection syndromes. *Curr Opin Neurobiol* (2007) 17:103–11. doi: 10.1016/j.conb.2007.01.009
77. Palva JM, Monto S, Kulashekhar S, Palva S. Neuronal synchrony reveals working memory networks and predicts individual memory capacity. *Proc Natl Acad Sci U.S.A.* (2010) 107:7580–5. doi: 10.1073/pnas.0913113107
78. Roux F, Uhlhaas PJ. Working memory and neural oscillations: α-γ versus θ-γ codes for distinct WM information? *Trends Cognit Sci* (2014) 18:16–25. doi: 10.1016/j.tics.2013.10.010
79. Johnson EL, Dewar CD, Solbakk A-K, Endestad T, Meling TR, Knight RT. Bidirectional frontoparietal oscillatory systems support working memory. *Curr Biol* (2017) 27:1829–35. doi: 10.1016/j.cub.2017.05.046
80. Sarnthein J, Petsche H, Rappelsberger P, Shaw GL, von Stein A. Synchronization between prefrontal and posterior association cortex during human working memory. *Proc Natl Acad Sci U.S.A.* (1998) 95:7092–6. doi: 10.1073/pnas.95.12.7092
81. Klimesch W, Freunberger R, Sauseng P. Oscillatory mechanisms of process binding in memory. *Neurosci Biobehav Rev* (2010) 34:1002–14. doi: 10.1016/j.neubiorev.2009.10.004
82. Liebe S, Hoerzer GM, Logothetis NK, Rainer G. Theta coupling between V4 and prefrontal cortex predicts visual short-term memory performance. *Nat Neurosci* (2012) 15:456–62. doi: 10.1038/nn.3038
83. Freunberger R, Klimesch W, Griesmayr B, Sauseng P, Gruber W. Alpha phase coupling reflects object recognition. *Neuroimage* (2008) 42:928–35. doi: 10.1016/j.neuroimage.2008.05.020
84. Payne L, Kounios J. Coherent oscillatory networks supporting short-term memory retention. *Brain Res* (2009) 1247:126–32. doi: 10.1016/j.brainres.2008.09.095
85. Doesburg SM, Herdman AT, Ribary U, Cheung T, Moiseev A, Weinberg H, et al. Long-range synchronization and local desynchronization of alpha oscillations during visual short-term memory retention in children. *Exp Brain Res* (2010) 201:719–27. doi: 10.1007/s00221-009-2086-9
86. Nyrenius J, Billstedt E. The functional impact of cognition in adults with autism spectrum disorders. *Nord J Psychiatry* (2020) 74:220–5. doi: 10.1080/08039488.2019.1694698
87. Carpentieri S, Morgan SB. Adaptive and intellectual functioning in autistic and nonautistic retarded children. *J Autism Dev Disord* (1996) 26:611–20. doi: 10.1007/BF02172350
88. Kirchner WK. Age differences in short-term retention of rapidly changing information. *J Exp Psychol* (1958) 55:352–8. doi: 10.1037/h0043688
89. Kundu B, Chang J-Y, Postle BR, Van Veen BD. Context-specific differences in fronto-parieto-occipital effective connectivity during short-term memory maintenance. *Neuroimage* (2015) 114:320–7. doi: 10.1016/j.neuroimage.2015.04.001
90. Tallon-Baudry C. Oscillatory synchrony and human visual cognition. *J Physiol* (2003) 97:355–63. doi: 10.1016/j.jphysparis.2003.09.009
91. Wilsch A, Henry MJ, Herrmann B, Herrmann CS, Obleser J. Temporal Expectation Modulates the Cortical Dynamics of Short-Term Memory. *J Neurosci* (2018) 38:7428–39. doi: 10.1523/JNEUROSCI.2928-17.2018
92. Schack B, Klimesch W. Frequency characteristics of evoked and oscillatory electroencephalic activity in a human memory scanning task. *Neurosci Lett* (2002) 331:107–10. doi: 10.1016/S0304-3940(02)00846-7
93. Düzel E, Penny WD, Burgess N. Brain oscillations and memory. *Curr Opin Neurobiol* (2010) 20:143–9. doi: 10.1016/j.conb.2010.01.004
94. Salazar RF, Dotson NM, Bressler SL, Gray CM. Content-specific fronto-parietal synchronization during visual working memory. *Science* (2012) 338:1097–101. doi: 10.1126/science.1224000
95. Daume J, Graetz S, Gruber T, Engel AK, Friese U. Cognitive control during audiovisual working memory engages frontotemporal theta-band interactions. *Sci Rep* (2017) 7:12585. doi: 10.1038/s41598-017-12511-3
96. Dai Z, de Souza J, Lim J, Ho PM, Chen Y, Li J, et al. EEG cortical connectivity analysis of working memory reveals topological reorganization in theta and alpha bands. *Front Hum Neurosci* (2017) 11:237. doi: 10.3389/fnhum.2017.00237
97. Bressler SL, Richter CG. Interareal oscillatory synchronization in top-down neocortical processing. *Curr Opin Neurobiol* (2015) 31:62–6. doi: 10.1016/j.conb.2014.08.010
98. Kopell N, Ermentrout GB, Whittington MA, Traub RD. Gamma rhythms and beta rhythms have different synchronization properties. *Proc Natl Acad Sci U.S.A.* (2000) 97:1867–72. doi: 10.1073/pnas.97.4.1867
99. von Stein A, Chiang C, König P. Top-down processing mediated by interareal synchronization. *Proc Natl Acad Sci U.S.A.* (2000) 97:14748–53. doi: 10.1073/pnas.97.26.14748
100. Johnson EL, King-Stephens D, Weber PB, Laxer KD, Lin JJ, Knight RT. Spectral imprints of working memory for everyday associations in the frontoparietal network. *Front Syst Neurosci* (2019) 12:65. doi: 10.3389/fnsys.2018.00065
101. Murray JD, Jaramillo J, Wang X-J. Working memory and decision-making in a frontoparietal circuit model. *J Neurosci* (2017) 37:12167–86. doi: 10.1523/JNEUROSCI.0343-17.2017
102. Sato J, Mossad SI, Wong SM, Hunt BAE, Dunkley BT, Lou SM, et al. Alpha keeps it together: Alpha oscillatory synchrony underlies working memory maintenance in young children. *Dev Cognit Neurosci* (2018) 34:114–23. doi: 10.1016/j.dcn.2018.09.001
103. Sauseng P, Klimesch W, Doppelmayr M, Pecherstorfer T, Freunberger R, Hanslmayr S. EEG alpha synchronization and functional coupling during top-down processing in a working memory task. *Hum Brain Mapp* (2005) 26:148–55. doi: 10.1002/hbm.20150
104. Crespo-Garcia M, Pinal D, Cantero JL, Díaz F, Zurrón M, Atienza M. Working memory processes are mediated by local and long-range synchronization of alpha oscillations. *J Cognit Neurosci* (2013) 25:1343–57. doi: 10.1162/jocn_a_00379
105. Jensen O, Gelfand J, Kounios J, Lisman JE. Oscillations in the alpha band (9-12 Hz) increase with memory load during retention in a short-term memory task. *Cereb Cortex* (2002) 12:877–82. doi: 10.1093/cercor/12.8.877
106. Wechsler D. *Wechsler Abbreviated Scale of Intelligence (WASI)*. San Antonio, TX: Psychological Corporation (1999).
107. Wechsler D. *Wechsler Abbreviated Scale of Intelligence, Second Edition (WASI-II)*. San Antonio, TX: NCS Pearson (2011).
108. Lord C, Rutter M, DiLavore PC, Risi S, Gotham K, Bishop SL. *Autism Diagnostic Observation Schedule, Second Edition (ADOS-2) Manual (Part I): Modules 1-4*. Torrance, CA: Western Psychological Services (2012).
109. Lord C, Risi S, Lambrecht L, Cook EH Jr., Leventhal BL, DiLavore PC, et al. The Autism Diagnostic Observation Schedule-Generic: A standard measure of social and communication deficits associated with the spectrum of autism. *J Autism Dev Disord* (2000) 30:205–23. doi: 10.1023/A:1005592401947
110. Roth RM, Isquith PK, Gioia GA. *Behavior Rating Inventory of Executive Function – Adult Version*. Lutz, FL: Psychological Assessment Resources (2005).
111. Constantino JN, Gruber CP. *Social Responsiveness Scale, Second Edition*. Los Angeles, CA: Western Psychological Services (2012).
112. Oostenveld R, Fries P, Maris E, Schoffelen J-M. FieldTrip: Open source software for advanced analysis of MEG, EEG, and invasive electrophysiological data. *Comput Intell Neurosci* (2011) 2011:156869. doi: 10.1155/2011/156869
113. Nolte G. The magnetic lead field theorem in the quasi-static approximation and its use for magnetoenchephalography forward calculation in realistic volume conductors. *Phys Med Biol* (2003) 48:3637–52. doi: 10.1088/0031-9155/48/22/002
114. Tzourio-Mazoyer N, Landeau B, Papathanassiou D, Crivello F, Etard O, Delcroix N, et al. Automated anatomical labeling of activations in SPM using

a macroscopic anatomical parcellation of the MNI MRI single-subject brain. *Neuroimage* (2002) 15:273–89. doi: 10.1006/nimg.2001.0978
115. Van Veen BD, Van Drongelen W, Yuchtman M, Suzuki A. Localization of brain electrical activity via linearly constrained minimum variance spatial filtering. *IEEE Trans BioMed Eng* (1997) 44:867–80. doi: 10.1109/10.623056
116. Breakspear M, Williams LM, Stam CJ. A novel method for the topographic analysis of neural activity reveals formation and dissolution of "dynamic cell assemblies." *J Comput Neurosci* (2004) 16:49–68. doi: 10.1023/B:JCNS.0000004841.66897.7d
117. Tewarie P, Liuzzi L, O'Neill GC, Quinn AJ, Griffa A, Woolrich MW, et al. Tracking dynamic brain networks using high temporal resolution MEG measures of functional connectivity. *Neuroimage* (2019) 200:38–50. doi: 10.1016/j.neuroimage.2019.06.006
118. Zalesky A, Fornito A, Bullmore ET. Network-based statistic: Identifying differences in brain networks. *Neuroimage* (2010) 53:1197–207. doi: 10.1016/j.neuroimage.2010.06.041
119. Xia M, Wang J, He Y. BrainNet Viewer: A network visualization tool for human brain connectomics. *PloS One* (2013) 8:e68910. doi: 10.1371/journal.pone.0068910
120. Koelewijn L, Lancaster TM, Linden D, Dima DC, Routley BC, Magazzini L, et al. Oscillatory hyperactivity and hyperconnectivity in young APOE-ε4 carriers and hypoconnectivity in Alzheimer's disease. *Elife* (2019) 8:e36011. doi: 10.7554/eLife.36011
121. Lever AG, Werkle-Bergner M, Brandmaier AM, Ridderinkhof KR, Geurts HM. Atypical working memory decline across the adult lifespan in autism spectrum disorder? *J Abnorm Psychol* (2015) 124:1014–26. doi: 10.1037/abn0000108
122. Haigh SM, Walsh JA, Mazefsky CA, Minshew NJ, Eack SM. Processing speed is impaired in adults with autism spectrum disorder, and relates to social communication abilities. *J Autism Dev Disord* (2018) 48:2653–62. doi: 10.1007/s10803-018-3515-z
123. Oliveras-Rentas RE, Kenworthy L, Roberson RB, Martin A, Wallace GL. WISC-IV profile in high-functioning autism spectrum disorders: Impaired processing speed is associated with increased autism communication symptoms and decreased adaptive communication abilities. *J Autism Dev Disord* (2012) 42:655–64. doi: 10.1007/s10803-011-1289-7
124. Travers BG, Bigler ED, Tromp DPM, Adluru N, Froehlich AL, Ennis C, et al. Longitudinal processing speed impairments in males with autism and the effects of white matter microstructure. *Neuropsychologia* (2014) 53:137–45. doi: 10.1016/j.neuropsychologia.2013.11.008
125. Hedvall Å, Fernell E, Holm A, Åsberg Johnels J, Gillberg C, Billstedt E. Autism, processing speed, and adaptive functioning in preschool children. *Sci World J* (2013) 2013:158263. doi: 10.1155/2013/158263
126. Mayes SD, Calhoun SL. Learning, attention, writing, and processing speed in typical children and children with ADHD, autism, anxiety, depression, and oppositional-defiant disorder. *Child Neuropsychol* (2007) 13:469–93. doi: 10.1080/09297040601112773
127. Luna B, Doll SK, Hegedus SJ, Minshew NJ, Sweeney JA. Maturation of executive function in autism. *Biol Psychiatry* (2007) 61:474–81. doi: 10.1016/j.biopsych.2006.02.030
128. Cardillo R, Lanfranchi S, Mammarella IC. A cross-task comparison on visuospatial processing in autism spectrum disorders. *Autism* (2020) 24:765–79. doi: 10.1177/1362361319888341
129. Wallace GL, Anderson M, Happé F. Brief report: Information processing speed is intact in autism but not correlated with measured intelligence. *J Autism Dev Disord* (2009) 39:809–14. doi: 10.1007/s10803-008-0684-1
130. Mayes SD, Calhoun SL. WISC-IV and WIAT-II profiles in children with high-functioning autism. *J Autism Dev Disord* (2008) 38:428–39. doi: 10.1007/s10803-007-0410-4
131. Fried R, Joshi G, Bhide P, Pope A, Galdo M, Koster A, et al. A study of the neuropsychological correlates in adults with high functioning autism spectrum disorders. *Acta Neuropsychiatr* (2016) 28:286–95. doi: 10.1017/neu.2016.12
132. Braaten EB, Ward AK, Forchelli G, Vuijk PJ, Cook NE, McGuinness P, et al. Characteristics of child psychiatric outpatients with slow processing speed and potential mechanisms of academic impact. *Eur Child Adolesc Psychiatry* (2020). doi: 10.1007/s00787-019-01455-w
133. Tsukiura T, Fujii T, Takahashi T, Xiao R, Inase M, Iijima T, et al. Neuroanatomical discrimination between manipulating and maintaining processes involved in verbal working memory; a functional MRI study. *Cognit Brain Res* (2001) 11:13–21. doi: 10.1016/s0926-6410(00)00059-8
134. Paulesu E, Frith CD, Frackowiak RSJ. The neural correlates of the verbal component of working memory. *Nature* (1993) 362:342–5. doi: 10.1038/362342a0
135. Sheremata SL, Somers DC, Shomstein S. Visual short-term memory activity in parietal lobe reflects cognitive processes beyond attentional selection. *J Neurosci* (2018) 38:1511–9. doi: 10.1523/JNEUROSCI.1716-17.2017
136. Bettencourt KC, Xu Y. Decoding the content of visual short-term memory under distraction in occipital and parietal areas. *Nat Neurosci* (2016) 19:150–7. doi: 10.1038/nn.4174
137. Nee DE, Brown JW, Askren MK, Berman MG, Demiralp E, Krawitz A, et al. A meta-analysis of executive components of working memory. *Cereb Cortex* (2013) 23:264–82. doi: 10.1093/cercor/bhs007
138. Berryhill ME. Insights from neuropsychology: Pinpointing the role of the posterior parietal cortex in episodic and working memory. *Front Integr Neurosci* (2012) 6:31. doi: 10.3389/fnint.2012.00031
139. Andersen RA, Essick GK, Siegel RM. Encoding of spatial location by posterior parietal neurons. *Science* (1985) 230:456–8. doi: 10.1126/science.4048942
140. Alain C, Shen D, Yu H, Grady C. Dissociable memory- and response-related activity in parietal cortex during auditory spatial working memory. *Front Psychol* (2010) 1:202. doi: 10.3389/fpsyg.2010.00202
141. Passaro AD, Elmore LC, Ellmore TM, Leising KJ, Papanicolaou AC, Wright AA. Explorations of object and location memory using fMRI. *Front Behav Neurosci* (2013) 7:105. doi: 10.3389/fnbeh.2013.00105
142. Rottschy C, Caspers S, Roski C, Reetz K, Dogan I, Schulz JB, et al. Differentiated parietal connectivity of frontal regions for "what" and "where" memory. *Brain Struct Funct* (2013) 218:1551–67. doi: 10.1007/s00429-012-0476-4
143. Courtney SM, Ungerleider LG, Keil K, Haxby JV. Object and spatial visual working memory activate separate neural systems in human cortex. *Cereb Cortex* (1996) 6:39–49. doi: 10.1093/cercor/6.1.39
144. Thomas KM, King SW, Franzen PL, Welsh TF, Berkowitz AL, Noll DC, et al. A developmental functional MRI study of spatial working memory. *Neuroimage* (1999) 10:327–38. doi: 10.1006/nimg.1999.0466
145. Harrison A, Jolicoeur P, Marois R. "What" and "Where" in the Intraparietal Sulcus: An fMRI Study of Object Identity and Location in Visual Short-Term Memory. *Cereb Cortex* (2010) 20:2478–85. doi: 10.1093/cercor/bhp314
146. Olson IR, Berryhill M. Some surprising findings on the involvement of the parietal lobe in human memory. *Neurobiol Learn Mem* (2009) 91:155–65. doi: 10.1016/j.nlm.2008.09.006
147. Duggirala SX, Saharan S, Raghunathan P, Mandal PK. Stimulus-dependent modulation of working memory for identity monitoring: A functional MRI study. *Brain Cognit* (2016) 102:55–64. doi: 10.1016/j.bandc.2015.12.006
148. Finke K, Bublak P, Zihl J. Visual spatial and visual pattern working memory: Neuropsychological evidence for a differential role of left and right dorsal visual brain. *Neuropsychologia* (2006) 44:649–61. doi: 10.1016/j.neuropsychologia.2005.06.015
149. Xu Y, Chun MM. Dissociable neural mechanisms supporting visual short-term memory for objects. *Nature* (2006) 440:91–5. doi: 10.1038/nature04262
150. Konstantinou N, Constantinidou F, Kanai R. Discrete capacity limits and neuroanatomical correlates of visual short-term memory for objects and spatial locations. *Hum Brain Mapp* (2017) 38:767–78. doi: 10.1002/hbm.23416
151. Menon V, Uddin LQ. Saliency, switching, attention and control: A network model of insula function. *Brain Struct Funct* (2010) 214:655–67. doi: 10.1007/s00429-010-0262-0
152. Sridharan D, Levitin DJ, Menon V. A critical role for the right fronto-insular cortex in switching between central-executive and default-mode networks. *Proc Natl Acad Sci U S A* (2008) 105:12569–74. doi: 10.1073/pnas.0800005105
153. Eckert MA, Menon V, Walczak A, Ahlstrom J, Denslow S, Horwitz A, et al. At the heart of the ventral attention system: The right anterior insula. *Hum Brain Mapp* (2009) 30:2530–41. doi: 10.1002/hbm.20688

154. Uddin LQ, Kinnison J, Pessoa L, Anderson ML. Beyond the tripartite cognition-emotion-interoception model of the human insular cortex. *J Cognit Neurosci* (2014) 26:16–27. doi: 10.1162/jocn_a_00462
155. Cauda F, Costa T, Torta DME, Sacco K, D'Agata F, Duca S, et al. Meta-analytic clustering of the insular cortex: Characterizing the meta-analytic connectivity of the insula when involved in active tasks. *Neuroimage* (2012) 62:343–55. doi: 10.1016/j.neuroimage.2012.04.012
156. D'Esposito M, Postle BR. The cognitive neuroscience of working memory. *Annu Rev Psychol* (2015) 66:115–42. doi: 10.1146/annurev-psych-010814-015031
157. Barbey AK, Koenigs M, Grafman J. Dorsolateral prefrontal contributions to human working memory. *Cortex* (2013) 49:1195–205. doi: 10.1016/j.cortex.2012.05.022
158. Wager TD, Smith EE. Neuroimaging studies of working memory: A meta-analysis. *Cognit Affect Behav Neurosci* (2003) 3:255–74. doi: 10.3758/cabn.3.4.255
159. O'Reilly RC, Braver TS, Cohen JD. A biologically based computational model of working memory. In: Miyake A, Shah P, editors. *Models of Working Memory: Mechanisms of Active Maintenance and Executive Control*. New York, NY: Cambridge University Press (1999). p. 375–411. doi: 10.1017/CBO9781139174909.014
160. Feredoes E, Heinen K, Weiskopf N, Ruff C, Driver J. Causal evidence for frontal involvement in memory target maintenance by posterior brain areas during distracter interference of visual working memory. *Proc Natl Acad Sci U S A* (2011) 108:17510–5. doi: 10.1073/pnas.1106439108
161. Edin F, Klingberg T, Johansson P, McNab F, Tegnér J, Compte A. Mechanism for top-down control of working memory capacity. *Proc Natl Acad Sci U S A* (2009) 106:6802–7. doi: 10.1073/pnas.0901894106
162. Cavanna AE, Trimble MR. The precuneus: A review of its functional anatomy and behavioural correlates. *Brain* (2006) 129:564–83. doi: 10.1093/brain/awl004
163. Zhang S, Li CR. Functional connectivity mapping of the human precuneus by resting state fMRI. *Neuroimage* (2012) 59:3548–62. doi: 10.1016/j.neuroimage.2011.11.023
164. Margulies DS, Vincent JL, Kelly C, Lohmann G, Uddin LQ, Biswal BB, et al. Precuneus shares intrinsic functional architecture in humans and monkeys. *Proc Natl Acad Sci U S A* (2009) 106:20069–74. doi: 10.1073/pnas.0905314106
165. Mahayana IT, Tcheang L, Chen C-Y, Juan C-H, Muggleton NG. The precuneus and visuospatial attention in near and far space: A transcranial magnetic stimulation study. *Brain Stimul* (2014) 7:673–9. doi: 10.1016/j.brs.2014.06.012
166. Selemon LD, Goldman-Rakic PS. Common cortical and subcortical targets of the dorsolateral prefrontal and posterior parietal cortices in the rhesus monkey: Evidence for a distributed neural network subserving spatially guided behavior. *J Neurosci* (1988) 8:4049–68. doi: 10.1523/JNEUROSCI.08-11-04049.1988
167. Leichnetz GR. Connections of the medial posterior parietal cortex (area 7m) in the monkey. *Anat Rec* (2001) 263:215–36. doi: 10.1002/ar.1082
168. Suchan B, Yágüez L, Wunderlich G, Canavan AGM, Herzog H, Tellmann L, et al. Hemispheric dissociation of visual-pattern processing and visual rotation. *Behav Brain Res* (2002) 136:533–44. doi: 10.1016/s0166-4328(02)00204-8
169. Fletcher PC, Frith CD, Baker SC, Shallice T, Frackowiak RSJ, Dolan RJ. The mind's eye–precuneus activation in memory-related imagery. *Neuroimage* (1995) 2:195–200. doi: 10.1006/nimg.1995.1025
170. Sugiura M, Shah NJ, Zilles K, Fink GR. Cortical representations of personally familiar objects and places: Functional organization of the human posterior cingulate cortex. *J Cognit Neurosci* (2005) 17:183–98. doi: 10.1162/0898929053124956
171. Nyberg L, Dahlin E, Stigsdotter Neely A, Bäckman L. Neural correlates of variable working memory load across adult age and skill: Dissociative patterns within the fronto-parietal network. *Scand J Psychol* (2009) 50:41–6. doi: 10.1111/j.1467-9450.2008.00678.x
172. Robitaille N, Grimault S, Jolicœur P. Bilateral parietal and contralateral responses during maintenance of unilaterally encoded objects in visual short-term memory: Evidence from magnetoencephalography. *Psychophysiology* (2009) 46:1090–9. doi: 10.1111/j.1469-8986.2009.00837.x
173. Linden DEJ, Bittner RA, Muckli L, Waltz JA, Kriegeskorte N, Goebel R, et al. Cortical capacity constraints for visual working memory: dissociation of fMRI load effects in a fronto-parietal network. *Neuroimage* (2003) 20:1518–30. doi: 10.1016/j.neuroimage.2003.07.021
174. Vogan VM, Morgan BR, Powell TL, Smith ML, Taylor MJ. The neurodevelopmental differences of increasing verbal working memory demand in children and adults. *Dev Cognit Neurosci* (2016) 17:19–27. doi: 10.1016/j.dcn.2015.10.008
175. Rypma B, Prabhakaran V, Desmond JE, Glover GH, Gabrieli JDE. Load-dependent roles of frontal brain regions in the maintenance of working memory. *Neuroimage* (1999) 9:216–26. doi: 10.1006/nimg.1998.0404
176. Gould RL, Brown RG, Owen AM, Ffytche DH, Howard RJ. fMRI BOLD response to increasing task difficulty during successful paired associates learning. *Neuroimage* (2003) 20:1006–19. doi: 10.1016/S1053-8119(03)00365-3
177. Höller-Wallscheid MS, Thier P, Pomper JK, Lindner A. Bilateral recruitment of prefrontal cortex in working memory is associated with task demand but not with age. *Proc Natl Acad Sci U S A* (2017) 114:E830–9. doi: 10.1073/pnas.1601983114
178. Heinzel S, Lorenz RC, Duong Q-L, Rapp MA, Deserno L. Prefrontal-parietal effective connectivity during working memory in older adults. *Neurobiol Aging* (2017) 57:18–27. doi: 10.1016/j.neurobiolaging.2017.05.005
179. Wianda E, Ross B. The roles of alpha oscillation in working memory retention. *Brain Behav* (2019) 9:e01263. doi: 10.1002/brb3.1263
180. Aron AR, Robbins TW, Poldrack RA. Inhibition and the right inferior frontal cortex: One decade on. *Trends Cognit Sci* (2014) 18:177–85. doi: 10.1016/j.tics.2013.12.003
181. Vidal J, Mills T, Pang EW, Taylor MJ. Response inhibition in adults and teenagers: Spatiotemporal differences in the prefrontal cortex. *Brain Cognit* (2012) 79:49–59. doi: 10.1016/j.bandc.2011.12.011
182. Vara AS, Pang EW, Vidal J, Anagnostou E, Taylor MJ. Neural mechanisms of inhibitory control continue to mature in adolescence. *Dev Cognit Neurosci* (2014) 10:129–39. doi: 10.1016/j.dcn.2014.08.009
183. Rubia K, Smith AB, Brammer MJ, Taylor E. Right inferior prefrontal cortex mediates response inhibition while mesial prefrontal cortex is responsible for error detection. *Neuroimage* (2003) 20:351–8. doi: 10.1016/s1053-8119(03)00275-1
184. Forstmann BU, Jahfari S, Scholte HS, Wolfensteller U, van den Wildenberg WPM, Ridderinkhof KR. Function and structure of the right inferior frontal cortex predict individual differences in response inhibition: A model-based approach. *J Neurosci* (2008) 28:9790–6. doi: 10.1523/JNEUROSCI.1465-08.2008
185. Anderson MC, Ochsner KN, Kuhl B, Cooper J, Robertson E, Gabrieli SW, et al. Neural systems underlying the suppression of unwanted memories. *Science* (2004) 303:232–5. doi: 10.1126/science.1089504
186. Emch M, von Bastian CC, Koch K. Neural correlates of verbal working memory: An fMRI meta-analysis. *Front Hum Neurosci* (2019) 13:180:180. doi: 10.3389/fnhum.2019.00180
187. Bomyea J, Taylor CT, Spadoni AD, Simmons AN. Neural mechanisms of interference control in working memory capacity. *Hum Brain Mapp* (2018) 39:772–82. doi: 10.1002/hbm.23881
188. Geurts HM, van den Bergh SFWM, Ruzzano L. Prepotent response inhibition and interference control in autism spectrum disorders: Two meta-analyses. *Autism Res* (2014) 7:407–20. doi: 10.1002/aur.1369
189. Adams NC, Jarrold C. Inhibition in autism: Children with autism have difficulty inhibiting irrelevant distractors but not prepotent responses. *J Autism Dev Disord* (2012) 42:1052–63. doi: 10.1007/s10803-011-1345-3
190. Christ SE, Kester LE, Bodner KE, Miles JH. Evidence for selective inhibitory impairment in individuals with autism spectrum disorder. *Neuropsychology* (2011) 25:690–701. doi: 10.1037/a0024256
191. Lever AG, Ridderinkhof KR, Marsman M, Geurts HM. Reactive and proactive interference control in adults with autism spectrum disorder across the lifespan. *Dev Psychol* (2017) 53:379–95. doi: 10.1037/dev0000219
192. Ozonoff S, Strayer DL. Inhibitory function in nonretarded children with autism. *J Autism Dev Disord* (1997) 27:59–77. doi: 10.1023/a:1025821222046
193. Sauseng P, Griesmayr B, Freunberger R, Klimesch W. Control mechanisms in working memory: A possible function of EEG theta oscillations. *Neurosci Biobehav Rev* (2010) 34:1015–22. doi: 10.1016/j.neubiorev.2009.12.006

194. Sauseng P, Klimesch W, Freunberger R, Pecherstorfer T, Hanslmayr S, Doppelmayr M. Relevance of EEG alpha and theta oscillations during task switching. *Exp Brain Res* (2006) 170:295–301. doi: 10.1007/s00221-005-0211-y
195. Cavanagh JF, Frank MJ. Frontal theta as a mechanism for cognitive control. *Trends Cognit Sci* (2014) 18:414–21. doi: 10.1016/j.tics.2014.04.012
196. Sauseng P, Klimesch W, Doppelmayr M, Hanslmayr S, Schabus M, Gruber WR. Theta coupling in the human electroencephalogram during a working memory task. *Neurosci Lett* (2004) 354:123–6. doi: 10.1016/j.neulet.2003.10.002
197. Picci G, Gotts SJ, Scherf KS. A theoretical rut: Revisiting and critically evaluating the generalized under/over-connectivity hypothesis of autism. *Dev Sci* (2016) 19:524–49. doi: 10.1111/desc.12467
198. Just MA, Keller TA, Malave VL, Kana RK, Varma S. Autism as a neural systems disorder: A theory of frontal-posterior underconnectivity. *Neurosci Biobehav Rev* (2012) 36:1292–313. doi: 10.1016/j.neubiorev.2012.02.007
199. Vissers ME, Cohen MX, Geurts HM. Brain connectivity and high functioning autism: A promising path of research that needs refined models, methodological convergence, and stronger behavioral links. *Neurosci Biobehav Rev* (2012) 36:604–25. doi: 10.1016/j.neubiorev.2011.09.003
200. Holz EM, Glennon M, Prendergast K, Sauseng P. Theta–gamma phase synchronization during memory matching in visual working memory. *Neuroimage* (2010) 52:326–35. doi: 10.1016/j.neuroimage.2010.04.003
201. Polanía R, Nitsche MA, Korman C, Batsikadze G, Paulus W. The Importance of Timing in Segregated Theta Phase-Coupling for Cognitive Performance. *Curr Biol* (2012) 22:1314–8. doi: 10.1016/j.cub.2012.05.021
202. Jacobs J, Hwang G, Curran T, Kahana MJ. EEG oscillations and recognition memory: Theta correlates of memory retrieval and decision making. *Neuroimage* (2006) 32:978–87. doi: 10.1016/j.neuroimage.2006.02.018
203. Schack B, Klimesch W, Sauseng P. Phase synchronization between theta and upper alpha oscillations in a working memory task. *Int J Psychophysiol* (2005) 57:105–14. doi: 10.1016/j.ijpsycho.2005.03.016
204. Popov T, Popova P, Harkotte M, Awiszus B, Rockstroh B, Miller GA. Cross-frequency interactions between frontal theta and posterior alpha control mechanisms foster working memory. *Neuroimage* (2018) 181:728–33. doi: 10.1016/j.neuroimage.2018.07.067
205. Klimesch W, Freunberger R, Sauseng P, Gruber W. A short review of slow phase synchronization and memory: Evidence for control processes in different memory systems? *Brain Res* (2008) 1235:31–44. doi: 10.1016/j.brainres.2008.06.049
206. Hunt BAE, Wong SM, Vandewouw MM, Brookes MJ, Dunkley BT, Taylor MJ. Spatial and spectral trajectories in typical neurodevelopment from childhood to middle age. *Netw Neurosci* (2019) 3:497–520. doi: 10.1162/netn_a_00077
207. Vogan VM, Morgan BR, Lee W, Powell TL, Smith ML, Taylor MJ. The neural correlates of visuo-spatial working memory in children with autism spectrum disorder: Effects of cognitive load. *J Neurodev Disord* (2014) 6:19. doi: 10.1186/1866-1955-6-19

Conflict of Interest : The authors declare that the research was conducted in the absence of any commercial or financial relationships that could be construed as a potential conflict of interest.

frontiers in Psychiatry

ORIGINAL RESEARCH
published: 19 November 2020
doi: 10.3389/fpsyt.2020.584557

Maturation of Auditory Cortex Neural Activity in Children and Implications for Auditory Clinical Markers in Diagnosis

J. Christopher Edgar[1,2], Lisa Blaskey[1,3,4], Heather L. Green[1], Kimberly Konka[1], Guannan Shen[1], Marissa A. Dipiero[1], Jeffrey I. Berman[1,2], Luke Bloy[1], Song Liu[1], Emma McBride[1], Matt Ku[1], Emily S. Kuschner[1,3,4], Megan Airey[1], Mina Kim[1], Rose E. Franzen[1], Gregory A. Miller[5,6] and Timothy P. L. Roberts[1,2]*

[1] Department of Radiology, Lurie Family Foundations Magnetoencephalography Imaging Center, The Children's Hospital of Philadelphia, Philadelphia, PA, United States, [2] Department of Radiology, Perelman School of Medicine, University of Pennsylvania, Philadelphia, PA, United States, [3] Department of Pediatrics, Center for Autism Research, The Children's Hospital of Philadelphia, Philadelphia, PA, United States, [4] Department of Psychiatry, Perelman School of Medicine, University of Pennsylvania, Philadelphia, PA, United States, [5] Department of Psychology, University of California, Los Angeles, Los Angeles, CA, United States, [6] Department of Psychiatry and Biobehavioral Sciences, University of California, Los Angeles, Los Angeles, CA, United States

OPEN ACCESS

Edited by:
Peter Uhlhaas, University of Glasgow, United Kingdom

Reviewed by:
Burkhard Maess, Max Planck Institute for Human Cognitive and Brain Sciences, Germany
Donald C. Rojas, Colorado State University, United States
Brian A. Coffman, University of Pittsburgh, United States

***Correspondence:**
J. Christopher Edgar
edgarj@chop.edu

Specialty section:
This article was submitted to Neuroimaging and Stimulation, a section of the journal Frontiers in Psychiatry

Received: *17 July 2020*
Accepted: *15 October 2020*
Published: *19 November 2020*

Citation:
Edgar JC, Blaskey L, Green HL, Konka K, Shen G, Dipiero MA, Berman JI, Bloy L, Liu S, McBride E, Ku M, Kuschner ES, Airey M, Kim M, Franzen RE, Miller GA and Roberts TPL (2020) Maturation of Auditory Cortex Neural Activity in Children and Implications for Auditory Clinical Markers in Diagnosis. Front. Psychiatry 11:584557. doi: 10.3389/fpsyt.2020.584557

Functional brain markers that can inform research on brain abnormalities, and especially those ready to facilitate clinical work on such abnormalities, will need to show not only considerable sensitivity and specificity but enough consistency with respect to developmental course that their validity in individual cases can be trusted. A challenge to establishing such markers may be individual differences in developmental course. The present study examined auditory cortex activity in children at an age when developmental changes to the auditory cortex 50 ms (M50) and 100 ms (M100) components are prominent to better understand the use of auditory markers in pediatric clinical research. MEG auditory encoding measures (auditory evoked fields in response to pure tone stimuli) were obtained from 15 typically developing children 6–8 years old, with measures repeated 18 and 36 months after the initial exam. MEG analyses were conducted in source space (i.e., brain location), with M50 and M100 sources identified in left and right primary/secondary auditory cortex (Heschl's gyrus). A left and right M50 response was observed at all times (Time 1, Time 2, Time 3), with M50 latency (collapsing across hemisphere) at Time 3 (77 ms) 10 ms earlier than Time 1 (87 ms; $p < 0.001$) and with M50 responses on average (collapsing across time) 5 ms earlier in the right (80 ms) than left hemisphere (85 ms; $p < 0.05$). In the majority of children, however, M50 latency changes were not constant across the three-year period; for example, whereas in some children a ∼10 ms latency reduction was observed from Time 1 to Time 2, in other children a ∼10 ms latency reduction was observed from Time 2 to Time 3. M100 responses were defined by a significant "peak" of detected power with magnetic field topography opposite M50 and occurring 50–100 ms later than the M50. Although M100s were observed in a few children at Time 1 and Time 2 (and more often in the right than left hemisphere), M100s were not observed in the majority of children except in the

right hemisphere at Time 3. In sum, longitudinal findings showed large between- and within-subject variability in rate of change as well as time to reach neural developmental milestones (e.g., presence of a detectable M100 response). Findings also demonstrated the need to examine whole-brain activity, given hemisphere differences in the rate of auditory cortex maturation. Pediatric research will need to take such normal variability into account when seeking clinical auditory markers.

Keywords: auditory, pediatric, maturation, M50, M100, auditory, magnetoencephalography (MEG)

INTRODUCTION

Researchers conducting EEG and MEG clinical studies have long sought to identify auditory brain measures that predict patient group status. Especially prominent are studies seeking to identify auditory encoding and gating deficits in adults with schizophrenia (1–13), and studies seeking to identify auditory encoding and auditory discrimination deficits in children and adults with autism spectrum disorder (14–21). As detailed in Edgar (22), control and case group differences in the rate of brain maturation may constrain the use of brain markers. As an example, given normal maturation of a brain measure in controls and abnormally slow maturation in cases, the use of the measure to differentiate groups may be of use only for a certain age range.

A different view of auditory neural measures reveals a shifting landscape of auditory measures across the lifespan, with some evoked components such as the 50 ms auditory response thought to be present throughout life, some responses such as the 100 ms response appearing only by early adolescence (see details in Discussion), and some responses such as the 40 Hz steady-state response not reliably observed until late adolescence [e.g., see (23–26)]. As such, although several different auditory components are of interest, as they allow assessment of different aspects of auditory cortex neural function (see Discussion), selection of auditory brain markers in clinical pediatric studies is often—or should be—constrained by the age of the sample. And for each component of interest, information regarding the rate of maturation in typically developing populations is lacking, information that is needed in order to identify abnormal maturation in patient populations.

The present study sought to begin to understand maturation of primary/secondary auditory cortex activity in typically-developing young children via assessing the maturation of the 50 ms (M50 MEG and P50/P1 EEG) response and the 100 ms auditory response (M100 MEG and N100/N1 EEG). M50 and M100 responses were examined in children 6–8 years old (Time 1) and again at ∼18 months (Time 2) and 36 months (Time 3) after the initial exam. Given many studies showing hemisphere differences in the functional maturation of left and right auditory cortex activity (15, 27–33), analyses were conducted in source space (i.e., brain location), obtaining measures for left and right primary/secondary auditory cortex.

Based on cross-sectional findings (see Discussion), it was hypothesized that in each child M50 latency would decrease across the 3-year period and that M50 responses would peak earlier in the right than left hemisphere at all 3 time points (16, 34, 35). It was also hypothesized that in the majority of children M100 responses, as defined by a significant "peak" of detected power with opposite magnetic field topography occurring 50–100 ms later than the M50, would be observed only at Time 3 (36–38). Finally, qualitative assessment of Time 1 to Time 3 auditory cortex maturation (i.e., inspecting individual differences in maturation rate) was performed to assess between- and within-subject (between-hemisphere) rate-of-change variability in the M50 and M100 measures. It is hoped that findings will provide information that will benefit the design of pediatric auditory clinical studies (e.g., choice of age range to target given study goals).

METHODS AND MATERIALS

This study was approved by the local Institutional Review Board, and all families gave written informed consent. When competent to do so, children over 7 years of age gave verbal assent to participate.

Participants

Data were obtained from 15 typically developing children (13M/2F; more males than females given that these controls were recruited for an autism spectrum disorder study). Children were selected according to the following criteria: (1) no history of traumatic brain injury, significant medical or neurological abnormality, known genetic syndrome, or diagnosed neurodevelopmental or learning disorders, (2) no active psychosis, (3) no MRI contraindications, (4) no sensory impairments (somatosensory, visual, or hearing), and (5) English as a first language. In addition, all children were evaluated by licensed clinical psychologists who ruled out the presence of DSM-5 Axis I disorders based on clinical judgment, review of parent-completed standardized, norm-referenced behavior rating scales, and parent screening interview (39–43). Finally, in all subjects, an estimate of full-scale IQ was obtained via a highly reliable 4-subtest short form (44) of the Wechsler Intelligence Scale for Children-5th edition (45).

MEG Data Acquisition

MEG data were obtained using a 275-channel MEG system (VSM MedTech Inc., Coquitlam, BC). Electro-oculogram (EOG) (vertical EOG on the upper and lower left side) and electrocardiogram (ECG) were also obtained. After applying a band-pass filter (0.03–150 Hz), EOG, ECG, and MEG signals were digitized at 1,200 Hz with 3rd-order gradiometer

environmental noise reduction. The participants' head position was monitored using three head position indicator (HPI) coils attached to the scalp. Children were scanned in a supine position.

The auditory exam consisted of sinusoidal tones of 500 Hz frequency and 300 ms duration. Tones were presented using E-Prime v1.1 via a sound pressure transducer and sound conduction tubing to the participant's peripheral auditory canal via ear-tip inserts (ER3A, Etymotic Research, IL, USA). Prior to each session, tones were presented binaurally and incrementally until reaching auditory threshold for each ear (i.e., stepwise approach). Tones were presented at 45 dB sensation level above threshold. Stimuli were presented with the inter-trial interval varying randomly between 600 and 2,000 ms, and with 520 trials collected over ∼14 min. To minimize fatigue, during the task participants viewed a movie (without auditory track) projected onto a screen positioned at a comfortable viewing distance. After each MEG session, structural magnetic resonance imaging (sMRI) provided T1-weighted, 3-D MPRAGE anatomical images for source localization (3T Siemens Prisma scanner).

Source Localization

MEG data were downsampled to 500 Hz. Artifact correction was applied to remove eye-blink activity using BESA 6.1, as outlined in Edgar et al. (14). Non-eye-blink artifacts trials were rejected by amplitude and gradient criteria (amplitude >1,200 fT/cm, gradients >800 fT/cm/sample). Artifact-free trials (from −500 ms to +500 ms) were then averaged.

Source localization for each subject was performed using their grand-average evoked response (e.g., collapsing across all ISIs). The average number of artifact-free trials was 477 at Time 1 (SD = 20), 470 at Time 2 (SD = 21), and 479 at Time 3 (SD = 20). To co-register MEG and sMRI data, three anatomical landmarks (nasion and right and left preauriculars) as well as an additional 200+ points on the scalp and face were digitized for each participant using the Probe Position Identification (PPI) System (Polhemus, Colchester, VT), and a transformation matrix that involved rotation and translation between the MEG and sMRI coordinate systems was obtained via a least-squares match of the PPI points to the surface of the scalp and face.

Left and right 50 ms (M50) and 100 ms (M100) sources were examined. As the primary generator of the M50 and M100 is well-modeled by a single dipole in left and right superior temporal gyrus (STG) and surrounding regions [(37, 46–49); see Edgar et al. (16) for an extended discussion on the generators of the M50 and M100 response], source localization was performed using an anatomical constraint. In particular, after co-registering the MEG and sMRI data, each child's left and right Heschl's Gyrus was visually identified and a dipole regional source [i.e., two orthogonal orientations (50)] manually placed at the "center" of each Heschl's Gyrus (i.e., at an anterior to posterior midpoint, and approximately two-thirds from the medial termination of Heschl's Gyrus; if two Heschl's Gyri were evident in a hemisphere, the dipole was placed between the two Heschl's Gyri).

After manually placing the left and right STG dipoles, the principle axis of each left- and right-hemisphere regional dipole source was oriented at the maximum of the left and right M50 and then left and right M100 response for each child in order to optimize the orientation of the standard regional sources (location fixed). Dipole orientations were obtained after applying a 2 Hz (24 dB/octave, zero-phase) to 55 Hz (48 dB/octave, zero-phase) band-pass filter to the scalp data used in source localization. Once oriented, the non-dominant source was removed and only the oriented source waveform examined. Goodness-of-fit (GOF = percent of sensor data explained) values for the M50 and M100 source models are provided in the Results.

Presence of an M50 and an M100 response was determined based on amplitude, latency, and hemisphere ingoing and outgoing flux topography. An M100 was scored if the magnetic flux topography was characteristic of the M100 response (i.e., for M100 left hemisphere ingoing anterior, outgoing posterior, and vice-versa for the right hemisphere), was preceded by M50 (i.e., flux topography opposite M100), and followed by M200 (i.e., flux topography same as M100), and with source strength greater than baseline. M50 was operationally defined as the first reversal in magnetic-field topography preceding M100 (or simply within a 35–125 ms range if M100 not present). In many children, a left- or right-hemisphere M100 response, defined as above, was not observed. For these children, left and right STG dipoles were oriented at the maximum of M200 [typically, M200 has a magnetic topography similar to M100 (16)]. When an M50 or M100 response was observed, left and right M50 (35–125 ms) and M100 (80–195 ms) scoring windows were used to identify the signal maxima in each window. This extended latency range allows capturing M50 and M100 responses in younger children.

Statistical Analyses

As a left and right M50 response was observed in all participants, M50 latency was examined via an ANOVA with hemisphere and Time (1, 2, and 3) as repeated measures. Where appropriate, Huynh-Feldt corrections are reported. For the two participants unable to come to the Time 2 visit, the Time 2 M50 latency group mean was used to estimate their Time 2 M50 latency, and their M100 response was scored as missing. As left and right M100 were absent in the majority of participants, rather than examine M100 latency, the presence/absence of an M100 across hemisphere and time was examined via a Fisher's Exact Test and then follow-up McNemar analyses. Finally, correlations examined associations between age and M50 latency and between full-scale IQ and M50 latency, and Mann-Whitney *U*-tests examined associations between the presence/absence of an M100 and age and full-scale IQ.

RESULTS

Demographics

Table 1 shows mean age and full-scale IQ at each time.

M50 and M100 Recordings and Source Models

Motion during the recording was minimal, with average motion across the exam at Time 1 = 1.42 mm, Time 2 = 1.18 mm, and Time 3 = 0.95 mm. The lack of motion was largely due to the fact that the children were watching a video (with no sound track) during the exam.

TABLE 1 | Demographic information as well as left and right M50 (latency) and M100 (presence) values at each time.

	Age	IQ	M50 latency		M100 present	
	Mean (SD)	Mean (SD)	Left mean (SD)	Right mean (SD)	Left	Right
Time 1	7.83 years (0.70)	113 (13)	91 ms (13)	84 ms (10)	7%	40%
Time 2	9.23 years (0.70)	111 (14)	85 ms (14)	80 ms (8)	7%	40%
Time 3	10.82 years (0.70)	111 (10)	79 ms (12)	74 ms (5)	27%	67%

TABLE 2 | Left and right: M50 latency for each child at each time (orange cells note the two children without Time 2 data, with their M50 latency values the group mean).

	Age (years)			Left M50 latency (ms)			Right M50 latency (ms)			Left M100 0 = no 1 = yes			Right M100 0 = no 1 = yes		
Subject	Time 1	Time 2	Time 3	Time 1	Time 2	Time 3	Time 1	Time 2	Time 3	Time 1	Time 2	Time 3	Time 1	Time 2	Time 3
L023	6.7	8.2	9.7	83	77	73	85	77	77	0	0	0	1	0	1
L024	6.7	8.1	9.8	91	75	79	83	73	75	0	0	0	1	1	1
L011	7.2	8.8	10.3	101	103	67	101	69	67	0	0	0	0	1	1
L006	7.3	8.9	10.3	79	73	71	83	81	83	0	0	1	1	0	0
L013	7.5	9	10.5	85	85	83	79	83	85	0	0	1	1	1	1
L010	7.6	9	10.5	83	77	73	81	75	69	0	0	0	0	0	1
L014	7.7	9.2	10.7	77	71	67	73	75	75	1	1	1	1	1	1
L032	7.8	Missed visit	10.8	93	85	81	81	80	75	0	0	0	0	0	0
L026	8.1	9.6	11.1	103	99	91	89	87	81	0	0	0	0	0	0
L015	8.2	9.7	11.2	97	89	81	79	77	75	0	0	0	0	0	1
L027	8.3	9.8	11.4	101	79	83	77	75	73	0	0	0	0	1	1
L018	8.3	9.8	11.3	103	105	93	107	101	75	0	0	0	0	0	0
L028	8.6	Missed visit	11.6	77	85	71	71	80	69	0	0	1	0	0	1
L007	8.7	10.2	11.9	115	111	107	89	89	71	0	0	0	0	0	0
L001	8.9	10.4	12	71	63	61	77	73	71	0	0	1	1	1	1

Gray highlighting showing that whereas a M50 10ms latency reduction was observed in some participants from Time 1 to Time 2, this large latency reduction was observed in other participants from Time 2 to Time 3.

Left and right M50 responses were observed in all recordings. GOF values indicated that the M50 source models (left and right oriented M50 dipole) accounted for a vast majority of the variance in M50 activity: Time 1 = 88%, Time 2 = 90%, and Time 3 = 88%. An ANOVA showed that M50 GOF values did not change as a function of Time, $F_{(2,24)} = 0.47$, $p > 0.05$, and M50 GOF did not correlate with age (correlation values at each Time ranged from −0.34 to + 0.22, all non-significant).

As detailed in the following section, M100 responses were not observed in the majority of children. Examining only those individuals with a left, right, or bilateral M100 response, GOF values for the M100 source models were: Time 1 = 79%, Time 2 = 83%, and Time 3 = 79%. M100 GOF values were lower than M50 GOF values, in large part due to the fact that M100 responses were often very weak and also often only observed in a single hemisphere (see following section). Given very few children with an M100, change in M100 GOF across time and M100 GOF and age associations were not examined.

Maturation of M50 and Associations With Age and IQ

Table 1 shows the left and right M50 mean latency at each time, and **Table 2** left and right M50 latency for each child at each time (orange cells note the two children without Time 2 data, with their M50 latency values the group mean). ANOVA with Hemisphere and Time (1, 2, and 3) as repeated measures and M50 latency as the dependent variable showed main effects for Hemisphere [$F_{(1, 14)} = 5.19$, $p < 0.05$] and Time [$F_{(1.94, 27.18)} = 16.24$, $p < 0.001$], with M50 responses on average 5 ms earlier in the right than left hemisphere, and with M50 latency 10 ms earlier at Time 3 [77 ms (SD = 7)] than at Time 1 [87 ms (SD = 10); collapsing across hemisphere]. Neither age nor IQ was associated with M50 latency at any time point or with Time 1 to Time 3 M50 latency change (*ps* > 0.05).

Although the Time main effect confirmed the expected effect of an earlier M50 latency at Time 3 than Time 1 (i.e., statistically comparing Time 1 vs. Time 3 M50 latency), a qualitative review of the data showed that in many children, M50 latency changes were not constant between Time 1 to Time 2 and Time 2 to Time 3. This is detailed in **Table 2**, providing left and right M50 latency values for each participant at all three time points, with gray highlighting showing that whereas a 10 ms latency reduction was observed in some participants from Time 1 to Time 2, this large latency reduction was observed in other participants from Time 2 to Time 3. Also shown in **Table 2**, in some children M50 latency changes were consistent across the 3-year period, with a ∼5 ms change from Time 1 to Time 2 and a ∼5 ms change from Time 2 to Time 3. Finally, in some children (even the younger

children) M50 latencies appeared to be adult-like across all three time points. **Figure 1** plots left and right M50 latency values at each time point for five representative children (referred to in Discussion, and also see **Supplementary Material** for similar figure including all children).

Maturation of M100 and Associations With Age and IQ

Table 1 shows the percentage of children with a left or right M100 at each time, and **Table 2** the presence/absence of a left or right M100 for each child (orange cells note the two children without Time 2 data, with their M100 response scored as missing). Except for the right hemisphere at Time 3, an M100 was not present in the majority of children at any time. A Fisher's Exact Test examining the presence/absence of an M100 between hemisphere (2 levels) and across time (3 levels) was marginally significant ($p = 0.07$; the two participants with missing MEG data at Time 2 were scored as not having an M100). Simple-effects analyses, performed using the McNemar Test, showed that M100 responses tended to be observed more often in the right than left hemisphere at Time 1 (McNemar test $p = 0.06$) and Time 2 (McNemar test $p = 0.06$), but not Time 3 (McNemar test $p = 0.13$).

Mann-Whitney *U*-tests showed that the presence/absence of an M100 did not differ as a function of age or IQ at any time point. These analyses, however, were generally uninformative, as there were few children with an M100 response at Time 1, Time 2, or Time 3. Qualitative observations about the M100 are provided in the Discussion.

Finally, given two studies suggesting that in young children it might be difficult to observe M100 responses at short ISIs (31, 51), analyses examining the absence/presence of an M100 were rerun examining only trials with ISIs >1,600 ms (~120 trials). Although paired *t*-tests showed stronger M100 responses in the >1,600 ms ISI condition vs. shorter ISIs ($p < 0.05$; examining only those cases with a present M100), there was no evidence that M100s were more often observed at the longer vs. shorter ISIs. In particular, a review of all cases (15 children × 3 times) showed only two instances where an M100 would have been scored "present" when examining >1,600 ms ISI vs. scored "absent" when examining the "All" condition. A single child provided both instances (Time 2 right hemisphere and Time 3 right hemisphere).

DISCUSSION

Functional brain markers that can inform research on auditory processing abnormalities, and especially those ready to facilitate clinical work on such abnormalities, will need to show not only considerable sensitivity and specificity but enough consistency with respect to developmental course that their validity in individual cases can be trusted. A challenge to establishing such markers is individual difference in developmental course. Even in the present modest sample of typically developing children, large within- and between-subject variability was observed in the maturation of left and right primary/secondary auditory cortex function, a potential obstacle to establishment of useful auditory encoding markers in this age range.

Three findings were of note. First, although in almost all children M50 latencies decreased by ~10 ms across a 3-year period, the time course of this latency change varied across children. As an example, whereas in some children an M50 latency reduction occurred between Time 1 and Time 2, in others the M50 latency reduction occurred between Time 2 and Time 3. Second, the M100 response slowly developed across the 3-year period examined, with an M100 still not present in many children at their Time 3 visit (9–12 years old). Finally, and contributing to the large literature documenting hemisphere differences in auditory cortex activity, M50 and M100 findings underscored the need to examine left- and right-hemisphere auditory cortex neural activity separately (see **Figure 1** and **Table 2**). In the following paragraphs, present findings are discussed with respect to previous studies examining the maturation of auditory cortex

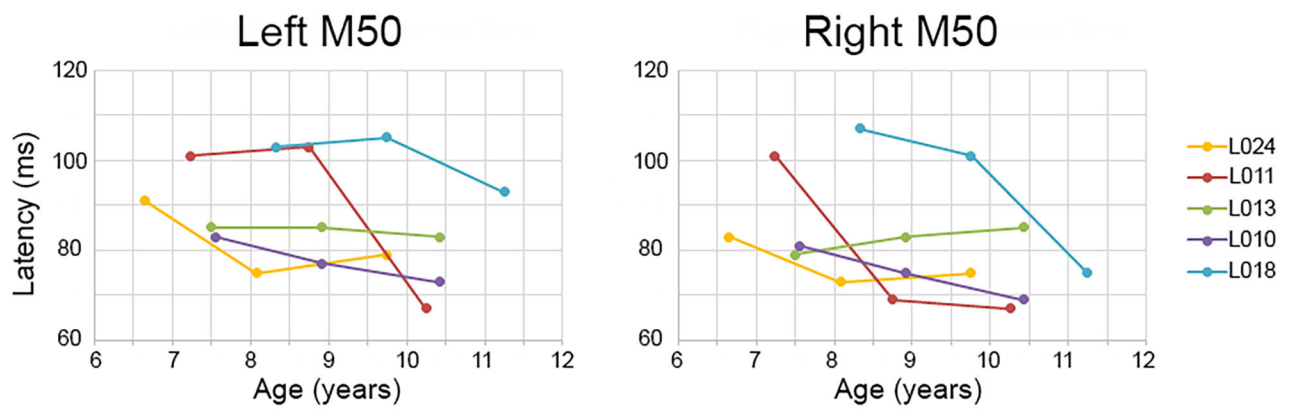

FIGURE 1 | Examples of between- and within-subject variability in M50 latency change. Time 1, 2, and 3 (x axis) left and right M50 latency values (y axis) are plotted for five children. Whereas some children showed a constant M50 latency change from Time 1 to Time 2 to Time 3 (e.g., L010), in other children the M50 latency change occurred only between Time 1 and Time 2 (L011 right) or between Time 2 and Time 3 (L011 left).

activity in children as well as with respect to the broader literature on brain markers in pediatric clinical populations.

With respect to M50, left and right M50 responses were observed in all subjects, a finding reported in many previous studies [e.g., see Ponton et al. (37)]. In young children, the P50 (EEG)/M50 (MEG) is readily evoked (52), with the peak latency of this component in 5- and 6-year-old children 85–95 ms (46, 53). These latency values are consistent with those observed in the present study (see **Table 1**, Time 1). P50 and M50 latency and amplitude decrease as a function of age (31, 54), with present findings indicating a ∼10 ms change across the examined 3-year period. As noted, however, in many children this ∼10 ms change was not constant across the 3-year period, with many different maturation scenarios observed. For example, as shown in **Figure 1**, in child L011 a large left M50 latency reduction was observed from Time 2 to Time 3 vs. a large right M50 latency reduction from Time 1 to Time 2. Many other patterns were observed; in child L018, left and right M50 latency changes were most prominent from Time 2 to Time 3, in child L010 a constant M50 latency reduction was observed across the 3-year interval, and in L013 the left and right M50 latency appeared stable across all three time points. **Table 2** provides several additional examples of between- and within-subject variability in M50 latency rate of change.

Thus, despite a small sample of 15 children, present findings suggest a very wide variety of normal M50 development (assessed in terms of latency), including many younger children having earlier M50 latencies than older children (see **Table 2**). Although denser sampling, such as obtaining brain measures every 6 months, is needed to more exactly determine how rapidly M50 latency change can occur in this age range, the present data indicate an M50 latency "growth spurt" in many children, similar to how height can change rapidly in infants and children. Given the marked single time point as well as rate-of-change between-subject variability in M50 latency in this cohort (Time 1 age 6–8 years), "expected" associations between age and M50 latency were not observed, as changes in M50 latency in this cohort did not exceed the between-subject variability in M50 latency in this age range. Finally, and relatedly, previous research indicates that rate-of-change in M50 latency differs across the lifespan. As an example, examining cross-sectional infant data, Edgar et al. (30) estimated a ∼0.6 ms/month latency change (= ∼7.2 ms/year) for M50, with this rate-of-change estimate consistent with prior studies in this age range (55, 56). And, of course, in adults (young to middle-aged, pre-degenerative), M50 latency is expected to be stable.

Although less common in young children, when present, N100 appears around 100–150 ms [e.g., (57–59)], with an adult morphology typically observed around 10–12 years of age (58), and thus with EEG N100 and MEG M100 auditory responses generally observed by late childhood and early adolescence (37, 58). Present findings showing missing left and right M100 responses in many of the children even at Time 3 (see **Table 2**), suggest that a N100/M100 response would not be observed in all children until early adolescence. Present findings, however, also demonstrated large variability in the absence/presence of M100 both between and within children. As an example, as shown in **Figure 2** and **Table 2**, whereas an M100 response was observed in some children at all three time points (e.g., L024 in right and L014 bilaterally), many of the older children showed neither a left nor right M100 at any time (e.g., L018). And, analogous to M50 latency, within this age range, age was a poor predictor of the presence/absence of an M100 and the presence/absence of an M100 did not predict IQ, suggesting that variability in the presence/absence of an M100 in this age range is "normal."

M50 and M100 maturation likely reflects changes to cortical gray matter such as changes in synaptic efficiency (32, 60) as well as maturational changes to the morphology of primary auditory cortex pyramidal cells (61, 62). Of note is that whereas development of deep layers (lower layer III to layer VI) in auditory cortex occurs between 6 months and 5 years of age (36), the superficial layers (upper layer III and layer II) continue to mature until about age 12 (63, 64). Based on this, researchers have hypothesized that the 50 ms auditory response reflects recurrent activation in layers III and IV, the termination zone of thalamo-cortical pathways that are almost fully developed by age 6 years. Observation of an M50 response in all children in the present study is consistent with early development of cortical layers III and IV, with changes to M50 latency likely reflecting, in part, continued maturation of thalamo-cortical white matter (e.g., myelination) through childhood and early adolescence (65, 66). As the M50 and P50 EEG response is observed in infants (30, 53, 67–69), the M50 response appears to be present throughout the lifespan and thus can be tracked from infancy through adulthood [e.g, see Figure 3 in Chen et al. (26)]. To the extent that M50 primarily reflects activity from cortical layers III and IV, the M50 response thus allows assessment of the maturation of these cortical layers across the lifespan.

As previously noted, M100 is observed less frequently in young children. It has been hypothesized that this is due to the fact that generation of M100 likely reflects activation of cortical layers upper III and II, areas not fully developed until at least age 12 [e.g., (36, 37, 58)]. In **Figure 2** (and see all source waveforms plots in **Supplementary Material**), the gradual emergence of an M100 response is observed, with the slow development of M100 perhaps reflecting greater synchronization in the afferent activity arriving at the synapses in layer II and upper layer III (38) across childhood.

Maturational changes to auditory cortex function, as assessed via the use of electrophysiology, thus likely occur within a landscape of altering feedforward and feedback inputs to primary/secondary auditory areas. Ponton et al. (37) suggested that during development, the magnitude of the earlier maturing tangential "50 ms" auditory response decreases as the magnitude of the later maturing tangential "100 ms" auditory response increases. Given this pattern, in the present study, a developing M100 response could result in an earlier M50 response via "cancelation" of M50 activity via an increasingly dominant M100 response.

Whereas, in young children M50 activity may "cancel" M100 activity, it is also hypothesized that in older children the feedback activity giving rise to the M100 response increases in strength, such that in adults the neural activity associated with M100 is strong enough to largely "cancel" the M50 response. As suggested

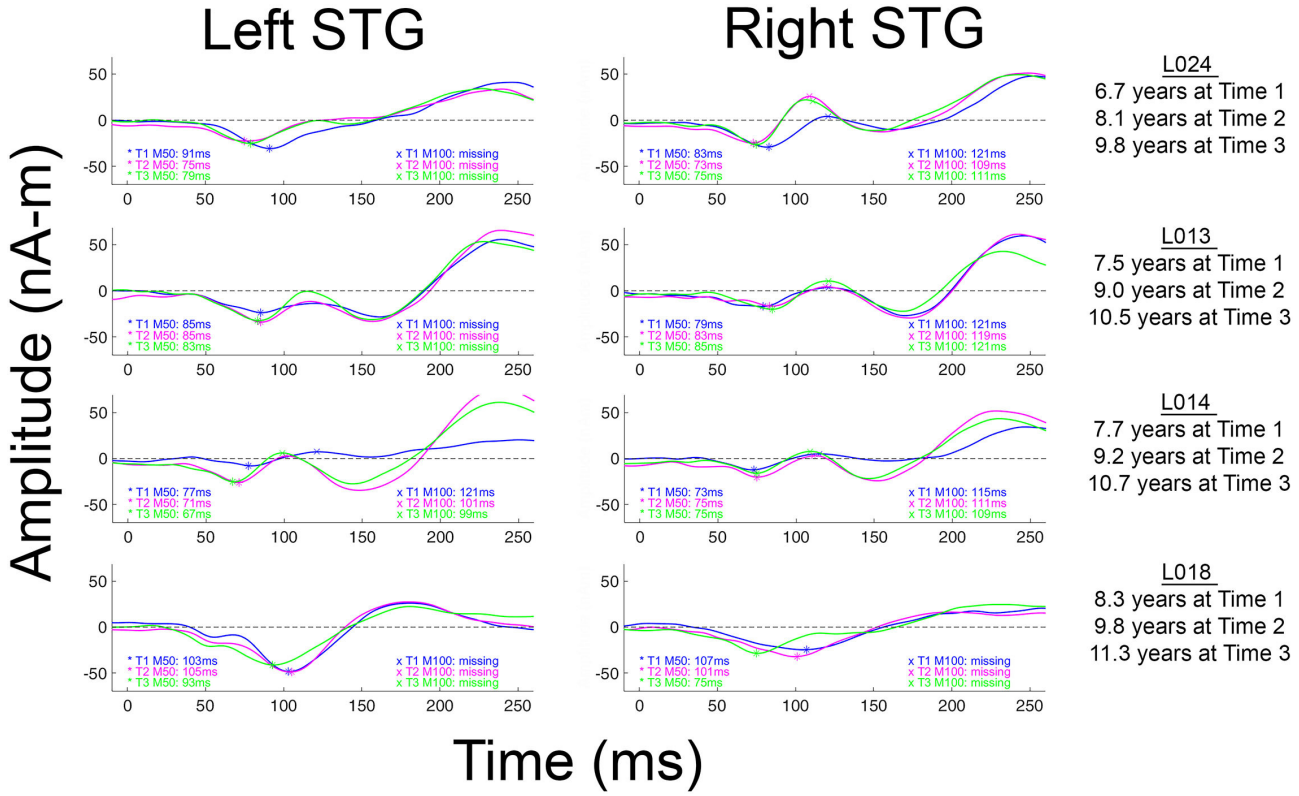

FIGURE 2 | Left and right M100 source waveforms for all three times shown for four children. The x axis shows latency (ms) and the y axis source strength (nAm). When an M50 or M100 response was present, the peak latency value is provided. Children are ordered from youngest to oldest.

by Ponton et al. (37) and Ceponiene et al. (46), what is possible is that rather than M50 decreasing as a function of age, the M50 response simply appears smaller in EEG and MEG recordings given cancelation of an external M50/P50 response by stronger electrical currents associated with the M100 response. Of course, another possibility is that the M50 response truly becomes weaker as a function of age. Although corticography studies could help differentiate between these two alternatives, such studies will be difficult given the need to study sulcal auditory cortex neural activity in children at different ages.

In several papers, including a paper by our group, it has been suggested that the M100 develops "out of" the later N200 (EEG) or M200 (MEG) response (16, 36, 37). The N200/M200, a response occurring after N100/M100 and with the same topography as N100/M100, has a maximum amplitude at ∼8 years and then decays until it is often not present in individuals 18 years and older (37, 70). In **Figure 2** (and see **Supplementary Material**), the M200 response is clearly observed in all children. Present findings, however, do not support the claim that the M100 develops out of the M200. Indeed, as shown in the **Figure 2** and the **Supplementary Material** source waveforms, in most children the M100 appears as a distinct component, slowly emerging in-between M50 and M200. As a specific example, in L013 (**Figure 2**), the "M100" is at all times clearly distinct from the later M200.

In the present study, M100 was scored as present if there was a peak with a rising and falling slope distinct from M200, with an M100 magnetic-field topography, with a non-zero source strength, and with a latency between 80 and 185 ms. **Figure 3** shows examples of how the study scoring criteria were applied to determine the absence/presence of an M100. Specifically, **Figure 3** shows left and right STG source waveforms (−75–500 ms), magnetic field maps (20 ms intervals), and left and right Heschl's gyri dipole locations for three children. In all three children, M50 responses were observed bilaterally (M50 responses are plotted "downward"), with the source waveforms showing an M50 response that exceeds baseline and the magnetic field maps showing the expected M50 field pattern (e.g., in the left hemisphere an anterior magnetic field source and a posterior magnetic field sink). None of the three children showed a left M100 response, mirroring what was observed in the vast majority of the sample. And of note, although in all three children a left M100 is suggested, in none of the children did the left magnetic field maps indicate an M50 to M100 field pattern reversal, and thus a left M100 was scored as absent in all three children. In contrast in children L013V1 and L027V3, a right M100 was scored as present. In L013V1, although a full field reversal from M50 to M100 is not observed, the magnetic field pattern clearly indicates a field reversal (although not as purely dipolar as an adult M100) and the M100 response exceeded

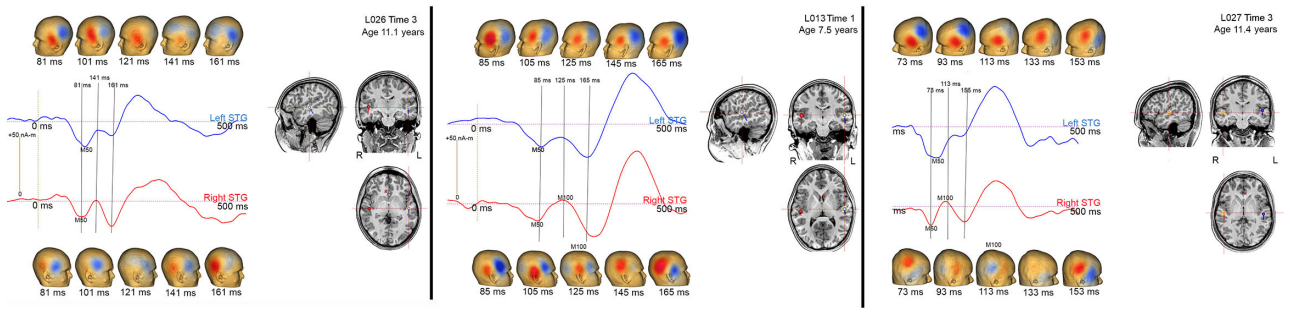

FIGURE 3 | Left (blue) and right (red) STG source waveforms (−75 to 500 ms), magnetic field maps (20 ms intervals), and left and right Heschl's gyri dipole locations for 3 children. Data are presented to provide examples of the criteria used to determine an absent/present M50 and M100.

the baseline (barely), and thus an M100 was scored as present. In L027V3, a more mature right M100 is observed, with an M100 magnetic field pattern clearly observed and M100 weak but clearly exceeding the baseline. These three children provide examples where researchers using different scoring criteria, for example not requiring a magnetic field reversal from M50 to M100, might have scored M100s as present (e.g., scoring based on examining only the source waveforms or only the EEG or MEG sensor responses). Notably, these three cases differ from the many other children where there was no source waveform deflection suggesting an emerging M100 (e.g., see L018V1).

Some researchers may regard the M100 scoring criteria applied in this study as too conservative; although in many children M100 was scored as missing (e.g., an M100 magnetic field topography was not observed), what is likely the "M100" response could be observed in the source waveforms at Time 1, Time 2, and Time 3 (e.g., L013 left in **Figure 2**). Although conservative, this is a safe strategy, as the longitudinal data indicate risks associated with a more liberal approach. In particular, the present three-time-point data likely provide a false sense of security; although in this study the Time 3 data in many children often provided visual confirmation that a Time 1 or Time 2 M100 could be identified based only on source waveform morphology (e.g., L013 left in **Figure 2**), in most studies, investigators do not have the ability to look into the future to determine whether they made the right choice.

Difficulty scoring the M100 in this age range is of note when examining the multi-determined sensor data rather than source waveforms. Indeed, present findings indicate that developmental studies examining N100 activity at a single midline scalp site (e.g., Cz or Fz) are problematic, as latency and amplitude measures at a single site in many children will reflect activity from only a single hemisphere (e.g., see L024 in **Figure 2**). Without separately examining left and right auditory cortex activity, it is not possible to determine which hemisphere or perhaps even which components (M100 or M200) contribute to the midline EEG N100 response.

Other study findings also demonstrated the need to separately examine left and right auditory cortex activity. An example is the left vs. right STG M50 latency difference observed in the present study, a finding reported in previous studies examining children and adolescents (15, 16, 27–29). Given left and right M50 latency differences in pediatric populations, examination of the latency of the 50 ms latency response at EEG midline sites would be problematic. More generally, Ponton et al. (37) and Sussman et al. (71) have noted that examining sensor auditory data is problematic as the activity at any given sensor location reflects the weighted contribution of activity from different sources, each with potentially different maturation rates. The Edgar et al. (72) left and right auditory cortex simulations provide a detailed examination of the problems with scoring auditory cortex activity at the sensor level, with hemisphere differences in the latency or amplitude of an auditory response providing very misleading EEG midline auditory measures. In addition to the above concerns, an analysis strategy that provides separate measures for left and right auditory activity is critical in pediatric clinical studies as studies show hemisphere-specific abnormalities in neurodevelopmental disorders [e.g., see (15, 73)].

Considered as a whole, the present M50 and M100 findings indicate that variability in the maturation of auditory cortex neural activity occurs in a manner analogous to maturation of behavioral phenotypes observed "by eye." For example, although most typically developing infants take their first steps between 9 and 12 months and are walking by 14 or 15 months, some normally developing children do not take their first steps until 16 to 17 months (74). Furthermore, within this almost 1-year range, age of first step does not predict future intelligence or coordination (75). Only by 20 months does an infant who does not walk become of clinical concern (76, 77).

As observable "by eye" behaviors relate in some way to brain activity, it is thus perhaps not unexpected that the relatively large between-subject variability observed in behaviors that develop during infancy and childhood (walking, talking, skipping) is also observed in brain measures. In the present study, large between- as well as within-subject (between-hemisphere) variability was observed in the maturation of M50 (latency change), with the M50 and M100 measures not related to age at time of first exam or to general cognitive ability (IQ). The slow development of auditory cortex neural activity is perhaps is related to the slow process of language development, extending from birth to teenage years. For example, although children have essentially mastered the phonology of their language by

5 years of age, their articulation continues to develop as they start to use more complex stress and intonations (78). Regarding speech perception, their ability to understand speech in noisy circumstances continues to improve up to age 15 (79).

As detailed in Edgar et al. (22), an understanding of normal brain maturation is needed whether one takes a DSM-5 or an RDoC approach to research. What differentiates these approaches is primarily a matter of granularity (80), with a DSM-5 approach focusing on diagnosis and an RDoC approach focusing on smaller units of analysis that may cut across DSM-5 diagnostic categories, such as psychological concepts and biological phenomena associated with disease (80, 81). The present study provides specific examples of potential RDoC biological phenomena—M50 and M100—and demonstrate the need to consider hemisphere differences (M50 and M100) and also demonstrate that some measures are of use only after a certain age (M100).

Presented in a "RDoC format," **Figure 4** suggests a way to conceptualize assessment of auditory system neural function, with the selection of auditory measures of interest considered with respect to what neural and cognitive functions are of clinical interest as well as what research tells us so far about the presence/absence of specific auditory components across the lifespan. Although not comprehensive, **Figure 4** sketches out some of the relevant features to consider [including noting hemisphere differences in rate of maturation via lighter (slower) to deeper (faster) shades of green]. Although scientists might disagree with some of the details, such disagreements simply indicate that there is more to learn. And although the present study focuses on electrophysiology auditory cortex measures, as detailed in Edgar (22), these concerns are relevant to other imaging modalities and other ages.

With respect to identifying clinical auditory neural brain markers (e.g., brain measures diagnostic of autism spectrum disorder or learning disability), the present longitudinal findings also provide some perspective. For example, although it is likely that control and patient group differences in M50 latency can be detected with a moderate-sized sample [see Edgar et al. (16) for an example in autism spectrum disorder], examination of the present longitudinal data suggests that it is unlikely that an M50 latency diagnostic marker with high sensitivity (correctly identifying all patients) and specificity (not mistakenly identifying a control as a patient) could be developed. This is because it is doubtful that in a given patient group all the patient's auditory measures would exist at the tail of the control distribution (the state of affairs needed to obtain high sensitivity and specificity). As a specific example, using right M50 latency as a marker in the clinic for children 6–8 years old, and given the Time 1 right M50 latency standard deviation of 10 ms (mean = 84 ms; range = 71–107 ms), almost all members of the patient group would need to have a latency great than 104 ms (i.e., showing delayed M50 latencies) to obtain high sensitivity and specificity. The above example simply provides another example of what functional and structural brain imaging clinical research findings already show. In particular, in most neurodevelopmental disorders a single brain marker has not been shown to have the sensitivity and specificity needed to serve as a diagnostic brain marker, this claim supported by the fact that large sample studies show at most small to medium group effects for most brain measures [e.g., (82–84)].

Of course, single auditory measures may prove useful in other ways, such as predicting treatment response (85). And as evidenced in other papers, multiple brain measures can be combined to provide greater group separation (86). Such composite diagnostic measures, however, may be difficult to obtain given that different brain measures may provide optimal group separation at different ages [see Edgar et al. (22) for a discussion].

A few study limitations are of note. First, findings are generally specific to right-handed typically developing males (only two female participants), with studies needed to determine whether there are sex differences in the maturation of auditory cortex (from birth to late adolescence). Second, larger samples

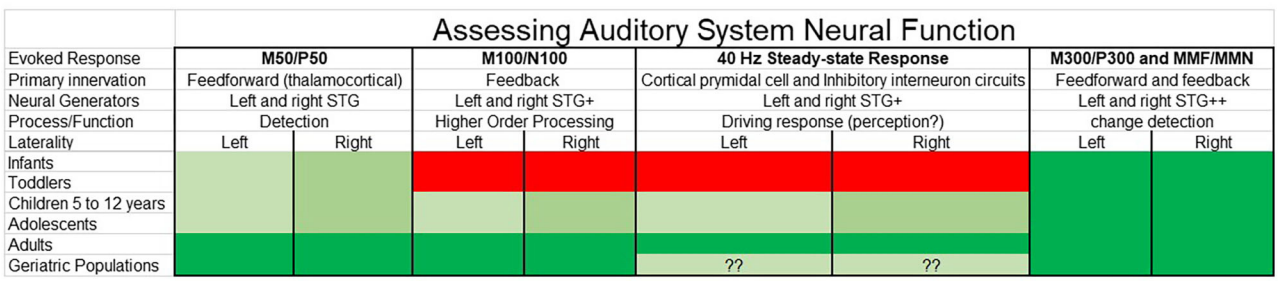

FIGURE 4 | Auditory system neural measures for clinical research considered as a function of the human lifespan (green = possible, red = not possible) as well as with respect to neural and cognitive functions of interest. Although not comprehensive, relevant features to consider are noted, such as the likely brain regions involved, and with hemisphere differences in rate of maturation [hemisphere showing slower maturation (lighter green) compared to hemisphere showing faster maturation (deeper green)]. Whereas research indicates that some auditory evoked responses such as M50 and P50 can be measured throughout the lifespan, other measures such as the M100 and N100 and the auditory 40 Hz steady-state response are reliably obtained only in older adolescents and adults. Also of note are differences in the "complexity" of the evoked response—whereas some evoked responses such as M50 and P50 are thought to primarily reflect activity from left and right primary/secondary auditory regions, other evoked responses reflect activity from multiple brain regions, such as the M300 and P300 (and with almost no research examining rates of maturation for each M300 and P300 generator).

(males and females) are needed to determine what is normal vs. what is atypical, similar to the growth charts available for height and weight (e.g., 95% confidence intervals for a given age). However, although larger samples are needed to fully characterize M50 and M100 auditory cortex development, the present sample is sufficient (and sufficiently well-screened) to demonstrate that large variability across typically developing children in the maturation of auditory cortex is typical, just as similarly large variability in age of first step is typical. Third, as study participants have not yet been followed into adolescence, it is unknown at what age all participants will show a left and right M100 response. Fourth, the present study focused on evoked components, with future studies examining maturation of time-frequency measures (e.g., intra-trial coherence, event-related synchronization/desynchronization) certainly of interest in neurodevelopmental patient populations [e.g., (14, 87–91)]. Finally, the present study did not examine associations between maturation of brain function and brain structure (e.g., local gray matter). Such function-structure analyses will be conducted once the samples are much larger.

In conclusion, the present paper examined within- and between-subject variability in the development of auditory cortex neural activity in children. Relatively large between-subject as well as within-subject (left- and right-hemisphere) variability in reaching neural developmental milestones (e.g., showing an M100 response) was observed. Findings also clearly demonstrated the need to examine whole-brain activity given regional differences (e.g., hemisphere) in the rate of brain maturation.

DATA AVAILABILITY STATEMENT

The datasets presented in this article are not readily available because data will be made available upon request at the conclusion of this longitudinal study. Requests to access the datasets should be directed to edgarj@chop.edu.

ETHICS STATEMENT

This study was approved by the Institutional Review Board at the Children's Hospital of Philadelphia and all families gave written informed consent. Written informed consent to participate in this study was provided by the participants' legal guardian/next of kin.

AUTHOR CONTRIBUTIONS

LBla, KK, EM, EK, MA, and MKi: individuals contributed via developing and administering clinical assessments. JCE, HG, GS, MD, JB, LBlo, SL, and MKu: analysis of MEG data. JCE, LBlo, RF, GM, and TR: statistical analysis. All authors were involved in writing and editing the manuscript.

FUNDING

This study was supported in part by NIH grant R01DC008871 (TR), R01MH107506 (JE), R21MH098204 (JCE), R21 NS090192 (JCE), NICHD grant R01HD093776 (JCE), and the Clinical Translational Core, Biostatistics & Bioinformatics Core and the Neuroimaging Core of the Intellectual and Developmental Disabilities Research Center funded by NICHD grant 5U54HD086984 (to RTS, TR, and MP; principal investigator, M. Robinson, PhD).

ACKNOWLEDGMENTS

TR gratefully acknowledges the Oberkircher Family for the Oberkircher Family Chair in Pediatric Radiology at CHOP.

SUPPLEMENTARY MATERIAL

The Supplementary Material for this article can be found online at: https://www.frontiersin.org/articles/10.3389/fpsyt.2020.584557/full#supplementary-material

REFERENCES

1. Edgar JC, Fisk CL, Chen YH, Stone-Howell B, Liu S, Hunter MA, et al. Identifying auditory cortex encoding abnormalities in schizophrenia: the utility of low-frequency versus 40 Hz steady-state measures. *Psychophysiology*. (2018) 55:e13074. doi: 10.1111/psyp.13074
2. Edgar JC, Hanlon FM, Huang MX, Weisend MP, Thoma RJ, Carpenter B, et al. Superior temporal gyrus spectral abnormalities in schizophrenia. *Psychophysiology*. (2008) 45:812–24. doi: 10.1111/j.1469-8986.2008.00682.x
3. Smith AK, Edgar JC, Huang M, Lu BY, Thoma RJ, Hanlon FM, et al. Cognitive abilities and 50- and 100-msec paired-click processes in schizophrenia. *Am J Psychiatry*. (2010) 167:1264–75. doi: 10.1176/appi.ajp.2010.09071059
4. Adler LE, Pachtman E, Franks RD, Pecevich M, Waldo MC, Freedman R. Neurophysiological evidence for a defect in neuronal mechanisms involved in sensory gating in schizophrenia. *Biol Psychiatry*. (1982) 17:639–54.
5. Waldo MC, Adler LE, Freedman R. Defects in auditory sensory gating and their apparent compensation in relatives of schizophrenics. *Schizophr Res*. (1988) 1:19–24. doi: 10.1016/0920-9964(88)90035-7
6. Greenwood TA, Braff DL, Light GA, Cadenhead KS, Calkins ME, Dobie DJ, et al. Initial heritability analyses of endophenotypic measures for schizophrenia: the consortium on the genetics of schizophrenia. *Arch Gen Psychiatry*. (2007) 64:1242–50. doi: 10.1001/archpsyc.64.11.1242
7. Turetsky BI, Greenwood TA, Olincy A, Radant AD, Braff DL, Cadenhead KS, et al. Abnormal auditory N100 amplitude: a heritable endophenotype in first-degree relatives of schizophrenia probands. *Biol Psychiatry*. (2008) 64:1051–9. doi: 10.1016/j.biopsych.2008.06.018
8. Johannesen JK, Kieffaber PD, O'Donnell BF, Shekhar A, Evans JD, Hetrick WP. Contributions of subtype and spectral frequency analyses to the study of P50 ERP amplitude and suppression in schizophrenia. *Schizophr Res*. (2005) 78:269–84. doi: 10.1016/j.schres.2005.05.022
9. Rosburg T, Boutros NN, Ford JM. Reduced auditory evoked potential component N100 in schizophrenia–a critical review. *Psychiatry Res*. (2008) 161:259–74. doi: 10.1016/j.psychres.2008.03.017
10. Blumenfeld LD, Clementz BA. Response to the first stimulus determines reduced auditory evoked response suppression in schizophrenia: single trials analysis using MEG. *Clin Neurophysiol*. (2001) 112:1650–9. doi: 10.1016/S1388-2457(01)00604-6

11. Clementz BA, Blumenfeld LD, Cobb S. The gamma band response may account for poor P50 suppression in schizophrenia. *Neuroreport.* (1997) 8:3889–3. doi: 10.1097/00001756-199712220-00010
12. Ethridge LE, Hamm JP, Pearlson GD, Tamminga CA, Sweeney JA, Keshavan MS, et al. Event-related potential and time-frequency endophenotypes for schizophrenia and psychotic bipolar disorder. *Biol Psychiatry.* (2015) 77:127–36. doi: 10.1016/j.biopsych.2014.03.032
13. Popov T, Jordanov T, Weisz N, Elbert T, Rockstroh B, Miller GA. Evoked and induced oscillatory activity contributes to abnormal auditory sensory gating in schizophrenia. *Neuroimage.* (2011) 56:307–14. doi: 10.1016/j.neuroimage.2011.02.016
14. Edgar JC, Khan SY, Blaskey L, Chow VY, Rey M, Gaetz W, et al. Neruomagnetic noise predicts evoked-response delays and core language deficits in autism spectrum disorders. *J Autism Dev Disord.* (2015) 45:395–405. doi: 10.1007/s10803-013-1904-x
15. Edgar JC, Fisk Iv CL, Berman JI, Chudnovskaya D, Liu S, Pandey J, et al. Auditory encoding abnormalities in children with autism spectrum disorder suggest delayed development of auditory cortex. *Mol Autism.* (2015) 6:69. doi: 10.1186/s13229-015-0065-5
16. Edgar JC, Lanza MR, Daina AB, Monroe JF, Khan SY, Blaskey L, et al. Missing and delayed auditory responses in young and older children with autism spectrum disorders. *Front Hum Neurosci.* (2014) 8:417. doi: 10.3389/fnhum.2014.00417
17. Roberts TP, Khan SY, Rey M, Monroe JF, Cannon K, Blaskey L, et al. MEG detection of delayed auditory evoked responses in autism spectrum disorders: towards an imaging biomarker for autism. *Autism Res.* (2010) 3:8–18. doi: 10.1002/aur.111
18. Matsuzaki J, Ku M, Berman JI, Blaskey L, Bloy L, Chen YH, et al. Abnormal auditory mismatch fields in adults with autism spectrum disorder. *Neurosci Lett.* (2019) 698:140–5. doi: 10.1016/j.neulet.2018.12.043
19. Roberts TP, Cannon KM, Tavabi K, Blaskey L, Khan SY, Monroe JF, et al. Auditory magnetic mismatch field latency: a biomarker for language impairment in autism. *Biol Psychiatry.* (2011) 70:263–9. doi: 10.1016/j.biopsych.2011.01.015
20. Chien YL, Hsieh MH, Gau SS. Mismatch negativity and P3a in adolescents and young adults with autism spectrum disorders: behavioral correlates and clinical implications. *J Autism Dev Disord.* (2018) 48:1684–97. doi: 10.1007/s10803-017-3426-4
21. Schwartz S, Shinn-Cunningham B, Tager-Flusberg H. Meta-analysis and systematic review of the literature characterizing auditory mismatch negativity in individuals with autism. *Neurosci Biobehav Rev.* (2018) 87:106–17. doi: 10.1016/j.neubiorev.2018.01.008
22. Edgar JC. Identifying electrophysiological markers of autism spectrum disorder and schizophrenia against a backdrop of normal brain development. *Psychiatry Clin Neurosci.* (2020) 74:1–11. doi: 10.1111/pcn.12927
23. Edgar JC, Fisk CLt, Liu S, Pandey J, Herrington JD, Schultz RT, et al. Translating adult electrophysiology findings to younger patient populations: difficulty measuring 40-Hz auditory steady-state responses in typically developing children and children with autism spectrum disorder. *Dev Neurosci.* (2016) 38:1–14. doi: 10.1159/000441943
24. Rojas DC, Maharajh K, Teale PD, Kleman MR, Benkers TL, Carlson JP, et al. Development of the 40Hz steady state auditory evoked magnetic field from ages 5 to 52. *Clin Neurophysiol.* (2006) 117:110–7. doi: 10.1016/j.clinph.2005.08.032
25. Cho RY, Walker CP, Polizzotto NR, Wozny TA, Fissell C, Chen CM, et al. Development of sensory gamma oscillations and cross-frequency coupling from childhood to early adulthood. *Cereb Cortex.* (2015) 25:1509–18. doi: 10.1093/cercor/bht341
26. Chen YH, Saby J, Kuschner E, Gaetz W, Edgar JC, Roberts TPL. Magnetoencephalography and the infant brain. *Neuroimage.* (2019) 189:445–58. doi: 10.1016/j.neuroimage.2019.01.059
27. Poulsen C, Picton TW, Paus T. Age-related changes in transient and oscillatory brain responses to auditory stimulation during early adolescence. *Dev Sci.* (2009) 12:220–35. doi: 10.1111/j.1467-7687.2008.00760.x
28. Yoshimura Y, Kikuchi M, Shitamichi K, Ueno S, Munesue T, Ono Y, et al. Atypical brain lateralisation in the auditory cortex and language performance in 3- to 7-year-old children with high-functioning autism spectrum disorder: a child-customised magnetoencephalography (MEG) study. *Mol Autism.* (2013) 4:38. doi: 10.1186/2040-2392-4-38
29. Albrecht R, Suchodoletz W, Uwer R. The development of auditory evoked dipole source activity from childhood to adulthood. *Clin Neurophysiol.* (2000) 111:2268–76. doi: 10.1016/S1388-2457(00)00464-8
30. Edgar JC, Murray R, Kuschner ES, Pratt K, Paulson DN, Dell J, et al. The maturation of auditory responses in infants and young children: a cross-sectional study from 6 to 59 months. *Front Neuroanat.* (2015) 9:131. doi: 10.3389/fnana.2015.00131
31. Paetau R, Ahonen A, Salonen O, Sams M. Auditory evoked magnetic fields to tones and pseudowords in healthy children and adults. *J Clin Neurophysiol.* (1995) 12:177–85. doi: 10.1097/00004691-199503000-00008
32. Gomes H, Dunn M, Ritter W, Kurtzberg D, Brattson A, Kreuzer JA, et al. Spatiotemporal maturation of the central and lateral N1 components to tones. *Brain Res Dev Brain Res.* (2001) 129:147–55. doi: 10.1016/S0165-3806(01)00196-1
33. Musacchia G, Choudhury NA, Ortiz-Mantilla S, Realpe-Bonilla T, Roesler CP, Benasich AA. Oscillatory support for rapid frequency change processing in infants. *Neuropsychologia.* (2013) 51:2812–24. doi: 10.1016/j.neuropsychologia.2013.09.006
34. Freedman R, Adler LE, Waldo M. Gating of the auditory evoked potential in children and adults. *Psychophysiology.* (1987) 24:223–7. doi: 10.1111/j.1469-8986.1987.tb00282.x
35. Myles-Worsley M, Coon H, Byerley W, Waldo M, Young D, Freedman R. Developmental and genetic influences on the P50 sensory gating phenotype. *Biol Psychiatry.* (1996) 39:289–95. doi: 10.1016/0006-3223(95)00134-4
36. Ponton CW, Moore JK, Eggermont JJ. Prolonged deafness limits auditory system developmental plasticity: evidence from an evoked potentials study in children with cochlear implants. *Scand Audiol Suppl.* (1999) 51:13–22.
37. Ponton C, Eggermont JJ, Khosla D, Kwong B, Don M. Maturation of human central auditory system activity: separating auditory evoked potentials by dipole source modeling. *Clin Neurophysiol.* (2002) 113:407–20. doi: 10.1016/S1388-2457(01)00733-7
38. Ponton CW, Eggermont JJ. Of kittens and kids: altered cortical maturation following profound deafness and cochlear implant use. *Audiol Neurootol.* (2001) 6:363–80. doi: 10.1159/000046846
39. Constantino JN. *GCP: Social Responsiveness Scale.* 2nd ed. Torrance, CA: Western Psychological Services (2012).
40. Gioia GA. *BRIEF: Behavior Rating Inventory of Executive Function: Professional Manual.* Odessa, FL: Psychological Assessment Resources (2000).
41. Achenbach T. *Diagnostic and Statistical Manual of Mental Disorders.* 5th ed. Washington, DC: American Psychiatric Association (2013).
42. Achenbach TM, Rescorla LA. *Manual for the ASEBA School-Age Forms & Profiles.* Burlington, VT: University of Vermont; Research Center for Children, Youth, & Families (2001).
43. Achenbach TME. *Child Behavior Checklist for Ages 6-18.* Burlington, VT: University of Vermont, Research Center for Children, Youth, & Families.
44. Sattler JM, Dunmont R, Coalson D. *Assessment of Children: WICS-V WPPSI-IV.* LaMesa, CA: Jerome Sattler, Publisher, Inc (2016).
45. Wechsler D. *Wechsler Intelligence Scale for Children.* 5th ed. Bloomington, MN: Pearson (2014).
46. Ceponiene R, Rinne T, Naatanen R. Maturation of cortical sound processing as indexed by event-related potentials. *Clin Neurophysiol.* (2002) 113:870–82. doi: 10.1016/S1388-2457(02)00078-0
47. Scherg M, Von Cramon D. Two bilateral sources of the late AEP as identified by a spatio-temporal dipole model. *Electroencephalogr Clin Neurophysiol.* (1985) 62:32–44. doi: 10.1016/0168-5597(85)90033-4
48. Herdman AT, Wollbrink A, Chau W, Ishii R, Ross B, Pantev C. Determination of activation areas in the human auditory cortex by means of synthetic aperture magnetometry. *Neuroimage.* (2003) 20:995–1005. doi: 10.1016/S1053-8119(03)00403-8
49. Ross B, Picton TW, Pantev C. Temporal integration in the human auditory cortex as represented by the development of the steady-state magnetic field. *Hear Res.* (2002) 165:68–84. doi: 10.1016/S0378-5955(02)00285-X
50. Scherg M, Berg P. New concepts of brain source imaging and localization. *Electroencephalogr Clin Neurophysiol Suppl.* (1996) 46:127–37.

51. Rojas DC, Walker JR, Sheeder JL, Teale PD, Reite ML. Developmental changes in refractoriness of the neuromagnetic M100 in children. *Neuroreport.* (1998) 9:1543–7. doi: 10.1097/00001756-199805110-00055
52. Oram Cardy JE, Ferrari P, Flagg EJ, Roberts W, Roberts TP. Prominence of M50 auditory evoked response over M100 in childhood and autism. *Neuroreport.* (2004) 15:1867–70. doi: 10.1097/00001756-200408260-00006
53. Wunderlich JL, Cone-Wesson BK, Shepherd R. Maturation of the cortical auditory evoked potential in infants and young children. *Hear Res.* (2006) 212:185–202. doi: 10.1016/j.heares.2005.11.010
54. Sharma A, Dorman MF, Spahr AJ. A sensitive period for the development of the central auditory system in children with cochlear implants: implications for age of implantation. *Ear Hear.* (2002) 23:532–9. doi: 10.1097/00003446-200212000-00004
55. Novak GP, Kurtzberg D, Kreuzer JA, Vaughan HG Jr. Cortical responses to speech sounds and their formants in normal infants: maturational sequence and spatiotemporal analysis. *Electroencephalogr Clin Neurophysiol.* (1989) 73:295–305. doi: 10.1016/0013-4694(89)90108-9
56. Ohlrich ES, Barnet AB, Weiss IP, Shanks BL. Auditory evoked potential development in early childhood: a longitudinal study. *Electroencephalogr Clin Neurophysiol.* (1978) 44:411–23. doi: 10.1016/0013-4694(78)90026-3
57. Bruneau N, Roux S, Guerin P, Barthelemy C, Lelord G. Temporal prominence of auditory evoked potentials (N1 wave) in 4-8-year-old children. *Psychophysiology.* (1997) 34:32–8. doi: 10.1111/j.1469-8986.1997.tb02413.x
58. Ponton CW, Eggermont JJ, Kwong B, Don M. Maturation of human central auditory system activity: evidence from multi-channel evoked potentials. *Clin Neurophysiol.* (2000) 111:220–36. doi: 10.1016/S1388-2457(99)00236-9
59. Satterfield JH, Schell AM, Backs RW, Hidaka KC. A cross-sectional and longitudinal study of age effects of electrophysiological measures in hyperactive and normal children. *Biol Psychiatry.* (1984) 19:973–90.
60. Eggermont JJ. On the rate of maturation of sensory evoked potentials. *Electroencephalogr Clin Neurophysiol.* (1988) 70:293–305. doi: 10.1016/0013-4694(88)90048-X
61. Elston GN, Fujita I. Pyramidal cell development: postnatal spinogenesis, dendritic growth, axon growth, and electrophysiology. *Front Neuroanat.* (2014) 8:78. doi: 10.3389/fnana.2014.00078
62. Elston GN, Okamoto T, Oga T, Dornan D, Fujita I. Spinogenesis and pruning in the primary auditory cortex of the macaque monkey (*Macaca fascicularis*): an intracellular injection study of layer III pyramidal cells. *Brain Res.* (2010) 1316:35–42. doi: 10.1016/j.brainres.2009.12.056
63. Moore JK, Guan YL. Cytoarchitectural and axonal maturation in human auditory cortex. *J Assoc Res Otolaryngol.* (2001) 2:297–311. doi: 10.1007/s101620010052
64. Moore JK, Linthicum FH Jr. The human auditory system: a timeline of development. *Int J Audiol.* (2007) 46:460–78. doi: 10.1080/14992020701383019
65. Roberts TP, Khan SY, Blaskey L, Dell J, Levy SE, Zarnow DM, et al. Developmental correlation of diffusion anisotropy with auditory-evoked response. *Neuroreport.* (2009) 20:1586–91. doi: 10.1097/WNR.0b013e3283306854
66. Roberts TP, Lanza MR, Dell J, Qasmieh S, Hines K, Blaskey L, et al. Maturational differences in thalamocortical white matter microstructure and auditory evoked response latencies in autism spectrum disorders. *Brain Res.* (2013) 1537:79–85. doi: 10.1016/j.brainres.2013.09.011
67. Kushnerenko E, Ceponiene R, Balan P, Fellman V, Huotilaine M, Naatane R. Maturation of the auditory event-related potentials during the first year of life. *Neuroreport.* (2002) 13:47–51. doi: 10.1097/00001756-200201210-00014
68. Kushnerenko E, Ceponiene R, Balan P, Fellman V, Naatanen R. Maturation of the auditory change detection response in infants: a longitudinal ERP study. *Neuroreport.* (2002) 13:1843–8. doi: 10.1097/00001756-200210280-00002
69. Barnet AB. Auditory evoked potentials during sleep in normal children from ten days to three years of age. *Electroencephalogr Clin Neurophysiol.* (1975) 39:29–41. doi: 10.1016/0013-4694(75)90124-8
70. Johnstone SJ, Barry RJ, Anderson JW, Coyle SF. Age-related changes in child and adolescent event-related potential component morphology, amplitude and latency to standard and target stimuli in an auditory oddball task. *Int J Psychophysiol.* (1996) 24:223–38. doi: 10.1016/S0167-8760(96)00065-7
71. Sussman E, Steinschneider M, Gumenyuk V, Grushko J, Lawson K. The maturation of human evoked brain potentials to sounds presented at different stimulus rates. *Hear Res.* (2008) 236:61–79. doi: 10.1016/j.heares.2007.12.001
72. Edgar JC, Huang MX, Weisend MP, Sherwood A, Miller GA, Adler LE, et al. Interpreting abnormality: an EEG and MEG study of P50 and the auditory paired-stimulus paradigm. *Biol Psychol.* (2003) 65:1–20. doi: 10.1016/S0301-0511(03)00094-2
73. Roberts TP, Heiken K, Zarnow D, Dell J, Nagae L, Blaskey L, et al. Left hemisphere diffusivity of the arcuate fasciculus: influences of autism spectrum disorder and language impairment. *AJNR Am J Neuroradiol.* (2014) 35:587–92. doi: 10.3174/ajnr.A3754
74. WHO Multicentre Growth Reference Study Group. WHO motor development study: windows of achievement for six gross motor development milestones. *Acta Paediatr Suppl.* (2006) 450:86–95. doi: 10.1111/j.1651-2227.2006.tb02379.x
75. Jenni OG, Chaouch A, Caflisch J, Rousson V. Infant motor milestones: poor predictive value for outcome of healthy children. *Acta Paediatr.* (2013) 102:e181–4. doi: 10.1111/apa.12129
76. Gerber RJ, Wilks T, Erdie-Lalena C. Developmental milestones: motor development. *Pediatr Rev.* (2010) 31:267–76; quiz 277. doi: 10.1542/pir.31-7-267
77. Prevention CfDCa. *Important Milestones: Your Baby by Eighteen Months*. (2019). Available online at: https://www.cdc.gov/ncbddd/actearly/milestones/milestones-18mo.html
78. Turnbull KP, Justice LM. *Language Development From Theory to Practice*. 3rd ed. Columbus, OH: The Ohio State University (2017).
79. Hoff E. *Langauge Development.* 2nd ed. Belmont, CA: Wadsworth/Thomson Learning (2001).
80. Kozak MJ, Cuthbert BN. The NIMH research domain criteria initiative: background, issues, and pragmatics. *Psychophysiology.* (2016) 53:286–97. doi: 10.1111/psyp.12518
81. Miller GA, Rockstroh BS, Hamilton HK, Yee CM. Psychophysiology as a core strategy in RDoC. *Psychophysiology.* (2016) 53:410–4. doi: 10.1111/psyp.12581
82. Thompson PM, Jahanshad N, Ching CRK, Salminen LE, Thomopoulos SI, Bright J, et al. ENIGMA and global neuroscience: a decade of large-scale studies of the brain in health and disease across more than 40 countries. *Transl Psychiatry.* (2020) 10:100. doi: 10.1016/j.biopsych.2020.02.167
83. van Erp TG, Hibar DP, Rasmussen JM, Glahn DC, Pearlson GD, Andreassen OA, et al. Subcortical brain volume abnormalities in 2028 individuals with schizophrenia and 2540 healthy controls via the ENIGMA consortium. *Mol Psychiatry.* (2016) 21:547–53. doi: 10.1038/mp.2015.63
84. van Rooij D, Anagnostou E, Arango C, Auzias G, Behrmann M, Busatto GF, et al. Cortical and subcortical brain morphometry differences between patients with autism spectrum disorder and healthy individuals across the lifespan: results from the ENIGMA ASD working group. *Am J Psychiatry.* (2018) 175:359–69. doi: 10.1176/appi.ajp.2017.17010100
85. Roberts TPL, Bloy L, Blaskey L, Kuschner E, Gaetz L, Anwar A, et al. A MEG study of acute arbaclofen (STX-209) administration. *Front Integr Neurosci.* (2019) 13:69. doi: 10.3389/fnint.2019.00069
86. Berman JI, Edgar JC, Blaskey L, Kuschner ES, Levy SE, Ku M, et al. Multimodal diffusion-MRI and MEG assessment of auditory and language system development in autism spectrum disorder. *Front Neuroanat.* (2016) 10:30. doi: 10.3389/fnana.2016.00030
87. Edgar JC, Chen YH, Lanza M, Howell B, Chow VY, Heiken K, et al. Cortical thickness as a contributor to abnormal oscillations in schizophrenia? *Neuroimage Clin.* (2014) 4:122–9. doi: 10.1016/j.nicl.2013.11.004
88. Wilson TW, Hernandez OO, Asherin RM, Teale PD, Reite ML, Rojas DC. Cortical gamma generators suggest abnormal auditory circuitry in early-onset psychosis. *Cereb Cortex.* (2008) 18:371–8. doi: 10.1093/cercor/bhm062
89. Uhlhaas PJ, Roux F, Rodriguez E, Rotarska-Jagiela A, Singer W. Neural synchrony and the development of cortical networks. *Trends Cogn Sci.* (2010) 14:72–80. doi: 10.1016/j.tics.2009.12.002
90. Uhlhaas PJ, Roux F, Singer W, Haenschel C, Sireteanu R, Rodriguez E. The development of neural synchrony reflects late maturation and restructuring of functional networks in humans. *Proc Natl Acad Sci USA.* (2009) 106:9866–71. doi: 10.1073/pnas.0900390106

91. Hirano Y, Oribe N, Kanba S, Onitsuka T, Nestor PG, Spencer KM. Spontaneous gamma activity in schizophrenia. *JAMA Psychiatry*. (2015) 72:813–21. doi: 10.1001/jamapsychiatry.2014.2642

Conflict of Interest: JB reports a consultancy with McGowan Associates. TR declares his position on the advisory boards of (1) CTF MEG, (2) Ricoh, (3) Spago Nano Medicine, (4) Avexis Inc., (5) Acadia Pharmaceuticals and equity interests in (1) Prism Clinical Imaging and (2) Proteus Neurodynamics. TR and JCE also declare intellectual property relating to the potential use of electrophysiological markers for treatment planning in clinical ASD. LBla reports a consultancy with KBT Technologies.

The remaining authors declare that the research was conducted in the absence of any commercial or financial relationships that could be construed as a potential conflict of interest.

frontiers in Psychiatry

ORIGINAL RESEARCH
published: 23 November 2020
doi: 10.3389/fpsyt.2020.561973

A MEG Study of Visual Repetition Priming in Schizophrenia: Evidence for Impaired High-Frequency Oscillations and Event-Related Fields in Thalamo-Occipital Cortices

Andreas Sauer[1,2], *Tineke Grent-'t-Jong*[3,4], *Michael Wibral*[5], *Michael Grube*[6], *Wolf Singer*[1,2,7] *and Peter J. Uhlhaas*[3,4]*

[1] Department of Neurophysiology, Max Planck Institute for Brain Research, Frankfurt am Main, Germany, [2] Singer Lab, Ernst Strüngmann Institute (ESI) for Neuroscience in Cooperation With Max Planck Society, Frankfurt am Main, Germany, [3] Institute of Neuroscience and Psychology, University of Glasgow, Scotland, United Kingdom, [4] Department of Child and Adolescent Psychiatry, Charité-Universitätsmedizin Berlin, Berlin, Germany, [5] Campus Institute for Dynamics of Biological Networks, Georg-August University, Göttingen, Germany, [6] Department of Psychiatry and Psychotherapy—Psychosomatics, Municipal Clinic, Frankfurt am Main, Germany, [7] Frankfurt Institute for Advanced Studies (FIAS), Frankfurt am Main, Germany

OPEN ACCESS

Edited by:
Vaibhav A. Diwadkar, Wayne State University, United States

Reviewed by:
Raymond Young-Jin Cho, Baylor College of Medicine, United States
Kevin M. Spencer, Harvard Medical School, United States

***Correspondence:**
Peter J. Uhlhaas
peter.uhlhaas@charite.de

Specialty section:
This article was submitted to Neuroimaging and Stimulation, a section of the journal Frontiers in Psychiatry

Received: *14 May 2020*
Accepted: *19 October 2020*
Published: *23 November 2020*

Citation:
Sauer A, Grent-'t-Jong T, Wibral M, Grube M, Singer W and Uhlhaas PJ (2020) A MEG Study of Visual Repetition Priming in Schizophrenia: Evidence for Impaired High-Frequency Oscillations and Event-Related Fields in Thalamo-Occipital Cortices. Front. Psychiatry 11:561973. doi: 10.3389/fpsyt.2020.561973

Background: Cognitive dysfunctions represent a core feature of schizophrenia and a predictor for clinical outcomes. One possible mechanism for cognitive impairments could involve an impairment in the experience-dependent modifications of cortical networks.

Methods: To address this issue, we employed magnetoencephalography (MEG) during a visual priming paradigm in a sample of chronic patients with schizophrenia ($n = 14$), and in a group of healthy controls ($n = 14$). We obtained MEG-recordings during the presentation of visual stimuli that were presented three times either consecutively or with intervening stimuli. MEG-data were analyzed for event-related fields as well as spectral power in the 1–200 Hz range to examine repetition suppression and repetition enhancement. We defined regions of interest in occipital and thalamic regions and obtained virtual-channel data.

Results: Behavioral priming did not differ between groups. However, patients with schizophrenia showed prominently reduced oscillatory response to novel stimuli in the gamma-frequency band as well as significantly reduced repetition suppression of gamma-band activity and reduced repetition enhancement of beta-band power in occipital cortex to both consecutive repetitions as well as repetitions with intervening stimuli. Moreover, schizophrenia patients were characterized by a significant deficit in suppression of the C1m component in occipital cortex and thalamus as well as of the late positive component (LPC) in occipital cortex.

Conclusions: These data provide novel evidence for impaired repetition suppression in cortical and subcortical circuits in schizophrenia. Although behavioral priming was

preserved, patients with schizophrenia showed deficits in repetition suppression as well as repetition enhancement in thalamic and occipital regions, suggesting that experience-dependent modification of neural circuits is impaired in the disorder.

Keywords: neural oscillations, repetition suppression (RS), visual priming, magentoencephalography (MEG), schizophrenia

INTRODUCTION

Schizophrenia is a severe mental disorder characterized by psychotic experiences and disorganized and negative symptoms. In addition, the disorder involves profound deficits in a range of cognitive processes (1). Importantly, cognitive deficits are not modified by current pharmacological treatments and are related to the poor functional outcomes in the majority of schizophrenia patients (2, 3). While cognitive impairments have so far been conceptualized primarily in terms of impairments in higher cognitive functions, such as attention, memory and executive processes (4), there is evidence that dysfunctional sensory processes are also involved (5, 6). Accordingly, the identification of neural mechanisms underlying cognitive impairments in schizophrenia remains one of the major challenges that is important for the development of novel treatments.

Impaired learning mechanisms may contribute to cognitive deficits in schizophrenia as there is evidence of dysfunctional synaptic plasticity (7, 8). Synaptic plasticity refers to synaptic changes in neuronal connections, such as long-term potentiation and depression (LTP/LTD), and is thought to be the primary mechanism for learning and memory (9–12). N-methyl-D-aspartate receptors (NMDA-Rs) play an important role during the induction of LTP/LTD (13). Moreover, there is consistent evidence for an involvement of NMDA-R hypofunctioning in the pathophysiology of schizophrenia (14, 15).

Patients with schizophrenia consistently show deficits in explicit learning and memory (16), while performance on implicit processing tasks appears relatively intact. Thus, studies using motor learning or grammar learning tasks found normal learning (17–19), while probabilistic learning was impaired (18, 19).

One form of implicit memory is repetition priming. Repetition priming refers to improvements in behavioral responses, such as accuracy or reaction time, when stimuli are repeatedly presented (20, 21). Stimulus repetition is associated with changes in single cortical neuron responses (22) as well as in functional magnetic resonance imaging (fMRI)- (23, 24) and in Electro-/Magnetoencephalography data (25, 26). Although stimulus repetition typically leads to repetition suppression, the converse phenomenon, repetition enhancement, has been also been observed in response to unfamiliar stimuli (23) or with low stimulus visibility (27). More recently, it has been shown that repetition suppression and enhancement can occur within one cortical region (28) and that stimulus repetition can induce both enhancement and suppression of neural responses, depending on the number of stimulus presentations (29).

Repetition suppression has been related to the "sharpening" of neural networks (30, 31) which involves a reduction of the number of neurons over successive presentations. More recent studies have shown that top-down processes contribute toward repetition suppression (32, 33). From this perspective, the reduction of neural activity is the result of a comparison between bottom-up (sensory evidence) and top-down activity (predictions), thus leading to a reduction of the prediction error (34, 35).

There is evidence that schizophrenia is associated with impaired repetition suppression. Deficits have been observed for early evoked auditory responses, such as the P50 component (36–40), as well as during pre-pulse inhibition (41–43), in the M170 component in visual cortex (44) and in fMRI-data (45, 46). However, there is also evidence for intact repetition suppression of ERPs (47–49) as well as in fMRI-data (50, 51).

To further investigate repetition priming and the associated neural signatures in schizophrenia, we employed a visual priming paradigm in combination with MEG. Specifically, we presented three visual objects consecutively to examine both repetition suppression and enhancement in MEG-data. In a second experimental condition, stimulus repetitions were interleaved with intervening stimuli to exclude habituation as an alternative explanation for repetition suppression effects.

We focused on the modification of neural oscillations, as beta-/gamma- (52, 53) but also theta-band oscillations (54) provide a temporal structure that allows for precise alignment of the temporal relations between pre- and postsynaptic activation, this relation being crucial in determining the occurrence and the polarity of activity dependent synaptic gain changes (LTP/LTD). More specifically, experience-dependent changes in neural networks appear to depend on the power of stimulus-induced gamma-band oscillations, suggesting a critical role of synchronized gamma-activity for synaptic plasticity (53).

Importantly, there is consistent evidence for aberrant neural oscillations and their synchronization in patients with schizophrenia (55) that could underlie impairments in sensory processing (56–59) as well as higher cognitive functions (60). These data are furthermore consistent with evidence for impaired GABAergic as well as impaired glutamatergic neurotransmission in the disorder (61–64).

Given the important role of neural oscillations in synaptic plasticity (53) as well as the evidence for impaired learning in schizophrenia, we hypothesized that schizophrenia patients would be characterized by impaired behavioral priming as well as reduced repetition suppression in visual cortex as reflected by aberrant gamma-band activity and impaired event-related fields (ERFs) in response to repeated presentation of visual stimuli. Moreover, we also expected close correlations between behavioral impairments, cognitive deficits, and dysfunctional oscillatory activity.

METHODS

Participants

Fourteen healthy control participants (mean ± SD age, 25.71 ± 4.64 years; 11 females) were recruited from the local community and screened for psychopathology with the German version of the Structured Clinical Interview for DSM-IV-R (SCID) (65). Fourteen patients with schizophrenia (mean ± SD age, 33.79 ± 11 years; three females) were recruited from the outpatient unit of the Psychiatry Department of the Clinic in Frankfurt-Hoechst. All patients fulfilled DSM-IV criteria for schizophrenia as verified by means of a SCID-interview prior to study inclusion. Average disease duration was 10.8 ± 7.1 years. All patients were medicated with atypical neuroleptics. Age and sex differed significantly between both groups (age: $t_{26} = -2.68$, $p = 0.012$; sex: $X^2(1) = 8.31$, $p < 0.01$). Current psychopathological symptoms were assessed using the Positive and Negative Syndrome Scale (PANSS) for schizophrenia (66). Symptoms were grouped into five factors – "Negative," "Positive," "Excitement," "Cognitive," and "Depression" – according to the model of Lindenmayer et al. (67) (**Table 1**). In addition, patients were also rated on the item "Inappropriate Affect," which allowed for a score on the factor "Disorganization" (68). Cognitive functions were assessed with the German version of the Brief Assessment of Cognition in Schizophrenia [BACS; (69)] (**Table 1**). BACS data were standardized (z-transformed) to a normative database, correcting for age and gender (70).

Participants were excluded if they reported any neurological disorder or current or past alcohol or substance dependence. All subjects were right-handed as assessed by the Edinburgh Handedness Inventory (71) and had normal or corrected-to-normal visual acuity. All participants gave written informed consent prior to the study. The study was carried out according to the declaration of Helsinki and approved by the ethical committee of the Goethe University Frankfurt.

Stimuli and Task

Stimuli consisted of 200 colored line drawings, picturing natural or man-made objects (72, 73). Stimuli were presented in the center of a translucent screen at a viewing distance of 51 cm and subtended 6.6 degrees of visual angle. A fixation cross was always present in the center of the screen to reduce eye-movements. An LCD projector located outside the magnetically shielded room of the MEG was used to project the stimuli onto the screen via two front-silvered mirrors. Presentation of experimental stimuli was controlled using Presentation (version 14.2, Neurobehavioral Systems, Inc.).

Stimuli were presented for 1000 ms with a randomized inter-stimulus interval of 1000–2000 ms. Each stimulus was presented three times, with either no or different intervening stimuli. The number of intervening stimuli (5–15) was randomized. This resulted in two different repetition conditions: (1) stimulus sequences with three consecutive presentations of the same

TABLE 1 | Demographic, neuropsychological and psychopathological data.

	Controls ($n = 14$)		SCZ-patients ($n = 14$)		Statistics
	Mean	SD	Mean	SD	
Gender (f/m)	11/3		3/11		$X^2(1) = 8.31$, $P < 0.01$
Age (years)	25.71	4.64	33.79	11.00	$t_{(26)} = 2.68$, $P < 0.05$
Education (years)	14.86	2.03	14.10	3.31	n.s.
Duration of Illness (years)	—	—	10.80	7.10	—
Handedness, left	0		0		
Behavioral priming					
%-change RT NOLAG	−21.42		−23.11		n.s.
%-change RT LAG	−8.72		−9.20		n.s.
BACS (total)	323.43	21.14	248.21	29.47	$t_{(26)} = 8.05$, $P < 0.001$
Memory	56.57	6.62	40.14	7.96	$t_{(26)} = 4.37$, $P < 0.001$
Digit span	21.50	3.52	16.21	2.58	$t_{(26)} = 5.15$, $P < 0.001$
Token motor	97.86	3.16	81.14	17.71	$t_{(26)} = 3.12$, $P < 0.005$
Fluency	63.86	14.84	45.43	14.27	$t_{(26)} = 3.27$, $P < 0.005$
Symbols	63.86	7.34	49.36	16.20	$t_{(26)} = 2.54$, $P < 0.05$
Tower of London	19.79	1.81	15.93	2.95	$t_{(26)} = 3.98$, $P < 0.001$
PANSS (total)			43.00	24.37	—
Negative	—	—	14.23	5.20	—
Excitement	—	—	6.86	3.91	—
Cognitive	—	—	8.86	2.40	—
Positive	—	—	9.43	3.56	—
Depression	—	—	10.71	2.63	—
Disorganization	—	—	4.64	2.35	—

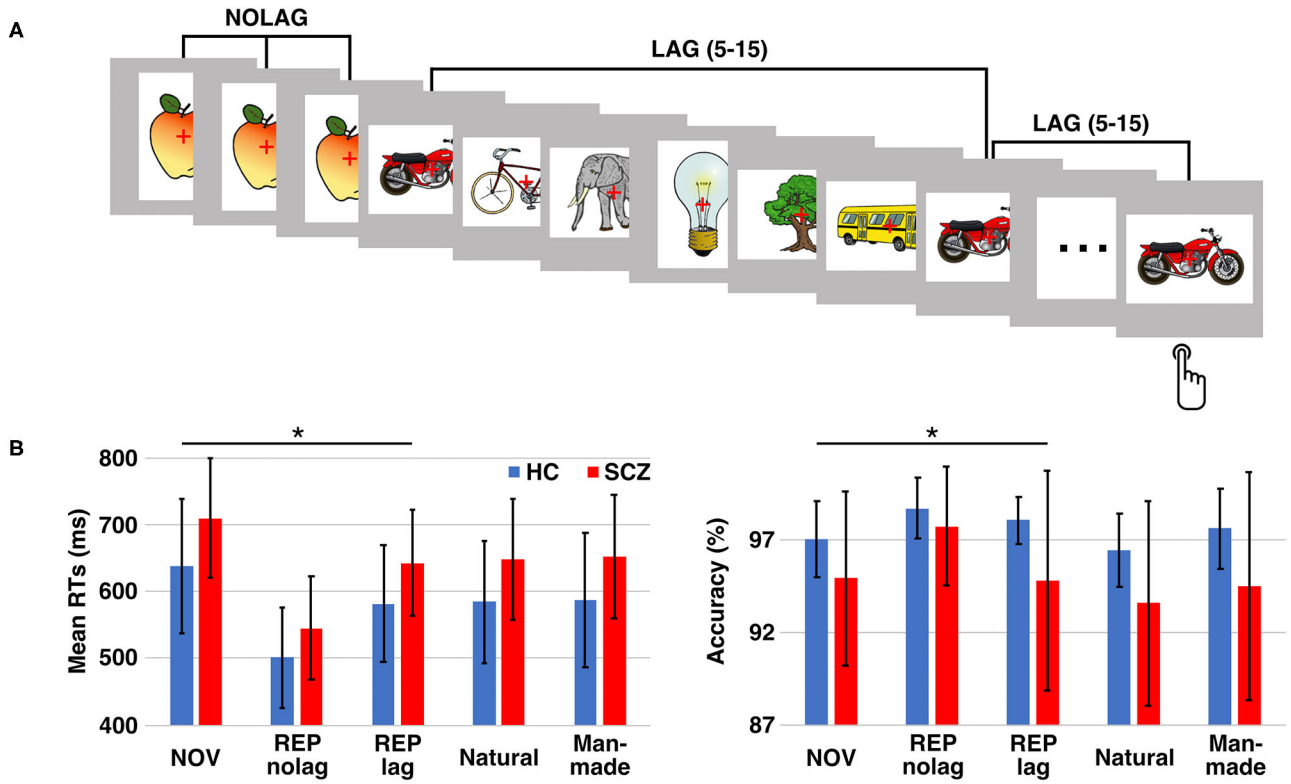

FIGURE 1 | Experimental design and behavioral performance. **(A)** Paradigm: participants had to decide whether the presented object is man-made or natural. Each stimulus was presented three times either in consecutive trials (NOLAG) or with 5–15 different intervening stimuli (LAG). **(B)** Mean response times (RTs; left) and response accuracy (right) ± SD for the different conditions/groups. Asterisk indicates significant group differences ($p < 0.05$, corr.). HC = control participants, SCZ, schizophrenia patients; NOV, Novel; REP, Repeated.

stimulus without different intervening stimuli (NOLAG) and (2) three presentations of the same stimulus separated by different intervening stimuli (LAG) (**Figure 1A**). The LAG condition was included to exclude habituation as an alternative explanation for repetition suppression effects and allowed to investigate the modulation of repetition effects by the lag between the repeated presentations of a stimulus (i.e., the "stability" of the repetition effect). Stimulus sequences were shuffled for each participant, resulting in individually randomized stimulus sequences with regards to experimental conditions and stimulus category. Participants were instructed to respond with a button press to indicate whether the presented object was natural or man-made. The assignment of buttons was counterbalanced across participants. Behavioral responses were recorded using a fiber-optic response device (Lumitouch, Photon Control Inc., Burnaby, BC, Canada). Participants were instructed to avoid eye movements and blinking during the presentation of stimuli.

Stimuli were administered in three experimental conditions: (1) novel pictures (i.e., the first presentation of a stimulus; NOV), (2) repeated presentations without lag (NOLAG) and (3) repeated presentations with lag (LAG). The experiment consisted of 600 trials, divided into five blocks of 120 trials each.

Neuroimaging

MEG data were acquired using a 275-sensor whole-head system (Omega 2005, VSM MedTech Ltd.) with a sampling rate of 600 Hz in a synthetic third order axial gradiometer configuration. Before and after each block, head position relative to the gradiometer array was measured. Recordings with head movements exceeding 5 mm were discarded. A high-resolution anatomical MRI scan was acquired for each participant on a 3 T Siemens Trio scanner, using a 3D-MPRAGE sequence (160 slices, voxel size: 1 × 1 × 1 mm; field of view: 256 mm, repetition time: 2300 ms, echo time: 3.93 ms), with markers placed at the same locations as the sensors used for recording head position in the MEG. These markers were used for subsequent co-registration of the MEG data to the anatomical T1 image.

MEG Data Analysis

MEG data were analyzed with MATLAB using the open source Fieldtrip toolbox (74). Trials were defined from the continuously recorded MEG signal from −1000 to 1500 ms with respect to the onset of the stimulus. Pre-processing included lowpass filtering of the MEG data (Butterworth filter fourth order) with a lowpass frequency of 200 Hz as well as detrending. Power line fluctuations (50 Hz and harmonics) and a 60 Hz

beamer noise signal were removed using a band-stop filter. Independent component analysis (ICA) was used to remove artifacts due to cardiac activity, eye movements and eye blinks. Trials containing muscle artifacts or sensor (SQUID) jumps were discarded using semi-automatic artifact rejection routines. Data epochs for NOV trials were pooled together from the NOLAG and LAG conditions, and only trials with correct responses were considered for further analyses.

All analyses were conducted on "virtual channel" reconstructed MEG data. Linearly constrained minimum variance (LCMV) beamformer spatial filters (75) were used to first reconstruct the MEG data from MNI source locations corresponding to centroids of 80 of 116 available AAL atlas regions (76).

Time-frequency power representations (TFRs) were computed on the LCMV reconstructed time-series, using a sliding window Fast Fourier Transform (FFT) approach with a fixed window of 200 ms and a step size of 10 ms across the length of the epochs. Power of all frequencies between 1 and 200 Hz was estimated based on data padded up to 4 s, using a frequency resolution of 1 Hz, and multiplying the data with a Hanning taper before power estimation.

To analyze ERFs, trials were low-pass filtered at 20 Hz (Butterworth filter fourth order) and baseline corrected using the first 200 ms of each epoch. Trials were averaged per condition and per participant. Based on previous studies (25, 77–79) ERFs were analyzed for early components C1m (30–80 ms) and M100 (80–120 ms) as well as the P300m (200–400 ms) and the late positive component (LPC, 400–600 ms).

Fourteen regions were included in the further analyses: 12 covering striate and extra-striate visual-cortical areas based on previous studies (25, 78) and two (bilateral) thalamic regions (see **Figures 4A,B**).

Statistical Analyses

Behavioral data were analyzed by means of repeated measures ANOVA using JASP (version 0.13.1; University of Amsterdam, NL). A probability level of $p < 0.05$ was considered as statistically significant. Statistical analyses of MEG data for factors GROUP (Controls vs. Patients), NOVELTY (Novel vs. Repetition) and PRESENTATION (NOLAG vs. LAG) were assessed using non-parametric Monte-Carlo permutation independent F-tests as implemented in Fieldtrip with 1999 permutations and cluster-based correction for multiple comparisons ($p < 0.05$, one sided). To examine differences between experimental conditions within and between groups, non-parametric Monte-Carlo permutation *t*-test statistics with 1999 permutations and cluster-based correction for multiple comparisons ($p < 0.05$, two sided) as implemented in Fieldtrip were performed. Cluster-based statistics were computed across the 12 occipital cortex regions of interest (ROIs) and for the two thalamic ROIs, separately. Effects of picture repetition on modulation of neural activity were statistically evaluated within each group in relation to the response to novel stimuli, with contrasting novel stimuli (NOV) against repeated stimuli for each repetition condition (NOLAG or LAG). For group effects, the difference between NOV and REP for each repetition condition (NOLAG or LAG) was calculated within each group and then contrasted against each other. As sex and age were significantly different between groups, the influence of these variables on group differences of repetition effects was analyzed with correlational analyses (see **Supplementary Figure 2**).

RESULTS

Neuropsychological Data

Schizophrenia patients were significantly impaired in the BACS-total score as well as in each of the subtests ($t = 7.76$, $p < 0.001$; mean z-score ± SD, controls: 4.33 ± 2.29, schizophrenia patients: −4.33 ± 3.31; **Table 1**).

Behavioral Data

Analysis of reaction times (RTs) revealed a main effect of GROUP [$F_{(1, 27)} = 13.97$, $p < 0.001$], a main effect of NOVELTY [$F_{(1, 27)} = 41.12$, $p < 0.001$], and a main effect of PRESENTATION [$F_{(1, 27)} = 7.18$, $p < 0.01$]. Tukey *post-hoc* analyses showed that schizophrenia patients responded significantly slower than controls (GROUP: $t = -3.72$, $p < 0.001$, mean difference: −71.20 ms, 95%-CI [−132.22, −10.17]; mean RT ± SD, controls: 638.62 ± 100.44 ms, schizophrenia patients: 709.82 ± 89.07 ms). Moreover, RTs were faster for repeated presentations (NOVELTY: $t = 6.41$, $p < 0.001$, mean difference: 106.47 ms, 95%-CI [73.55, 139.40]; mean RT ± SD, NOV: 674.22 ± 99.95 ms, REP: 567.75 ± 93.83 ms), and that participants responded faster for presentations without different intervening stimuli (PRESENTATION: $t = -3.72$, $p < 0.001$, mean difference: −44.48 ms, 95%-CI [−77.41, −11.56]; mean RT ± SD, NOLAG: 598.74 ± 117.23 ms, LAG: 643.23 ± 98.16 ms) (**Figure 1B**). There was no GROUP × NOVELTY interaction, indicating a comparable behavioral priming effect to repeated presentations in the two groups [$F_{(1, 27)} = 0.33$, $p = 0.569$] (**Table 1**). A significant NOVELTY × PRESENTATION interaction indicated that RTs were significantly different between novel and repeated presentation depending on the repetition condition [$F_{(1, 27)} = 7.18$, $p < 0.01$].

Analyses of accuracy showed a main effect of GROUP [$F_{(1, 27)} = 9.86$, $p < 0.005$]. Tukey *post-hoc* analysis showed that accuracy was higher in controls compared to schizophrenia patients ($t = 3.14$, $p = 0.002$; mean accuracy ± SD, controls: 98.37 ± 0.98%, patients: 96.69 ± 3.30%; **Figure 1B**).

MEG Data

Responses to Novel Stimuli

The schizophrenia group was characterized by a significantly reduced oscillatory response in occipital ROIs in the gamma-band to novel stimuli (63–141 Hz, 0.04–1.0 s, $t_{sum} = 14{,}470$, $p = 0.001$, 95%-CI [−0.0004, 0.0024]; **Figures 2A,B**, **Table 2**). This effect was observed in bilateral cuneus, calcarine sulci as well as bilateral superior, middle and inferior occipital gyri. Moreover, schizophrenia patients showed a significantly reduced C1m component in occipital ROIs ($t_{sum} = 25.45$, $p = 0.036$; **Figure 2C**, **Table 2**).

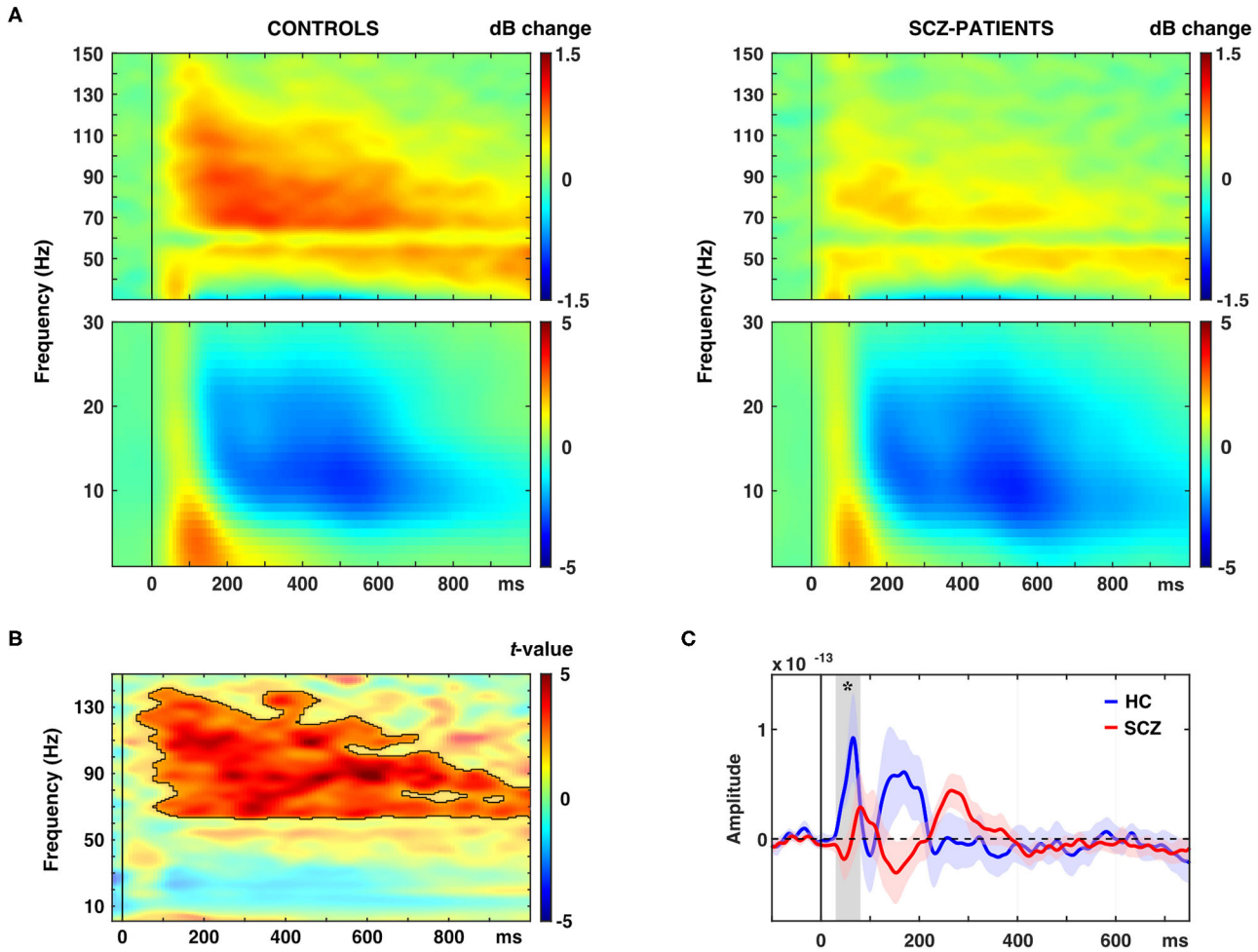

FIGURE 2 | Effects of novel pictures on spectral power and event-related fields (ERFs). **(A)** Time-frequency responses (TFR) of AAL atlas reconstructed virtual channel data. TFR show grand average ($N = 14$ per group) data from across 12 regions in the occipital cortex as displayed in **Figure 4A** (averaged dB power changes from baseline) for novel picture presentations in control participants (left) and schizophrenia patients (right). **(B)** TFR plot with statistical result (non-parametric, Monte-Carlo permutation independent *t*-test, cluster corrected, $p < 0.05$) of group difference with significant cluster outlined. **(C)** ERF time-course of grand average ($N = 14$ per group) data in the occipital cortex for novel picture presentations in control participants (HC) and schizophrenia patients (SCZ). Asterisk indicates a significant difference between groups (cluster corrected, $p < 0.05$).

Repetition Suppression/Enhancement

Spectral power

Analyses of factors GROUP, NOVELTY, and PRESENTATION revealed a main effect of GROUP ($p < 0.001$, $F_{sum} = 110785.70$), a main effect of NOVELTY ($p = 0.012$, $F_{sum} = 20049.06$), but no main effect of PRESENTATION ($p = 0.9$, $F_{sum} = 27.95$). *Post-hoc* pairwise *t*-test analyses revealed that stimulus repetitions led to a significant reduction of gamma-band power in occipital cortex ROIs in controls in both NOLAG (42–123 Hz, $t_{sum} = -11366$, $p = 0.001$; **Figures 3A,B**) and LAG (42–129 Hz, $t_{sum} = -8903.30$, $p = 0.001$; **Figures 3A,B**) conditions (**Table 2**). In the NOLAG condition, the effect was observed in all occipital cortex ROIs, whereas the effect in the LAG condition was observed only in right cuneus, right inferior occipital gyrus as well as bilateral calcarine sulci and superior and medial occipital gyri. Schizophrenia patients, however, showed a significant reduction of gamma-band power to repeated presentations only in the NOLAG condition and with a smaller bandwidth (66–88 Hz, $t_{sum} = -1262.30$, $p = 0.016$; **Figures 3A,B**, **Table 2**). Furthermore, this effect was spatially limited to the right lingual gyrus.

Importantly, schizophrenia patients showed an impaired repetition suppression of gamma-band power in both NOLAG (43–98 Hz, $t_{sum} = -3319.10$, $p = 0.001$; **Figure 3C**) and LAG (50–98 Hz, $t_{sum} = -1658.70$, $p = 0.015$; **Figure 3C**) conditions in occipital ROIs compared to controls (**Table 2**). For both conditions, impaired repetition suppression of gamma-band

TABLE 2 | Summary of significant within- and between-group effects in MEG data.

Effect	ROI	Frequency range	ERF latency	*P*
CONTROLS				
NOV vs. REPnolag	Occipital ROI	42–123 Hz		0.001
		2–35 Hz		0.008
	Occipital ROI		30–80 ms	0.029
			400–600 ms	0.020
	Thalamus		30–80 ms	0.053
NOV vs. REPlag	Occipital ROI	42–129 Hz		0.001
		1–36 Hz		0.003
	Occipital ROI		30–80 ms	0.031
SCZ-PATIENTS				
NOV vs. REPnolag	Occipital ROI	66–88 Hz		0.016
		1–37 Hz		0.001
NOV vs. REPlag	Occipital ROI	12–40 Hz		0.009
CON vs. SCZ				
NOV vs. REPnolag	Occipital ROI	43–98 Hz		0.001
		14–33 Hz		0.039
	Occipital ROI		30–80 ms	0.005
	Thalamus		30–80 ms	0.019
NOV vs. REPlag	Occipital ROI	50–98 Hz		0.015
		12–31 Hz		0.024
	Occipital ROI		30–80 ms	0.063
NOV	Occipital ROI	63–141 Hz		0.001
			30–80 ms	0.036

activity was observed in bilateral cuneus, calcarine sulci as well as bilateral superior occipital gyri.

In frequencies < 40 Hz, both groups showed repetition enhancement in occipital cortex ROIs to repeated presentations in both NOLAG (controls: 2–35 Hz, t_{sum} = 4,514, p = 0.008; schizophrenia patients: 1–37 Hz, t_{sum} = 2957.70, p = 0.001; **Figures 3A,B**) and LAG (controls: 1–36 Hz, t_{sum} = 4632.2, p = 0.003; schizophrenia patients: 12–40 Hz, t_{sum} = 1972.10, p = 0.009; **Figures 3A,B**) conditions (**Table 2**). For controls, the effect was observed in all occipital cortex ROIs in both NOLAG and LAG conditions. Schizophrenia patients, on the other hand, showed repetition enhancement of beta-band activity only in bilateral cuneus, calcarine sulci, superior and medial occipital gyri and the right lingual gyrus.

Repetition enhancement of beta-band-power was significantly reduced in the schizophrenia group compared to controls in both NOLAG (14–33 Hz, t_{sum} = 1238.70, p = 0.039; **Figure 3C**) and LAG (12–31 Hz, t_{sum} = 1407.20, p = 0.024; **Figure 3C**) conditions in occipital ROIs (**Table 2**). Group differences for repetition enhancement of beta-band power were found in bilateral calcarine sulci and the right superior occipital gyrus in the NOLAG condition and in the right calcarine sulcus as well as the left middle occipital gyrus in the LAG condition.

ERFs

Analyses of factors GROUP, NOVELTY and PRESENTATION showed no significant main effects. *Post-hoc* pairwise *t*-tests revealed that controls showed an early effect of stimulus repetition with a significant reduction of the C1m (30–80 ms) component in the NOLAG and LAG condition (NOLAG: t_{sum} = 19.83, p = 0.029; LAG: t_{sum} = 43.90, p = 0.031) in all occipital ROIs (**Figure 4A**, **Table 2**). In addition, we observed a statistical trend in the NOLAG condition in the thalamus (t_{sum} = 24.20, p = 0.053; **Figure 4B**, **Table 2**). Importantly, repetition suppression of the C1m was not present in schizophrenia patients neither in the NOLAG nor the LAG conditions across occipital and thalamic ROIs (**Figures 4A,B**). There was a significant group difference in C1m repetition suppression in the NOLAG condition in occipital ROIs ($t_{sum=}$ −43.70, p = 0.005) and thalamus ($t_{sum=}$ −32.36, p = 0.019) but only as a statistical trend in the LAG condition in occipital ROIs ($t_{sum=}$ −20.39, p = 0.063) (**Figures 4A,B**, **Table 2**). The group effect in the NOLAG condition was mainly driven by the left calcarine sulcus and left superior occipital gyrus as well as the left thalamus, respectively, while the group effect in the LAG condition was observed only in the left calcarine sulcus.

In addition, we observed repetition suppression of the LPC in occipital ROIs in the NOLAG condition in controls (400–600 ms, t_{sum} = 82.39, p = 0.02; **Figure 4A**). In schizophrenia patients, this effect did not reach statistical significance (t_{sum} = −56,19, p = 0.09), and the group difference showed only a trend toward statistical significance when averaged over all occipital ROIs (t_{sum} = −61.70, p = 0.058). However, there was a significant difference in right calcarine sulcus (tsum = −259.89, p = 0.002).

Analyses of the M100 (80–120 ms) and P300m (200–400 ms) revealed no significant differences within or between groups.

Correlations With Behavior and Psychopathology vs. MEG Data

Pearson's correlations were used on z-normalized data to investigate relationships between repetition suppression/enhancement of the C1m, spectral power in the low (12–33 Hz) and high frequency (43–98 Hz) range and response times, accuracy and PANSS ratings. Bootstrapping (1000 randomizations) was applied to control for spurious findings. We did not find any significant correlations between repetition suppression/enhancement and behavioral parameters in both groups as well as with psychopathology in schizophrenia patients.

DISCUSSION

The present study investigated repetition suppression in schizophrenia with MEG to examine changes in neural oscillations and ERFs during visual priming. While behavioral priming was intact in schizophrenia patients, we observed a dysregulation of both low- and high-frequency oscillations as well as impaired ERFs, suggesting an impairment in the experience-dependent modification of neural circuits.

Consistent with previous studies that examined implicit learning in schizophrenia (80, 81), we found no difference

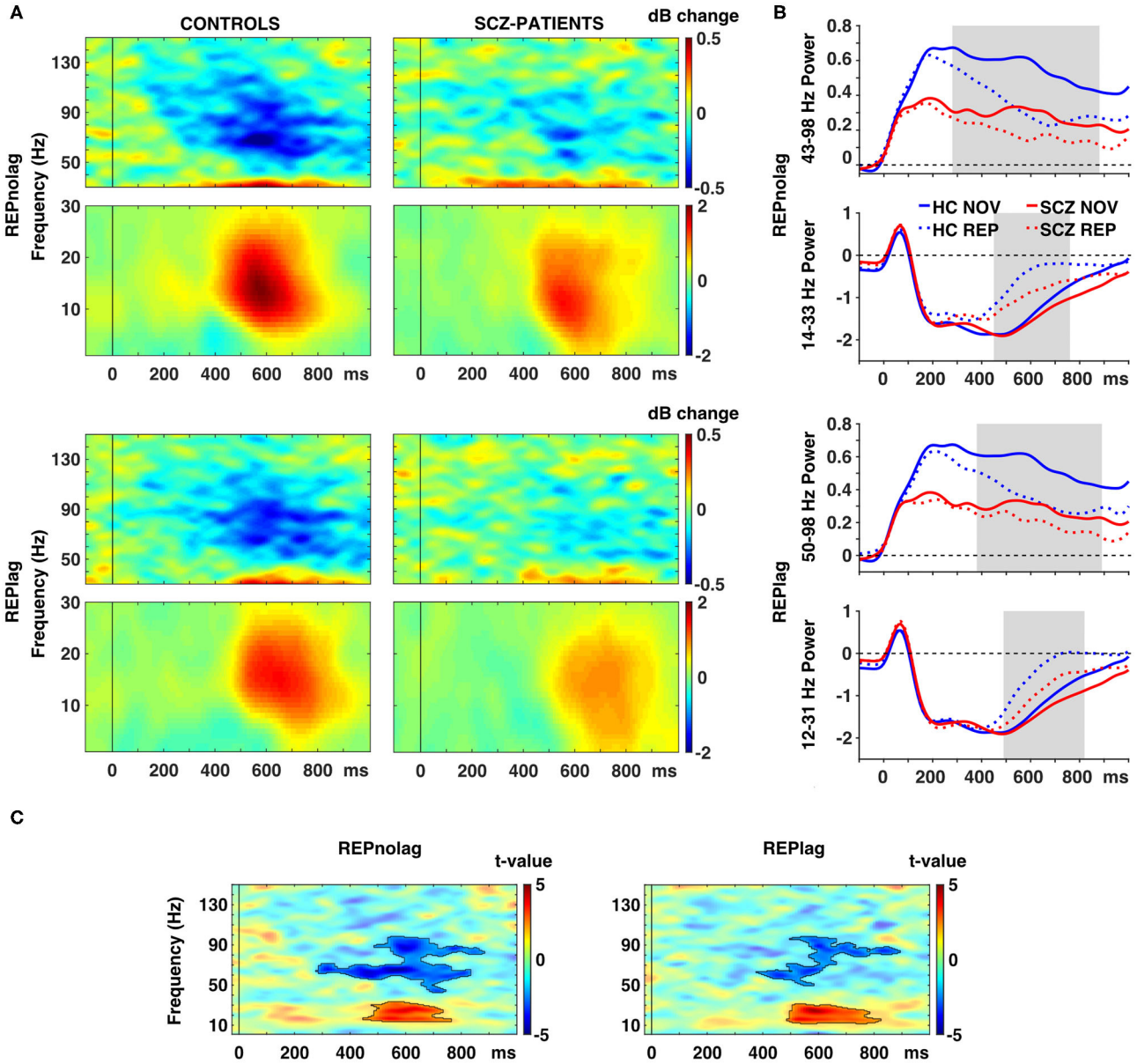

FIGURE 3 | Effects of picture repetition on spectral power. **(A)** Time-frequency responses (TFR) of AAL atlas reconstructed virtual channel data. TFR show grand average ($N = 14$ per group) data from across 12 regions in the occipital cortex as displayed in **Figure 4A** (averaged dB power changes from baseline) for the difference between novel and repeated pictures (REP minus NOV) for repetitions with no lag (first row) and lag (second row) in control participants (left) and schizophrenia patients (right). **(B)** Line graphs show averaged power for gamma (top) and beta (bottom) frequencies over time per group for novel and repeated picture presentations in the NOLAG (first row) and LAG (second row) condition. **(C)** TFR plots with statistical results (non-parametric, Monte-Carlo permutation independent *t*-test, cluster corrected, $p < 0.05$) of group difference for the effect of repetition (REP minus NOV) with significant clusters outlined. HC, control participants; SCZ, schizophrenia patients; NOV, novel; REP, repeated.

in behavioral priming between schizophrenia patients and controls. However, differences between groups emerged in MEG-parameters, suggesting a dissociation between repetition suppression/enhancement and behavioral priming. This is also supported by the fact that there were no significant correlations between MEG-data, cognitive and clinical variables. Moreover, previous studies failed to show a significant correlation between behavioral priming and neural suppression in occipital cortex during normal brain functioning (82–85), raising the possibility that behavioral priming and repetition suppression are distinct processes.

Consistent with previous studies that investigated repetition effects on neural oscillations and ERPs in healthy participants using visual paradigms (25, 78, 86), we observed repetition

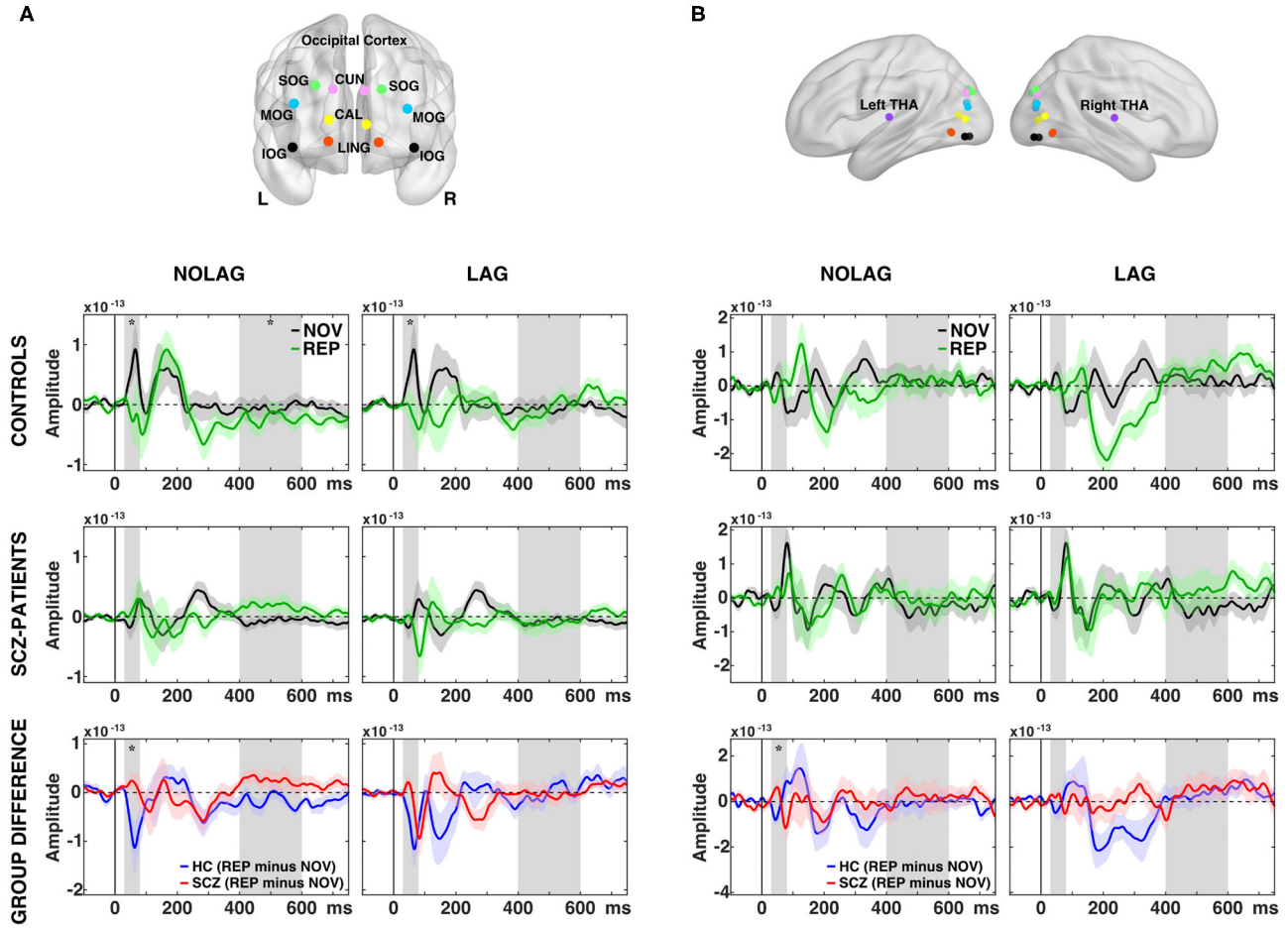

FIGURE 4 | Effects of picture repetition on event-related fields (ERFs). **(A)** Indication of regions of interest (ROI) used in the analysis for the occipital cortex, projected onto a transparent MNI template brain. CAL, calcarine sulcus; CUN, cuneus; LING, lingual gyrus; SOG/MOG/IOG, superior/middle/inferior occipital gyrus. ERF time-courses of grand average ($N = 14$ per group) data from across 12 regions in the occipital cortex for consecutively repetitions (NOLAG, left) and repetitions with intervening different stimuli (LAG, right) for control participants (first row) and schizophrenia patients (second row). Third row shows the group difference for the effect of repetition (REP minus NOV within group). **(B)** As in **(A)** but for the thalamus = THA. HC, controls participants; SCZ, schizophrenia patients; NOV, Novel; REP, Repeated. Gray boxes indicate the time window used for the statistical analyses (C1m = 30–80 ms; LPC = 400–600 ms). Asterisk indicates a significant difference between conditions/groups (cluster corrected, $p < 0.05$).

suppression of gamma-band frequencies and ERF components as well as repetition enhancement of beta-band frequencies in normal controls. Importantly, our data highlight an impairment in high-frequency oscillations in patients with schizophrenia during responses to novel stimuli as well as aberrant modulation of beta- and gamma-band activity during repetition suppression and enhancement. Consistent with a large body of EEG/MEG-data that demonstrated reduced power of high-frequency oscillations during sensory and perceptual processing (56, 59, 87, 88), we observed a pronounced (effect size: d = 1.48) and sustained reduction of high-gamma (>60 Hz) power that was extended over a large frequency range and time interval in occipital areas belonging to both dorsal and ventral processing streams.

Furthermore, modulation of spectral power during repetition suppression and enhancement at beta/gamma-band frequencies was also impaired in schizophrenia patients. Because of the pronounced reduction of gamma-band power to novel stimuli in schizophrenia patients, we have specifically examined repetition effects in relation to the response to novel stimuli within each group. Although the reduced gamma-band response to novel stimuli limits the range of repetition suppression in schizophrenia patients, our finding of impaired repetition enhancement of beta-band oscillations without a decreased beta-band response to novel stimuli, indicates a general deficit in repetition-related modulation of spectral power in schizophrenia patients.

Recently, Galuske et al. (53) have shown that changes of neuronal response properties induced by repetitive

visual stimulation depend on the magnitude of induced gamma-band oscillations. The authors observed changes in orientation tuning of neurons in visual cortex only when conditioning stimuli induced strong gamma-oscillations, suggesting a critical role of synchronized gamma-oscillations for facilitating experience-dependent plasticity. Accordingly, aberrant repetition suppression in schizophrenia patients might result from a persistent failure to generate gamma-band oscillations that in turn impairs synaptic plasticity.

As perception is dependent upon inferential processes whereby sensory evidence is weighted against prior knowledge (34, 89), it is possible that shallow processing, as indexed by reduced gamma-band responses to the initial stimulus, leads to a weaker formation of the prior in patients with schizophrenia. In the context of predictive coding, repetition suppression reflects the attenuation of the prediction error due to the decreasing mismatch between predictions and sensory input. As the magnitude of the prediction error signal reflects the match between prior and sensory data, weak priors in schizophrenia patients might result in a greater mismatch and thus in reduced repetition suppression. Interestingly, in the schizophrenia group repetition suppression effects were only observed in the NOLAG condition. This could index that interfering stimuli in the LAG condition further diminished the impact of the prior, thus leading to a further reduction of repetition suppression. In agreement with this interpretation is the recent finding (90) that the amplitude of induced gamma oscillations is positively correlated with the goodness of the match between sensory evidence and internal predictions.

Different oscillation frequencies have been related to different components of inferential processing. Top-down prediction signaling has been proposed to be predominantly mediated by alpha-/beta-frequencies and feed-forward prediction error signaling by gamma- and theta-band oscillations (91, 92). As group differences in gamma-band activity emerged in early visual areas, such as cuneus and calcarine sulcus, as well as higher-order visual regions, such as superior occipital gyrus, reduced gamma-band activity in patients with schizophrenia may lead to reduced feed-forward signaling as recently demonstrated by our group (59). According to the predictive coding framework, the predictive model at higher levels of the hierarchy is updated by the ascending prediction error, which has more impact on the prior when it conveys precise information (through precision weighting). Reduced gamma responses in patients with schizophrenia may lead to a deficient updating of priors through reduced precision of the prediction error signal resulting from imprecise sensory data input.

This is in line with our finding of impaired repetition enhancement of beta-band activity in schizophrenia patients. Precision of predictions increases as prediction error is minimized by repetitions, which may underlie repetition enhancement (35). Reduced repetition enhancement in schizophrenia patients could index reduced precision of predictions, which may result from a deficient interplay between top-down predictions and bottom-up prediction error signaling.

Consistent with a previous report (79) we also found that stimulus repetition was associated with an early (30–80 ms) reduction of the C1m component in healthy controls in visual cortex. The C1 component reflects the first visual evoked potential (VEP) component, with an onset latency between 40 and 70 ms and peak latency between 60 and 100 ms, and originates from primary visual cortex in striate cortex within the calcarine fissure (93–97). Importantly, repetition suppression of this early VEP was impaired in schizophrenia patients. This finding is in line with a large body of research on early-stage visual processing deficits in schizophrenia (59, 98).

Furthermore, we found impaired repetition suppression of early VEPs in schizophrenia patients in the thalamus. The thalamus plays a key role in information processing as nearly all sensory information must pass the thalamus before reaching the cerebral cortex, and there is consistent evidence for both anatomical (99) and functional abnormalities (100, 101) in schizophrenia.

In addition, we observed impaired repetition suppression of the LPC in the schizophrenia group in occipital ROIs. The LPC has been associated with recognition memory processes ["old/new effect;" (102)]. Specifically, Matsuoka et al. (103) using repetition priming found that schizophrenia patients showed no effect of immediate stimulus repetition on late ERPs that could index a failure to use information from preceding stimuli.

However, these deficits between groups only reached trend level in the LAG condition, which is consistent with previous studies showing that suppression of ERPs (78, 104) dissolves with lag between repetitions.

LIMITATIONS

There are several limitations associated with this study. Firstly, we only included a relatively small sample of patients with schizophrenia. As a result, the lack of significant correlations between behavioral and neuroimaging measures might be due to insufficient statistical power. In addition, we did not systematically assess the contribution of eye movements toward differences in both behavior and MEG-data. Finally, observations in deep brain structures like the thalamus with MEG can be challenging because of the decay of the magnetic field. However, the large effect size ($d = 0.98$) of our result support the feasibility of MEG in combination with individual anatomical information to assess thalamic signals (101, 105, 106).

SUMMARY

The present study provides novel evidence for impaired repetition suppression and repetition enhancement in schizophrenia as reflected by deficits in the experience-dependent modification of beta/gamma-band oscillations as well as ERFs during visual priming. Specifically, schizophrenia patients showed impaired repetition suppression of early and late evoked visual responses as well as gamma-band oscillations. In the context of predictive coding, reduced gamma-band activity may lead to impaired feed-forward signaling which could then lead to reduced repetition suppression and enhancement.

Since deficits in repetition suppression have been found to be present even before the onset of the disorder (107, 108), it will be important to further investigate neural mechanisms

of repetition suppression and their impairment in at-risk populations as well as in larger cohorts of schizophrenia patients to examine whether effects of reduced repetition suppression involve aberrant connectivity between cortical areas.

DATA AVAILABILITY STATEMENT

The raw data supporting the conclusions of this article will be made available by the authors, without undue reservation.

ETHICS STATEMENT

The study was approved by the ethical committee of the Goethe University Frankfurt. The patients/participants provided their written informed consent to participate in this study.

AUTHOR CONTRIBUTIONS

AS contributed to design, recordings, analyses, and write-up of the study. TG-'t-J contributed to analyses and write-up of the study. MW, MG, WS, and PU (leading investigator) are senior scientists who supervised the entire study, from design to final submission.

FUNDING

This study was supported by the German-Israeli Foundation for Scientific Research and Development (GIF-Grant No. 1071).

ACKNOWLEDGMENTS

We would like to thank Luiz Lana for help with programming the randomization to individually shuffle stimuli sequences.

SUPPLEMENTARY MATERIAL

The Supplementary Material for this article can be found online at: https://www.frontiersin.org/articles/10.3389/fpsyt.2020.561973/full#supplementary-material

REFERENCES

1. Heinrichs RW. The primacy of cognition in schizophrenia. *Am Psychol.* (2005) 60:229–42. doi: 10.1037/0003-066X.60.3.229
2. Green MF. What are the functional consequences of neurocognitive deficits in schizophrenia? *Am J Psychiatry.* (1996) 153:321–30. doi: 10.1176/ajp.153.3.321
3. Green MF, Kern RS, Braff DL, Mintz J. Neurocognitive deficits and functional outcome in schizophrenia: are we measuring the "right stuff"? *Schizophr Bull.* (2000) 26:119–36. doi: 10.1093/oxfordjournals.schbul.a033430
4. Heinrichs RW, Zakzanis KK. Neurocognitive deficit in schizophrenia: a quantitative review of the evidence. *Neuropsychology.* (1998) 12:426–45. doi: 10.1037/0894-4105.12.3.426
5. Javitt DC, Shelley AM, Silipo G, Lieberman JA. Deficits in auditory and visual context-dependent processing in schizophrenia: defining the pattern. *Arch Gen Psychiatry.* (2000) 57:1131–7. doi: 10.1001/archpsyc.57.12.1131
6. Uhlhaas PJ, Mishara AL. Perceptual anomalies in schizophrenia: integrating phenomenology and cognitive neuroscience. *Schizophr Bull.* (2007) 33:142–56. doi: 10.1093/schbul/sbl047
7. Stephan KE, Baldeweg T, Friston KJ. Synaptic plasticity and dysconnection in schizophrenia. *Biol Psychiatry.* (2006) 59:929–39. doi: 10.1016/j.biopsych.2005.10.005
8. Stephan KE, Friston KJ, Frith CD. Dysconnection in schizophrenia: from abnormal synaptic plasticity to failures of self-monitoring. *Schizophr Bull.* (2009) 35:509–27. doi: 10.1093/schbul/sbn176
9. Castellucci V, Pinsker H, Kupfermann I, Kandel ER. Neuronal mechanisms of habituation and dishabituation of the gill-withdrawal reflex in Aplysia. *Science.* (1970) 167:1745–8. doi: 10.1126/science.167.3926.1745
10. Bliss TVP, Collingridge GL. A synaptic model of memory: long-term potentiation in the hippocampus. *Nature.* (1993) 361:31–9. doi: 10.1038/361031a0
11. Pastalkova E, Serrano P, Pinkhasova D, Wallace E, Fenton AA, Sacktor TC. Storage of spatial information by the maintenance mechanism of LTP. *Science.* (2006) 313:1141–4. doi: 10.1126/science.1128657
12. Whitlock JR, Heynen AJ, Shuler MG, Bear MF. Learning induces long-term potentiation in the hippocampus. *Science.* (2006) 313:1093–7. doi: 10.1126/science.1128134
13. Collingridge GL, Bliss TVP. NMDA receptors - their role in long-term potentiation. *TINS.* (1987) 10:288–93. doi: 10.1016/0166-2236(87)90175-5
14. Kirov G, Pocklington AJ, Holmans P, Ivanov D, Ikeda M, Ruderfer D, et al. De novo CNV analysis implicates specific abnormalities of postsynaptic signaling complexes in the pathogenesis of schizophrenia. *Mol Psychiatry.* (2012) 17:142–53. doi: 10.1038/mp.2011.154
15. Moghaddam B, Javitt D. From revolution to evolution: the glutamate hypothesis of schizophrenia and its implication for treatment. *Neuropsychopharmacology.* (2012) 37:4–15. doi: 10.1038/npp.2011.181
16. Aleman A, Hijman R, de Haan EH, Kahn RS. Memory impairment in schizophrenia: a meta-analysis. *Am J Psychiatry.* (1999) 156:1358–66. doi: 10.1176/ajp.156.9.1358
17. Danion JM, Meulemans T, Kauffmann-Muller F, Vermaat H. Intact implicit learning in schizophrenia. *Am J Psychiatry.* (2001) 158:944–8. doi: 10.1176/appi.ajp.158.6.944
18. Horan WP, Green MF, Knowlton BJ, Wynn JK, Mintz J, Nuechterlein KH. Impaired implicit learning in schizophrenia. *Neuropsychology.* (2008) 22:606–17. doi: 10.1037/a0012602
19. Gomar JJ, Pomarol-Clotet E, Sarró S, Salvador R, Myers CE, McKenna PJ. Procedural learning in schizophrenia: reconciling the discrepant findings. *Biol Psychiatry.* (2011) 69:49–54. doi: 10.1016/j.biopsych.2010.07.013
20. Tulving E, Schacter DL. Priming and human memory systems. *Science.* (1990) 247:301–6. doi: 10.1126/science.2296719
21. Schacter DL, Buckner RL. Priming and the brain. *Neuron.* (1998) 20:185–95. doi: 10.1016/S0896-6273(00)80448-1
22. Miller EK, Li L, Desimone R. A neural mechanism for working and recognition memory in inferior temporal cortex. *Science.* (1991) 254:1377–9. doi: 10.1126/science.1962197
23. Henson R, Shallice T, Dolan R. Neuroimaging evidence for dissociable forms of repetition priming. *Science.* (2000) 287:1269–72. doi: 10.1126/science.287.5456.1269
24. Buckner RL, Goodman J, Burock M, Rotte M, Koutstaal W, Schacter D, et al. Functional-anatomic correlates of object priming in humans revealed by rapid presentation event-related fMRI. *Neuron.* (1998) 20:285–96. doi: 10.1016/S0896-6273(00)80456-0
25. Gruber T, Müller MM. Effects of picture repetition on induced gamma band responses, evoked potentials, and phase synchrony in the human EEG. *Cogn Brain Res.* (2002) 13:377–92. doi: 10.1016/S0926-6410(01)00130-6
26. Friese U, Rahm B, Hassler U, Kaiser J, Gruber T. Repetition suppression and effects of familiarity on blood oxygenation level dependent signal and gamma-band activity. *Neuroreport.* (2012) 23:757–61. doi: 10.1097/WNR.0b013e328356b173

27. Turk-Browne NB, Yi D-J, Leber AB, Chun MM. Visual quality determines the direction of neural repetition effects. *Cereb Cortex.* (2007) 17:425–33. doi: 10.1093/cercor/bhj159
28. de Gardelle V, Waszczuk M, Egner T, Summerfield C. Concurrent repetition enhancement and suppression responses in extrastriate visual cortex. *Cereb Cortex.* (2013) 23:2235–44. doi: 10.1093/cercor/bhs211
29. Müller NG, Strumpf H, Scholz M, Baier B, Melloni L. Repetition suppression versus enhancement–it's quantity that matters. *Cereb Cortex.* (2013) 23:315–22. doi: 10.1093/cercor/bhs009
30. Desimone R. Neural mechanisms for visual memory and their role in attention. *Proc Natl Acad Sci USA.* (1996) 93:13494–9. doi: 10.1073/pnas.93.24.13494
31. Wiggs CL, Martin A. Properties and mechanisms of perceptual priming. *Curr Opin Neurobiol.* (1998) 8:227–33. doi: 10.1016/S0959-4388(98)80144-X
32. Summerfield C, Trittschuh EH, Monti JM, Mesulam M-M, Egner T. Neural repetition suppression reflects fulfilled perceptual expectations. *Nat Neurosci.* (2008) 11:1004–6. doi: 10.1038/nn.2163
33. Todorovic A, van Ede F, Maris E, de Lange FP. Prior expectation mediates neural adaptation to repeated sounds in the auditory cortex: an MEG study. *J Neurosci.* (2011) 31:9118–23. doi: 10.1523/JNEUROSCI.1425-11.2011
34. Friston K. A theory of cortical responses. *Phil Trans R Soc B Biol Sci.* (2005) 360:815–36. doi: 10.1098/rstb.2005.1622
35. Auksztulewicz R, Friston K. Repetition suppression and its contextual determinants in predictive coding. *Cortex.* (2016) 80:125–40. doi: 10.1016/j.cortex.2015.11.024
36. Adler LE, Pachtman E, Franks RD, Pecevich M, Waldo MC, Freedman R. Neurophysiological evidence for a defect in neuronal mechanisms involved in sensory gating in schizophrenia. *Biol Psychiatry.* (1982) 17:639–54.
37. Adler LE, Waldo MC, Freedman R. Neurophysiologic studies of sensory gating in schizophrenia: comparison of auditory and visual responses. *Biol Psychiatry.* (1985) 20:1284–96. doi: 10.1016/0006-3223(85)90113-1
38. Freedman R, Adler LE, Gerhardt GA, Waldo M, Baker N, Rose GM, et al. Neurobiological studies of sensory gating in schizophrenia. *Schizophr Bull.* (1987) 13:669–78. doi: 10.1093/schbul/13.4.669
39. Freedman R, Waldo M, Bickford-Wimer P, Nagamoto H. Elementary neuronal dysfunctions in schizophrenia. *Schizophr Res.* (1991) 4:233–43. doi: 10.1016/0920-9964(91)90035-P
40. Olincy A, Braff DL, Adler LE, Cadenhead KS, Calkins ME, Dobie DJ, et al. Inhibition of the P50 cerebral evoked response to repeated auditory stimuli: results from the Consortium on Genetics of Schizophrenia. *Schizophr Res.* (2010) 119:175–82. doi: 10.1016/j.schres.2010.03.004
41. Braff DL, Geyer MA. Sensorimotor gating and schizophrenia. Human and animal model studies. *Arch Gen Psychiatry.* (1990) 47:181–8. doi: 10.1001/archpsyc.1990.01810140081011
42. Braff DL, Grillon C, Geyer MA. Gating and habituation of the startle reflex in schizophrenic patients. *Arch Gen Psychiatry.* (1992) 49:206–15. doi: 10.1001/archpsyc.1992.01820030038005
43. Braff DL, Geyer MA, Swerdlow NR. Human studies of prepulse inhibition of startle: normal subjects, patient groups, and pharmacological studies. *Psychopharmacology.* (2001) 156:234–58. doi: 10.1007/s002130100810
44. Rivolta D, Castellanos NP, Stawowsky C, Helbling S, Wibral M, Grützner C, et al. Source-reconstruction of event-related fields reveals hyperfunction and hypofunction of cortical circuits in antipsychotic-naive, first-episode schizophrenia patients during Mooney face processing. *J Neurosci.* (2014) 34:5909–17. doi: 10.1523/JNEUROSCI.3752-13.2014
45. Williams LE, Blackford JU, Luksik A, Gauthier I, Heckers S. Reduced habituation in patients with schizophrenia. *Schizophr Res.* (2013) 151:124–32. doi: 10.1016/j.schres.2013.10.017
46. Lee J, Reavis EA, Engel SA, Altshuler LL, Cohen MS, Glahn DC, et al. fMRI evidence of aberrant neural adaptation for objects in schizophrenia and bipolar disorder. *Hum Brain Mapp.* (2019) 40:1608–17. doi: 10.1002/hbm.24472
47. Coffman BA, Haigh SM, Murphy TK, Salisbury DF. Impairment in Mismatch Negativity but not Repetition Suppression in Schizophrenia. *Brain Topogr.* (2017) 30:521–30. doi: 10.1007/s10548-017-0571-1
48. Sauer A, Zeev-Wolf M, Grent-'t-Jong T, Recasens M, Wacongne C, Wibral M, et al. Impairment in predictive processes during auditory mismatch negativity in ScZ: Evidence from event-related fields. *Hum Brain Mapp.* (2017) 38:5082–93. doi: 10.1002/hbm.23716
49. Wynn JK, Engel SA, Lee J, Reavis EA, Green MF. Evidence for intact stimulus-specific neural adaptation for visual objects in schizophrenia and bipolar disorder: an ERP study. *PLoS ONE.* (2019) 14:e0221409. doi: 10.1371/journal.pone.0221409
50. Reavis EA, Lee J, Wynn JK, Engel SA, Cohen MS, Nuechterlein KH, et al. Assessing neural tuning for object perception in schizophrenia and bipolar disorder with multivariate pattern analysis of fMRI data. *Neuroimage Clin.* (2017) 16:491–7. doi: 10.1016/j.nicl.2017.08.023
51. Kovács G, Grotheer M, Münke L, Kéri S, Nenadić I. Significant repetition probability effects in schizophrenia. *Psychiatry Res Neuroimaging.* (2019) 290:22–9. doi: 10.1016/j.pscychresns.2019.05.006
52. Wespatat V, Tennigkeit F, Singer W. Phase sensitivity of synaptic modifications in oscillating cells of rat visual cortex. *J Neurosci.* (2004) 24:9067–75. doi: 10.1523/JNEUROSCI.2221-04.2004
53. Galuske RAW, Munk MHJ, Singer W. Relation between gamma oscillations and neuronal plasticity in the visual cortex. *PNAS.* (2019) 116:23317–25. doi: 10.1073/pnas.1901277116
54. Huerta PT, Lisman JE. Heightened synaptic plasticity of hippocampal CA1 neurons during a cholinergically induced rhythmic state. *Nature.* (1993) 364:723–5. doi: 10.1038/364723a0
55. Uhlhaas PJ, Singer W. Abnormal neural oscillations and synchrony in schizophrenia. *Nat Rev Neurosci.* (2010) 11:100–13. doi: 10.1038/nrn2774
56. Kwon JS, O'Donnell BF, Wallenstein GV, Greene RW, Hirayasu Y, Nestor PG, et al. Gamma frequency-range abnormalities to auditory stimulation in schizophrenia. *Arch Gen Psychiatry.* (1999) 56:1001–5. doi: 10.1001/archpsyc.56.11.1001
57. Spencer KM, Niznikiewicz MA, Shenton ME, McCarley RW. Sensory-evoked gamma oscillations in chronic schizophrenia. *Biol Psychiatry.* (2008) 63:744–7. doi: 10.1016/j.biopsych.2007.10.017
58. Sun L, Castellanos N, Grützner C, Koethe D, Rivolta D, Wibral M, et al. Evidence for dysregulated high-frequency oscillations during sensory processing in medication-naïve, first episode schizophrenia. *Schizophr Res.* (2013) 150:519–25. doi: 10.1016/j.schres.2013.08.023
59. Grent-'t-Jong T, Gajwani R, Gross J, Gumley AI, Krishnadas R, Lawrie SM, et al. Association of magnetoencephalographically measured high-frequency oscillations in visual cortex with circuit dysfunctions in local and large-scale networks during emerging psychosis. *JAMA Psychiatry.* (2020) 77:852. doi: 10.1001/jamapsychiatry.2020.0284
60. Ryman SG, Cavanagh JF, Wertz CJ, Shaff NA, Dodd AB, Stevens B, et al. Impaired midline theta power and connectivity during proactive cognitive control in schizophrenia. *Biol Psychiatry.* (2018) 84:675–83. doi: 10.1016/j.biopsych.2018.04.021
61. Benes FM, Berretta S. GABAergic interneurons: implications for understanding schizophrenia and bipolar disorder. *Neuropsychopharmacology.* (2001) 25:1–27. doi: 10.1016/S0893-133X(01)00225-1
62. Lewis DA, Curley AA, Glausier JR, Volk DW. Cortical parvalbumin interneurons and cognitive dysfunction in schizophrenia. *TINS.* (2012) 35:57–67. doi: 10.1016/j.tins.2011.10.004
63. Kegeles LS, Mao X, Stanford AD, Girgis R, Ojeil N, Xu X, et al. Elevated prefrontal cortex γ-aminobutyric acid and glutamate-glutamine levels in schizophrenia measured in vivo with proton magnetic resonance spectroscopy. *Arch Gen Psychiatry.* (2012) 69:449–9. doi: 10.1001/archgenpsychiatry.2011.1519
64. Pocklington AJ, Rees E, Walters JTR, Han J, Kavanagh DH, Chambert KD, et al. Novel findings from cnvs implicate inhibitory and excitatory signaling complexes in schizophrenia. *Neuron.* (2015) 86:1203–14. doi: 10.1016/j.neuron.2015.04.022
65. Saß H, Wittchen H-U, Zaudig M, Houben I. *Diagnostisches und Statistisches Manual Psychischer Störungen - Textrevision - DSM-IV-TR.* Göttingen: Hogrefe. (2003).

66. Kay SR, Fiszbein A, Opler LA. The positive and negative syndrome scale (PANSS) for schizophrenia. *Schizophr Bull.* (1987) 13:261–76. doi: 10.1093/schbul/13.2.261
67. Lindenmayer JP, Bernstein-Hyman R, Grochowski S. A new five factor model of schizophrenia. *Psychiatr Q.* (1994) 65:299–322. doi: 10.1007/BF02354306
68. Cuesta MJ, Peralta V. Psychopathological dimensions in schizophrenia. *Schizophr Bull.* (1995) 21:473–82. doi: 10.1093/schbul/21.3.473
69. Keefe R. The Brief Assessment of Cognition in Schizophrenia: reliability, sensitivity, and comparison with a standard neurocognitive battery. *Schizophr Res.* (2004) 68:283–97. doi: 10.1016/j.schres.2003.09.011
70. Keefe RSE, Harvey PD, Goldberg TE, Gold JM, Walker TM, Kennel C, et al. Norms and standardization of the Brief Assessment of Cognition in Schizophrenia (BACS). *Schizophr Res.* (2008) 102:108–15. doi: 10.1016/j.schres.2008.03.024
71. Oldfield RC. The assessment and analysis of handedness: the Edinburgh inventory. *Neuropsychologia.* (1971) 9:97–113. doi: 10.1016/0028-3932(71)90067-4
72. Snodgrass JG, Vanderwart M. A standardized set of 260 pictures: Norms for name agreement, image agreement, familiarity, and visual complexity. *J Exp Psychol Hum Learn Memory.* (1980) 6:174–215. doi: 10.1037/0278-7393.6.2.174
73. Rossion B, Pourtois G. Revisiting snodgrass and Vanderwart's object database: color and texture improve object recognition. *J Vision.* (2001) 1:413. doi: 10.1167/1.3.413
74. Oostenveld R, Fries P, Maris E, Schoffelen J-M. FieldTrip: open source software for advanced analysis of MEG, EEG, and invasive electrophysiological data. *Comput Intellig Neurosci.* (2011) 2011:156869–9. doi: 10.1155/2011/156869
75. Van Veen BD, van Drongelen W, Yuchtman M, Suzuki A. Localization of brain electrical activity via linearly constrained minimum variance spatial filtering. *IEEE Trans Biomed Eng.* (1997) 44:867–80. doi: 10.1109/10.623056
76. Tzourio-Mazoyer N, Landeau B, Papathanassiou D, Crivello F, Etard O, Delcroix N, et al. Automated anatomical labeling of activations in SPM using a macroscopic anatomical parcellation of the MNI MRI single-subject brain. *NeuroImage.* (2002) 15:273–89. doi: 10.1006/nimg.2001.0978
77. Rugg MD, Soardi M, Doyle MC. Modulation of event-related potentials by the repetition of drawings of novel objects. *Brain Res Cogn Brain Res.* (1995) 3:17–24. doi: 10.1016/0926-6410(95)00014-3
78. Gruber T, Malinowski P, Müller MM. Modulation of oscillatory brain activity and evoked potentials in a repetition priming task in the human EEG. *Europ J Neurosci.* (2004) 19:1073–82. doi: 10.1111/j.0953-816X.2004.03176.x
79. Pourtois G, Rauss KS, Vuilleumier P, Schwartz S. Effects of perceptual learning on primary visual cortex activity in humans. *Vision Res.* (2008) 48:55–62. doi: 10.1016/j.visres.2007.10.027
80. Gras-Vincendon A, Danion JM, Grangé D, Bilik M, Willard-Schroeder D, Sichel JP, et al. Explicit memory, repetition priming and cognitive skill learning in schizophrenia. *Schizophr Res.* (1994) 13:117–26. doi: 10.1016/0920-9964(94)90092-2
81. Spataro P, Saraulli D, Cestari V, Costanzi M, Sciarretta A, Rossi-Arnaud C. Implicit memory in schizophrenia: a meta-analysis. *Compr Psychiatry.* (2016) 69:136–44. doi: 10.1016/j.comppsych.2016.05.013
82. Maccotta L, Buckner RL. Evidence for neural effects of repetition that directly correlate with behavioral priming. *J Cog Neurosci.* (2004) 16:1625–32. doi: 10.1162/0898929042568451
83. Wig GS, Grafton ST, Demos KE, Kelley WM. Reductions in neural activity underlie behavioral components of repetition priming. *Nat Neurosci.* (2005) 8:1228–33. doi: 10.1038/nn1515
84. Sayres R, Grill-Spector K. Object-Selective Cortex Exhibits Performance-Independent Repetition Suppression. *J Neurophysiol.* (2006) 95:995–1007. doi: 10.1152/jn.00500.2005
85. McMahon DBT, Olson CR. Repetition suppression in monkey inferotemporal cortex: relation to behavioral priming. *J Neurophysiol.* (2007) 97:3532–43. doi: 10.1152/jn.01042.2006
86. Gilbert JR, Gotts SJ, Carver FW, Martin A. Object repetition leads to local increases in the temporal coordination of neural responses. *Front Hum Neurosci.* (2010) 4:30. doi: 10.3389/fnhum.2010.00030
87. Spencer KM, Nestor PG, Niznikiewicz MA, Salisbury DF, Shenton ME, McCarley RW. Abnormal neural synchrony in schizophrenia. *J Neurosci.* (2003) 23:7407–11. doi: 10.1523/JNEUROSCI.23-19-07407.2003
88. Thuné H, Recasens M, Uhlhaas PJ. The 40-Hz auditory steady-state response in patients with schizophrenia: a meta-analysis. *JAMA Psychiatry.* (2016) 73:1145–53. doi: 10.1001/jamapsychiatry.2016.2619
89. Rao RP, Ballard DH. Predictive coding in the visual cortex: a functional interpretation of some extra-classical receptive-field effects. *Nat Neurosci.* (1999) 2:79–87. doi: 10.1038/4580
90. Peter A, Uran C, Klon-Lipok J, Roese R, van Stijn S, Barnes W, et al. Surface color and predictability determine contextual modulation of V1 firing and gamma oscillations. *Elife.* (2019) 8:83. doi: 10.7554/eLife.42101
91. Arnal LH, Giraud A-L. Cortical oscillations and sensory predictions. *TICS.* (2012) 16:390–8. doi: 10.1016/j.tics.2012.05.003
92. Michalareas G, Vezoli J, van Pelt S, Schoffelen J-M, Kennedy H, Fries P. Alpha-beta and gamma rhythms subserve feedback and feedforward influences among human visual cortical areas. *Neuron.* (2016) 89:384–97. doi: 10.1016/j.neuron.2015.12.018
93. Jeffreys DA, Axford JG. Source locations of pattern-specific components of human visual evoked potentials. I. Component of striate cortical origin. *Exp Brain Res.* (1972) 16:1–21. doi: 10.1007/BF00233371
94. Jeffreys DA, Axford JG. Source locations of pattern-specific components of human visual evoked potentials. II. Component of extrastriate cortical origin. *Exp Brain Res.* (1972) 16:22–40. doi: 10.1007/BF00233372
95. Clark VP, Fan S, Hillyard SA. Identification of early visual evoked potential generators by retinotopic and topographic analyses. *Hum Brain Mapp.* (1994) 2:170–87. doi: 10.1002/hbm.460020306
96. Mangun GR. Neural mechanisms of visual selective attention. *Psychophysiology.* (1995) 32:4–18. doi: 10.1111/j.1469-8986.1995.tb03400.x
97. Di Russo F, Martínez A, Hillyard SA. Source analysis of event-related cortical activity during visuo-spatial attention. *Cereb Cortex.* (2003) 13:486–99. doi: 10.1093/cercor/13.5.486
98. Grent-'t-Jong T, Rivolta D, Sauer A, Grube M, Singer W, Wibral M, et al. MEG-measured visually induced gamma-band oscillations in chronic schizophrenia: evidence for impaired generation of rhythmic activity in ventral stream regions. *Schizophr Res.* (2016) 176:177–85. doi: 10.1016/j.schres.2016.06.003
99. Andreasen NC, Arndt S, Swayze V, Cizadlo T, Flaum M, O'Leary D, et al. Thalamic abnormalities in schizophrenia visualized through magnetic resonance image averaging. *Science.* (1994) 266:294–8. doi: 10.1126/science.7939669
100. Pratt J, Dawson N, Morris BJ, Grent-'t-Jong T, Roux F, Uhlhaas PJ. Thalamo-cortical communication, glutamatergic neurotransmission and neural oscillations: a unique window into the origins of ScZ? *Schizophr Res.* (2017) 180:4–12. doi: 10.1016/j.schres.2016.05.013
101. Grent-'t-Jong T, Rivolta D, Gross J, Gajwani R, Lawrie SM, Schwannauer M, et al. Acute ketamine dysregulates task-related gamma-band oscillations in thalamo-cortical circuits in schizophrenia. *Brain.* (2018) 141:2511–26. doi: 10.1093/brain/awy175
102. Rugg MD, Curran T. Event-related potentials and recognition memory. *TICS.* (2007) 11:251–7. doi: 10.1016/j.tics.2007.04.004
103. Matsuoka H, Matsumoto K, Yamazaki H, Sakai H, Miwa S, Yoshida S, et al. Lack of repetition priming effect on visual event-related potentials in schizophrenia. *Biol Psychiatry.* (1999) 46:137–40. doi: 10.1016/S0006-3223(98)00330-8
104. Nagy ME, Rugg MD. Modulation of event-related potentials by word repetition: the effects of inter-item lag. *Psychophysiology.* (1989) 26:431–6. doi: 10.1111/j.1469-8986.1989.tb01946.x
105. Attal Y, Bhattacharjee M, Yelnik J, Cottereau B, Lefèvre J, Okada Y, et al. Modeling and detecting deep brain activity with MEG & EEG. *Conf Proc IEEE Eng Med Biol Soc.* (2007) 2007:4937–40. doi: 10.1109/IEMBS.2007.4353448

106. Roux F, Wibral M, Singer W, Aru J, Uhlhaas PJ. The phase of thalamic alpha activity modulates cortical gamma-band activity: evidence from resting-state meg recordings. *J Neurosci.* (2013) 33:17827–35. doi: 10.1523/JNEUROSCI.5778-12.2013
107. Cadenhead KS, Light GA, Shafer KM, Braff DL. P50 suppression in individuals at risk for schizophrenia: the convergence of clinical, familial, and vulnerability marker risk assessment. *Biol Psychiatry.* (2005) 57:1504–9. doi: 10.1016/j.biopsych.2005.03.003
108. Brockhaus-Dumke A, Schultze-Lutter F, Mueller R, Tendolkar I, Bechdolf A, Pukrop R, et al. Sensory gating in schizophrenia: p50 and n100 gating in antipsychotic-free subjects at risk, first-episode, and chronic patients. *Biol Psychiatry.* (2008) 64:376. doi: 10.1016/j.biopsych.2008.02.006

Conflict of Interest: The authors declare that the research was conducted in the absence of any commercial or financial relationships that could be construed as a potential conflict of interest.

frontiers in Psychiatry

ORIGINAL RESEARCH
published: 16 December 2020
doi: 10.3389/fpsyt.2020.551952

Test–Retest Reliability of Magnetoencephalography Resting-State Functional Connectivity in Schizophrenia

Felicha T. Candelaria-Cook and Julia M. Stephen*

The Mind Research Network, Albuquerque, NM, United States

The reliability of magnetoencephalography (MEG) resting-state functional connectivity in schizophrenia (SZ) is unknown as previous research has focused on healthy controls (HC). Here, we examined reliability in 26 participants (13-SZ, 13-HC). Eyes opened and eyes closed resting-state data were collected on 4 separate occasions during 2 visits, 1 week apart. For source modeling, we used minimum norm software to apply dynamic statistical parametric mapping. Source analyses compared the following functional connectivity metrics from each data run: coherence (coh), imaginary coherence (imcoh), pairwise phase consistency (ppc), phase-locking value (plv), phase lag index (pli), weighted phase lag index (wpli), and weighted phase lag index debiased (wpli2). Intraclass correlation coefficients (ICCs) were calculated for whole brain, network, and network pair averages. For reliability, ICCs above 0.75 = excellent, above 0.60 = good, above 0.40 = fair, and below 0.40 = poor reliability. We found the reliability of these metrics varied greatly depending on frequency band, network, network pair, and participant group examined. Broadband (1–58 Hz) whole brain averages in both HC and SZ showed excellent reliability for wpli2, and good to fair reliability for ppc, plv, and coh. Broadband network averages showed excellent to good reliability across 1 hour and 1 week for coh, imcoh, ppc, plv, wpli within default mode, cognitive control, and visual networks in HC, while the same metrics had excellent to fair reliability in SZ. Regional network pair averages showed good to fair reliability for coh, ppc, plv within default mode, cognitive control and visual network pairs in HC and SZ. In general, HC had higher reliability compared to SZ, and the default mode, cognitive control, and visual networks had higher reliability compared to somatosensory and auditory networks. Similar reliability levels occurred for both eyes opened and eyes closed resting-states for most metrics. The functional connectivity metrics of coh, ppc, and plv performed best across 1 hour and 1 week in HC and SZ. We also found that SZ had reduced coh, plv, and ppc in the dmn average and pair values indicating dysconnectivity in SZ. These findings encourage collecting both eyes opened and eyes closed resting-state MEG, while demonstrating that clinical populations may differ in reliability.

Keywords: schizophrenia, MEG, test–retest reliability, resting-state, functional connectivity

OPEN ACCESS

Edited by:
Peter Uhlhaas,
University of Glasgow,
United Kingdom

Reviewed by:
Guido Nolte,
University Medical Center
Hamburg-Eppendorf, Germany
Srikantan S. Nagarajan,
University of California, San Francisco,
United States

****Correspondence:***
Felicha T. Candelaria-Cook
fccook@mrn.org

Specialty section:
This article was submitted to Neuroimaging and Stimulation, a section of the journal Frontiers in Psychiatry

Received: *14 April 2020*
Accepted: *23 November 2020*
Published: *16 December 2020*

Citation:
Candelaria-Cook FT and Stephen JM (2020) Test–Retest Reliability of Magnetoencephalography Resting-State Functional Connectivity in Schizophrenia. Front. Psychiatry 11:551952. doi: 10.3389/fpsyt.2020.551952

INTRODUCTION

Magnetoencephalography (MEG) is an advantageous neuroimaging tool to study psychosis due to its safety as a non-invasive test, along with the high dimensional data it provides on neuronal activity, oscillatory dynamics, and connectivity at a millisecond time scale. The spontaneous oscillatory signals captured by MEG during a resting-state can be used to estimate neural interactions between brain regions and reveal network disorganization and abnormalities in schizophrenia (SZ) and other clinical populations. Despite the increasing prevalence of resting-state MEG research, studies examining the reproducibility and reliability of MEG-derived functional connectivity measures remain scarce, especially in clinical populations where reliability is critical for clinical application.

Previous resting-state MEG test–retest reliability has been evaluated in healthy controls (HC) (1–5), patients with depression (6), and patients with SZ (5). Most test–retest studies use intraclass correlation coefficients (ICCs) or Spearman correlations to report and categorize degree of reliability. To model and interpret an ICC, with values ranging from 0 to 1, excellent reliability is defined as ICC $>$ 0.75, good reliability ICC $=$ 0.75-0.60, fair reliability ICC $=$ 0.59–0.40, and poor reliability ICC $<$ 0.40 (7). In HC, MEG spectral power has good reliability in theta, alpha, and beta bands (ICCs $>$ 0.6) over a 7 day test–retest interval (3) and excellent reliability in theta-gamma bands (ICCs $>$ 0.86) in global and regional spectral measures over both 1 hour and 1 week test–retest intervals (5). The reliability of MEG functional connectivity has varied greatly in HC depending on the connectivity metric used (1, 2, 5) and frequency band studied (4). For example, the reliability of phase-locking value (plv) in alpha, beta, and gamma bands average between ICCs $=$ 0.74–0.82, but dip to ICCs $<$ 0.1 when phase-lag index (pli) is used (2). Conversely, other studies have reported weighted phase-lag index (wpli) and the imaginary part of coherency had excellent to good reliability of global connectivity over 30 trials in alpha and theta bands, but often fair to poor reliability in other frequency bands and in vertex-based connectivity (4). It is clear given the variability of previous MEG functional connectivity findings that more research is needed to reach a consensus on which functional connectivity metric is best suited for MEG resting-state studies.

In clinical populations much less is known about the reliability of MEG functional connectivity metrics. Examining resting-state functional connectivity in patients with SZ can be especially informative given that SZ is often conceptualized as a disorder of altered brain connectivity by the disconnection hypothesis (8) with abnormal resting-state brain networks demonstrating disorganization (9). MEG functional connectivity abnormalities in patients with SZ, quantified by imaginary coherence (imcoh), include decreased left prefrontal cortex and right superior temporal cortex connectivity in alpha band which negatively correlated with negative symptoms, together with increased connectivity in left extrastriate cortex and right inferior prefrontal cortex (10). Other studies using spatial independent component analysis and pairwise correlations found hyperconnectivity within frontal and temporal networks in patients with SZ (11), information which was valuable in improving classification when combined with fMRI functional connectivity (12), in addition to hypoconnectivity between sensorimotor and task positive networks in the delta frequency band (13). Patients with SZ also have shown abnormalities in dynamic functional connectivity by changing meta-states more often than HC and exhibiting greater inter-individual variability (14), metrics which correlated with positive symptoms (15). For a more complete review of MEG abnormalities reported in SZ please refer to the following review papers (16–18). These previous findings, however, have not been replicated or shown test–retest reliability.

Recently we examined the 1 week reliability of MEG resting-state spectral power in a cohort of patients with SZ and HC. Overall we found that spectral power measures (power, normalized power, alpha reactivity) had excellent reliability for both HC and SZ in 1) global power averages in theta-gamma bands, 2) for all frequency bands across sensor regions, and 3) within parietal regions for alpha frequency (5). Furthermore, for patients, higher PANSS positive scores were negatively correlated with reduced parietal alpha normalized power. We also briefly examined a single functional connectivity metric, weighted phase lag index debiased (wpli2), and found poor reliability for the metric in both groups (5). The current study was designed as a follow-up to further explore other functional connectivity metrics which may perform better in patients with SZ. Where the previous study provided an in-depth analysis of MEG spectral power in patients with SZ and HC, the current study aims to provide an in-depth analysis of MEG functional connectivity in patients with SZ and HC.

The current study was designed to determine the test–retest reliability of MEG resting-state functional connectivity over 1 hour and 1 week intervals in psychosis. As such, it is one of the first studies to directly address MEG functional connectivity reliability in patients with SZ. MEG resting-state data were collected in 13 patients with SZ and 13 matched HC. Data were collected across 1 week (2 visits, 2 runs per visit). Each MEG session analyzed included both a 10 min and a 4 min rest session with rest phase alternating between an eyes open and eyes closed state. We hypothesized reliability would be lower in the patient group, when compared to HC, and that certain connectivity metrics, such as wpli2 would have poor reliability, similar to our previous study (5). Furthermore, when directly comparing functional connectivity metrics, we expected patients with SZ to have reduced connectivity when compared to HC, in line with (16). This study compared the reliability of various functional connectivity metrics in source space across 1 hour and 1 week intervals, using coherence (coh), imcoh (imaginary coherence), pairwise phase consistency (ppc), plv (phase-locking value), pli (phase-lag index), wpli (weighted phase lag index), and wpli2 (weighted phase lag index debiased). To determine reliability, ICCs were calculated and compared for whole brain averages, network connectivity averages, and regional connectivity pairs. Furthermore, ICCs were compared between patients with SZ and HC to determine which measures were most stable in a patient population.

TABLE 1 | Participant characteristics.

	Healthy Controls (Mean ±SD)	Patients with Schizophrenia (Mean ±SD)
Demographics		
Gender (M/F)	8/5	8/5
Age (Males)	32.65 ± 8.88	32.98 ± 7.18
Age (Females)	37.95 ± 6.51	38.35 ± 7.99
Education (years) **	15.23 ± 2.13	13.00 ± 1.41
Ethnicity (% Hispanic)	23%	46%
Ethnicity (% non-Hispanic)	77%	54%
Duration of Illness (yrs)	—	15.00 ± 9.34
Data quality		
% Epochs rejected eyes open	3.07 ± 3.47	5.62 ± 3.31
% Epochs rejected eyes closed	1.67 ± 2.40	3.65 ± 6.82
% Epochs rejected total	2.39 ± 2.71	4.64 ± 2.56
Avg # epochs Rest10 total	286.85 ± 20.49	282.81 ± 28.85
Avg # epochs Rest4 total	114.92 ± 7.84	115.23 ± 10.62
Avg Euclidean distance Rest10	4.62 mm	6.06 mm
Avg Euclidean distance Rest4	4.90 mm	6.12 mm

*Asterisks represent significant differences between groups (**$p < 0.05$). All other comparisons ($p > 0.05$).*

MATERIALS AND METHODS

Participants

The current study used existing data from 13 individuals diagnosed with SZ and 13 HC, age and gender matched (5). All participants were within 21–49 years of age, **Table 1**, and were compensated for their participation. Participant characteristics and procedures will be briefly described here, for further information on methods please refer to (5). Based on the Structured Clinical Interview for DSM-IV-Patient (SCID-IP), SZ participants had a DSM-IV-TR diagnosis of SZ, along with retrospective clinical stability. Based on the Structured Clinical Interview for DSM-IV-Non-patient (SCID-NP), HC participants had no psychiatric or neurological disorders and no history of developmental delays. All participants gave their informed consent according to institutional guidelines. The University of New Mexico Health Sciences Center Human Research Review Committee approved this study. Although participant data and rest preprocessing procedures used here overlap with that presented in (5), the analytic approach used here, specifically focusing on comparing different functional connectivity metrics, is novel and distinct.

Structural MRI Data Acquisition

To map source locations structural MRIs were obtained after MEG scans. Sagittal T1-weighted anatomical MR images were acquired using a Siemens TIM Trio 3 Tesla MRI system with a 32-channel head coil. Parameters of the T1-weighted MPRAGE sequence were: TR = 2,530 ms, TE = 1.64 ms, 3.5 ms, 5.36 ms, 7.22 ms, 9.08 ms, TI = 1,200 ms, 1.0 mm slice thickness, 192 slices, 7° flip angle, field of view (FOV) = 256 mm × 256 mm, matrix = 256 × 256, GRAPPA acceleration = 2 (5).

MEG Behavioral Tasks

Visits occurred 7 days apart. In order to avoid circadian rhythm influence on reliability, time of day was matched between visits. The average time for return visits for HC was 7.54 days ± 60 min and for SZ was 7.84 days ± 51 min. During each visit, the hour long MEG scan began with a 10-min rest task and ended with a 4-min rest task. At the start of each task participants were instructed to monitor prompts to close their eyes or open their eyes and fixate on a white cross. As shown in **Figure 1**, each task alternated between equal phases of eyes closed and eyes opened. The 10-min task, herein referred to as Rest10, changed phase every 2.5 min, while the 4-min task, herein referred to as Rest4, changed phase every 2 min. In total, resting-state activity was recorded during 4 separate runs (Visit1_Rest10, Visit1_Rest4, Visit2_Rest10, Visit2_Rest4).

MEG Data Acquisition and Preprocessing

MEG data were collected with a 306-channel whole-head MEG system (Elekta Neuromag) in a magnetically shielded room (Vacuumschmelze—Ak3B) at the Mind Research Network in Albuquerque, New Mexico. Electro-oculogram and electrocardiogram channels were placed on the participant to monitor heartbeat and eyeblink artifacts. In addition, using three-dimensional digitization equipment (Polhemus FastTrack), four electromagnetic coils were registered to the nasion and preauricular points. During the tasks, data were sampled at 1,000 Hz and a Continuous Head Position Indicator (cHPI) was used to correct for motion. During each visit participants sat upright and head position was monitored closely. Average Euclidean distance was calculated for each task, see **Table 1**. Head position consistency was similar between HC and SZ (all p's > 0.31) (5).

Using Neuromag MaxFilter 2.2 software, raw data were corrected for noise and head motion artifacts with the temporal extension of signal space separation (t-SSS) method with movement compensation (19, 20). For equivalent sensor locations, head position was transformed between visits with the MaxFilter 2.2, MaxMove option. Using signal space projection (SSP) (21) in MNE software (22), data were cleaned from heartbeat and eye-blink artifacts. Any data that failed the automated process was visually inspected and SSPs to remove artifacts were generated manually. After ensuring the data were artifact-free, continuous files were segmented into 2 sec epochs. Epochs were rejected if the magnetic field exceeded 5 pT. Data quality was equivalent between groups (all p's > 0.25), see **Table 1**.

MEG Source Analysis

Similar to previous processing (5), the cortical surface of each participant was reconstructed from T1-weighted MRI files using FreeSurfer. To create a source space of 4.9 m with 4,098 locations per hemisphere, a repeatedly subdivided octahedron was used as the spatial subsampling method. In MNE software (22, 23), dynamic statistical parametric mapping (dSPM) (24) was used

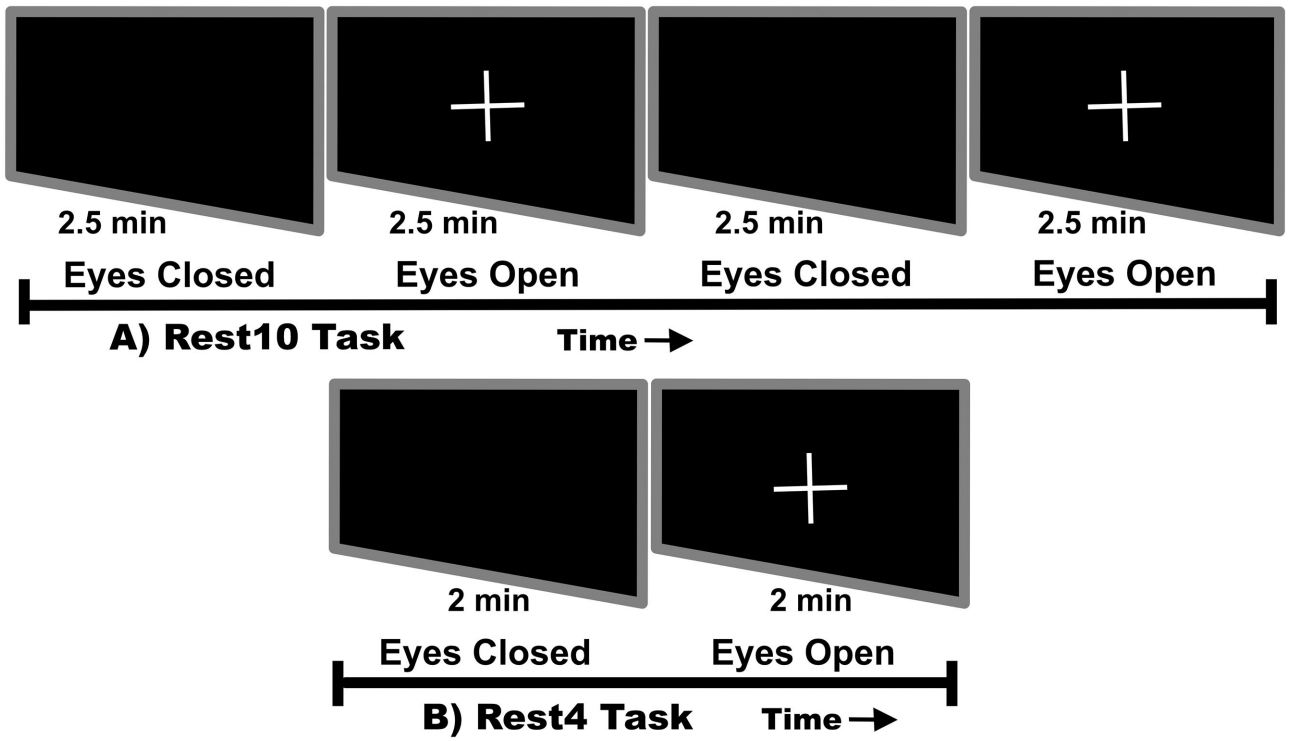

FIGURE 1 | Rest task design. Rest10 alternates between 2.5 min of eyes closed followed by 2.5 min of eyes open fixated on a cross. Rest4 alternates between 2 min of eyes closed followed by 2 min of eyes open fixated on a cross.

to create an anatomically constrained linear estimation inverse model. The dSPM inverse model identified where the estimated current at each cortical surface vertex differed significantly from empty room data. Other data parameters were: depth weight of 0.8, loose constraint of 0.2, orientation of none, and signal-to-noise ratio of 3. A single layer (inner skull) boundary element method (25) was used to create the forward solution. A surface-based source space was used to confine source locations to a fixed surface orientation. When using a fixed source space, loose/free orientations are not normed, leading to signed source activity.

Source estimates were derived from epoch files. Using the FreeSurfer DKT parcellation (26, 27), average time series were extracted for 62 regional labels. The spectral connectivity computation performed in MNE software (version 0.19.0) (22, 23) used multitaper spectrum estimation with 7 DPSS windows. The frequency bands used were defined as: broadband (1–58 Hz), delta (1–4 Hz), theta (5–8 Hz), alpha (9–13 Hz), beta (14–29 Hz), and gamma (31–58 Hz). The connectivity methods extracted were: coh, imcoh, ppc, plv, pli, wpli, and wpli2. Since an aim of the study was to compare available functional connectivity metrics, not create, or modify existing ones, we report connectivity values produced by MNE without modification. In the case of imcoh, MNE uses the original definition (28), not the absolute value, to calculate imcoh values. The results of the spectral connectivity computation were run through custom scripts in MATLAB (2019a, MathWorks) to create whole brain, network, and regional pair averages. Whole brain values were derived from averaging all 62 regional labels, network values were derived from averaging regional labels within predefined clusters (29), and regional pair values were predefined 1-to-1 select regional connections. The labeling used between functional and anatomical regions is shown in **Table 2**. These resting-state networks are semi-independent anatomical clusters of correlated brain activity commonly examined during rest (29). Regional pairs were chosen from the default mode, cognitive control, and visual networks. The pairs represent either unilateral or contralateral connecting nodes within the same resting-state network. The default mode pair was contralateral right hemisphere precuneus to left hemisphere medial orbitofrontal region, the cognitive control pair was unilateral left hemisphere inferior parietal to left hemisphere caudal middle frontal region and the visual network pair was contralateral left hemisphere lateral occipital to right hemisphere middle temporal, **Table 2**. These regions were chosen to maximize regional distance within networks in an effort to minimize the effects of signal leakage on connectivity measures.

Spectral Connectivity Estimation

Using MNE spectral connectivity commands, spectral connectivity was determined for the following 7 metrics: coh, imcoh, ppc, plv, pli, wpli, and wpli2. Coh is a generalization of correlation to the frequency domain, while imcoh is similar but is sensitive to synchronizations of two processes which are time-lagged to each other and avoids volume conduction artifacts by acknowledging that volume conduction does not cause a time-lag (28). Plv characterizes a stable phase relationship between two timecourses in a particular frequency band within

TABLE 2 | Labeling between functional and anatomical regions.

Network	Anatomical areas	
Auditory	superior temporal-L	superior temporal-R
Somatosensory	paracentral-L	paracentral-R
	superior parietal-L	superior parietal-R
	postcentral-L	postcentral-R
	supramarginal-L	supramarginal-R
Visual	cuneus-L	cuneus-R
	lingual-L	lingual-R
	fusiform-L	fusiform-R
	middle temporal-L	middle temporal-R*
	lateral occipital-L*	lateral occipital-R
	pericalcarine-L	pericalcarine-R
Cognitive control	caudal middle frontal-L*	caudal middle frontal-R
	entorhinal-L	entorhinal-R
	inferior parietal-L*	inferior parietal-R
	inferior temporal-L	inferior temporal-R
	insula-L	insula-R
	lateral orbitofrontal-L	lateral orbitofrontal-R
	parahippocampal-L	parahippocampal-R
	pars opercularis-L	pars opercularis-R
	pars orbitalis-L	pars orbitalis-R
	pars triangularis-L	pars triangularis-R
	precentral-L	precentral-R
	rostral middle frontal-L	rostral middle frontal-R
	transverse temporal-L	transverse temporal-R
Default mode	caudal anterior cingulate- L	caudal anterior cingulate- R
	isthmus cingulate-L	isthmus cingulate-R
	medial orbitofrontal-L*	medial orbitofrontal-R
	posterior cingulate-L	posterior cingulate-R
	precuneus-L	precuneus-R*
	rostral anterior cingulate-L	rostral anterior cingulate-R
	superior frontal-L	superior frontal-R

L, left hemisphere; R, right hemisphere.
**Denotes network pair.*

a predefined window (i.e., rhythmic neuronal synchronization) (30). Ppc is very similar to plv, but is bias-free and consistent with population parameter statistics by using an equivalent to squared plv (31). Pli uses similar information but improves upon plv by disregarding zero-lag phase differences (32). Furthermore, pli quantifies the asymmetry of the phase difference distribution and estimates the likelihood for a consistent phase lead or lag between signals from two sensors. Wpli builds upon phase lag index by weighting observed phase leads and lags by the magnitude of the imaginary component of the cross-spectrum (33). These additions reduce sensitivity to uncorrelated noise sources while increasing power. Wpli2 is a debiased estimator of the squared wpli which corrects for sample-size bias in phase-synchronization indices (33). Of the 7 metrics used, 2 are considered spectral coherence metrics (coh, imcoh) and 5 are considered phase estimation metrics (plv, ppc, pli, wpli, wpli2). Furthermore, 4 are robust against spatial leakage artifacts (imcoh, pli, wpli, wpli2) and 3 are not leakage corrected (coh, plv, ppc). Because the goal of the study was to compare available functional connectivity metrics from an already available software package, values were reported without modification. The formulas used by MNE were according to original definition, meaning coh, plv, pli, wpli yielded absolute values, while imcoh did not.

Intraclass Correlation Coefficient

ICCs were calculated with SPSS (version 26 for Macintosh). We used a two-way mixed effects model with absolute agreement, single measurement criteria to estimate ICCs and their 95% confidence intervals. This is often referred to as an ICC (3,1) model. The equation for calculating the ICC is: ICC (3,1) $= MS_B - MS_E/MS_B + (k - 1)\ MS_E$, where MS_E = Error Mean Square, MS_B = Between-subjects Mean Square, and k = number of measurements (34–36). In a two-way mixed effects model, variance consists of 3 components: between-subjects variance (between-subjects mean square), between-tests variance, and random error variance (residual mean squares). Furthermore, by specifying absolute agreement the model is described as: between-subjects variance/(between-subjects variance + between-tests variance + random error variance) (37). ICCs ranged from 0 to 1 with higher values indicating better reliability, any negative values were rescored to zero. Following the guidelines of (7), we defined ICCs as: excellent reliability >0.75, good reliability 0.75–0.60, fair reliability 0.59–0.40, and poor reliability <0.40, similar to (5). ICCs were calculated over 4 timepoints to estimate an average across all 4 runs, and over 2 timepoints to estimate 1 hour and 1 week reliability. In the current study, each rest run was modeled with a fixed effects model, given that identical scanning parameters were used and task familiarity may have occurred. Meanwhile, subjects were modeled with a random effects model, given that sampling and recruitment was random and there was no reason to expect similarity in a spontaneous resting-state task.

Statistical Analysis

To look at group differences in functional connectivity metrics, data from a single visit (Visit1-Run1, Rest10, a 10 min resting-state task) was analyzed. Analysis of Variance (ANOVA) was performed using SPSS (version 26 for Macintosh) with the between-subjects factor of Group (HC, SZ). Each resting state (eyes open, eyes closed) was analyzed separately. The statistical threshold was set at $p < 0.05$ for each individual connectivity metric.

RESULTS

Whole Brain Reliability

Connectivity values within all 62 regional labels were averaged to create a whole brain, global reliability measure. As **Figure 2** shows, global MEG connectivity reliability varied greatly depending on frequency band, connectivity measure, and participant group examined. Within the broadband (1–58 Hz) average ICC for HC, **Figure 2A**: there was excellent reliability

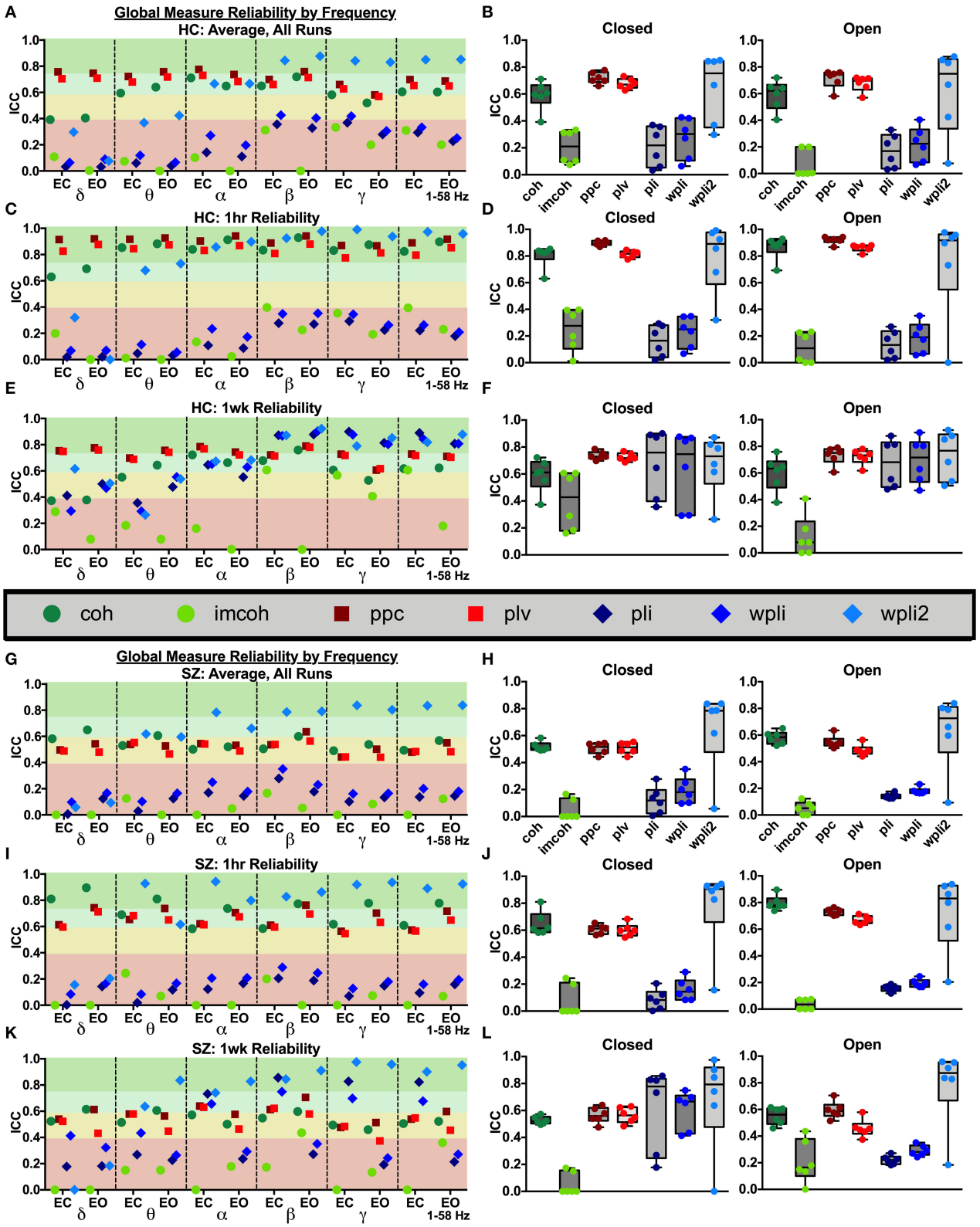

FIGURE 2 | Global reliability. Global ICC estimates for each connectivity measure were calculated in delta-gamma and broadband frequency bands as an average across all runs in HC **(A,B)** and SZ **(G,H)**, across 1 hour in HC **(C,D)** and SZ **(I,J)**, and across 1 week in HC **(E,F)** and SZ **(K,L)**. Data represent mean ICC value. Boxplots contain aggregate information for each connectivity measure in eyes closed and eyes open states.

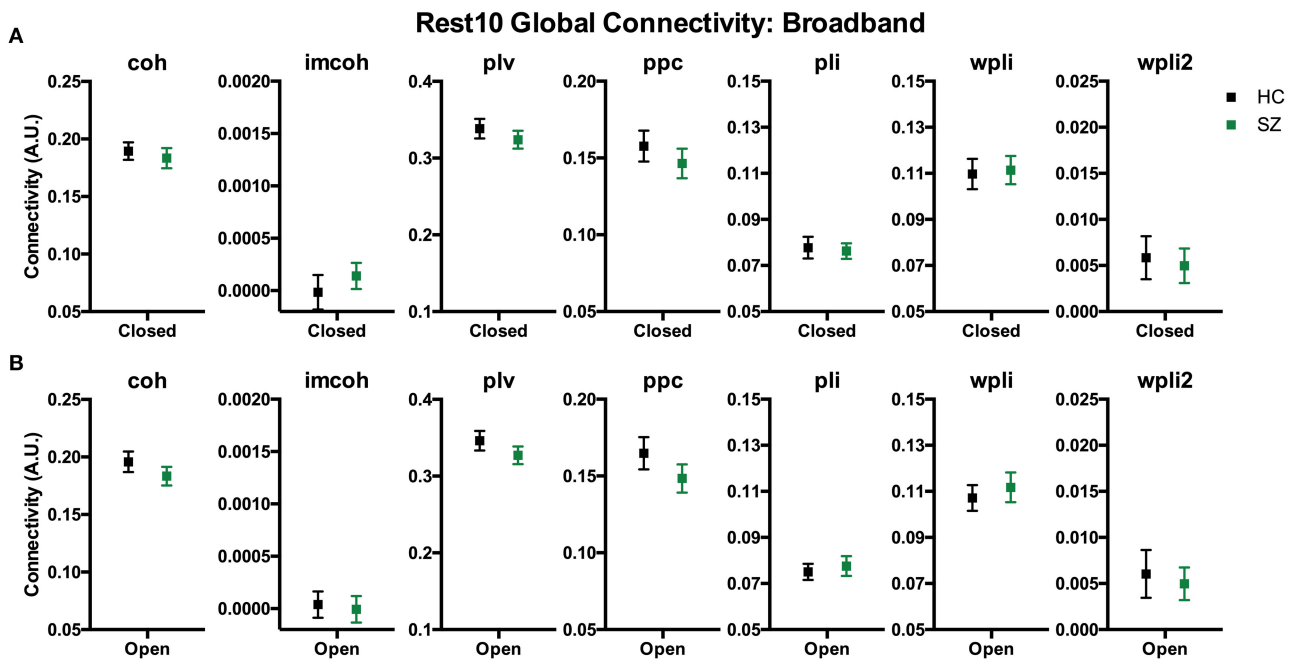

FIGURE 3 | Rest10 global broadband connectivity. Data represent mean (±SEM). Patients with schizophrenia and healthy controls were not significantly different in global broadband connectivity during the eyes closed resting-state **(A)** or eyes open resting-state **(B)**.

for wpli2 (ICC_{wpli2} = 0.85), good reliability for ppc, plv, and coh (ICC_{ppc} = 0.69, ICC_{plv} = 0.65, ICC_{coh} = 0.60), and poor reliability for imcoh, pli, and wpli (ICC_{imcoh} = 0.26, ICC_{pli} = 0.26, ICC_{wpli} = 0.29). Within the broadband average ICC for SZ, **Figure 2G**: there was excellent reliability for wpli2 (ICC_{wpli2} = 0.84), fair reliability for coh, ppc, and plv (ICC_{coh} = 0.53, ICC_{ppc} = 0.52, ICC_{plv} = 0.48) and poor reliability for imcoh, pli, and wpli2 (ICC_{imcoh} = 0.06, ICC_{pli} = 0.14, ICC_{wpli} = 0.19). In both groups, the coh, ppc, and plv had higher reliability across 1 hour than across 1 week, **Figures 2C,E** for HC and **Figures 2I,K** for SZ. Also, delta and theta bands generally had lower reliability than alpha, beta, and gamma bands. In HC and SZ, eyes open and eyes closed resting-states had similar reliability levels for most metrics, however, there were a couple metrics in SZ where eyes closed data had higher reliability than eyes open data, for example, 1 week reliability for pli and wpli (EC ICC_{pli} = 0.82 compared to EO ICC_{pli} = 0.21, and EC ICC_{wpli} = 0.68 compared to EO ICC_{wpli} = 0.27), **Figures 2K,L**.

To compare whole brain functional connectivity metrics between groups (SZ, HC) the main effect of group was examined during Visit 1 for the Rest 10 task. As shown in **Figure 3**, there were no significant group effects for any of the global connectivity metrics for broadband (1–58 Hz) frequency, p's > 0.251, suggesting there were no differences between patients with SZ and HC in the 7 functional connectivity metrics at the global level. Individual frequency bands (delta-gamma) were not explored further since broadband analyses did not reveal a group effect in global connectivity.

Network Reliability

Broadband connectivity averages within 5 networks, the default mode network (DMN), cognitive control network (COGN), visual network (VISN), somatosensory network (SOMN), and auditory network (AUDN), were examined, as shown in **Figure 4**. MEG connectivity network reliability varied greatly depending on network, connectivity measure and participant group. For both HC and SZ, the default mode, cognitive control, and visual networks had higher reliability compared to somatosensory and auditory networks. Within the default mode network, **Figures 4G,H** (DMN), HC had excellent reliability, for coh, imcoh, ppc, plv, and wpli2 (ICC_{coh} = 0.77, ICC_{imcoh} = 0.76, ICC_{ppc} = 0.82, ICC_{plv} = 0.79, ICC_{wpli2} = 0.85) and fair reliability for pli and wpli (ICC_{pli} = 0.48, ICC_{wpli} = 0.50), while SZ had excellent reliability in wpli2 (ICC_{wpli2} = 0.85), good reliability in plv (ICC_{plv} = 0.65), and fair reliability in coh and ppc (ICC_{coh} = 0.59, ICC_{ppc} = 0.57). Within the cognitive control network, **Figures 4G,H** (COGN), HC had excellent reliability for wpli2 (ICC_{wpli2} = 0.80), and good reliability for coh, imcoh, ppc, and plv (ICC_{coh} = 0.66, ICC_{imcoh} = 0.71, ICC_{ppc} = 0.70, ICC_{plv} = 0.64), while SZ had excellent reliability in wpli2 (ICC_{wpli2} = 0.87), and good reliability in coh, ppc, and plv (ICC_{coh} = 0.69, ICC_{ppc} = 0.72, ICC_{plv} = 0.63). Within the visual network, **Figures 4G,H** (VISN), HC had excellent reliability for coh, imcoh, ppc, plv and wpli2 (ICC_{coh} = 0.82, ICC_{imcoh} = 0.87, ICC_{ppc} = 0.86, ICC_{plv} = 0.87, ICC_{wpli2} = 0.80), while SZ had excellent reliability for coh, ppc, and plv (ICC_{coh} = 0.76, ICC_{ppc} = 0.77, ICC_{plv} = 0.79) and fair reliability for wpli2 (ICC_{wpli2} = 0.59). Within the somatosensory network, **Figures 4G,H** (SOMN), HC had excellent reliability for imcoh and wpli2 (ICC_{imcoh} = 0.84,

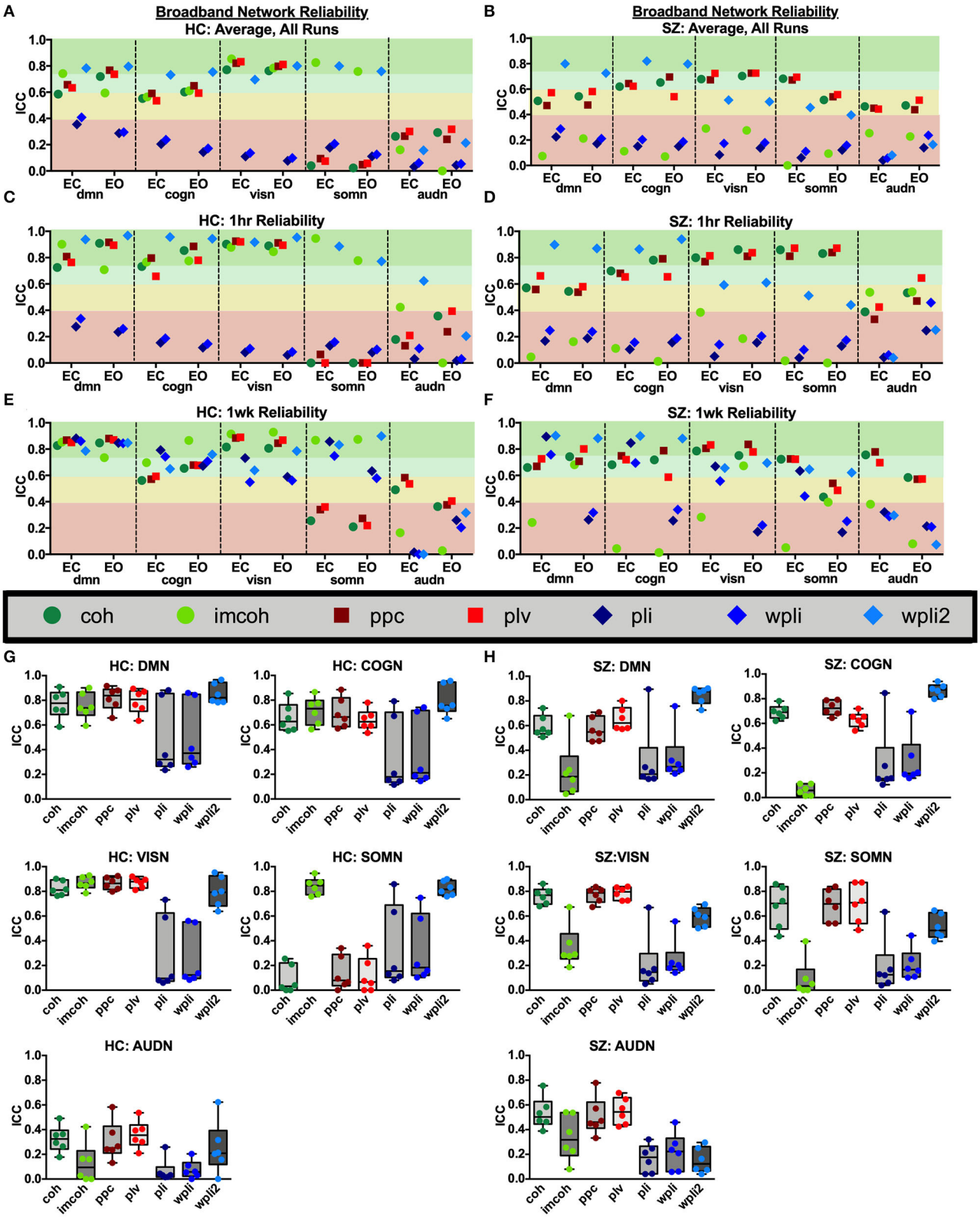

FIGURE 4 | Broadband network reliability. Broadband network ICC estimates for each connectivity measure were calculated for network averages across all runs, for 1 hour and 1 week in the broadband frequency band in HC **(A,C,E)** and SZ **(B,D,F)**. Data represent mean ICC value. Boxplots **(G,H)** contain aggregate information for each connectivity measure within networks.

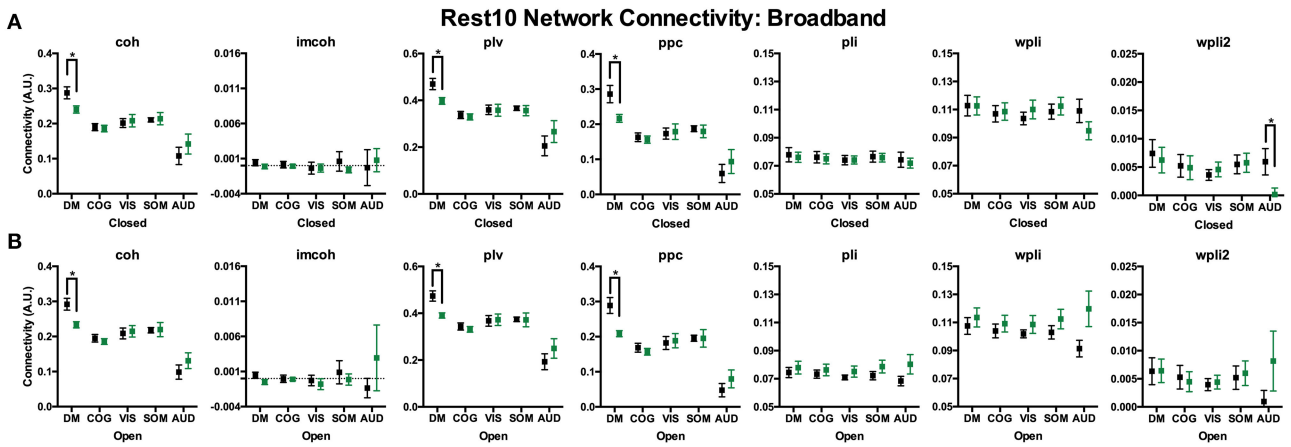

FIGURE 5 | Rest10 network broadband connectivity. Data represent mean (±SEM), asterisks denote $p<0.05$. Patients with schizophrenia had reduced broadband default mode network average coherence, phase-locking value, and pairwise phase consistency during the eyes closed resting-state **(A)** and eyes open resting-state **(B)**. Patients with schizophrenia also had reduced broadband auditory network average weight phase lag index debiased during the eyes closed resting-state **(A)**.

$ICC_{wpli2} = 0.83$), while SZ had good reliability for coh, ppc, and plv ($ICC_{coh} = 0.67$, $ICC_{ppc} = 0.69$, $ICC_{plv} = 0.70$), and fair reliability for wpli2 ($ICC_{wpli2} = 0.51$). Within the auditory network, **Figures 4G,H** (AUDN), SZ had fair reliability for coh, ppc, and plv ($ICC_{coh} = 0.53$, $ICC_{ppc} = 0.51$, $ICC_{plv} = 0.55$). Any measure not listed in the above networks had poor reliability.

To compare broadband network functional connectivity metrics between groups (SZ, HC) the main effect of group was examined during Visit 1 for the Rest 10 task. As shown in **Figure 5**, SZ had significantly reduced coh, plv, ppc in the dmn, when compared to HC, during both eyes closed [Group effect for coh: $F(1,24) = 5.631$, $p = 0.026$, plv: $F(1,24) = 6.766$, $p = 0.016$, ppc: $F(1,24) = 6.564$, $p = 0.017$] and eyes open [Group effect for coh: $F(1,24) = 9.464$, $p = 0.005$, plv: $F(1,24) = 11.172$, $p = 0.003$, ppc: $F(1,24) = 10.864$, $p = 0.003$] resting states, **Figures 5A,B**, respectively. Furthermore, SZ had significantly reduced wpli2 in the audn during an eyes closed resting state [Group effect for wpli2: $F(1,24) = 5.001$, $p = 0.035$].

Average network reliability within frequency bands is shown in **Figure 6**. To help determine which measurement time (1 hour vs. 1 week) drove the average, **Supplementary Figures 1**, **2** further break down network reliability within frequency bands for 1 hour and 1 week. An alternative version of **Figure 6**, showing variability across networks is also provided in **Supplementary Figure 3**. As with broadband data, the somatosensory and auditory networks across all frequencies had the lowest reliability. Similar reliability levels were found in both resting-states for all metrics (average HC mean difference = 0.01, SZ mean difference = 0.02).

Regional Pair Reliability

Broadband connectivity metrics within 3 individual network pairs (DMN pair, COGN pair, VISN pair) were examined, as shown in **Figure 7**. MEG connectivity network reliability varied greatly depending on network pair, connectivity measure and participant group. Within the default mode network pair, **Figures 7G,H** (DMN Pair), HC had fair reliability for coh, ppc, and plv ($ICC_{coh} = 0.46$, $ICC_{ppc} = 0.42$, $ICC_{plv} = 0.49$), and SZ had fair reliability for coh, ppc, and plv ($ICC_{coh} = 0.48$, $ICC_{ppc} = 0.49$, $ICC_{plv} = 0.55$). Within the cognitive control network pair, **Figures 7G,H** (COGN Pair), HC had good reliability for coh, ppc, and plv ($ICC_{coh} = 0.68$, $ICC_{ppc} = 0.66$, $ICC_{plv} = 0.68$), while SZ had good to fair reliability for coh, ppc, and plv ($ICC_{coh} = 0.49$, $ICC_{ppc} = 0.69$, $ICC_{plv} = 0.68$). Within the visual network pair, **Figures 7G,H** (VISN Pair), HC had good reliability for coh, ppc, and plv ($ICC_{coh} = 0.73$, $ICC_{ppc} = 0.73$, $ICC_{plv} = 0.75$), while SZ had fair reliability for ppc, and plv ($ICC_{ppc} = 0.41$, $ICC_{plv} = 0.51$). Any measure not listed in the above networks had poor reliability. For both groups, the connectivity metrics imcoh, pli, wpli, and wpli2 had poor reliability in all 3 network pairs tested. Eyes open and eyes closed had similar reliability levels in HC and SZ for all metrics (average HC mean difference = 0.01, SZ mean difference = 0.01).

To compare regional pair functional connectivity metrics between groups (SZ, HC) the main effect of group was examined during Visit 1 for the Rest 10 task. As shown in **Figure 8**, SZ had significantly reduced coh, plv, ppc in the dmn connectivity pair (precuneus right hemisphere to medial orbitofrontal cortex left hemisphere), during both eyes closed [Group effect for coh: $F(1,24) = 7.817$, $p = 0.010$, plv: $F(1,24) = 6.891$, $p = 0.015$, ppc: $F(1,24) = 6.518$, $p = 0.017$] and eyes open [Group effect for coh: $F(1,24) = 11.071$, $p = 0.003$, plv: $F(1,24) = 10.789$, $p = 0.003$, ppc: $F(1,24) = 10.154$, $p = 0.004$] resting states when compared to HC, **Figures 8A,B**, respectively. Furthermore, SZ had significantly reduced coh, plv, ppc in the visn connectivity pair (lateral occipital left hemisphere to middle temporal right hemisphere) during an eyes closed resting state, [Group effect for coh: $F(1,24) = 9.004$, $p = 0.010$, plv: $F(1,24) = 10.132$, $p = 0.004$, ppc: $F(1,24) = 7.345$, $p = 0.012$] **Figure 8A**, when compared to HC.

DISCUSSION

Following source analysis various FNC metrics were compared, specifically coh, imcoh, ppc, plv, pli, wpli, and wpli2. The

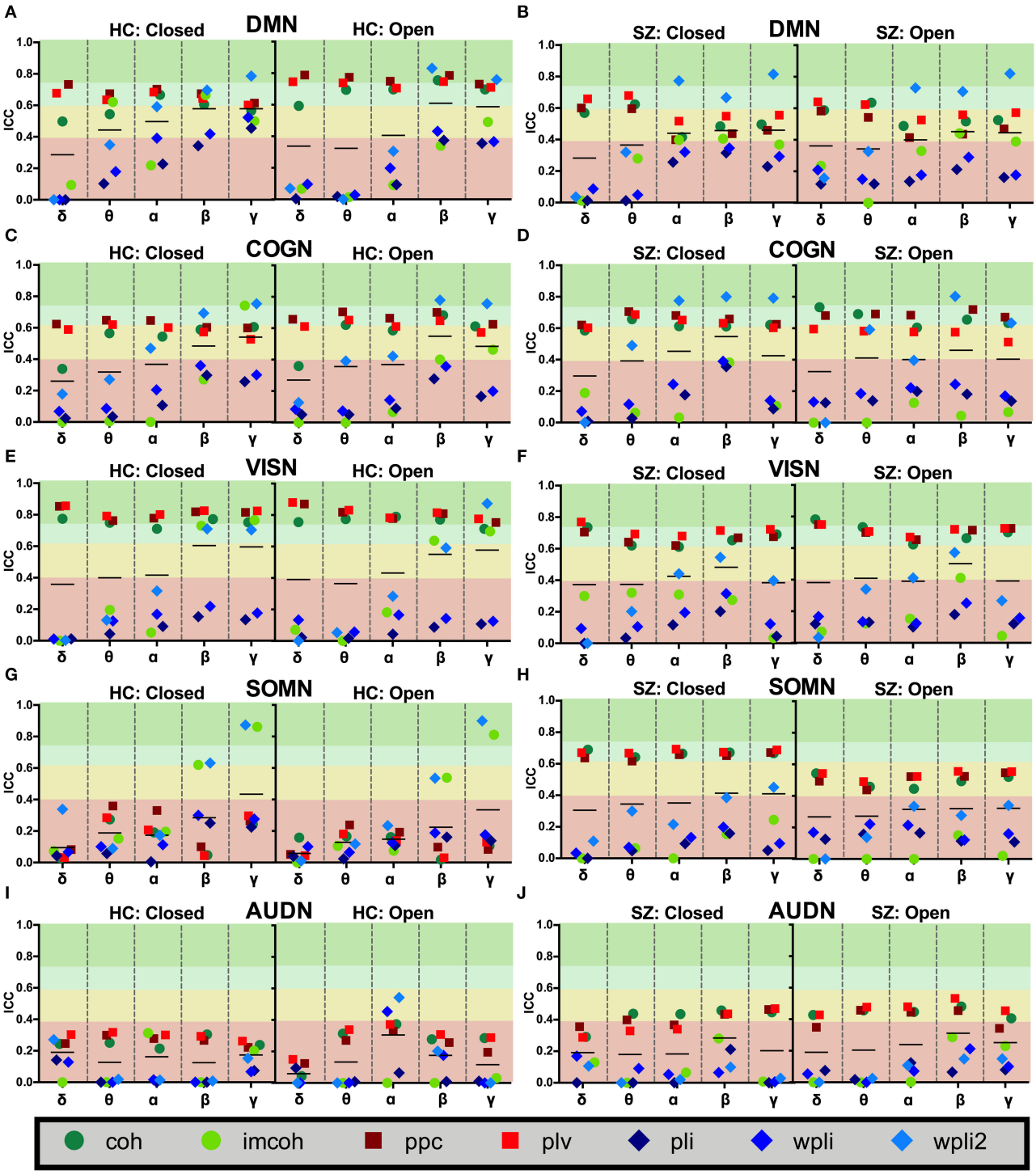

FIGURE 6 | Network reliability across frequency. Network ICC estimates for each connectivity measure were calculated as an average across all runs for each frequency band (delta-gamma) and in each resting state (eyes closed and eyes open). Network averages for DMN **(A,B)**, COGN **(C,D)**, VISN **(E,F)**, SOMN **(G,H)**, and AUDN **(I,J)** are shown in HC and SZ, respectively. Data represent mean ICC value.

reliability of these metrics varied greatly depending on frequency band, network, network pair, and participant group examined. To summarize a few key findings: (1) Broadband whole brain averages in both HC and SZ showed excellent reliability for wpli2, good to fair reliability for ppc, plv, and coh and poor reliability for imcoh, pli, and wpli, (2) Network averages showed

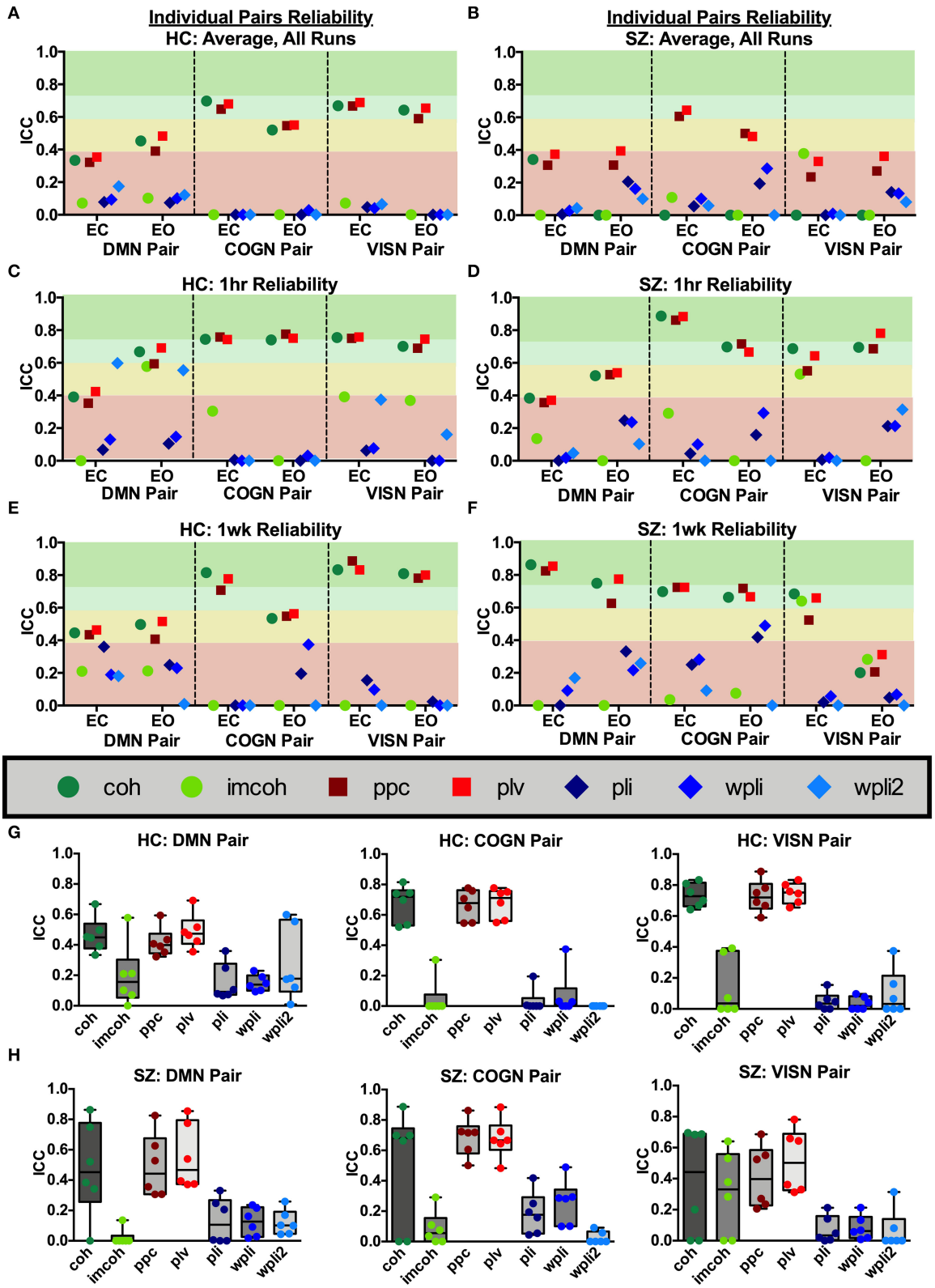

FIGURE 7 | Network pair reliability. Network pair ICC estimates for each connectivity measure were calculated as an average across all runs, for 1 hour and 1 week in the broadband frequency band in HC **(A,C,E)** and SZ **(B,D,F)**. Data represent mean ICC value. Boxplots **(G,H)** contain aggregate information for each connectivity measure within each network pair.

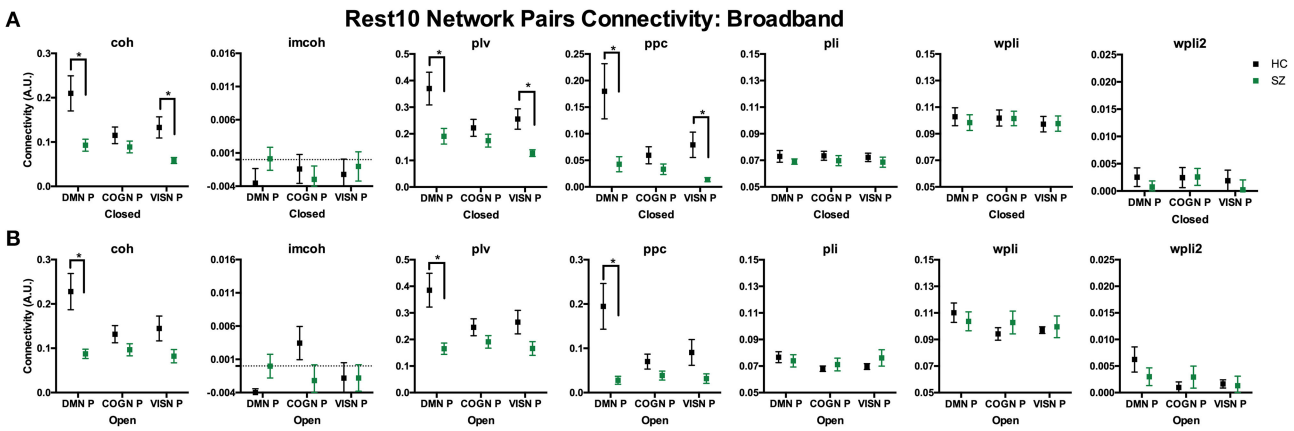

FIGURE 8 | Rest10 network pairs broadband connectivity. Data represent mean (±SEM), asterisks denote $p < 0.05$. Patients with schizophrenia had reduced default mode network pair (right precuneus to left medial orbitofrontal cortex) and visual network pair (left lateral occipital to right middle temporal) coherence, phase-locking value, and pairwise phase consistency during the eyes closed resting-state **(A)**. Patients with schizophrenia had reduced default mode network pair (right precuneus to left medial orbitofrontal cortex) coherence, phase-locking value, and pairwise phase consistency during the eyes open resting-state **(B)**.

excellent to good reliability for coh, imcoh, ppc, plv, and wpli within default mode, cognitive control, and visual networks in HC, while the same metrics had excellent to fair reliability in SZ, (3) Regional network pair averages showed good to fair reliability for coh, ppc, and plv within default mode, cognitive control and visual network pairs, while imcoh, pli, wpli, and wpli2 all had poor reliability, (4) For both HC and SZ, the default mode, cognitive control, and visual networks had higher reliability compared to somatosensory and auditory networks, and (5) Eyes open and eyes closed states had similar reliability levels in HC and SZ for all metrics. When taken together, the results indicate functional connectivity reliability is highly dependent on connectivity metric, frequency band, and region or network size.

In HC, we confirmed some patterns of functional connectivity for certain metrics and frequency bands, which were in line with previous research. Our results in HC were fairly consistent with previous resting-state MEG studies, although there were a few differences. For example, in MEG whole-brain functional connectivity comparisons plv has been found to range from excellent to good reliability (ICC range 0.74–0.82) in alpha-gamma bands, while pli has been found to have poor reliability (ICCs < 0.1) for all frequency bands in both eyes open and eyes closed resting-states (2). Here, we found similar results that global functional connectivity averages for plv had excellent to good reliability across 1 hour and 1 week in delta-gamma bands and in broadband ($ICC_{plv} = 0.65$), while pli had poor reliability in all bands across 1 hour and in broadband ($ICC_{pli} = 0.26$). We also found that both eyes open and eyes closed resting states had similar reliability levels. However, in contrast to the previous paper, we found that pli had excellent reliability in beta, gamma, and broadband across 1 week. Another previous study examining MEG global whole brain reliability found that coh and wpli had good to excellent reliability in delta-gamma bands (4). In contrast to this, the present study found that imcoh and wpli generally had poor reliability in all frequencies with a few exceptions, such as fair to good reliability for imcoh during an eyes closed state in beta, gamma, and broadband and fair to excellent reliability for wpli across 1 week. A potential difference between the two studies may be how imcoh was calculated. Here, we reported the imcoh measure without using absolute values, which is the default formula used by MNE software and the original publication (28). To get undirected connectivity for imcoh, certain source models benefit from using imcoh absolute values, as (4) did. At the resting-state network level, there is often poor reliability in phase or coh based metrics which are robust to spatial leakage artifacts, such as pli and its derivatives, as well as imcoh (1). We found similar results here and reported that our network averages showed lower reliability in metrics robust to spatial leakage artifacts, e.g., imcoh, pli, wpli, and wpli2. It is interesting that both results showed low reliability for the metrics considering that we used an anatomical parcellation and dSPM algorithm, whereas the previous publication used a data-driven parcellation from fMRI along with a beamformer algorithm. Poor reliability of phase based metrics has also been seen in another MEG study which found poor reliability in pli in all frequency bands and networks, but good to excellent reliability in plv in alpha-gamma bands for visual, sensorimotor, auditory, and default mode networks (2). Here, we found excellent to good reliability for coh, plv, and ppc within default mode, cognitive control, and visual networks, with mixed reliability for pli and wpli dependent on network and interval length (1 hour vs. 1 week). Although graph analysis was not used in the current study, it should be mentioned that the reliability of those derived resting-state MEG functional connectivity networks have also been variable, ranging from poor to good (ICCs 0.256–0.655) depending on band and metric defining nodal centrality, with greatest reliability in eyes open resting state networks when assessed with Dnodal and Enodal metrics (38). Further direct comparison between our research and (1, 2, 4) is difficult to interpret given that each study used different source analysis

and network modeling methods. Functional connectivity metrics based on phase-related connectivity can minimize the impact of spatial leakage and zero-lag synchronization, however, the estimates may be more variable in short or noisy recordings, or across connectivity pair data. It has been previously suggested that amplitude envelope correlation and partial correlation measures have higher reliability and are the most consistent functional connectivity methods for an MEG resting-state (1), however, those metrics were not tested in the current study. Phase-related connectivity metrics perform better when averaged across larger brain regions, more voxels, and in larger datasets, as sample size negatively impacts pli and imcoh metrics.

Magnetic field spread or spatial leakage artifacts is a problem in MEG functional connectivity estimation (39–41) that can influence measures of functional connectivity and artificially inflate reliability (1); therefore, metrics which avoid those confounds, such as imcoh, pli, wpli, phase slope index, amplitude envelope correlation, are generally recommended. However, the confounds introduced into connectivity estimation due to spatial leakage have been shown to be highly repeatable across scans and between subjects (1). Here, we also found that the metrics which are prone to spatial leakage, e.g., coh, plv, and ppc, generally have higher repeatability or reliability across sessions. The higher reliability may be spurious in nature, but coh, plv, and ppc remained consistently higher in reliability even when region size and number of regions averaged fluctuated in our data, e.g., throughout global, network, and regional pair data.

While signal leakage is expected to be highly reliable and may on the surface appear to influence the reliability of certain connectivity metrics, there are two additional factors which indicate that the reliability of coh, ppc, and plv is not solely attributed to signal leakage. First, signal leakage, especially for MEG, does not spread across the entire brain but remains relatively localized (41). In our data, the regional network pairs we selected represented "distant" intra network sources, e.g., parietal to anterior frontal or left occipital to right temporal, greatly decreasing the likelihood of the increased reliability of the coh, ppc and plv metrics to be influenced by signal leakage alone. Importantly also, these metrics that cannot directly eliminate the possibility of signal leakage also retain additional signal (zero-phase correlations) that metrics robust to signal leakage ignore. Invasive measures have demonstrated zero-phase correlations across broad regions of the brain indicating that not all zero-phase correlations are related to artifact alone, but contain real signal; therefore, eliminating all zero-phase correlations may reduce reliability by removing signal. There are other spatial leakage correction methods for MEG, besides removing zero-phase correlations, which may improve reliability, such as geometric correction scheme which removes spurious local connections without impacting dynamic hub regions and networks at rest (42) or adaptive cortical parcellations (43). In fact, it has been suggested that using a non-zero-lag connectivity metric does not obviate the need for adaptive parcellation. Based on this information, we consider the current results to support the reliability of coh, ppc, and pli across region, network and whole brain analyses.

Interestingly, our research found that the non-zero-lag connectivity metrics pli, wpli, and wpli2 had variable reliability depending on the size and number of regions averaged (i.e., as spatial resolution was increased, reliability decreased). Those metrics had their highest reliability in global averages, followed by network averages, and lowest reliability in individual network pair connections. For example, when wpli2 was not averaged across the whole brain or across a network, but in an individual network pair, HC and SZ groups both had poor reliability (HC ICC Avg = 0.14, SZ ICC Avg = 0.11), similar to previous results (5), yet global averages with all regions showed excellent reliability (HC ICC Avg = 0.85, SZ ICC Avg = 0.84). Even within network averages, the networks which contained more regions (default mode-14 regions, cognitive control-26 regions, and visual-12 regions) had higher reliability than networks defined by fewer regions (somatosensory-8 regions and auditory-2 regions). While some have used 2 or 3 nodes to characterize a resting-state network (2), we decided to use networks defined by the fMRI ICA resting-state network approach (12, 29, 44), a technique which has been successfully applied to MEG resting-state networks in SZ clinical populations (11, 14, 15).

Here, we showed several instances where patients with SZ had lower reliability in functional connectivity metrics, e.g., lower broadband whole brain averages and network averages when compared to HC. In our previous test–retest paper, which only examined wpli2 in select superior parietal regional connectivity pairs, we also found poor reliability in the metric for patients with SZ (ICC = 0.03), as well as HC (ICC = 0.12) (5). Although reliability was low, meaning significant effects were not consistent across run, we found instances of increased functional connectivity between superior parietal to lateral occipital and superior parietal to entorhinal connections in patients with SZ (5). However, these results may not replicate because the metric is unreliable. Previous research has shown that abnormal resting-state functional connectivity is a key process underlying SZ (9). While there are no other test–retest functional connectivity reliability studies to directly compare to, one study used imcoh and found decreased alpha-band connectivity in left prefrontal cortex and right superior temporal cortex together with increased connectivity in left extrastriate cortex and right inferior prefrontal cortex in patients with SZ (10). Our research would suggest that imcoh is a connectivity metric with low reliability in this patient population. We also found higher variability in ICC 95% confidence intervals (data not shown) in patients with SZ suggesting greater between subjects variability, similar to the dynamic functional connectivity finding that patients change meta-states more often than HC and exhibit greater inter-individual variability (14). Despite the difficulties in interpreting the functional meaning of lower reliability and higher variability in patients with SZ, the current findings are consistent with deficits in functional connectivity and neural oscillations previously reported (5, 11, 14, 16, 39, 45). Aside from differences in ICC, here, we also found that patients with SZ had significantly reduced coh, plv, and ppc metrics in the default mode network average and pair (right precuneus to left medial orbitofrontal cortex) values when compared to HC, in the Rest10 task during Visit 1. We also found reductions for patients

with SZ in coh, plv, and ppc metrics in the visual network pair, and for wpli2 in the auditory network during an eyes closed resting-state. When combined with the information that ICCs for these metrics (coh, plv, ppc) were relatively high, it implies the reduction in default mode functional connectivity seen in patients with SZ is somewhat stable during both eyes open and eyes closed resting-states.

A key question in examining test–retest reliability of resting state networks with MEG is whether there are stable networks within the time window assessed. Simulations have shown that at the network level, only longer window lengths were sufficient to detect resting-state networks that matched the ground truth, especially for plv, amplitude envelope correlation, and coh (46). While fMRI has presented multiple studies demonstrating the reliability of connectivity between different regions, the timescale of MEG is different and may present as more or less reliable depending on how these connectivity patterns are assessed. However, the visual occipital alpha activation that shows often reliable patterns of activation when changing between eyes open and eyes closed within subject provide evidence for the reliability of oscillatory networks. An additional question that remains is why clinical populations may exhibit different test–retest reliability than HC. A core characteristic of SZ is that patients experience repeated relapses even after initiation of medication (47). This supports the general idea that brain dynamics in patients are more variable and is consistent with the general hypothesis that healthy brain dynamics are maintained through homeostasis and deviations from this stable state lead to functional consequences (48). Future research is needed to determine if this reduction in reliability of measures in patients with SZ is dependent on medication, disease severity or disease duration and may further inform clinical treatment.

The current study was designed to compare available functional connectivity metrics in a test–retest dataset of patients with SZ and HC. We reported connectivity values without modification from the MNE provided functions and used a surface-based source space with a fixed surface orientation. However, it should be noted that certain functional connectivity metrics, e.g., imcoh, can become difficult to interpret when source direction is not well-defined. The other metrics used (coh, plv, ppc, pli, wpli, wpli2) are the result of absolute value calculations which account for sign flips across sessions. Others using imcoh should carefully evaluate their models to avoid introducing extra variability.

There are several limitations in the present study which warrant caution. The patient population recruited was a stable, medicated cohort of patients with SZ. As such, the results may not generalize to a more varied group of individuals with psychosis, other populations and/or imaging sites. Furthermore, it remains unknown if the functional connectivity abnormalities found were due to underlying neurophysiology of schizophrenia or were driven by medication, as all patients were antipsychotic medications. Another cautionary note is the small sample size. Although ICCs were calculated across 4 separate runs, the small group size ($n = 13$) warrants caution when generalizing to larger samples. Also, it is important to consider the ICC model itself. An ICC examines variance changes within and between subjects over time. Occasionally, a low ICC can reflect that a within-subject change occurred, and may not imply that a measure itself is inaccurate. While results between our study and others are similar, each study modeled ICC estimates differently and ICC values will fluctuate based on the model and variance assumptions (35, 36, 49). Another aspect to consider is the localization algorithm used. The optimal source localization algorithm to examine functional connectivity remains to be determined. One advantage of the dSPM algorithm is that its assumptions do not limit the ability to capture synchronous activity, which remains a limitation of most implementations of the beamformer approach. However, the dSPM algorithm is also known to have limited spatial resolution and also can propagate noise throughout the brain. As such, using dSPM may impact the sensitivity of the functional connectivity metrics measured. Future studies should examine realistic simulated connectivity patterns to determine the conditions under which the best results are obtained. Finally, the current study included a single MEG system, definitive conclusions on reliability cannot be made until a larger sample size and multiple sites are included.

Our research demonstrates that resting-state connectivity in clinical populations can be informative and reliable. Certain functional connectivity metrics should be preferred due to their higher reliability. MEG can be used to capture neural oscillatory networks in resting-states with good spatial precision and reliability. Both eyes open and eyes closed resting states were reliable over sessions and should be reported to best capture neural dynamics.

DATA AVAILABILITY STATEMENT

The original contributions generated for the study are included in the article/**Supplementary Files**, further inquiries can be directed to the corresponding author.

ETHICS STATEMENT

The studies involving human participants were reviewed and approved by University of New Mexico Health Sciences Center Human Research Review Committee. The patients/participants provided their written informed consent to participate in this study.

AUTHOR CONTRIBUTIONS

FC-C and JS: design and writing. FC-C: data collection and processing, formal analysis, and funding acquisition. JS: supervision. Both authors contributed to and have approved the final manuscript.

FUNDING

This work was supported in part by grants from the National Institutes of Health (P20GM103472 and P30GM122734) and

National Science Foundation (NSF) 1539067. The funding sources had no role in study design, analysis, and interpretation of the data, or the writing of this manuscript.

ACKNOWLEDGMENTS

We thank the participants who graciously offered their time for this study. Special thanks to Cesar Ojeda, and Nattida Payaknait from the UNM Department of Psychiatry for clinical research coordination and data entry, MRN technicians Dathan Gleichmann, Cathy Smith, and Diana South for their contributions with data collection, and MRN technician Megan Schendel for data preprocessing. This work was supported in part by grants from the National Institutes of Health (P20GM103472 and P30GM122734) and National Science Foundation (NSF) 1539067.

SUPPLEMENTARY MATERIAL

The Supplementary Material for this article can be found online at: https://www.frontiersin.org/articles/10.3389/fpsyt.2020.551952/full#supplementary-material

REFERENCES

1. Colclough GL, Woolrich MW, Tewarie PK, Brookes MJ, Quinn AJ, Smith SM. How reliable are MEG resting-state connectivity metrics? *Neuroimage*. (2016) 138:284–93. doi: 10.1016/j.neuroimage.2016.05.070
2. Garces P, Martin-Buro MC, Maestu F. Quantifying the test–retest reliability of magnetoencephalography resting-state functional connectivity. *Brain Connect*. (2016) 6:448–60. doi: 10.1089/brain.2015.0416
3. Martin-Buro MC, Garces P, Maestu F. Test–retest reliability of resting-state magnetoencephalography power in sensor and source space. *Hum Brain Mapp*. (2016) 37:179–90. doi: 10.1002/hbm.23027
4. Marquetand J, Vannoni S, Carboni M, Li Hegner Y, Stier C, Braun C, et al. Reliability of magnetoencephalography and high-density electroencephalography resting-state functional connectivity metrics. *Brain Connect*. (2019) 9:539–53. doi: 10.1089/brain.2019.0662
5. Candelaria-Cook FT, Schendel ME, Ojeda CJ, Bustillo JR, Stephen JM. Reduced parietal alpha power and psychotic symptoms: test–retest reliability of resting-state magnetoencephalography in schizophrenia and healthy controls. *Schizophr Res*. (2020) 215:229–40. doi: 10.1016/j.schres.2019.10.023
6. Nugent AC, Robinson SE, Coppola R, Furey ML, Zarate CA Jr. Group differences in MEG-ICA derived resting state networks: application to major depressive disorder. *Neuroimage*. (2015) 118:1–12. doi: 10.1016/j.neuroimage.2015.05.051
7. Cicchetti D, Sparrow SA. developing criteria for establishing interrater reliability of specific items: applications to assessment of adaptive behavior. *Am J Ment Defic*. (1981) 86:127–37.
8. Friston KJ. The disconnection hypothesis. *Schizophr Res*. (1998) 30:115–25. doi: 10.1016/S0920-9964(97)00140-0
9. Friston K, Brown HR, Siemerkus J, Stephan KE. The dysconnection hypothesis. *Schizophr Res*. (2016) 176:83–94. doi: 10.1016/j.schres.2016.07.014
10. Hinkley LB, Vinogradov S, Guggisberg AG, Fisher M, Findlay AM, Nagarajan SS. Clinical symptoms and alpha band resting-state functional connectivity imaging in patients with schizophrenia: implications for novel approaches to treatment. *Biol Psychiatry*. (2011) 70:1134–42. doi: 10.1016/j.biopsych.2011.06.029
11. Houck JM, Cetin MS, Mayer AR, Bustillo JR, Stephen J, Aine C, et al. Magnetoencephalographic and functional MRI connectomics in schizophrenia *via* intra- and inter-network connectivity. *Neuroimage*. (2017) 145(Pt A):96–106. doi: 10.1016/j.neuroimage.2016.10.011
12. Cetin MS, Houck JM, Rashid B, Agacoglu O, Stephen JM, Sui J, et al. Multimodal classification of schizophrenia patients with MEG and fMRI data using static and dynamic connectivity measures. *Front Neurosc*. (2016) 10:466. doi: 10.3389/fnins.2016.00466
13. Lottman KK, Gawne TJ, Kraguljac NV, Killen JF, Reid MA, Lahti AC. Examining resting-state functional connectivity in first-episode schizophrenia with 7T fMRI and MEG. *NeuroImage Clin*. (2019) 24:101959. doi: 10.1016/j.nicl.2019.101959
14. Sanfratello L, Houck J, Calhoun VD. Dynamic functional network connectivity in schizophrenia with MEG and fMRI, do different time scales tell a different story? *Brain Connect*. (2019). doi: 10.1101/432385
15. Sanfratello L, Houck JM, Calhoun VD. Relationship between MEG global dynamic functional network connectivity measures and symptoms in schizophrenia. *Schizophr Res*. (2019) 209:129–34. doi: 10.1016/j.schres.2019.05.007
16. Alamian G, Hincapie A-S, Pascarella A, Thiery T, Combrisson E, Saive A-L, et al. Measuring alterations in oscillatory brain networks in schizophrenia with resting-state MEG: state-of-the-art and methodological challenges. *Clin Neurophysiol*. (2017) 128:1719–36. doi: 10.1016/j.clinph.2017.06.246
17. Hinkley LB, Owen JP, Fisher M, Findlay AM, Vinogradov S, Nagarajan SS. Cognitive impairments in schizophrenia as assessed through activation and connectivity measures of magnetoencephalography (MEG) data. *Front Hum Neurosci*. (2010) 3:73. doi: 10.3389/neuro.09.073.2009
18. Siekmeier PJ, Stufflebeam SM. Patterns of spontaneous magnetoencephalographic activity in patients with schizophrenia. *J Clin Neurophysiol*. (2010) 27:179–90. doi: 10.1097/WNP.0b013e3181e0b20a
19. Taulu S, Hari R. Removal of magnetoencephalographic artifacts with temporal signal-space separation: demonstration with single-trial auditory-evoked responses. *Human Brain Mapping*. (2009) 30:1524–34. doi: 10.1002/hbm.20627
20. Taulu S, Kajola M. Presentation of electromagnetic multichannel data: the signal space separation method. *J Appl Phys*. (2005) 97:124905. doi: 10.1063/1.1935742
21. Uusitalo MA, Ilmoniemi RJ. Signal-space projection method for separating MEG or EEG into components. *Med Biol Eng Comput*. (1997) 35:135–40. doi: 10.1007/BF02534144
22. Gramfort A, Luessi M, Larson E, Engemann D, Strohmeier D, Brodbeck C, et al. MEG and EEG data analysis with MNE-Python. *Front Neurosc*. (2013) 7(267). doi: 10.3389/fnins.2013.00267
23. Gramfort A, Luessi M, Larson E, Engemann DA, Strohmeier D, Brodbeck C, et al. MNE software for processing MEG and EEG data. *NeuroImage*. (2014) 86:446–60. doi: 10.1016/j.neuroimage.2013.10.027
24. Dale AM, Liu AK, Fischl BR, Buckner RL, Belliveau JW, Lewine JD, et al. Dynamic statistical parametric mapping: combining fMRI and MEG for high-resolution imaging of cortical activity. *Neuron*. (2000) 26:55–67. doi: 10.1016/S0896-6273(00)81138-1
25. Hamalainen MS, Sarvas J. Realistic conductivity geometry model of the human head for interpretation of neuromagnetic data. *IEEE Trans Biomed Eng*. (1989) 36:165–71. doi: 10.1109/10.16463
26. Desikan RS, Ségonne F, Fischl B, Quinn BT, Dickerson BC, Blacker D, et al. An automated labeling system for subdividing the human cerebral cortex on MRI scans into gyral based regions of interest. *NeuroImage*. (2006) 31:968–80. doi: 10.1016/j.neuroimage.2006.01.021
27. Klein A, Tourville J. 101 labeled brain images and a consistent human cortical labeling protocol. *Front Neurosc*. (2012) 6:171. doi: 10.3389/fnins.2012.00171
28. Nolte G, Bai O, Wheaton L, Mari Z, Vorbach S, Hallett M. Identifying true brain interaction from EEG data using the imaginary part of coherency. *Clin Neurophysiol*. (2004) 115:2292–307. doi: 10.1016/j.clinph.2004.04.029
29. Allen EA, Damaraju E, Plis SM, Erhardt EB, Eichele T, Calhoun VD. Tracking whole-brain connectivity dynamics in the resting state. *Cerebral Cortex*. (2014) 24:663–76. doi: 10.1093/cercor/bhs352

30. Lachaux JP, Rodriguez E, Martinerie J, Varela FJ. Measuring phase synchrony in brain signals. *Hum Brain Mapp*. (1999) 8:194–208. doi: 10.1002/(SICI)1097-0193(1999)8:4<194::AID-HBM4>3.0.CO;2-C
31. Vinck M, van Wingerden M, Womelsdorf T, Fries P, Pennartz CM. The pairwise phase consistency: a bias-free measure of rhythmic neuronal synchronization. *Neuroimage*. (2010) 51:112–22. doi: 10.1016/j.neuroimage.2010.01.073
32. Stam CJ, Nolte G, Daffertshofer A. Phase lag index: assessment of functional connectivity from multi-channel EEG and MEG with diminished bias from common sources. *Hum Brain Mapp*. (2007) 28:1178–93. doi: 10.1002/hbm.20346
33. Vinck M, Oostenveld R, van Wingerden M, Battaglia F, Pennartz CM. An improved index of phase-synchronization for electrophysiological data in the presence of volume-conduction, noise and sample-size bias. *Neuroimage*. (2011) 55:1548–65. doi: 10.1016/j.neuroimage.2011.01.055
34. Chen G, Taylor PA, Haller SP, Kircanski K, Stoddard J, Pine DS, et al. Intraclass correlation: improved modeling approaches and applications for neuroimaging. *Human brain mapping*. (2018) 39:1187–206. doi: 10.1002/hbm.23909
35. Shrout PE, Fleiss JL. Intraclass correlations: uses in assessing rater reliability. *Psychol Bull*. (1979) 86:420–8. doi: 10.1037/0033-2909.86.2.420
36. McGraw KO, Wong SP. Forming inferences about some intraclass correlation coefficients. *Psychol Methods*. (1996) 1:30–46. doi: 10.1037/1082-989X.1.1.30
37. Li L, Zeng L, Lin Z-J, Cazzell M, Liu H. Tutorial on use of intraclass correlation coefficients for assessing intertest reliability and its application in functional near-infrared spectroscopy-based brain imaging. *J Biomed Opt*. (2015) 20:050801. doi: 10.1117/1.JBO.20.5.050801
38. Jin S-H, Seol J, Kim JS, Chung CK. How reliable are the functional connectivity networks of MEG in resting states? *J Neurophysiol*. (2011) 106:2888–95. doi: 10.1152/jn.00335.2011
39. Brookes MJ, Tewarie PK, Hunt BAE, Robson SE, Gascoyne LE, Liddle EB, et al. A multi-layer network approach to MEG connectivity analysis. *Neuroimage*. (2016) 132:425–38. doi: 10.1016/j.neuroimage.2016.02.045
40. Hipp JF, Hawellek DJ, Corbetta M, Siegel M, Engel AK. Large-scale cortical correlation structure of spontaneous oscillatory activity. *Nat Neurosci*. (2012) 15:884–90. doi: 10.1038/nn.3101
41. O'Neill G, Barratt E, Hunt B, Tewarie P, Brookes M. Measuring electrophysiological connectivity by power envelope correlation: a technical review on MEG methods. *Phys Med Biol*. (2015) 60. doi: 10.1088/0031-9155/60/21/R271
42. Della Penna S, Corbetta M, Wens V, de Pasquale F. The impact of the geometric correction scheme on MEG functional topology at rest. *Front Neurosc*. (2019) 13:1114. doi: 10.3389/fnins.2019.01114
43. Farahibozorg SR, Henson RN, Hauk O. Adaptive cortical parcellations for source reconstructed EEG/MEG connectomes. *Neuroimage*. (2018) 169:23–45. doi: 10.1016/j.neuroimage.2017.09.009
44. Cetin MS, Christensen F, Abbott CC, Stephen JM, Mayer AR, Canive JM, et al. Thalamus and posterior temporal lobe show greater inter-network connectivity at rest and across sensory paradigms in schizophrenia. *Neuroimage*. (2014) 97:117–26. doi: 10.1016/j.neuroimage.2014.04.009
45. Zeev-Wolf M, Levy J, Jahshan C, Peled A, Levkovitz Y, Grinshpoon A, et al. MEG resting-state oscillations and their relationship to clinical symptoms in schizophrenia. *NeuroImage Clin*. (2018) 20:753–61. doi: 10.1016/j.nicl.2018.09.007
46. Liuzzi L, Quinn AJ, O'Neill GC, Woolrich MW, Brookes MJ, Hillebrand A, et al. How sensitive are conventional MEG functional connectivity metrics with sliding windows to detect genuine fluctuations in dynamic functional connectivity? *Front Neurosc*. (2019) 13:797. doi: 10.3389/fnins.2019.00797
47. Buckley PF, Foster A. Schizophrenia: current concepts and approaches to patient care. *Am Health Drug Benefits*. (2008) 1:13–22.
48. Boison D, Masino SA. *Homeostatic Control of Brain Function*. New York, NY: Oxford University Press (2016).
49. Koo TK, Li MY. A guideline of selecting and reporting intraclass correlation coefficients for reliability research. *J Chiropr Med*. (2016) 15:155–63. doi: 10.1016/j.jcm.2016.02.012

Conflict of Interest: The authors declare that the research was conducted in the absence of any commercial or financial relationships that could be construed as a potential conflict of interest.

Advantages of publishing in Frontiers

OPEN ACCESS
Articles are free to read for greatest visibility and readership

FAST PUBLICATION
Around 90 days from submission to decision

HIGH QUALITY PEER-REVIEW
Rigorous, collaborative, and constructive peer-review

TRANSPARENT PEER-REVIEW
Editors and reviewers acknowledged by name on published articles

Frontiers
Avenue du Tribunal-Fédéral 34
1005 Lausanne | Switzerland

Visit us: www.frontiersin.org
Contact us: frontiersin.org/about/contact

REPRODUCIBILITY OF RESEARCH
Support open data and methods to enhance research reproducibility

DIGITAL PUBLISHING
Articles designed for optimal readership across devices

FOLLOW US
@frontiersin

IMPACT METRICS
Advanced article metrics track visibility across digital media

EXTENSIVE PROMOTION
Marketing and promotion of impactful research

LOOP RESEARCH NETWORK
Our network increases your article's readership